University of Alberta

Drug Delivery to Bone: Chemical Modification with Bisphosphonates and Physical Encapsulation with Nanoparticles

by

Sufeng Zhang 

A thesis submitted to the Faculty of Graduate Studies and Research
in partial fulfillment of the requirements for the degree of

Doctor of Philosophy

in

Chemical Engineering

Department of Chemical and Materials Engineering

Edmonton, Alberta
Fall 2008

Your file Votre référence
ISBN: 978-0-494-46457-1
Our file Notre référence
ISBN: 978-0-494-46457-1

DEDICATION

This thesis is dedicated to:

My parents, Mr. Maolin Zhang and Mrs. Xiangzhi Li, for their continuous encouragement and unwavering support.

My supervisor, Dr. Hasan Uludağ, for his enlightening advice and generosity throughout this entire process.

ABSTRACT

An effective therapeutic agent for treatment of bone diseases is expected to exhibit a high affinity to bone. Several drug delivery approaches were taken in this thesis work in order to develop a bone targeting platform. A method was first developed to obtain cleavable protein-bisphosphonates (BPs) conjugates with 2-(3-mercapto-propylsulfanyl)-ethyl-1,1-bisphosphonic acid (thiolBP) through disulfide linkage. The resultant protein-BP conjugates were readily cleaved in the presence of physiological thiols. To increase bone targeting efficiency while minimizing chemical modification of proteins, polymeric ligands containing multiple copies of BPs were constructed for protein conjugation by using thiolBP incorporated into poly(*L*-lysine) (PLL) and poly(ethylenimine) (PEI), respectively. The *in vitro* and *in vivo* mineral affinity of the polymer-BP conjugates and unmodified polymers showed that the cationic polymers displayed a strong affinity to hydroxyapatite (HA), which makes them suitable for designing delivery systems to bone. In virtue of better retention of protein integrity without direct modification, a nanoparticulate (NP) drug delivery system was then explored for growth factors – based on NPs fabricated from bovine serum albumin (BSA) and stabilized with PEI coating. Using the bone morphogenetic protein-2 (BMP-2), an encapsulation efficiency of > 90% was obtained in NPs. *In vitro* release kinetics showed PEI coating on the NPs efficiently controlled the release of BMP-2. The bioactivity and toxicity results indicated that BMP-2 in BSA NPs coated with 0.1 mg/mL PEI demonstrated tolerable toxicity, and retained BMP-2 bioactivity. The *in vivo* pharmacokinetics showed that PEI coating effectively reduced the initial burst release of BMP-2, and prolonged the BMP-2 retention time at implantation site in the rat

subcutaneous model. However, no bone formation was found in PEI-coated NP implants due to the toxicity of PEI in NP formulations that abolished BMP-2 activity. PEGylated PEI was then employed to reduce the toxicity of PEI, and PEI-PEG coated NPs not only possessed reduced size and zeta potential compared with PEI-coated NPs, but also successfully induced bone formation in the rat ectopic model. All together, the work presented herein expands the utilization of BPs in bone targeting efforts, as well as establishes a foundation for BMP-2 delivery based on a nanoparticulate formulation.

ACKNOWLEDGEMNETS

This research work was financially supported by a Biomedical Engineering Grant from the Whitaker Foundation, an operating Grant from the Canadian Institutes of Health Research and Infrastructure Grants from the Canadian Foundation for Innovation and the Alberta Heritage Foundation for Medical Research. Personally, I was primarily funded by the FS Chia PhD Scholarship provided by the University of Alberta.

My colleagues in Dr. Uludağ's laboratory supported me in my research work, and I would like to thank them for their interest and valuable hints. Especially, I would like to express my great gratitude to the laboratory technician, Mr. Cezary Kucharski, for his generous help with the animal study.

I am indebted to Dr. Phillip Y. K. Choi (Department of Chemical and Materials Engineering, University of Alberta) and Dr. John C. Vederas (Department of Chemistry, University of Alberta) for giving me very valuable suggestions and great support during my research. I am also obliged to Dr. Afsaneh Lavasanifar (Faculty of Pharmacy and Pharmaceutical Sciences, University of Alberta) for her inspiring lectures and kind encouragement.

I am very grateful to Dr. Michael Doschak, Mr. Michael Jones, Ms. Jillian Foster and Mr. Guang Li (the Pharmaceutical Orthopaedic Research Laboratory, Faculty of Pharmacy and Pharmaceutical Sciences, University of Alberta), for their great help with the micro-CT scanning and 3D imaging reconstruction. I would also like to thank Sara Elhasi (Faculty of Pharmacy and Pharmaceutical Sciences, University of Alberta) for her assistance with the Zetasizer.

TABLE OF CONTENTS

LIST OF TABLES

LIST OF FIGURES

LIST OF SCHEMES

LIST OF ABBREVIATIONS

1. ACS; Absorbable Collagen Sponge

2. AFM; Atomic Force Microscopy

3. Alendronate; 4-Aminobutylene-1,1-Bisphosphonate

4. ALP; Alkaline Phosphatase

5. aminoBP; 1-Amino-1,1-Diphosphonate Methane

6. AMP; 2-Amino-2-Methyl-Propan-1-ol

7. BMPs; Bone Morphogenetic Proteins

8. BMP-2; Bone Morphogenetic Protein-2

9. BMP-2/BSA NPs; BMP-2 encapsulated Bovine Serum Albumin Nanoparticles

10. BPs; Bisphosphonates

11. BSA; Bovine Serum Albumin

12. CDDS; Colloidal Drug Delivery System

13. CHOL-TOE-BP; Cholesteryl-Trisoxyethylene-Bisphosphonic acid

14. DMEM; Dulbecco's Modified Eagle Medium

15. DMSO; Dimethyl Sulfoxide

16. DTNB; 5,5'-Dithio-bis(2-Nitrobenzoic Acid)

17. EDC/NHS; 1-Ethyl-3-(3-Dimethylamino-propyl)-Carbodiimide/N-Hydroxy-Succinimide

18. EE; Encapsulation Efficiency

19. ELISA; Enzyme-Linked ImmunoSorbent Assay

20. FDA; Food and Drug Administration

21. FGFs; Fibroblast Growth Factors

22. FITC; Fluorescein Isothiocyanate

23. GPC; Gel Permeation Chromatography

24. HA; Hydroxyapatite

25. HBSS; Hank's Buffered Salt Solution

26. HMPA; N-(2-Hydroxypropyl)Methacrylamide

27. hPTH; Human Parathyroid Hormone

28. IGFs; Insulin-like Growth Factors

29. IgG; Imunoglobulin G

30. Micro-CT; Micro Computer Tomography

31. MMCCH; 4-(MaleimidoMethyl)Cyclohexane-1-Carboxyl-Hydrazide

32. MTT; 3-(4,5-Dimethylthiazol-2-yl)-2,5-diphenyltetrazolium Bromide

33. MW; Molecular Weight

34. NEM; N-ethylmaleimide

35. NHS-PEG-MAL; N-Hydroxysuccinimidyl-Polyethylene glycol-Maleimide

36. NPs; Nanoparticles

37. ODNs; Oligodexyonucleotides

38. Pamidronate; 3-Amino-1-Hydroxypropylidene-1,1-Bisphosphonate

39. PAMAM; Polyamidoamine

40. PDGFs; Platelet-Derived Growth Factors

41. PBS; Phosphate Buffer Saline

42. PEG; Poly(ehtyleneglycol)

43. PEI; Polyethylenimine

44. PLA; Poly(Lactic Acid)

45. PLGA; Poly(Lactic-co-Glycolic Acid)

46. PLL; Poly(*L*-lysine)

47. p-NPP; p-Nitrophenol Phosphate

48. p/s; Penicillin and Streptomycin

49. RES; Reticuloendothelial System

50. SD; Standard Deviation

51. SEM; Scanning Electron Microscopy

52. SHPP; N-Succinimidyl-3-(4-Hydroxy-Phenyl) Propionate

53. SMCC; Succinimidyl-4-(N-Maleimidomethyl)-Cyclohexane-1-Carboxylate

54. SPDP; N-Succinimidyl-3-(2-Pyridyldithio) Propionate

55. TCA; Trichloroacetic Acid

56. TCDG; 1,3,4,6-Tetrachloro-3α,6α-Diphenylglycouril

57. ThiolBP; 2-(3-Mercaptopropylsulfanyl)-ethyl-1,1-Bisphosphonic acid

58. TGF-β1; Transforming Growth Factor β-1

59. TNBS; 2,4,6-Trinitrobenzenesulfonic Acid (also called picrylsulfonic acid)

60. Triton X-100; Rein-pure Octylphenol-polyethyleneglycol Ether

CHAPTER I

Progress in Bone-Seeking Medicinal Agents and The Need for Drug Delivery to Bone[1]

[1]Some of the contents in this chapter have been previously published in: S. Zhang, G. Gangal, and H. Uludağ. 'Magic bullets' for bone diseases: progress in rational design of bone seeking medicinal agents. *Chem. Soc. Rev.*, 36 (2007) 507-531.

2.1 Local and Systemic Bone Regeneration

Bone tissue constitutes our bodily scaffold around which our organs are compartmentalized. It is a dynamic tissue that maintains the mineral balance in an organism, as well as providing an environment for cellular machinery involved in different physiological functions [1]. The bone tissue undergoes constant remodeling, where tightly regulated anabolic and catabolic processes enable bone adaptation during the lifespan of an organism. In addition to the cells involved in regulating bone tissue mass, i.e., bone-depositing osteoblasts, bone-resorbing osteoclasts and regulatory osteocytes, bone tissue also provides a home for a diverse array of cells involved in systemic functions. Immune regulatory cells involved in host defense, mesenchymal stem cells involved in tissue healing/repair, and hematopoietic precursors destined for systemic gas transport, are distinct cell populations residing in the bone tissue.

Bone remodeling occurs in focal and discrete packets, namely, bone remodeling unit, throughout the skeleton, and it takes a finite period of time estimated to be about 3~4 months for each packet remodeling which is geographically and chronologically separated from other packets. The sequence of this process is — osteoclastic bone resorption followed by osteoblastic bone formation to repair the defect, which formed the bone structural unit [2]. A sudden injury to the skeletal integrity can be recuperated because of the innate regeneration capability of the mineralized tissue. However, bone tissue regeneration is problematic when the skeletal challenge of bone disorders were mainly associated with the aberrant behavior of cellular components residing in the skeletal system [3], for example, the imbalance in bone remodeling favoring osteoclast-mediated bone resorption resulted in osteoporosis, and the malignant differentiated B

lymphocytes localized exclusively in bone marrow led to multiple myeloma [3]. The potential candidate for alternating cell behavior is growth factors, which are endogenous proteins present in bone matrix, regulating cellular activity and capable of stimulating new bone formation [4]. Benefiting from the recombinant DNA technology, large quantity of proteins were produced and pursued as pharmacological agents for bone regeneration.

Bone grafting was traditionally employed in local bone regeneration at specific skeletal sites where bone integrity was compromised. Though effective acceleration of bone healing and augmentation of bone mass were achieved by bone grafting [5], the disadvantages associated were donor-site morbidity and potentially limited supply of suitable bone from patients of autografts, and the possibility of diseases transmission for allografts. With the demonstration of efficacy and safety, localized delivery of growth factors is becoming increasingly prevalent in treatment of local bone defects, and recently the recombinant human bone morphogenetic protein-2 (rhBMP-2) in type I collagen sponge has been approved by U.S. FDA (Food and Drug Administration) for spinal fusion, tibial fractures, as well as dental applications in humans (InFUSE® Bone Graft) [6]. In the InFUSE® Bone Graft Kit, the concentration of rhBMP-2 is 1.5 mg/mL in the solution upon reconstitution, and then applies to the absorbable collagen sponge (ACS) for no less than 15 minutes before placement inside the Fusion device (spinal fusion) or to the defect site (tibial fractures and dental applications). The InFUSE® Bone Graft should not be used for patients: 1) with a known hypersensitivity to rhBMP-2 or bovine-derived ACS or titanium/titanium alloy; 2) with a malignant tumor in the vicinity of the surgery area; 3) with pregnancy, or 4) with an active infection at the operative site (from

www.fda.gov). Currently, growth factors that are principle regulators of the skeleton are employed in preclinical and clinical studies for local bone repair, such as BMPs [6], transforming growth factor β-1 (TGF-β1) [7], TGF-β2 [8], fibroblast growth factors (FGFs) [9], insulin-like growth factors (IGFs) [10], platelet-derived growth factors (PDGFs) [11] and the combination of growth factors for a synergistic effect [12]. By the combination of matrices or scaffolds with these bioactive growth factors, local introduction of such agents for bone repair can minimize the systemic side effects since a gradual release of growth factors from the implantation site limited critical concentration to be reached at other sites.

As a non-invasive mean for bone regeneration, systemic administration of growth factors was explored as an alternative to local surgical implantation. The typical administration routes are intravenous (IV) and subcutaneous (SC) injection. Systemic bone formation is quite beneficial for bone diseases where a generalized bone loss is associated, for example, osteoporosis. Growth factors investigated in animal models by systemic administration, such as bFGF [13] and BMP-2 [14], were shown to be capable of stimulating bone formation systemically. Recently, the human parathyroid hormone (hPTH) 1-34, has been approved for osteoporosis therapy [15]. Despite the achievement of growth factors in systemic bone regeneration, there are two critical drawbacks associated: i) the instability of proteins under *in vivo* conditions due to their short half-lives, which necessitates repeated administration of proteins to maintain a certain level of concentration at bone sites for pharmacological effects; and ii) since proteins are ubiquitous modulators of cellular activities, and they do not have the affinity specific to bone mineral; consequently, systemic administration of a given protein is likely to exhibit

non-specific distribution at extraskeletal sites, resulting in undesired side effects. These undesirable activities have been the main impediment in the clinical evaluation of systemic administration of growth factors. Therefore, drug delivery techniques that can guide the proteins specifically to bone are expected to facilitate this process.

There are two distinct delivery systems to target drugs to bone: the conjugation of "bone-seeking" moieties directly onto drugs or drug carrier and the colloidal drug delivery system where the drug is physically encapsulated into the delivery system. The former was exemplified as drug modification with tetracycline, bisphosphonates (BPs) or poly (aspartic acid) based on their high bone affinity. The latter consists of liposomes, natural or synthetic polymeric nanoparticles (NPs) and micelles, etc. This thesis will focus on protein-BPs modification and polymeric nanoparticulate drug delivery system in these two categories. With the benefit of bone-targeting delivery, protein drugs are expected to exhibit high affinity to bone, restrict its pharmacological activity at bone sites with minimal side effects at extraskeletal sites, and effectively be applied for systemic therapy by injection, or local therapy by implantation.

2.2 Drug Targeting to Skeletal Tissue

Bone tissue is distinguished from the rest of our tissues by the presence of a massive mineral phase, i.e., biological apatite. Approximately 3-4 kg of mineral mass is present in our bodies, and two-third of this mineral mass is estimated to be present in the bone tissue [16]. More than 99% of bodily calcium deposits are located in the bone. Except the dental tissue and pathological calcifications, such as kidney stones and calcified atherosclerotic plaques, no other tissue systems contain such a concentrated

mineral phase. The mineral phase in bones can serve as a unique receptacle for absorption of molecules from the systemic circulation, and molecules in circulation that display a preferential affinity to the biological apatite have the potential to seek and concentrate in the bone tissue. Several endogenous proteins exhibit a significant affinity to biological apatite, so that their interactions with mineralizing surfaces serve to facilitate or inhibit mineral formation process *in vivo*. However, the current recombinant proteins useful for medicinal purposes do not express a strong affinity to bone. Below the structure of biological apatite, as well as the structural features of proteins responsible for mineral affinity are reviewed, since these features will help to understand interactions of endogenous molecules with bone, and might ultimately be utilized as a means for bone targeting.

2.2.1 Biological Apatite of Bone

Bone mineral was recognized as an analog of naturally-occurring geological HA in the 1920s [17]. The unit cell of crystalline HA has the chemical formula of $Ca_{10}(PO_4)_6(OH)_2$ with an ideal Ca:P stoichiometric ratio of 1.67:1 **(Figure 1-1A)**. However, the analysis of bone mineral shows a Ca:P ratio ranging from 1.3:1 to 1.9:1 [18]. This deviation is mainly attributed to the carbonated groups that present distorting the crystal structure of most biological apatites [19,20]. The kinetic factors arise in solid-solution equilibrium during mineralization, which may give rise to creation of vacancies at Ca^{2+}, PO_4^{3-}, and OH^- sites, substitution of other cations (such as Mg^{2+} for Ca^{2+}), and protonation of PO_4^{3-} to substitute HPO_4^{2-} in the crystal lattice **(Figure 1-1B and 1-1C)** [21]. Moreover, the organic phosphate in the bone matrix might also partly contribute to

this deviation [18]. Two primary classes of binding sites in such a structure are provided by the superficial Ca^{2+} for anions and PO_4^{3-} for cations. Zeta (ζ) potential of synthetic HA ("HA" refers to synthetic HA herein till the end of this paragraph) surface increases from negative to positive with increasing Ca:P ratio from 1.55 to 1.70 [22]. This effect is likely due to excess Ca^{2+} neutralizing the surface anions such as CO_3^{2-} or OH^- located in the PO_4^{3-} defects. The surface charge of HA was recently probed by titration to determine the ability of the surface to adsorb H^+ (and/or OH^-) in an indifferent (non-interacting) electrolyte solution [23]. The pH at which the point of zero charge occurs for synthetic HA was found to be ~7.3. HA accumulated positive charge more readily below the point of zero charge than it accumulated negative charge above the point of zero charge, consistent with previous observations [22]. The Ca^{2+} ions in solution were readily exchanged during deprotonation of HPO_4^{2-}, indicating the dynamic nature of HA surfaces [23].

Unique insights into HA surfaces are beginning to be acquired with the Atomic Force Microscope (AFM) [24,25]. By virtue of functionalizing the AFM tip with specific chemical groups, the nature of surface charge on HA crystals could be probed in addition to the surface topography. To obtain precise and positionally-sensitive measurement of surface properties of HA, Vandiver et al. [26] measured the electrostatic forces between AFM tips derivatized with $-COO^-$ and $-NH_3^+$, and the synthetic polycrystalline HA at nm-resolution. The results revealed that HA has a net negative surface charge per unit area with an average value of -0.019C/m^2, consistent with previous measurements [27,28], at the given pH (6.0) of the system. More importantly, HA did not present a uniform charge density over its surface; the surface charges varied greatly as a function of

distance within a grain boundary; a ~7-fold variation over a distance of ~400 nm within the boundaries of a grain. This variation presumably resulted from a variation of surface PO_4^{3-} groups, and suggests a heterogeneous template for molecular binding within a single grain. The same approach (with $-COO^-$ and $-NH_3^+$ functionalized tips) was also adopted for probing protein-free apatite enamel surfaces [29]. These surfaces exhibited a net positive surface charge at the neutral pH due to Ca^{2+} rich surface layers on biologically derived crystals [30,31]. Within each crystal (approximately 90 nm in width, 50 nm in thickness and >1000 nm long,) the surfaces exhibited a 'striated' pattern of alternative surface charge, perpendicular to the crystal "*c*"-axis in the absence of any topographical changes on the surfaces. Using enamel surfaces where the endogenous proteins were extracted under neutral conditions, the striated pattern of the surface became more pronounced under low pH (4-5.5) conditions [32]; i.e., the functionalized tips exhibited significant frictional variations while sliding on the etched surface. The striated pattern was readily observed with AFM tips derivatized with $-COO^-$, but not $-NH_3^+$ derivatized tips. Therefore, it is likely that this striated pattern corresponds to the distribution of Ca^{2+} on the HA surface **(Figure 1-1D)**. Other mechanisms, such as protonation surface moieties, mobility of charges in and out of buffer environment and/or dissolution of crystal interfaces, are also likely reasons for appearance such striated patterns.

An important consideration for the design of bone-seeking agents is the relationship between the observed heterogeneity in charge distribution and molecular binding: do such variations lead to differences in quantitative and/or selective molecular binding? A well-studied molecule in this context is amelogenin, a peptide macromolecule

known to play a physiological role in mediating mineralization in enamel formation. Recent studies have indicated that the –COOH rich C-terminus of the protein binds and orients the molecule on HA surfaces [33]. The protein forms 10-20 nm aggregates under physiological conditions [34], so that its HA binding is not likely to involve specific secondary motifs. However, the aggregated protein still binds to the discrete regions on enamel surfaces consistent with the cationic banding pattern [25,35]. Even with synthetic HA, a recombinant amelogenin exhibited ~64% surface coverage, selectively interacting with some of the crystal faces, but not uniformly with all available surfaces [36]. The binding pattern is not unique to the amelogenin, and heterogeneous binding patterns were also observed by two other anionic proteins: (i) bovine serum albumin, which has no significant role in biomineralization [35], and; (ii) phosphophoryn, which is also involved in modulating biomineralization [36]. Whereas albumin desorption was complete with a high molar (500 mM) phosphate buffer, a significant fraction of amelogenin nanospheres remained bound to enamel crystals under these conditions, indicating also a variation in the strength of binding among the surface sites.

The striated pattern of biological apatite (enamel) was also revealed after investigating the surface binding of a totally synthetic macromolecule, a –COOH-terminated 7^{th}-generation polyamidoamine (PAMAM) dendrimer [37,38]. However, a –NH_2-terminated PAMAM dendrimer exhibited a diffuse, as opposed to a striated, binding pattern. Both functional groups were >95% ionized under the utilized experimental conditions (in distilled water, at pH 7.4), so that the electrostatic interactions were considered to be the main contributor to the surface binding. In fact, a -CH_3-terminated PAMAM, unlike its –COOH and -NH_2-terminated analogs, was readily removed from

the enamel surfaces (the desorption buffer: 100 mM and 200 mM phosphate buffer at pH 7.4) [37], indicating the terminal groups of the PAMAM, rather than the internal hydrophobic moieties or polar amide linkages, to be the participants in the enamel matrix interactions. These results were indicative of a diffuse pattern of anionic charges (presumably PO_4^{3-}) on enamel surfaces, unlike the 'clustered' cationic charges (primarily Ca^{2+}). Although the exact structural features responsible for these variations are not known, the substitution of H-bonding for Ca^{2+}, or variations in apatite solubility (due to carbonate or Mg^{2+} substitutions) could be likely reasons [32,39]. These results might also suggest a stronger interaction between the basic groups and the surface, whose variations in ionic composition do not necessarily influence the conducive binding of basic groups.

2.2.2 Bone Affinity of Proteins

The amphoteric nature of the bone mineral presents a complex mosaic of charges to proteins due to Ca^{2+}, PO_4^{3-}, OH^- and other ill-defined substituents formed under physiological conditions. Such ionic species provide ample sites for binding of proteins via electrostatic interactions. The affinity of specific proteins for HA is the basis for influencing the nucleation, orientation, and growth of bone apatite under physiological conditions [40], ultimately regulating mineralization to suit the needs of an organism. The interactions of proteins with HA were first probed in 1956 under chromatographic conditions by Tiselius et al. [41], revealing the electrostatic nature of the underlying interactions. Gorbunoff and Timasheff [42-44] subsequently conducted a comprehensive investigation of HA binding using an extensive set of proteins whose isoelectric points

(pI) ranged from 3.5 to 11.0. Basic proteins (high pI) were proposed to bind to HA primarily via non-specific electrostatic interactions between the $-NH_3^+$ groups and anionic moieties on the HA surface, while acidic proteins (low pI) were bound specifically by complexation of their $-C(O)-O^-$ moieties to Ca^{2+} sites on HA. A concentrated charge density was necessary for a significant protein binding, and diffuse distribution of the charged groups on a protein generally weakened the HA binding (see below). The binding mediated by the $-C(O)-O^-$ groups was proposed to be rather specific, since replacement of –C(O)-OH by –S(O)(O)-OH obliterated the binding [45]. Both the ionic composition and the pH of the immediate environment influenced the interactions of proteins with HA. For acidic proteins, HA binding is enhanced in the presence of Ca^{2+} ions in medium [46], and elution of the acidic proteins is difficult to achieve even with Ca^{2+} concentration as high as 3 M. In addition to direct effects on HA binding, Ca^{2+} in solution was proposed to facilitate HA binding by inducing an optimal configuration of protein α-helixes most suitable for HA binding [47], which was observed in circular dichroism spectra for an analog of matrix Gla protein [48]. The α-helical conformation was proposed to act as a scaffold, aligning the charged residues of proteins in a complementary pattern to the Ca^{2+} ions in a hydroxyapatite crystal lattice. The PO_4^{3-} in solution suppresses the HA binding of acidic proteins, possibly due to competitive binding of the phosphate ions with the Ca^{2+} on HA. On the other hand, the basic proteins are eluted by cationic ions Na^+, K^+, and especially Mg^{2+} and Ca^{2+} [49]. Acidic proteins generally display increased HA binding with decreasing pH. Since protein –C(O)-OH groups will be less ionized at lower pH, and, hence, display a lower propensity towards cationic moieties in HA, this pH effect was likely due to increased hydrogen bonding

interaction between acidic proteins and HA surface and/or an overall decrease in the collective surface charge of HA (i.e., protonation of PO_4^{3-} to HPO_4^{2-} at lower pH) [50]. Also the possible change in the conformation of the proteins (i.e., more favorable binding configuration at lower pH) [51,52], a stronger HA interactions mediated by the protein – NH_3^+ groups (i.e., due to higher extent of amine protonation at lower pH) are all likely factors contributing to enhanced protein binding at lower pH.

An active area of mineralization research has focused on elucidating protein structural motifs responsible for HA binding, with the expectation that optimal distribution of "point" interactions imparts a unique, and stronger mineral affinity as compared to simple additive effect of the interacting components [53-58]. Consecutive aspartic acid residues found in osteopontin, and consecutive glutamic acid residues found in osteonectin and bone sialoprotein are two specific protein motifs shown to concentrate anionic groups for a superior mineral affinity [53]. A minimum length of six anionic residues was necessary, and poly(aspartic acid) was shown to be superior for HA binding [59]. This simple sequence of consecutive amino acids have been utilized to facilitate binding of RGD-peptides (arginine-glycine-aspartic acid peptides involved in cell-surface integrin binding) to HA [60,61], as well as in drug delivery efforts to design model drugs with high affinity to bone mineral [62].

In the absence of consecutive aspartic/glutamic acid residues, post-translational modification of proteins with acidic moieties provides an alternative means for imparting mineral affinity. Phosphorylation of serine/tyrosine imparts a high affinity to proteins by virtue of phosphate binding to the mineral, analogous to pyrophosphate binding to HA. Phosphophoryn binding to bone is a well-known example where dephosphorylation of

specific protein residues reduces its mineral binding [63]. Partial dephosphorylation of bovine osteopontin with alkaline phosphatase also reduced its ability to bind HA [64]. Phosphorylated sequences may act in concert with other acidic residues for HA binding; using several isoforms of salivary statherins, the N-terminal sequence Asp-pSer-pSer-Glu-Glu [65-67] was found to be responsible for the HA affinity. The phosphorylated serines in this case provided the appropriate high-charge density in the absence of long acidic amino acid repeats, and induced a helical conformation conducive for HA binding. Several uncharged polar residues (e.g., glutamine, tyrosine and threonine) adjacent to the Asp-pSer-pSer-Glu-Glu sequence additionally participated in H-bonding interactions with the HA surface. γ-Carboxylation of glutamic acid residues also enhances mineral affinity. In a recent model of HA binding [68], osteocalcin was found to display 3 α-helical regions, where 3 glutamic acid residues in helix α-1 were γ-carboxylated to create an extensively anionic surface, and in conjunction with an adjacent aspartic acid, coordinated 5 Ca^{2+} ions on HA surfaces. The spatial arrangement of the Ca^{2+} binding moieties on osteocalcin was well-aligned with the Ca^{2+} arrangement in a synthetic analogue of HA (note that exact arrangement of Ca^{2+} ions in bone mineral might be significantly different from this HA model). Other post-translation modifications, such as carbohydrate moieties, sulfation and sialic acid addition, may also contribute to increased bone binding (as observed after comparison of native bone sialoprotein, and unmodified bone sialoprotein expressed in *E-coli* without post-translational modification [52,69]). Gericke et al. [70] suggested that osteopontin, whose binding propensity was usually ascribed to aspartic acid-rich sequences, incorporates phosphorylated sequences that caused alternations in protein conformation (detected by Fourier Transform-Infrared

spectroscopy, FT-IR) to influence the interaction of osteopontin with HA. Finally, transglutaminase-sensitive sequences present in osteopontin can be crosslinked to form an osteopontin-network, and provide another avenue for post-translational control of mineral affinity [71]. Upon polymerization, a conformational change in osteopontin structure was observed with circular dichroism spectroscopy, suggesting a more-ordered structure for the osteopontin polymer as compared to the monomeric form of the protein [71]. A more ordered structure was more likely to provide the HA binding motif by the spatial arrangement well-aligned with the HA lattice. It was suggested that the initiation of HA crystallization required protein aggregates rather than the single osteopontin monomers [72].

The structural studies in recent years have clearly indicated the availability of several distinct acidic protein motifs for HA binding. It is likely that the strength and the specific protein binding sites on HA will depend on the details of the interacting motif. No information is available about the differences in the binding mode of the different motifs on biological apatite. A recent study, which utilized octacalcium phosphate as a model matrix, indicated poly(aspartic acid) interacted preferentially with Ca^{2+} ions exposed on the hydrated {100} surface parallel to the *c*-axis of the crystals [73]. The phosphorylated proteins, on the other hand, interacted specially with the apatite-like motifs on the {010} surface through occupation of the exact lattice site of the crystal phosphate groups. The availability of both motifs in a single protein, such as osteopontin, is likely to enhance the affinity due to additive binding of the two motifs to different sites on apatite.

Relatively little is known about the structural motifs responsible for HA binding of basic proteins. It is generally accepted that the binding arises due to interactions between the protein $-NH_3^+$ and the anionic moieties of HA. Using site-directed mutagenesis of lysozyme (pI~11), where individual amino acids were replaced with alanine, Lys-1, Lys-13, Arg-14 and Arg-10 residues were found critical for HA contact, which were all located on the protein surface away from the active site of the enzyme [74,75]. This preliminary study also suggested that cationic charges on a protein may form 'clustered' patterns on a protein site, possibly enhancing the strength of HA interactions reminiscent of anionic protein motifs.

Unfortunately, these mineral-interacting proteins do not have a medicinal value at the present time. On the other hand, the current recombinant proteins useful for medicinal purposes do not express a strong affinity to bone due to lack of structural motifs or lack of post-translational modification. One then is faced with engineering the proteins to impart a mineral affinity to make them useful in bone diseases. This is most effectively achieved with BP substitution.

2.3 Progress in Bone-Seeking Medicinal Agents

2.3.1 Non-BP Medicinal Agents for Bone Targeting

Several molecules demonstrated bone affinity that can be used as osteotropic moieties [76]. The well-known antibacterial agent tetracycline exhibits a strong affinity to bone. As one of the earliest studies on tetracycline conjugation with drugs, Pierce et al. reported the delivery of a carbonic anhydrase inhibitor, acetazolamide [77]. *In vitro* results showed high HA affinity of the conjugate, and the drug was able to release from

the conjugate after hydrolysis with some retention of its activity. Later, β-estradiol-3-benzoate [78], 3-Estrone [79], and bone growth factor TGF-β [80] were successively conjugated to tetracycline for bone-targeting delivery. Another moiety demonstrated bone affinity was 4-carboxy-3-hydroxy-1,2-pyrazole, which was examined in a study conducted by Willson et al. for the enhancement of estrogen's affinity to HA [81]. Due to the complicated chemical structure and poor stability during chemical modification of tetracyclines, their further utilization as bone-targeting moiety was hindered. As an alternative, BPs, with exceptional osteotropicity, are very attractive for bone-targeting delivery because of their suitability for chemical modification and "universal" carrier property – their ability to load almost any drug (This will be discussed in details later). Recently, the mineral-binding protein motifs provide a guide to develop more physiological molecules for bone targeting. Poly(aspartic acid) and poly(glutamic acid) are prototypical molecules where the mineral affinity is afforded by totally metabolizable and endogenous moieties. *In vivo* targeting for small molecules, fluorescein isothiocyanate (FITC) [62] and 17β-estradiol [82], and recently a polymeric ligand [45], was successfully demonstrated by using poly(amino acids). γ-Carboxyglutamic acid in an α-helix conformation [47], phosphorylated serines/tyrosines [83,84], and lysine/arginine are other elements found in protein motifs that may be assembled into bone-seeking agents [74]. Their potential to be physiologically metabolized with no trace of targeting moiety left behind makes them worthwhile to explore.

2.3.2 Structural Basis of Bisphosphonate Affinity to Bone

The exceptional selectivity of BPs to bone mineral rather than other tissues lacking a mineral phase is the basis for their value in clinical practice. Due to the affinity of spatially-optimized, deprotonated $-O^-$ to the bone apatite, the bisphosphonic acid form of the compound is the bone-seeking entity. Monophosphonates, phosphonate esters, chemically-modified phosphonate groups (e.g., methylated phosphonates, phosphono-phosphinates or bisphosphinates), or compounds with P-N-P and P-C-C-P backbones all display reduced affinity to mineral to make them not useful for bone therapy [85]. Though non-geminal diphosphonates are biologically inactive as anti-calcification agents, introduction of a keto group at the α-carbon makes bisacryl-phosphonates active as anti-resorptive agents with lower potency than the BPs [86] (**Figure 1-2**). The pharmacological activity of BPs varies a great deal from compound to compound [87], in line with variations in the R_1 and R_2 substituents shown in **Figure 1-3**. Whereas an increased affinity to HA is desirable to further increase bone concentrations of active agents, it is important for the BP levels not to reach inhibitory concentrations on mineralization of osteoid in bones [88].

There are two main considerations in the design of BP-based drugs: (1) the relative affinity for bone mineral, and (2) the inhibitory effect on cellular mechanisms responsible for bone resorption. These aspects are fulfilled by different parts of the BP molecules and early studies suggested they did not necessarily rely on each other. The P-C-P linkage along with the 3-D configuration of the R_2 substituent determines the interaction with specific cellular targets essential for the pharmacological activity. The $_2$(HO)-(O)P-C-P(O)-$(OH)_2$ moiety, on the other hand, is responsible for chelation of Ca^{2+}

in HA; the bite distance of deprotonated oxygens, $-O^{-}\cdots{}^{-}O-$, between the two phosphonates is 2.9-3.1 Å, and this separation is within the range found for the oxygens in HA [89,90]. This is presumably the ideal distance for the chelation of Ca^{2+} ions in HA. The affinity of BPs for bone mineral was proposed to bear no relationship to their marked differences in antiresorptive potencies [91]. BPs with a –OH group in the R_1 position have increased affinity for bone mineral (so called 'bone-hook' effect, as suggested by Russell et al. [92]) and the R_2 substituent was believed to play a nominal role in the bone affinity; BPs with variable R_2 substituents but a common –OH in the R_1 position bound with equal affinity to bone mineral; For example, olpadronate and etidronate (see **Figure 1-3**), two BPs with considerably different R_2 substituents, could displace [^{14}C]-3-dimethylamino-1-hydroxypropylidene-1,1-bisphopshonate (dimethyl-pamidronate) from mouse fetal bones with equal potency, but clodronate, which lacked the –OH moiety on the R_1 position, was ~10 times less potent in such a displacement [91]. The differences in binding can be explained with the mode of binding [88]; i.e., **bidentate** binding, involving two de-protonated $-O^{-}$ from each phosphonate moiety binding to HA Ca^{2+} (as in the case of clodronate) vs. **tridentate** binding involving participation of the –OH at the R_1 position. Although tridentate binding is generally accepted, the amino-BPs pamidronate and alendronate contain -OH groups in *gauche* configuration, which enable formation of an intramolecular N-H···O (hydroxyl) H-bond and impairs tridentate binding under some conditions [89,90]. Tridentate binding can also be obtained with an $-NH_2$ group in the R_1 position [93,94]. The amino-substituted BPs and their -OH analogs (etidronate, pamidronate and olpadronate, in this case) bound with similar affinity to

mouse bones *in vitro*, and inhibited the growth of calcium oxalate crystals to the same extent [94].

Recent studies, however, indicated that R_2 substituent may also influence the HA affinity of BPs [95,96]. Nancollas et al. compared the binding affinities of several BPs to HA, all of which consisted of the same R_1 substituent (–OH), but differing R_2 substituents [95]. Different HA binding affinities were observed among the BPs, with a decreasing rank order of zoledronate > alendronate > ibandronate $\approx$ risedronate > etidronate. The corresponding affinity constant *K*, which was calculated from kinetics of HA crystal growth, were 3.47, 2.94, 2.36, 2.19, and 1.19 x 10^6 M^{-1}, respectively. These results were attributed to the differences in the protonation of R_2 substituent, dictated by the pK_a of the ionizable moieties. In addition, measurement of ζ-potential of the BP-treated HA suggested that changes in the overall charge of the crystal surface, which was best explained by molecular charges on the R_2 substituent. The latter affected HA binding of additional BPs by enhancing or suppressing further binding on the surface. Under physiological conditions, higher binding was obtained when the pK_a of the R_2 substituent was $\geq$7. Consistent with the HA growth studies, the BP affinity to HA was determined by a direct method under chromatographic conditions; a decreasing order of HA affinity was obtained with zoledronate, risedronate and an risedronate analogue in which one of the phosphonate groups was replaced by a -C(O)-OH. Moreover, a recent computational model (3D) demonstrated the differences in HA affinities of different BPs, with the consideration of the interaction of the N side chain conformations with the [001] surface of HA [97]. This model also showed similar rank order in HA affinity as the above studies (note that ibandronate was not included in the simulation study). Along the same

lines, a sulfate-bearing BP, whose R_1 and R_2 substituents were -H and $-CH_2-SO_3H$, respectively, was compared *in vivo* to the –OH-bearing etidronate's capacity to target to bone [98]. Equivalent or better bone targeting was achieved (at 1 hr and at 24 hrs, respectively) with this non-hydroxyl bearing BP as compared to etidronate. Therefore, increasing evidence is accumulating to confirm the subtle contribution of R_2 substituent to the mineral affinity, which could be utilized to further enhance the ability of BPs to seek bone.

Finally, the overall hydrophobicity of BPs has been shown to influence the bone targeting ability [99]. This observation was derived from studies where BP conjugates from a diverse group of compounds and drugs (e.g., 17β-estradiol, diclofenac, and benzene) were constructed. As expected, the hydrophobicity of the conjugates was significantly different among BPs with different side-group (R_2 substituent being the major variable), based on the calculated octanol/water partition coefficient (calculated log P) of the acid-form of the compounds. The use of the acid form is a simplification, but it is justifiable considering that the exact nature of the BP complexes with metal ions such as Ca^{2+} and Na^+ *in vivo* is difficult to predict. The calculated log P of the acid form will presumably be closely related to the calculated log P of the ion-chelated form. After systemic administration, an inverse correlation was obtained between the calculated log P and the ability of the compounds to deposit to bones, which ranged from 6 to 70% of the administered dose. All compounds used in that study contained a hydrogen on the α-carbon, and lacked either a –OH or $–NH_2$ at this position. Using such a uniform population of BP conjugates has likely contributed to the relatively good correlation between the calculated log P and the skeletal deposition. The authors expected the

hydrophobicity of BPs to determine the propensity of the BP-metal chelates formed between the endogenous ions in circulation and exogenous BPs through the interaction between negatively charged phosphate groups on BPs and positively charged metal ions to precipitate in systemic circulation; i.e. chelates with more hydrophobic character will presumably be removed faster by the macrophages. These results highlight the need to use smaller, hydrophilic BPs as the basis of bone-specific carriers.

2.3.3 Functional Bisphosphonates for Protein Targeting to Bone

The exceptional affinity of BPs to HA has previously been used to transport several classes of therapeutic agents to bone tissue. These included: (i) anti-neoplastic agents intended to control cancerous cell growth, (ii) anti-bacterial agents to inhibit bacterial colonization, and (iii) anti-osteoporosis agents acting to protect against the excessive bone loss with advancing age. In addition, BPs are beginning to be utilized as the building blocks of generic carriers that can transport a spectrum of molecules to bone, rather than linking them directly to a given molecule for its delivery to bone.

To impart a mineral affinity to a protein, one needs to couple the BPs to proteins in aqueous media. Unlike the majority of BP constructs summarized here and in the previous reviews [3,100,101], this consideration rules out the possibility of using BP esters that are not soluble under aqueous conditions, and whose de-esterification after protein coupling is likely to abolish the protein activity. High-temperature conditions, pH extremes, and exposure to highly reactive, non-specific reagents (e.g., free radicals) are not possible if one wishes to retain the activity of the proteins. Water-soluble BPs with readily-reactive functional groups need to be employed for this purpose. Three most

common moieties for convenient protein chemistry are $-NH_2$, -SH, and –C(O)OH groups; hence, BPs with these groups will be ideal for chemical schemes designed for protein substitution. The current schemes for the synthesis of such BPs were previously provided [3], and below the strategies for modifying such groups for protein attachment were summarized.

2.3.3.1 Amino-Bisphosphonates The ethyl/methyl ester of 1-aminomethylene-1,1-bisphosphonate has been the starting compound for synthesis of several BP conjugates of small molecular drugs. 2-iminothiolane derivatization of the $-NH_2$ group was readily achieved to provide a free -SH group (**Scheme 1-1**), which was used for further conjugation with proteins [102]. The heterofunctional crosslinkers, such as *N*-succinimidyl-3-2(pyridyldithiopropionate) (SPDP) [103] and *N*-succinimidyl-4-(*N*-maleimido-methyl)cyclohexane-1-carboxylate (SMCC) [104], were capable of reacting with the introduced -SH group to give an NHS ester of the BP with labile disulfide (–S–S–) linkage or stable thioether (–S–C–) linkage, respectively (**Scheme 1-1**). In both cases, the ε–NH_2 of protein lysines readily reacted with the NHS ester to link the BPs to the proteins via relatively-stable amide linkages. 4-(Maleimidomethyl)-cyclohexane-1-carboxyl-hydrazide (MMCCH) has been also used in this approach to link the thiolated 1-aminomethylene-1,1-bisphosphonate to the protein carbohydrate groups [104]. In this case, the carbohydrate moieties were first oxidized with $NaIO_4$ to convert the vicinal –OH groups into –C(O) –H groups, which were reactive with the hydrazide moiety of MMCCH [104]. Modifying carbohydrate moieties could be preferable since they are not usually an integral part of the protein pharmacophore, unlike the amino acids in the

peptide core. In the absence of carbohydrate residues, which is the case for *E-coli*-derived recombinant proteins, conjugating BPs to proteins via cleavable –S–S– linkages offers the obvious advantage of slowly releasing the protein from the conjugated BP to exert its pharmacological activity freely.

It was reported that 3-amino-1-hydroxypropylidene-1,1-bisphosphonate (pamidronate) were utilized to prepare a near-infrared emitting diagnostic after reaction with an NHS-ester of a fluorescent dye [105]. Similarly, 4-aminobutylene-1,1-bisphosphonate (alendronate) was reacted with an NHS ester of poly(ethylene glycol) before conjugation to a polymeric carrier [45]. As an alternative to NHS esters, 4-aminobutylene-1,1-bisphosphonate was capable of coupling to a tetrafluorophenol ester of a short peptide, triglycine, leading to a BP-$(glycine)_3$ conjugate with an amide linkage [105]. The feasibility of $-NH_2$ coupling to aldehyde groups have been also reported [106].

2.3.3.2 Thiol-Bisphosphonates To obviate the need for thiolating amino-BPs, a thiol-containing BP, 2-(3-mercapto-propylsulfanyl)-ethyl-1,1-bisphosphonic acid [103] was recently utilized for protein coupling. It was shown to be effective in imparting a mineral affinity to proteins after SMCC and SPDP mediated couplings (**Scheme 1-2**). Under equivalent reaction conditions, a similar extent of BP substitution could be obtained on the model protein albumin when either thiolated 1-aminomethylene-1,1-bisphosphonate or 2-(3-mercapto-propylsulfanyl)-ethyl-1,1-bisphosphonic acid were utilized [103], suggesting that the reactivity of the –SH group being the primary determinant of coupling efficiency. Unlike the NHS-mediated reactions with amino-BPs, which require a relatively high pH, the –SH group of the BP could be derivatized within a broader pH

range; coupling in the pH range of 4.5 to 8 was successful. This could be advantageous to accommodate proteins with minimal solubility or undergoing denaturation at the higher pH.

The thiol groups of BPs are also reactive with epoxides under neutral pH conditions (**Scheme 1-2**) [107]. An amine group at the β-position was found necessary for this reaction, since a –SH linked to the α-carbon of BPs with an aliphatic chain was unreactive with the epoxide moieties. The conjugates will yield a thioether in the tether, which is expected to be more stable than the disulfide linkages. This chemistry was successfully used to graft thiol-BPs onto biological matrices (i.e., heart valves, [107]), and it should be straight-forward to adopt it with epoxide-containing linkers for modification of soluble proteins.

2.3.3.3 Carboxyl-Bisphosphonates The length of the tether between protein lysine groups and the substituted BPs was found to influence the imparted mineral affinity [108]; a shorter tether length gave a higher mineral affinity as compared to longer tether lengths. BPs with –C(O)-OH groups could be utilized to minimize tether length, since this group affords activation with carbodiimides for coupling to protein amines with "zero" tether length. Two –C(O)-OH-bearing BPs with dendritic structures were recently reported [109,110]. The compounds incorporated two (diBPs) and four bisphosphonic acids (tetraBPs) with a single –COOH moiety, as shown in **Figure 1-4**. In addition to minimal tether lengths, the compounds were designed to 'load' multiple copies of BPs per protein substitution site, so that a higher substitution efficiency could be achieved with reduced extent of protein modifications. This is an important consideration in order to minimize

any changes in the protein activity as a result of BP substitution. It was feasible to attach a maximum of 3-4 diBPs molecules per albumin (~66 kD), 6-7 diBPs molecules per IgG (~150 kD), and 3-4 tetraBPs molecules per albumin after activation with water-soluble 1-ethyl-3-(3-dimethylamino-propyl)-carbodiimide/N-hydroxy-succinimide (EDC/NHS). These levels of substitutions were generally lower than the SMCC- and SPDP-mediated coupling of conventional BPs, where a maximum of 15-20 BPs could be attached per albumin or IgG. The lower extent of conjugation efficiency for the dendritic BPs is possibly due to the steric hindrance of the substituted ligands, but the obtained substitution efficiencies were sufficient for bone targeting.

2.4 Colloidal Drug Delivery Systems Targeting to Bone

An exciting area beginning to be explored is the development of bone-specific carriers that complexes the medicinal agent without the need for direct modification of the agent *per se*. Colloidal drug delivery systems (CDDS) provide a promising approach in this regard. CDDS consists of liposomes, nanoparticles, dendrimers, emulsions and micelles, with the length scales below a micron [111]. CDDS offers protection of drugs against chemical and enzymatic degradation when delivered *in vivo* and optimizes the release profile of the loaded drug in a controlled manner. The flexibility in tailoring the internal and surface structure of CDDS has led to the adoption of colloidal drug carriers as the platform for a wide range of current therapeutics, as a mean to achieve new delivery modes and improve their therapeutic potentials.

To attain the goal of bone-specific CDDS, it is important to note that bones possess a membrane consisting of lining cells, which function as a marrow-blood barrier;

the accessibility of exogenous large substances to the bone surface is extremely limited [112]. Thus, drug carriers prefer to be small size; complexes with large diameter are not suitable. This is not likely to be a critical issue when NPs are utilized for local delivery of proteins after implantation, but it will be a significant issue when NPs are injected systemically. Since HA is the most practical template for bone-targeting, CDDS should exhibit high affinity to HA in systemic delivery and prolong the retention of the loaded drug at bone defect site to maximize the pharmacological effect. Furthermore, it is imperative that the CDDS composition should be biocompatible and biodegradable, to minimize the interference with normal cellular activities by excessive inflammatory reactions, and the possible adverse effects of residual carriers influence on the mechanical integrity of repaired bone [113]. Given the many types of CDDS, this section will focus on the local and systemic delivery of growth factors by polymeric NPs for bone regeneration.

Polymeric NPs delivery system has been fabricated from polyesters (e.g. poly(lactic acid) (PLA) and poly(lactic-co-glycolic acid) (PLGA)), proteins (e.g. albumin, gelatin and protamine), polysaccharide (chitosan), polycyanoacrylate (e.g. poly(butylcyanoacrylate)), lipids (e.g. trimyristin and glyceryl behenate) and polyelectrolyte (e.g. polyethylenimine) [114]. Among them, the conventional synthetic polyester, with PLA and PLGA as representatives, have been extensively studied due to their low toxicity, well-understood degradation pattern and established processing methodologies, which ensures better prediction and control the system behavior [115]. Protein NPs, made from natural polymers, possess excellent biocompatibility and biodegradability in physiological system. Albumin NPs have been extensively studied as

drug delivery systems, and Abraxane® as a carrier of anticancer drug paclitaxel has been accepted in human use [116]. One concern about protein NPs is the immunogenic reactions and disease transmission, but proteins produced from recombinant technology or plant origin should overcome this concern [6]. The abundant functional groups (amines, carboxylic groups and thiol groups) on proteins provide plentiful opportunities, including covalent or non-covalent interactions with ligands, to tailor the protein carrier for the appropriate targeting of NPs delivery system. Solid lipid NPs is another attractive approach with their good tolerability and biodegradation, but their lipophilic nature might pose an impediment for the encapsulation of hydrophilic peptides, and the fabrication procedure with high pressure could possibly induce protein degradation [117]. Except the abovementioned polymeric NPs, other materials were less popular in clinical development due to their less understood biologic fate after administration [115].

In current preclinical and clinical trials, the primary focus is local delivery of growth factors for bone repair [113]. The prolonged retention of bioactive growth factor at the bone repair site can maintain the concentration of these factors to allow the migration of responsive cells to the area for proliferation and differentiation. The simplest delivery system for growth factor is to incorporate the growth factor directly into the carrier, for example, the impregnation of BMP solutions with collagen sponge is a commonly used technique to fabricate BMP-2 delivery devices [118]. However, the passive adsorption might induce the conformational change of the proteins and could not afford precisely control over the release of protein [113]. One possible solution is the utilization of growth factor-binding heparin in combination with the carrier, so that the growth factors, such as bFGF, BMP-2, TGF-β, could be bound specially to the carrier for

a more sustained release [119]. This approach limited to the special binding property of the growth factors. Another alternative and more attractive approach is to incorporate the growth factor containing-NPs in matrices or scaffolds, so that the release of growth factor can be controlled in a more desirable way, since the NPs surface can be engineered appropriately for the preferred release pattern [120,121]. Recent studies provided various engineering approach to modify and control the growth factor release from the carrier. Wei et al. investigated BMP-7 encapsulated into PLGA NPs which were then post-seeded into PLLA scaffold in rat ectopic model [122]. The *in vitro* release kinetics indicated the NPs-containing scaffold could provide a sustained release of BMP-7 for up to 6 weeks, and the release profile was controlled by the PLGA molecular weight and composition. This NP-containing scaffold induced significant bone formation while passive adsorption of BMP-7 into PLLA scaffold failed to generate bone at 6 weeks. The suggested reason was the BMP-7 nanosphere-scaffold delivery system released and localized BMP-7 for a desired duration at the implantation site, while simple adsorption of BMP-7 into the scaffold likely gave a bolus or pulse release of BMP-7 with substantial loss of bioactivity, leading to the failure of bone formation. Another study conducted by Park et al. investigated the controlled release of growth factor from TGF-β3-containtaing heparin/poly(*L*-lysine) NPs immobilized on PLGA microsphere matrix [123]. The NPs and matrix combination provided sustained delivery of TGF-β 3, and were able to promote neocartilage formation after 4-week cultivation with mesenchymal stem cells *in vitro*. By using NPs for BMP-2 delivery, Chung et al. studied the BMP-2 loaded heparin-functionalized PLGA NPs in fibrin hydrogel on the rat calvarial critical size defect model [124]. Heparin was entrapped onto the surface of PLGA NPs with the purpose of specific

complexation with BMP-2, and then BMP-2 loaded NPs were incorporated into fibrin gel. Significantly higher bone formation was found in the BMP-2 loaded NP-fibrin gel complex, compared to the BMP-2 loaded fibrin gel without functionalized NPs at 4 weeks, which suggested that a more controlled release of BMP-2 was achieved in the former carrier. Encapsulation of growth factors into NP then combined with different matrix or scaffold as hybrid carrier for local bone defect replacement has been demonstrated to be a successful strategy to achieve prolonged release of bioactive growth factors. The release of protein from the carrier can be tailored by the modification of NPs. This is a versatile approach that can be expanded to many bioactive molecules. Since size of particles is not a critical issue in local delivery of growth factors, massive studies were also performed by encapsulating growth factors into microspheres for an prolonged retention time and enhanced pharmacological effect [7,125-127].

Unlike growth factor delivery by NPs for local therapy, size and surface charge of NPs are the main properties that can influence the clearance and biodistribution of NP carriers upon systemic administration [128]. The smaller size of particles seems to be an advantage since smaller NPs were removed more slowly from blood circulation than larger ones [129] , and the longer circulating carriers have a better chance to reach their target and lead to a therapeutic effect. Studies showed a size-dependent activation of the complement system for particles sizes below 1 μm [130]. It was also reported that no enhancement of phagocytic uptake was recorded at particle sizes below 200 nm [128]. Yet, the particles with extremely small size (<<100nm) was reported to be able to cross the fenestration in the hepatic sinusoidal endothelium, leading to a hepatic accumulation, although this was associated with the deformity of particles such as liposome particles

[131]. Moghimi et al suggested the size of solid NPs should not exceed 200 nm for effective long-circulating time in *vivo* [128]. With regard to bone tissue, due to a membrane of lining cells forming a marrow-blood barrier [112], not all NPs localized to bone are accessible to bone-resident cells. One study showed that NPs < 150 nm exhibited an increased localization in bone marrow, while NPs ~ 250 nm were mostly sequestered in the spleen and liver, presumably by the selective filtration in these organs [132]. Surface charge is another factor that plays an important role in determining the *in vivo* fate of NPs. Ionic interaction was considered as one of the principal driving forces for protein adsorption, and subsequently activated the opsonization process with promoted particle recognition and uptake [133]. Though this process can be reduced by smaller NPs size, neutral and hydrophilic NPs surface possesses a much lower opsonization rate than the charged and hydrophobic NPs [134]. Another alternative to reduce the opsonization and phagocytosis of NPs is surface-modified NPs with polyethylene glycol (PEG), an established method to reduce non-specific protein adsorption. Some factors, including PEG density, the spatial conformation and PEG chain flexibility should be in consideration for this approach [129].

So far, few studies were performed on systemic delivery of growth factors based on NP system for bone-targeting. Recently, two NP delivery systems with the potential to target to bone were reported: liposome/PEG/BPs NPs [135] and PLGA-PEG/PLGA-BPs NPs [136]. The former composed of liposomes as drug reservoir and cholesteryl-trisoxyethylene-bisphosphonic acid (CHOL-TOE-BP) serving as bone-targeting ligand, was prepared by lipid film extrusion method. The average size of NPs was between 100 and 135 nm with a polydispersity index < 0.1. The zeta potential was negative, and

increased as the BP content increased. *In vitro* binding assay showed the NPs possessed a high affinity to HA (~100%). The latter, PLGA-PEG/PLGA-BPs NP system, was prepared from the dialysis method, with a hydrophobic drug estrogen encapsulated and alendronate as the targeting moiety. The NP possessed a size of ~50 nm, but no report on zeta potential values. This NP system demonstrated an in vitro HA affinity (~ 50% to 80%), and the observed binding was increased as PLGA-BP content increased, but the binding of unfunctionalized NPs were not reported. *In vivo* evaluations of the pharmacokinetics and tissue distribution of these two NP systems still need to be probed for their bone-targeting capability. Nevertheless, these studies provided useful information in the design of bone-targeting delivery based on NPs, and with the appearance of more bone-binding ligands, such as N-(2-hydroxypropyl)methacrylamide (HPMA)-alendronate copolymer [137] and poly(N-acryl pamidronate-*co*-N-isopropylacrylamide [138], as well as cationic polymer PEI and PLL [139], more related investigations will be inspired in the near future. Such a developed NP delivery system for growth factor will be truly "generic", in that a design system should be able to deliver a range of therapeutic agents rather than molecule-specific.

SCHEMES

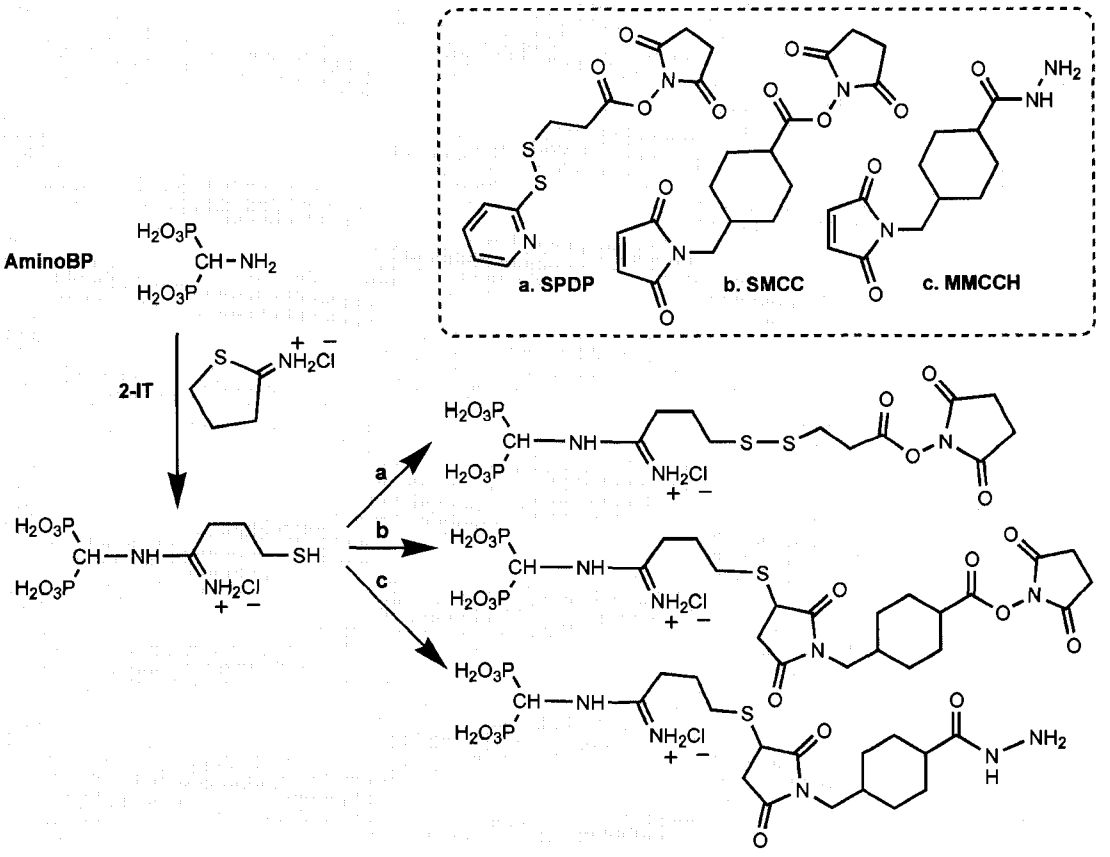

Scheme 1-1. Different linkers for aminoBP coupling with protein.

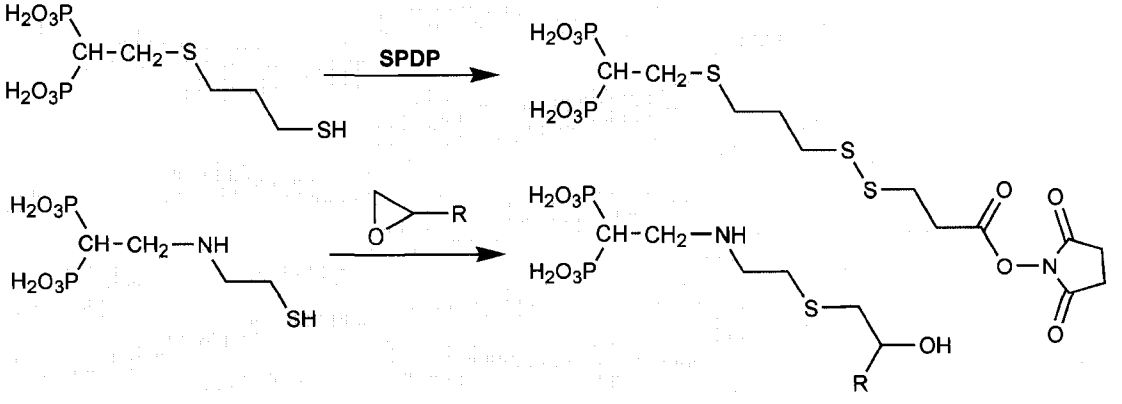

Scheme 1-2. Thiol-containing BP reaction with SPDP and epoxides.

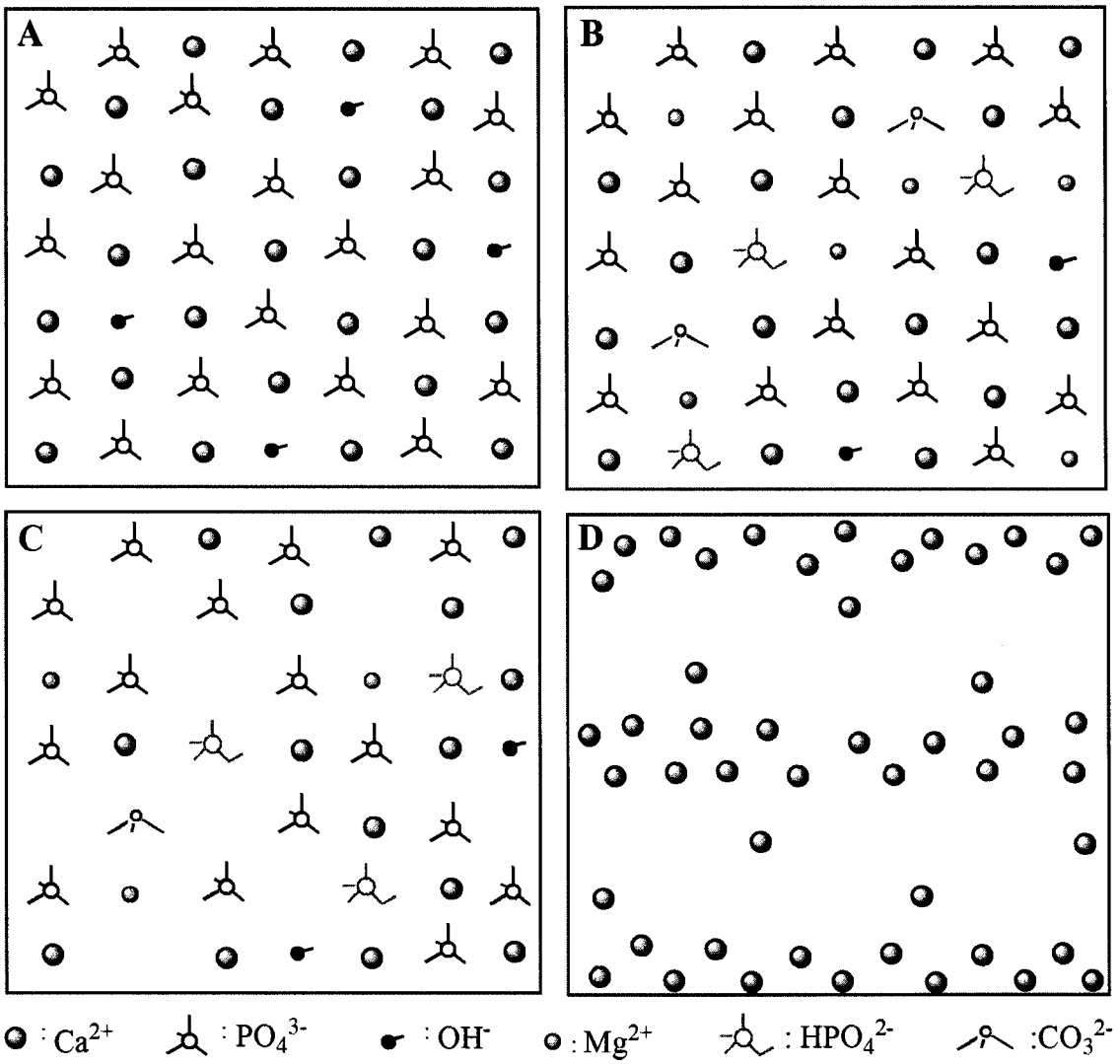

Figure 1-1. Schematic representation of the biological apatite. **A**. The synthetic hydroxyapatite (HA; $Ca_{10}(PO_4)_6(OH)_2$) is represented by the stoichiometric ratio of Ca^{2+}, PO_4^{3-} and OH- ions. **B**. Substitution of other cations (e.g., Mg^{2+}) and anions (e.g., HPO_4^{2-}) are typical for the physiological apatite. **C**. Non-equilibrium formation conditions also create defects in the apatite structure, leading to ionic gaps in the crystal structure. **D**. Recent investigations of physiological apatite crystals have suggested charge densities organized in larger scales (>10 nm) in the form of 'bands' (as revealed by probing surfaces with charged atomic force microscope tips).

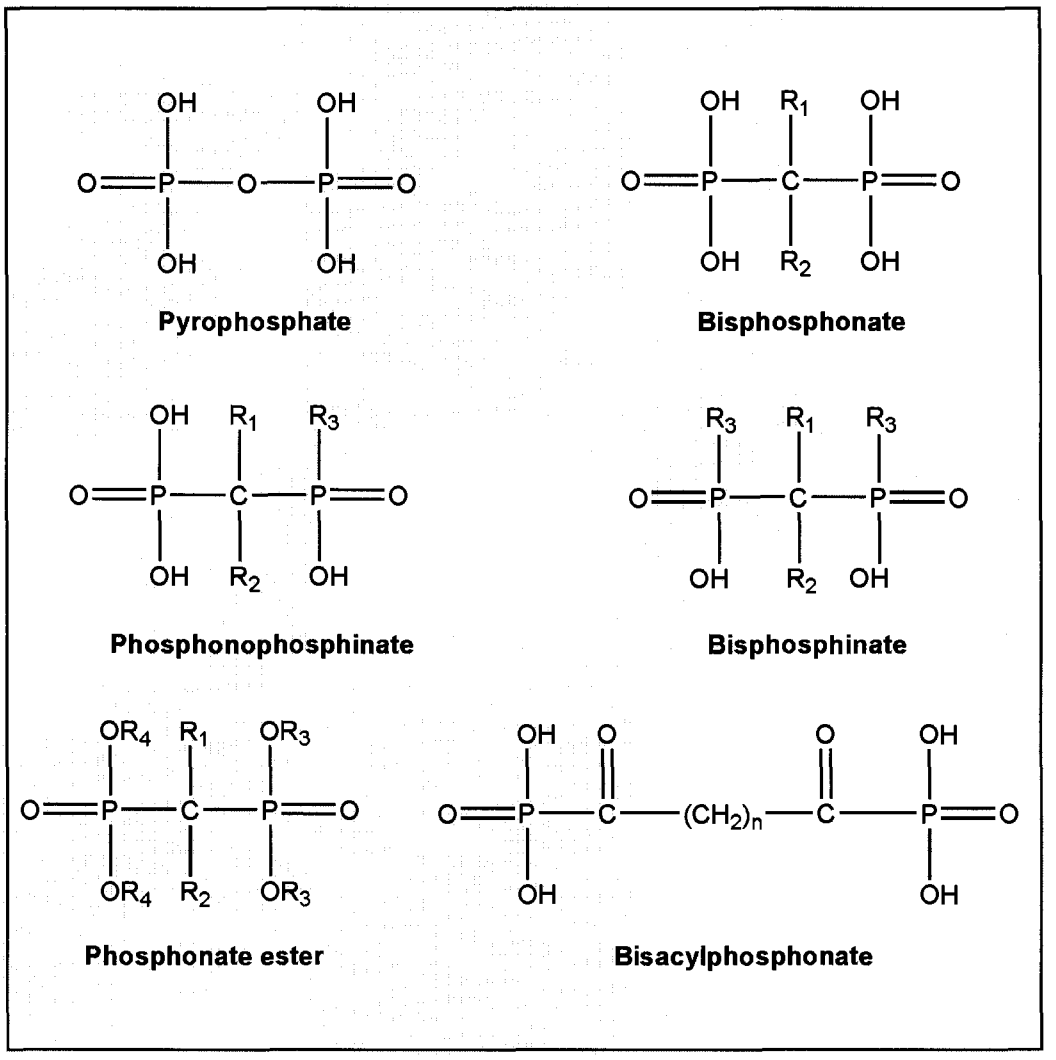

Figure 1-2. Structure of the endogenous pyrophosphonate, and its synthetic analogue, bisphosphonate (BP), which exhibit a strong bone affinity. The geminal (α) carbon in BPs typically contains two separate substituents, R_1 and R_2, which may significantly affect both the mineral affinity and the pharmacological activity. Other BP-related compounds are also shown, but the latter compounds either lack or exhibit a reduced affinity to the bone apatite.

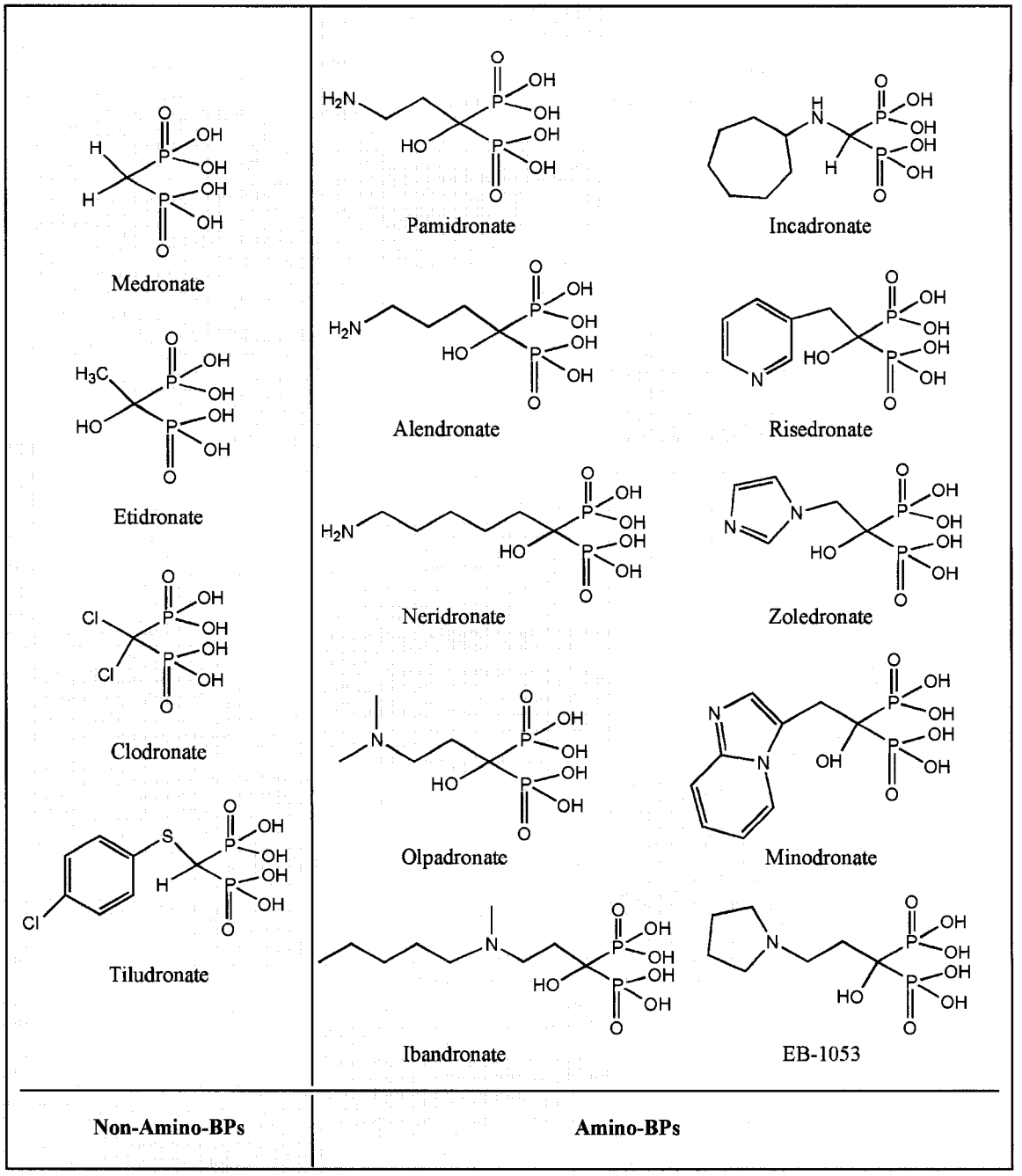

Figure 1-3. Examples of BP class of compounds currently used in a clinical setting. The compounds have been categorized into two classes, based on the presence of an amino group in the R_2 side-chain. The amino-BPs typically exhibit a higher potency in anti-resorptive effects, the primary clinical utility of BPs. Most of the BPs contain a geminal –OH group that enhances the mineral affinity of the compound.

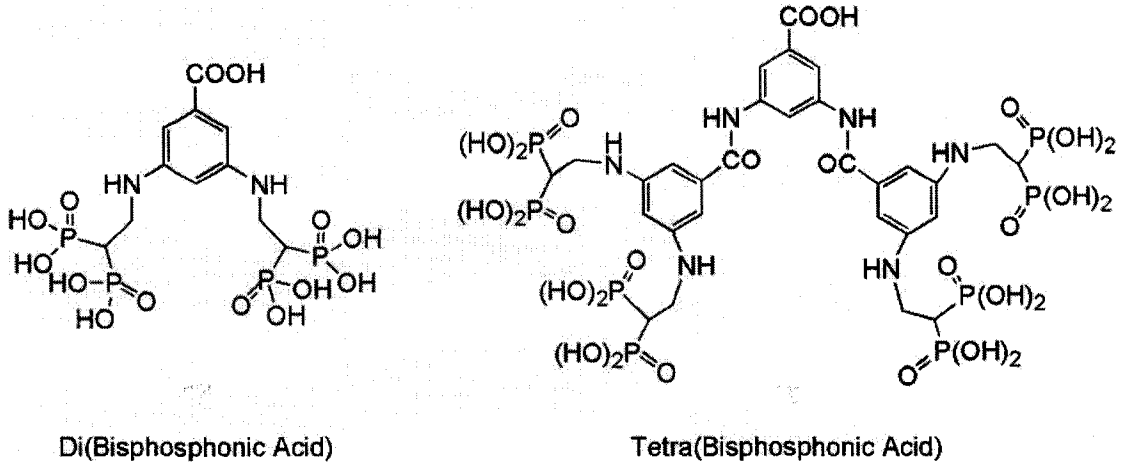

Figure 1-4. Novel dendritic BP-containing compounds. The compounds contained a single-COOH moiety for protein coupling, and either two or four BPs.

References

[1] J. P. Bilezikian, L. G. Raisz, and G. A. Rodan, *Principles of Bone Biology*, Academic Press, San Diego 2002.

[2] H. M. Frost, Dynamics of bone remodeling, in: *Bone Biodynamics,* Boston, 1964.

[3] S. A. Gittens, G. Bansal, R. F. Zernicke, and H. Uludağ, Designing proteins for bone targeting, *Adv. Drug Deliv. Rev.*, 57 (2005) 1011-1036.

[4] S. B. Trippel, R. D. Coutts, T. A. Einhorn, G. R. Mundy, and R. G. Rosenfeld, Growth factors as therapeutic agents, *J. Bone Joint. Surg. Am.*, 78 (1996) 1272-1286.

[5] S. Stevenson and S. P. Arnoczky, Transplantation of musculoskeletal tissues, in: *Orthopaedic Basic Science,* American Academy of Orthopaedic Surgeons, 2008, pp. 567-579.

[6] P. C. Bessa, M. Casal, and R. L. Reis, Bone morphogenetic proteins in tissue engineering: the road from laboratory to clinic, part II (BMP delivery), *J. Tissue Eng. Regen. Med.*, 2 (2008) 81-96.

[7] H. Fan, Y. Hu, L. Qin, X. Li, H. Wu, and R. Lv, Porous gelatin-chondroitin-hyaluronate tricopolymer scaffold containing microspheres loaded with TGF-β1 induces differentiation of mesenchymal stem cells *in vivo* for enhancing cartilage repair, *J. Biomed. Mater. Res.*, 77A (2006) 785-794.

[8] U. Ripamonti, J. Crooks, T. Matsaba, and J. Tasker, Induction of endochondral bone formation by recombinant human transforming growth factor-β2 in the baboon (*Papio ursinus*), *Growth Factors*, 17 (2000) 269-285.

[9] Y. Tabata, K. Yamada, S. Miyamoto, N. Hashimoto, and Y. Ikada, Skull bone regeneration in primates in response to basic fibroblast growth factor, *J. Neurosurg.*, 91 (1999) 851-856.

[10] S. B. Trippel, Role of insulin-like growth factors in the regulation of chondrocytes, in: M. Adolphe (Ed.), *Biological Regulation of the Chondrocytes,* CPC Press, Boca Raton, 1992, pp. 161-190.

[11] M. C. Adornato, I. Morcos, and J. Rozanski, The treatment of bisphosphonate-associated osteonecrosis of the jaws with bone resection and autologous platelet-derived growth factors, *J. Am. Dent. Assoc.*, 138 (2007) 971-977.

[12] W. V. Giannobile, R. A. Hernandez, R. D. Finkelman, S. Ryarr, C. P. Kiritsy, M. D'Andrea, and S. E. Lynch, Comparative effects of plateletderived growth factor-BB and insulin-like growth factor-I, individually and in combination, on periodontal regeneration in *Macaca fascicularis*, *J. Periodontal. Res.*, 31 (1996) 301-312.

[13] S. Pun, C. L. Florio, and T. J. Wronski, Anabolic effects of basic fibroblast growth factor in the tibial diaphysis of ovariectomized rats, *Bone*, 27 (2000) 197-202.

[14] G. Turgeman, Y. Zilberman, S. Zhou, P. Kelly, I. K. Moutsatsos, Y. P. Kharode, L. E. Borella, F. J. Bex, B. S. Komm, P. V. N. Bodine, and D. Gazit, Systemically administered rhBMP-2 promotes MSC activity and reverses bone and cartilage loss in osteopenic mice, *J. Cell. Biochem.*, 86 (2002) 461-474.

[15] M. Varkey, S. A. Gittens, and H. Uludağ, Growth factor delivery for bone tissue repair: an update, *Expert Opin. Drug Deliv.*, 1 (2004) 19-36.

[16] S. F. Siconolfi, R. J. Gretebeck, W. W. Wong, S. S. Moore, and J. H. Gilbert III, Determining bone and total body mineral content from body density and bioelectrical response spectroscopy, *J. Appl. Physiol.*, 85 (1998) 1578-1582.

[17] W. F. deJong, La substance minérale dans le os, *Rec. Trav. Chim.*, 45 (1926) 445-448.

[18] A. L. Boskey, The organic and inorganic matrices, in: J. O. Hollinger, T. A. Einhorn, B. A. Doll, and C. Sfeir (Eds.), *Bone tissue engineering,* CRC Press, Boca Raton, 2005, pp. 111-114.

[19] L. Pramatarova, E. Pecheva, R. Presker, M. T. Pham, M. F. Maitz, and M. Stutzmann, Hydroxyapatite growth induced by native extracellular matrix deposition on solid surfaces, *Eur. Cell Mater.*, 9 (2005) 9-12.

[20] S. V. Dorozhkin and M. Epple, Biological and medical significance of calcium phosphates, *Angew. Chem. Int. Ed.*, 41 (2002) 3130-3146.

[21] P. W. Brown and R. I. Martin, An analysis of hydroxyapatite surface layer formation, *J. Phys. Chem.*, 103 (1999) 1671-1675.

[22] K. Kandori, S. Sawai, Y. Yamamoto, H. Saito, and T. Ishikawa, Adsorption of albumin on calcium hydroxylapatite, *Colloids Surf.*, 68 (1992) 283-289.

[23] I. S. Harding, N. Rashid, and K. A. Hing, Surface charge and the effect of excess calcium ions on the hydroxyapatite surface, *Biomaterials*, 26 (2005) 6818-6826.

[24] L. M. Siperko and W. J. Landis, Atomic scale imaging of hydroxyapatite and brushite in air by force microscopy, *Appl. Phys. Lett.*, 61 (1992) 2610.

[25] J. Kirkham, J. Zhang, S. J. Brookes, R. C. Shore, S. R. Wood, D. A. Smith, M. L. Wallwork, O. H. Ryu, and C. Robinson, Evidence for charge domains on developing enamel crystal surfaces, *J. Dent. Res.*, 79 (2000) 1943-1947.

[26] J. Vandiver, D. Dean, N. Patel, W. Bonfield, and C. Ortiz, Nanoscale variation in surface charge of synthetic hydroxyapatite detected by chemically and spatially specific high-resolution force spectroscopy, *Biomaterials*, 26 (2005) 271-283.

[27] K. Kandori, M. Mukai, A. Yasukawa, and T. Ishikawa, Competitive and cooperative adsorptions of bovine serum albumin and lysozyme to synthetic calcium hydroxyapatites, *Langmuir*, 16 (2000) 2301-2305.

[28] P. X. Zhu, Y. Masuda, and K. Koumoto, Site-selective adhesion of hydroxyapatite microparticles on charged surfaces in a supersaturated solution, *J. Colloid Interface Sci.*, 243 (2001) 31-36.

[29] D. A. Smith, S. D. Connell, C. Robinson, and J. Kirkham, Chemical force microscopy: applications in surface characterisation of natural hydroxyapatite, *Anal. Chim. Acta*, 479 (2003) 39-57.

[30] S. Mafe, J. A. Manzanares, H. Reiss, J. M. Thomann, and P. Gramain, Model for the dissolution of calcium hydroxyapatite powder, *J. Phys. Chem.*, 96 (1992) 861-866.

[31] J. Zhang, J. Kirkham, M. L. Wallwork, D. A. Smith, S. J. Brookes, R. C. Shore, S. R. Wood, and C. Robinson, Use of self-assembled monolayers as substrates for atomic force imaging of hydroxyapatite crystals from mammalian skeletal tissues, *Langmuir*, 15 (1999) 8178-8183.

[32] C. Robinson, S. Connell, J. Kirkham, R. Shore, and A. Smith, Dental enamel - a biological ceramic: regular substructures in enamel hydroxyapatite crystals revealed by atomic force microscopy, *J. Mater. Chem.*, 14 (2004) 2242-2248.

[33] W. J. Shaw, A. A. Campbell, M. L. Paine, and M. L. Snead, The COOH terminus of the amelogenin, LRAP, is oriented next to the hydroxyapatite surface, *J. Biol. Chem.*, 279 (2004) 40263-40266.

[34] N. Bouropoulos and J. Moradian-Oldak, Analysis of hydroxyapatite surface coverage by amelogenin nanospheres following the Langmuir model for protein adsorption, *Calcif. Tissue Int.*, 72 (2003) 599-603.

[35] M. Wallwork, J. Kirkham, J. Zhang, D. A. Smith, S. Brookes, R. Shore, S. Wood, O. Ryu, and C. Robinson, Binding of matrix proteins to developing enamel crystals: an Atomic force microscopy study, *Langmuir*, 17 (2001) 2508-2513.

[36] M. L. Wallwork, J. Kirkham, H. Chen, S. X. Chang, C. Robinson, D. A. Smith, and B. H. Clarkson, Binding of dentin noncollagenous matrix proteins to biological mineral crystals: an atomic force microscopy study, *Calcif. Tissue Int.*, 71 (2002) 249-256.

[37] H. Chen, Y. Chen, B. G. Orr, M. M. BanaszakHoll, I. Majoros, and B. H. Clarkson, Nanoscale probing of the enamel nanorod surface using polyamidoamine dendrimers, *Langmuir*, 20 (2004) 4168-4171.

[38] H. Chen, M. Banaszak Holl, B. G. Orr, I. Majoros, and B. H. Clarkson, Interaction of dendrimers (artificial proteins) with biological hydroxyapatite crystals, *J. Dent. Res.*, 82 (2003) 443-448.

[39] M. J. Dallemagne, *Bone and teeth*, Pergamon Press, Oxford, UK. 1964.

[40] S. G. Rees, D. T. H. Wassell, R. J. Waddington, and G. Embery, Interaction of bone proteoglycans and proteoglycan components with hydroxyapatite, *Biochim. Biophys. Acta*, 1568 (2001) 118-128.

[41] A. Tiselius, S. Hjertén, and O. Levin, Protein chromatography on calcium phosphate columns, *Arch. Biochem. Biophys.*, 65 (1956) 132-155.

[42] M. J. Gorbunoff, The interaction of proteins with hydroxyapatite: I. Role of protein charge and structure, *Anal. Biochem.*, 136 (1984) 425-432.

[43] M. J. Gorbunoff, The interaction of proteins with hydroxyapatite: II. Role of acidic and basic groups, *Anal. Biochem.*, 136 (1984) 433-439.

[44] M. J. Gorbunoff and S. N. Timasheff, The interaction of proteins with hydroxyapatite: III. Mechanism, *Anal. Biochem.*, 136 (1984) 440-445.

[45] D. Wang, S. Miller, M. Sima, P. Kopeckova, and J. Kopecek, Synthesis and evaluation of water-soluble polymeric bone-targeted drug delivery systems, *Bioconjug. Chem.*, 14 (2003) 853-859.

[46] V. Hlady and H. Fnredi-Milhofer, Adsorption of human serum albumin on precipitated hydroxyapatite, *J. Colloid Interface Sci.*, 69 (1979) 460-468.

[47] P. V. Hauschka and S. A. Carr, Calcium-dependent α-helical structure in osteocalcin, *Biochemistry*, 21 (1982) 2538-2547.

[48] R. Wallin, D. Cain, S. M. Hutson, D. C. Sane, and R. Loeser, Modulation of the binding of matrix Gla protein (MGP) to bone morphogenetic protein-2 (BMP-2), *Thromb. Haemost.*, 84 (2000) 1039-1044.

[49] K. Ohta, H. Monma, J. Tanaka, and H. Eda, Interaction between hydroxyapatite and proteins by liquid chromatography using simulated body fluids as eluents, *J. Mater. Sci. Mater. Med.*, 13 (2002) 633-637.

[50] C. Robinson, S. Connell, S. J. Brookes, J. Kirkham, R. C. Shore, and D. A. M. Smith, Surface chemistry of enamel apatite during maturation in relation to pH: implications for protein removal and crystal growth, *Arch. Oral Biol.*, 50 (2005) 267-270.

[51] W. M. Rathman, M. J. van Zeyl, P. A. M. van den Keybus, R. A. Bank, E. C. I. Veerman, and A. V. Nieuw Amerongen, Isolation and characterization of three non-mucinous human salivary proteins with affinity for hydroxyapatite, *J. Biol. Buccale*, 17 (1989) 199-208.

[52] A. V. Nieuw Amerongen, C. H. Oderkerk, and E. C. I. Veerman, Interaction of human salivary mucins with hydroxyapatite, *J. Biol. Buccale*, 17 (1989) 85-92.

[53] R. Fujisawa, Y. Wada, Y. Nodasaka, and Y. Kuboki, Acidic amino acid-rich sequences as binding sites of osteonectin to hydroxyapatite crystals, *Biochim. Biophys. Acta*, 1292 (1996) 53-60.

[54] D. A. Pampena, K. A. Robertson, O. Litvinova, G. Lajoie, H. A. Goldberg, and G. K. Hunter, Inhibition of hydroxyapatite formation by osteopontin phospho-peptides, *Biochem. J.*, 378 (2004) 1083-1087.

[55] C. E. Tye, K. R. Rattray, K. J. Warner, J. A. R. Gordon, J. Sodek, G. K. Hunter, and H. A. Goldberg, Delineation of the hydroxyapatite-nucleating domains of bone sialoprotein, *J. Biol. Chem.*, 278 (2003) 7949-7955.

[56] H. A. Goldberg, K. J. Warner, M. C. Li, and G. K. Hunter, Binding of bone sialoprotein, osteopontin and synthetic polypeptides to hydroxyapatite, *Connect. Tissue Res.*, 42 (2001) 25-37.

[57] M. Wuttke, S. Muller, D. P. Nitsche, M. Paulsson, F. G. Hanisch, and P. Maurer, Structural characterization of human recombinant and bone-derived bone sialoprotein. Functional implications for cell attachment and hydroxyapatite binding, *J. Biol. Chem.*, 276 (2001) 36839-36848.

[58] H. A. Goldberg, K. J. Warner, M. J. Stillman, and G. K. Hunter, Determination of the hydroxyapatite-nucleating region of bone sialoprotein, *Connect. Tissue Res.*, 35 (1996) 385-392.

[59] F. Poumier, P. Schaad, Y. Haikel, J. C. Voegel, and P. Gramain, Dissolution of synthetic hydroxyapatite in the presence of acidic polypeptides, *J. Biomed. Mater. Res.*, 45 (1999) 92-99.

[60] A. A. Sawyer, D. M. Weeks, S. S. Kelpke, M. S. McCracken, and S. L. Bellis, The effect of the addition of a polyglutamate motif to RGD on peptide tethering to hydroxyapatite and the promotion of mesenchymal stem cell adhesion, *Biomaterials*, 26 (2005) 7046-7056.

[61] D. Itoh, S. Yoneda, S. Kuroda, H. Kondo, A. Umezawa, K. Ohya, T. Ohyama, and S. Kasugai, Enhancement of osteogenesis on hydroxyapatite surface coated with synthetic peptide (EEEEEEEPRGDT) *in vitro*, *J. Biomed. Mater. Res.*, 62 (2002) 292-298.

[62] S. Kasugai, R. Fujisawa, Y. Waki, K. Miyamoto, and K. Ohya, Selective drug delivery system to bone: small peptide (Asp)6 conjugation, *J. Bone Miner. Res.*, 15 (2000) 936-943.

[63] R. Fujisawa, Y. Kuboki, and S. Sasaki, Changes in interaction of bovine dentin phosphophoryn with calcium and Hydroxyapatite by chemical modifications, *Calcif. Tissue Int.*, 39 (1986) 248-251.

[64] A. L. Boskey, M. Maresca, W. Ullrich, S. B. Doty, W. T. Butler, and C. W. Prince, Osteopontin-hydroxyapatite interactions in vitro: inhibition of hydroxyapatite formation and growth in a gelatin-gel., *Bone Miner.*, 22 (1993) 147-159.

[65] N. Ramasubbu, L. M. Thomas, K. K. Bhandary, and M. J. Levine, Structural characteristics of human salivary statherin: a model for boundary lubrication at the enamel surface, *Crit. Rev. Oral. Biol. Med.*, 4 (1993) 363-370.

[66] P. S. Stayton, G. P. Drobny, W. J. Shaw, J. R. Long, and M. Gilbert, Molecular recognition at the protein-hydroxyapatite interface, *Crit. Rev. Oral Biol. Med.*, 14 (2003) 370-376.

[67] P. A. Raj, M. Johnsson, M. J. Levine, and G. H. Nancollas, Salivary statherin. Dependence on sequence, charge, hydrogen bonding potency, and helical conformation for adsorption to hydroxyapatite and inhibition of mineralization, *J. Biol. Chem.*, 267 (1992) 5968-5976.

[68] Q. Q. Hoang, F. Sicheri, A. J. Howard, and D. S. C. Yang, Bone recognition mechanism of porcine osteocalcin from crystal structure, *Nature*, 425 (2003) 977-980.

[69] J. T. Stubbs III, K. Mintz, E. D. Eanes, D. A. Torchia, and L. W. Fisher, Characterization of native and recombinant bone sialoprotein: delineation of the mineral-binding and cell adhesion domains and structural analysis of the RGD domain, *J. Bone Miner. Res.*, 12 (1997) 1210.

[70] A. Gericke, C. Qin, L. Spevak, Y. Fujimoto, W. T. Butler, E. S. Sørensen, and A. L. Boskey, Importance of phosphorylation for osteopontin regulation of biomineralization, *Calcif. Tissue Int.*, 77 (2005) 45-54.

[71] M. T. Kaartinen, A. Pirhonen, A. Linnala-Kankkunen, and P. H. Maenpaa, Cross-linking of osteopontin by tissue transglutaminase increases its collagen binding properties, *J. Biol. Chem.*, 274 (1999) 1729-1735.

[72] M. T. Kaartinen, A. Pirhonen, A. Linnala-Kankkunen, and P. H. Maenpaa, Transglutaminase-catalyzed cross-linking of osteopontin is inhibited by osteocalcin, *J. Biol. Chem.*, 272 (1997) 22736-22741.

[73] H. Furedi-Milhofer, J. Moradian-Oldak, S. Weiner, A. Veis, K. P. Mintz, and L. Addadf, Interactions of matrix proteins from mineralized tissues with octacalcium phosphate, *Connect. Tissue Res.*, 30 (1994) 251-264.

[74] T. Aizawa, N. Koganesawa, A. Kamakura, K. Masaki, A. Matsuura, H. Nagadome, Y. Terada, K. Kawano, and K. Nitta, Adsorption of human lysozyme onto hydroxyapatite: Identification of its adsorbing site using site-directed mutagenesis, *FEBS Lett.*, 422 (1998) 175-178.

[75] K. Kandori, N. Horigami, H. Kobayashi, A. Yasukawa, and T. Ishikawa, Adsorption of lysozyme onto various synthetic hydroxyapatites, *J. Colloid Interface Sci.*, 191 (1997) 498-502.

[76] D. Stepensky, L. Kleinberg, and A. Hoffman, Bone as an effect compartment, *Clin. Pharmacokinet.*, 42 (2003) 863-882.

[77] W. M. Pierce Jr. and L. C. Waite, Bone-targeted carbonic anhydrase inhibitors: effect of a proinhibitor on bone resorption *in vitro*, *Proc. Soc. Exp. Biol. Med.*, 186 (1984) 96-102.

[78] M. W. Orme and V. M. Labroo, Synthesis of β-estradiol-3-benzoate-17-(succinyl-12*a*-tetracycline): a potential bone-seeking estrogen, *Bioorg. Med. Chem. Lett.*, 4 (1994) 1375-1380.

[79] Zheng, H. and Weng, L. L, Bone resorption inhibition/osteogenesis promotion pharmaceutical composition. [US 5,698,542]. 1997.

[80] Bentz, H. and Rosen, D. Targeted delivery of bone growth factors. [EP 0 512 844]. 1992.

[81] T. M. Willson, B. R. Kenke, T. M. Momtahen, D. T. Garrison, L. B. Moore, N. G. Geddie, and P. G. Baer, Bone targeted drugs: 2. Synthesis of estrogens with hydroxyapatite affinity, *Bioorg. Med. Chem. Lett.*, 6 (1996) 1047-1050.

[82] K. Yokogawa, K. Miya, T. Sekido, Y. Higashi, M. Nomura, R. Fujisawa, K. Morito, Y. Masamune, Y. Waki, S. Kasugai, and K. I. MIYAMOTO, Selective delivery of estradiol to bone by aspartic acid oligopeptide and its effects on ovariectomized mice, *Endocrinology*, 142 (2001) 1228-1233.

[83] M. Missbach, M. Jeschke, J. Feyen, K. Mnller, M. Glatt, J. Green, and M. Susa, A novel inhibitor of the tyrosine kinase Src suppresses phosphorylation of its major cellular substrates and reduces bone resorption *in vitro* and in rodent models *in vivo*, *Bone*, 24 (1999) 437-449.

[84] W. Shakespeare, M. Yang, R. Bohacek, F. Cerasoli, K. Stebbins, R. Sundaramoorthi, M. Azimioara, C. Vu, S. Pradeepan, C. Metcalf, C. Haraldson, T. Merry, D. Dalgarno, S. Narula, M. Hatada, X. Lu, M. R. van Schravendijk, S. Adams, S. Violette, J. Smith, W. Guan, C. Bartlett, J. Herson, J. Iuliucci, M.

Weigele, and T. Sawyer, Structure-based design of an osteoclast-selective, nonpeptide Src homology 2 inhibitor with in vivo antiresorptive activity, *Proc. Natl. Acad. Sci. U.S.A.*, 97 (2000) 9373-9378.

[85] M. J. Rogers, R. C. Watts, R. G. G. Russell, X. Ji, X. Xiong, G. M. Blackburn, A. V. Bayless, and F. H. Ebetino, Inhibitory effects of bisphosphonates on growth of amoebae of the cellular slime mould Dictyostelium discoideum, *J. Bone Miner. Res.*, 9 (1994) 1029-1039.

[86] B. Y. Klein, H. Ben-Bassat, E. Breuer, V. Solomon, and G. Golomb, Structurally different bisphosphonates exert opposing effects on alkaline phosphatase and mineralization in marrow osteoprogenitors, *J. Cell. Biochem.*, 68 (1998) 186-194.

[87] L. Widler, K. A. Jaeggi, M. Glatt, K. Muller, R. Bachmann, M. Bisping, A. R. Born, R. Cortesi, G. Guiglia, H. Jeker, R. Klein, U. Ramseier, J. Schmid, G. Schreiber, Y. Seltenmeyer, and J. R. Green, Highly potent geminal bisphosphonates. From pamidronate disodium (Aredia) to zoledronic acid (Zometa), *J. Med. Chem.*, 45 (2002) 3721-3738.

[88] R. G. Russell, M. J. Rogers, J. C. Frith, S. P. Luckman, F. P. Coxon, H. L. Benford, P. I. Croucher, C. Shipman, and H. A. Fleisch, The pharmacology of bisphosphonates and new insights into their mechanisms of action, *J. Bone Miner. Res.*, 14 (1999) 53-65.

[89] D. Fernández, D. Vega, and A. Goeta, Alendronate zwitterions bind to calcium cations arranged in columns, *Acta Crystallogr. C.*, 59 (2003) m543-m545.

[90] D. Fernández, D. Vega, and A. Goeta, The calcium-binding properties of pamidronate, a bone-resorption inhibitor, *Acta Crystallogr. C*, 58 (2002) m494.

[91] E. van Beek, M. Hoekstra, M. van de Ruit, C. Löwik, and S. Papapoulos, Structural requirements for bisphosphonate actions *in vitro*, *J. Bone Miner. Res.*, 9 (1994) 1875-1882.

[92] R. Russell, R. Muhlbauer, S. Bisaz, D. Williams, and H. Fleisch, The influence of pyrophosphate, condensed phosphates, phosphonates and other phosphate compounds on the dissolution of hydroxyapatite *in vitro* and on bone resorption induced by parathyroid hormone in tissue culture and in thyroparathyroidectomised rats, *Calcif. Tissue Int.*, 6 (1970) 183-196.

[93] S. H. Szajnman, E. L. Ravaschino, R. Docampo, and J. B. Rodriguez, Synthesis and biological evaluation of 1-amino-1,1-bisphosphonates derived from fatty acids against Trypanosoma cruzi targeting farnesyl pyrophosphate synthase, *Bioorg. Med. Chem. Lett.*, 15 (2005) 4685-4690.

[94] E. van Beek, C. Löwik, I. Que, and S. Papapoulos, Dissociation of binding and antiresorptive properties of hydroxybisphosphonates by substitution of the hydroxyl with an amino group, *J. Bone Miner. Res.*, 11 (1996) 1492-1497.

[95] M. A. Lawson, J. T. Triffitt, F. H. Ebetino, R. J. Phipps, D. J. White, and R. G. G. Russell, The use of hydroxyapatite column chromatography as a novel method to reveal differences in relative binding affinities of bisphosphonates, *Bone*, 36 (2005) 308.

[96] G. H. Nancollas, R. Tang, R. J. Phipps, Z. Henneman, S. Gulde, W. Wu, A. Mangood, R. G. G. Russell, and F. H. Ebetino, Novel insights into actions of bisphosphonates on bone: Differences in interactions with hydroxyapatite, *Bone*, 38 (2006) 617-627.

[97] F. H. Ebetino, B. L. Barnett, R. G. G. Russell, Z. Henneman, and G. H. Nancollas, A computational model explains bisphosphonate binding affinity differences on hydroxyapatite, *Bone*, 38 (2006) 48-49.

[98] E. C. Lisic, M. Phillips, D. Ensor, K. L. Nash, A. Beets, and F. F. Knapp, Synthesis of a new bisphosphonic acid ligand (SEDP) and preparation of a ^{188}Re-(Sn)SEDP bone seeking radiotracer, *Nucl. Med. Biol.*, 28 (2001) 419-424.

[99] H. Hirabayashi, T. Sawamoto, J. Fujisaki, Y. Tokunaga, S. Kimura, and T. Hata, Relationship between physicochemical and osteotropic properties of bisphosphonic derivatives: rational design for osteotropic drug delivery system (ODDS), *Pharm. Res.*, 18 (2001) 646-651.

[100] H. Uludağ, Bisphosphonates as a foundation of drug delivery to bone, *Curr. Pharm. Des.*, 8 (2002) 1929-1944.

[101] H. Hirabayashi and J. Fujisaki, Bone-specific drug delivery systems, *Clin. Pharmacokinet.*, 42 (2003) 1319-1330.

[102] H. Uludağ, N. Kousinioris, T. Gao, and D. Kantoci, Bisphosphonate conjugation to proteins as a means to impart bone affinity, *Biotechnol. Prog.*, 16 (2000) 258-267.

[103] G. Bansal, J. E. I. Wright, S. Zhang, R. F. Zernicke, and H. Uludağ, Imparting mineral affinity to proteins with thiol-labile disulfide linkages, *J. Biomed. Mater. Res. Part A*, 74 (2005) 618-628.

[104] S. A. Gittens, J. R. Matyas, R. F. Zernicke, and H. Uludağ, Imparting bone affinity to glycoproteins through the conjugation of bisphosphonates, *Pharm. Res.*, 20 (2003) 978-987.

[105] A. Zaheer, R. E. Lenkinski, A. Mahmood, A. G. Jones, L. C. Cantley, and J. V. Frangioni, *In vivo* near-infrared fluorescence imaging of osteoblastic activity, *Nature Biotechnol.*, 19 (2001) 1148-1154.

[106] C. L. Webb, F. J. Schoen, and R. J. Levy, Covalent binding of aminopropanehydroxydiphosphonate to glutaraldehyde residues in pericardial

bioprosthetic tissue: Stability and calcification inhibition studies, *Exp. Mol. Pathol.*, 50 (1989) 291-302.

[107] I. S. Alferiev, J. M. Connolly, and R. J. Levy, A novel mercapto-bisphosphonate as an efficient anticalcification agent for bioprosthetic tissues, *J. Organomet. Chem.*, 690 (2005) 2543-2547.

[108] S. Gittens, P. Kitov, J. Matyas, R. Lobenberg, and H. Uludağ, Impact of tether length on bone mineral affinity of protein-bisphosphonate conjugates, *Pharm. Res.*, 21 (2004) 608-616.

[109] G. Bansal, S. A. Gittens, and H. Uludağ, A di(bisphosphonic acid) for protein coupling and targeting to bone, *J. Pharm. Sci.*, 93 (2004) 2788-2799.

[110] G. Bansal, J. E. I. Wright, C. Kucharski, and H. Uludağ, A dendritic tetra(bisphosphonic acid) for improved targeting of proteins to bone, *Angew. Chem. Int. Ed.*, 44 (2005) 3710-3714.

[111] B. J. Boyd, Past and future evolution in colloidal drug delivery systems, *Expert Opin. Drug Deliv.*, 5 (2008) 69-85.

[112] R. V. Talmage, Morphological and physiological consideration in a new concept of calcium transport in bone, *Am. J. Anat.*, 129 (1970) 467-476.

[113] V. Luginbuehl, L. Meinel, H. P. Merkle, and B. Gander, Localized delivery of growth factors for bone repair, *Eur. J. Pharm. Biopharm.*, 58 (2004) 197-208.

[114] M. N. V. Ravi Kumar, Nano and microparticles as controlled drug delivery devices, *J. Pharm. Pharmaceut. Sci.*, 3 (2000) 234-258.

[115] G. Wang and H. Uludağ, Recent developments in nanoparticle-based drug delivery and targeting systems with emphasis on protein-based nanoparticles, *Expert Opin. Drug Deliv.*, 5 (2008) 499-515.

[116] M. Socinski, Update on nanoparticle albumin-bound paclitaxel, *Clin. Adv. Hematol. Oncol.*, 4 (2006) 745-746.

[117] W. Mehnert and K. Mäder, Solid lipid nanoparticles: production, characterization and applications, *Adv. Drug Deliv. Rev.*, 47 (2001) 165-196.

[118] G. E. Riedel and A. Valentin-Opran, Clinical evaluation of rhBMP-2/ACS in orthopedic trauma: a progress report, *Orthopedics*, 22 (1999) 663-665.

[119] F. Blanquaert, F. D. Barritault, and J. P. Caruelle, Effects of heparan-like polymers associated with growth factors on osteoblast proliferation and phenotype expression, *J. Biomed. Mater. Res.*, 44 (1999) 63-72.

[120] T. C. Yih and M. Al-Fandi, Engineered nanoparticles as precise drug delivery systems, *J. Cell. Biochem.*, 97 (2006) 1184-1190.

[121] K. S. Soppimath, T. M. Aminabhavi, A. R. Kulkarni, and W. E. Rudzinski, Biodegradable polymeric nanoparticles as drug delivery devices, *J. Control Release*, 70 (2001) 1-20.

[122] G. Wei, Q. Jin, W. V. Giannobile, and P. X. Ma, The enhancement of osteogenesis by nano-fibrous scaffolds incorporating rhBMP-7 nanospheres, *Biomaterials*, 28 (2007) 2087-2096.

[123] J. S. Park, K. Park, D. G. Woo, H. N. Yang, H. M. Chung, and K. H. Park, PLGA microsphere construct coated with TGF-β 3 loaded nanoparticles for neocartilage formation, *Biomacromolecules*, 9 (2008) 2162-2169.

[124] Y. I. Chung, K. M. Ahn, S. H. Jeon, S. Y. Lee, J. H. Lee, and G. Tae, Enhanced bone regeneration with BMP-2 loaded functional nanoparticle-hydrogel complex, *J. Control Release*, 121 (2007) 91-99.

[125] F. M. Chen, Z. F. Wu, Y. Jin, Q. T. Wang, Y. Du, and G. F. Wang, Preparation and property of recombinant human bone morphogenetic protein-2 loaded hydrogel nanospheres and their biological effects on the proliferation and differentiation of bone mesenchymal stem cells, *Shanghai Kou Qiang Yi Xue,* 14 (2005) 485-489.

[126] F. m. Chen, Z. f. Wu, H. h. Sun, H. Wu, S. n. Xin, Q. t. Wang, G. y. Dong, Z. w. Ma, S. Huang, Y. j. Zhang, and Y. Jin, Release of bioactive BMP from dextran-derived microspheres: a novel delivery concept, *Int. J. Pharm.*, 307 (2006) 23-32.

[127] F. m. Chen, Y. M. Zhao, R. Zhang, T. Jin, H. h. Sun, Z. f. Wu, and Y. Jin, Periodontal regeneration using novel glycidyl methacrylated dextran (Dex-GMA)/gelatin scaffolds containing microspheres loaded with bone morphogenetic proteins, *J. Control Release*, 121 (2007) 81-90.

[128] S. M. Moghimi, A. C. Hunter, and J. C. Murray, Long-circulating and target-specific nanoparticles: theory to practice, *Pharmacol. Rev.*, 53 (2001) 283-318.

[129] A. Vonarbourg, C. Passirani, P. Saulnier, and J. P. Benoit, Parameters influencing the stealthiness of colloidal drug delivery systems, *Biomaterials*, 27 (2006) 4356-4373.

[130] Y. Tabata and Y. Ikada, Phagocytosis of polymer microspheres by macrophages, *Adv. Polym. Sci.*, 94 (1990) 107-141.

[131] E. L. Romero, M. J. Morilla, J. Regts, G. A. Koning, and G. L. Scherphof, On the mechanism of hepatic transendothelial passage of large liposomes, *FEBS Lett.*, 448 (1999) 193-196.

[132] C. J. H. Porter, S. M. Moghimi, L. Illum, and S. S. Davis, The polyoxyethylene/polyoxypropylene block co-polymer Poloxamer-407 selectively redirects intravenously injected microspheres to sinusoidal endothelial cells of rabbit bone marrow, *FEBS Lett.*, 305 (1992) 62-66.

[133] P. M. Claesson, E. Blomberg, J. C. Fröberg, T. Nylander, and T. Arnebrant, Protein interactions at solid surfaces, *Adv. Colloid Interface Sci.*, 57 (1995) 161-227.

[134] M. Roser, D. Fischer, and T. Kissel, Surface-modified biodegradable albumin nano- and microspheres. II: effect of surface charges on *in vitro* phagocytosis and biodistribution in rats, *Eur. J. Pharm. Biopharm.*, 46 (1998) 255-263.

[135] V. Hengst, C. Oussoren, T. Kissel, and G. Storm, Bone targeting potential of bisphosphonate-targeted liposomes: Preparation, characterization and hydroxyapatite binding *in vitro*, *Int. J. Pharm.*, 331 (2007) 224-227.

[136] S. W. Choi and J. H. Kim, Design of surface-modified poly(D,L-lactide-co-glycolide) nanoparticles for targeted drug delivery to bone, *J. Control Release*, 122 (2007) 24-30.

[137] H. Pan, M. Sima, P. Kopeckova, K. Wu, S. Gao, J. Liu, D. Wang, S. C. Miller, and J. Kopecek, Biodistribution and pharmacokinetic studies of bone-targeting N-(2-hydroxypropyl)methacrylamide copolymer-alendronate conjugates, *Mol. Pharm.*, 5 (2008) 548-558.

[138] L. Wang, M. Zhang, Z. Yang, and B. Xu, The first pamidronate containing polymer and copolymer, *Chem. Commun.*, (2006) 2795-2797.

[139] S. Zhang, J. E. I. Wright, N. Özber, and H. Uludağ, The interaction of cationic polymers and their bisphosphonate derivatives with hydroxyapatite, *Macromol. Biosci.*, 7 (2007) 656-670.

CHAPTER II

Scope of Dissertation

This thesis is comprised of a total of eight chapters. Each chapter is intended to be self-sufficient as a complete study and each chapter is formatted in such a way that it can serve as a 'manuscript' suitable as a stand-alone publication.

CHAPTER I introduces the necessity for systemic and local bone regeneration, as well as the most recent advances in development of bone-seeking medicinal agents. Given the specific advantages of protein therapy, the utilization of protein growth factors to stimulate new bone formation was discussed in this chapter. In order to overcome the side-effects elicited by protein distribution to extraskeletal sites, bone-specific drug delivery system is needed to restrict the therapeutic agents to bone for effective bone regeneration. As the basis for drug targeting to bone, the structure of biological apatite and bone affinity of proteins are presented. With the emphasis on bisphosphonates (BPs), bone-seeking agents are discussed and several functional BPs for protein conjugation were explored. As an approach to better retain the integrity of growth factors, colloidal drug delivery system is subsequently discussed, with a focus on polymeric nanoparticulate (NP) delivery system.

The scope of the dissertation is presented in **CHAPTER II** (the present chapter).

Based on the exceptional bone affinity of BPs, protein-BPs conjugation was initially developed by Uludag and co-workers, and it was demonstrated to be a feasible means to impart bone affinity to proteins. Protein-BP conjugates with cleavable linkages, which can allow proteins to be released from such conjugates, are preferable over conjugates with stable linkages. To this end, 2-(3-mercaptopropylsulfanyl)-ethyl-1,1-bisphosphonic acid (thiolBP) was conjugated onto fetuin, a model protein, using N-succinimidyl-3-(2-pyridyldithio) propionate (SPDP) in order to create disulfide-linked

conjugates. This work is summarized in **CHAPTER III**. The mineral affinity of disulfide-linked protein-BP conjugates was assessed by hydroxyapatite (HA) binding assay. The cleavage of the disulfide linkage was investigated in the presence of the physiological thiols, *L*-cysteine, *DL*-homocysteine, and *L*-glutathione. The cleavage rate of the three thiols was compared, as well as the cleavage of the conjugates in solution and bound to HA.

In order to increase bone targeting efficiency while minimizing the extent of protein modification, a polymeric molecule containing multiple copies of BPs was constructed for protein conjugation. This work is summarized in **CHAPTER IV**. Poly(*L*-lysine) (PLL) and poly(ethyleneimine) (PEI) were utilized as the polymeric backbones to incorporate the thiolBP, by using *N*-hydroxysuccinimidyl polyethyleneglycol maleimide (NHS-PEG-MAL) and succinimidyl-4-(N-maleimidomethyl)-cyclohexane-1-carboxylate (SMCC) as linkers, respectively. *In vitro* mineral affinity of the polymer-BP conjugates was assessed, in comparison with the unmodified cationic polymers. A strong affinity of cationic polymers to HA was unexpectedly observed. This led to more detailed studies on polymer binding, including the effect of polymer concentrations and molecular weight (MW) on binding. Furthermore, the mineral affinity of polymer-BP conjugates was investigated in a subcutaneous implant model in rats with a commercially available calcium phosphate implant matrix (Skelite^{TM}). This data not only provided information about the factors controlling the extent of cationic polymer adsorption to HA, but also pointed out to the potential of cationic polymers for drug delivery to bone.

Recently, NP-based drug delivery has gained importance for improving the potency of therapeutic agents. To explore the potential of NPs for growth factor delivery,

bovine serum albumin (BSA) NPs, obtained by a coacervation process, was fabricated and surface modified with cationic PEI. Such NPs were intended for delivery of a bone-inducing growth factor, Bone Morphogenetic Protein-2 (BMP-2) and my work on this approach is summarized in **CHAPTER V**. Different concentrations of PEI were utilized for coating BSA NPs to stabilize the colloidal system and to control the release of BMP-2. The PEI coating for NP stabilization eliminated the commonly used but undesirable chemical cross-linker glutaraldehyde. The NPs were characterized by size and zeta-potential measurements, as well as by Scanning Electron Microscopy and Atomic Force Microscopy. The encapsulation efficiency and *in vitro* release kinetics during a 10-day period was determined by NP-encapsulated ^{125}I-labeled BMP-2. The bioactivity of the encapsulated BMP-2 and the toxicity of the NPs were examined by the Alkaline Phosphatase (ALP) induction assay and the MTT assay, respectively, using human C2C12 cells. The results indicated that BMP-2 encapsulated BSA NPs (BMP-2/BSA NPs) coated with 0.1 mg/mL PEI demonstrated tolerable toxicity, retained the bioactivity of BMP-2, and efficiently controlled the release rate of BMP-2 *in vitro*.

Based on the promising *in vitro* results with NP delivery system, **CHAPTER VI** describes the *in vivo* pharmacokinetics and osteoinductivity studies of the BMP-2/BSA NPs coated with PEI in a rat ectopic model. *In vivo* pharmacokinetics showed that PEI coating effectively reduced the initial burst release of BMP-2, and prolonged the retention of BMP-2 at the implantation site. Despite the advantage from release kinetics, the PEI-coated BMP-2/BSA NPs failed to induce bone formation in implants. The subsequent experiments identified the increased PEI concentration in implantation formulations to abolish the BMP-2 osteogenic activity. The results generated in this

chapter demonstrated the benefits of PEI coating in release kinetics, but highlighted the toxicity of PEI coating which resulted in unsuccessful bone induction.

An established method for decreasing polymer toxicity and improving biocompatibility, namely PEGylation, was employed to reduce the toxicity of NP formulations in **CHAPTER VII**. The toxicity of PEI-PEG conjugate was determined and compared to the unmodified PEI. The BSA NPs coated with PEI-PEG were characterized by size, zeta potential measurement and the morphology by AFM. In comparison with PEI-coated NPs, dramatic reduction in size and zeta potential were observed by PEI-PEG coated BSA NPs. The ALP induction activity and toxicity of the PEI-PEG coated BMP-2/BSA NPs were subsequently studied. Finally, the osteoinductive activity of the PEI-PEG coated NPs were investigated in a rat ectopic model, which resulted in successful bone formation in this assay. The work described in **CHAPTERS V, VI,** and **VII** established the foundation of a novel drug delivery system based on polymer-coated, protein NPs that can control the release of encapsulated drugs and have the potential to target bone after further engineering.

All together, the work presented in this dissertation expands the utilization of BPs for protein targeting to bone. It provides a foundation for a nanoparticulate drug delivery system based on albumin particles surface modified by cationic polymers. As discussed in **CHAPTER VIII** on future studies, this dissertation also provides information for numerous additional studies to further expand our knowledge in the fields of drug delivery and bone tissue engineering.

CHAPTER III

Cleavage of Disulfide-Linked Fetuin-Bisphosphonate Conjugates with Three Physiological Thiols[1]

[1]The contents of this chapter have been previously published in: S. Zhang, J. E. I. Wright, G. Bansal, P. Cho and H. Uludağ. Cleavage of disulfide-linked fetuin-bisphosphonate conjugates with three physiological thiols, *Biomacromolecules*, 6 (2005) 2800-2808.

INTRODUCTION

Hydroxyapatite (HA: $Ca_{10}(PO_4)_6(OH)_2$) is one of the most important bioceramics for medical and dental applications, as it is the main inorganic constituent of hard tissues like bone and teeth [1]. HA has been used in conjugation with protein growth factors to stimulate bone formation locally. The binding of proteins to the mineral is dependent on different structural properties of proteins; whereas some proteins, such as the members of Bone Morphogenetic Proteins (BMPs) exhibit strong affinity to mineralized matrices, other proteins do not exhibit a strong affinity to mineral matrices [2]. Previous studies showed that chemical derivatization of proteins with bisphosphonates (BPs) is an effective means to enhance the mineral affinity of a wide-range of proteins, irrespective of their size and the overall charge [3-9]. The BP-class of molecules has an exceptional affinity for bone mineral HA. They are chemical analogues of the endogenous pyrophosphate (H_2O_3P-O-PO_3H_2), where the central, hydrolytically liable P-O-P linkage has been replaced by the hydrolysis-resistant P-C-P linkage. This substitution also provides a center for derivatization so that a variety of structural modifications can be made on BPs [3].

Fetuin has been used as a model protein to investigate the factors influencing the imparted mineral affinity as a result of BP conjugation. Fetuin is one of the most abundant noncollagenous proteins found in bone, with a concentration of about 1 mg/g of bone in rat, bovine and human bone [10], and it plays an important role in modulating bone growth and remodeling as well as ectopic calcification *in vivo*. BPs were conjugated to both the peptide core and carbohydrate residues of the protein, and both types of conjugations imparted a high mineral affinity to the fetuin in proportion to the number of

BP substituted per protein [8]. The effect of tether length on the mineral affinity of fetuin-BP conjugates were also reported; it was possible to construct fetuin-BP conjugates with various tether lengths, but the shorter tether lengths gave a superior affinity to mineral matrices [9]. The BP conjugation scheme used to construct the desired conjugates relied on chemical cross-linkers that coupled the thiol group of a BP to an amine group of proteins via thioether linkages. These linkages were initially chosen since they are known to be stable under various conditions, such as the medium pHs and the presence of serum [5]. However, for *in vivo* applications, conjugates with cleavable linkage might be desirable since proteins can be released in free form *in situ* to perform their functions [11]. Bioconjugates with cleavable linkages are typically based on ester or disulfide linkages, which are both regarded as liable under physiological conditions [12,13]. In contrast to ester linkages that are sensitive to the presence of water (hence, making it difficult to work with ester-conjugates in aqueous buffers), the disulfide linkages are stable in aqueous conditions, but susceptible to cleavage with free thiols.

The purpose of this study was to explore the feasibility of constructing fetuin-BP conjugates with cleavable disulfide linkages. Commercially available *N*-succinimidyl-3-(2-pyridyldithio)propionate (SPDP) was used as a cross-linker to construct fetuin conjugates with a thiol-containing BP, 2-(3-mercaptopropylsulfanyl)-ethyl-1,1-bisphosphonic acid (thiolBP). The cleavage of the fetuin-thiolBP conjugates was investigated in the presence of three thiols: *L*-cysteine, *DL*-homocysteine, and *L*-glutathione. These compounds are the most abundant thiols in physiological milieu such as serum. Our results indicated that fetuin-thiolBP conjugates formed with disulfide

linkage imparted the desired mineral affinity to the fetuin, and that this affinity was eliminated upon cleavage of the disulfide linkage with thiols.

MATERIALS AND METHODS

Materials

SPDP was acquired from Molecular Biosciences (Boulder, CO). Fetuin, *L*-glutathione (reduced) and picrylsulfonic acid solution (TNBS; 5 (w/v) %) were obtained from Sigma (St. Louis, MO). N-ethylmaleimide (NEM) was obtained from Eastman Organic Chemicals (Rochester, NY). N,N-dimethylformamide (DMF) was from Caledon Laboratories (Georgetown, Ontario). Tetraethyl methyelenebisphosphonate, diethylamine, paraformaldehyde, calcium hydride (CaH_2), p-toluenesulfonic acid monohydrate, 1,3-propanedithiol, *DL*-homocysteine, aqueous tetrabutyl ammonium hydroxide and 60-270 mesh silica gel were acquired from Aldrich (Milwaukee, WI). Bromotrimethyl silane ($BrSi(CH_3)_3$) was obtained from Acros Organics (Fairlawn, NJ). Methanol, 1-butanol, carbontetrachloride (CCl_4), methylene dichloride (CH_2Cl_2), chloroform ($CHCl_3$), dimethyl sulphoxide (DMSO) and boric acid were from Fisher (Fairlawn, NJ). *L*-cysteine was obtained from J.T. Baker Chemical Co. (Phillipsburg, NJ). Toluene was obtained from BDH (Toronto, Ontario). 5,5'-Dithio-bis-(2-nitrobenzoic acid) (DTNB) was obtained from PIERCE (Rockford, IL). The Spectra/Por dialysis tubing with MW cutoff of 12–14,000 Da was acquired from Spectrum Laboratories (Rancho Dominguez, CA). The phosphate buffer (pH=7.0) used for conjugation reactions was obtained by mixing 0.1 M dibasic sodium phosphate and 0.1 M monobasic sodium phosphate solutions. The carbonate buffer (pH=10.0) used for dialysis was obtained by mixing 0.2 M sodium

bicarbonate and 0.2 M sodium carbonate solutions. The borate buffer (pH=9.4) used for TNBS assay was obtained by mixing 0.2 M boric acid in 0.1 M NaOH and 0.1 M NaOH to the appropriate pH value. In-house deionized water (ddH_2O) used for dialysis, and buffer preparations were derived from a Milli-Q purification system.

Synthesis of 2-(3-mercapto-propylsulfanyl)-ethyl-1,1-bisphosphonic acid (thiolBP, **Scheme 1**) [14]

Briefly, a mixture of diethylamine (0.58 g, 8 mmol) and paraformaldehyde (1.21 g, 40 mmol) in 24 mL of methanol was warmed until clear. Heat was removed, tetraethylmethylene-bisphosphonate ***1*** (2.33 g, 8 mmol) was added and the mixture was refluxed for 24 hours. Methanol was removed in *vacuo* and then toluene was added. Catalytic amount of p-toluenesulfonic acid monohydrate was added to the intermediate ***2***. The mixture was refluxed and concentrated after 14 hours. The product was diluted with $CHCl_3$ and washed with water, and then the organic layer was dried over $MgSO_4$. This gave 1.54 g (71% yield) of tetraethyl ethylidenebisphosphonate ***3***. Then ***3*** (0.79 g, 2.64 mmol) was dissolved in CH_2Cl_2 (10 mL) and $BrSi(CH_3)_3$ (3.85 ml, 29.10 mmol) was added dropwise using syringe at 0 °C, then reacted for 48 hours at room temperature. CH_2Cl_2 was evaporated under vacuum, the free acid was extracted into ddH_2O (1 mL) and neutralized with 40% aqueous tetrabutyl-ammonium hydroxide to pH=4. The solution was dried in *vacuo* at 50-60 °C and evaporated under the same conditions with 1-butanol (5 mL) to an oily residue ***4***. Then ***4*** was dissolved in 1-butanol (1 mL) and stirred with 1, 3-propanedithiol (1.33 mL, 13.22 mmol) for 2.5 hours at 118-124 °C under N_2 atmosphere. The mixture was cooled and diluted with H_2O. The unreacted materials

were thoroughly extracted with hexane. The aqueous layer was vacuum concentrated to give a yellow colored oily product, thiolBP ***5***, along with residual 1-butanol (1-butanol was not completely removed since it does not participate in conjugation reactions). The structure of thiolBP was confirmed by ^{1}H-NMR: δ_H (D_2O): 3.01 (td, 2H, J=6.7 and J=15.3), 2.71 (t, 2H, J=7.2), 2.63 (t, 2H, J=7.1), 2.37 (tt, 1H, J=6.7 and J=22.3), 1.90 (p, 2H, J=7.2), which were consistent with the reported values in the literature [15,16].

ThiolBP Conjugation to Fetuin (Scheme 2)

The conjugation method used in this study was similar to the published procedure from our group [5], except the thiol-reactive succinimidyl-4-(N-maleimidomethyl)-cyclohexane-1-carboxylate (SMCC) was replaced with thiol-reactive dithiopyridine-containing SPDP. Briefly, a fetuin solution (5 mg/mL in 100 mM phosphate buffer, pH=7.0) was incubated for 30 minutes with 5 mM NEM to extinguish any free thiols in fetuin. The NEM-treated fetuin solution was then incubated for 3 hours with various concentrations of SPDP (see **Figure** legends), which was initially dissolved in DMF. To remove the unreacted linker, the samples were thoroughly dialyzed against 100 mM phosphate buffer (pH=5.0). ThiolBP solutions (in 100 mM phosphate buffer, pH=7.0) were then added directly to the SPDP-reacted fetuin solutions at equal volumes to give final thiolBP concentrations of 2 mM. The reaction was allowed to proceed for 1 hour at room temperature, and the unreacted thiolBP was removed by dialysis against 200 mM carbonate buffer (×3) and ddH_2O (×2).

Extent of ThiolBP Substitution

The protein concentrations in dialyzed samples were determined using the Bradford Protein assay [17]: a 50 μL sample was added to 1 mL of the protein reagent, which consisted of 0.01% (w/v) Coomassie Blue R-250, 4.7% (w/v) ethanol, and 8.5% (w/v) phosphoric acid. The sample absorbances were determined at 595 nm. A calibration curve was based on known concentrations of fetuin standards. An organic phosphate assay [18] was then used to determine thiolBP concentration in samples. Briefly, 50 μL of sample was mixed with 30 μL of 10% $Mg(NO_3)_2$ in 95% ethanol in glass tubes and ashed over a flame. After boiling in 0.3 mL of 0.5 N HCl for 15 minutes, 0.1 mL of ascorbic acid (10% w/v) and 0.6 mL of $(NH_4)_6Mo_7O_{24}{\cdot}4H_2O$ (0.42% w/v in 1 N H_2SO_4) were added to the tubes and the samples were incubated at 37 °C for 1 hour. The absorbances were determined at 820 nm and a calibration curve based on known concentrations of thiolBP standards was used to calculate the thiolBP concentrations in the conjugate samples. The thiolBP concentration of a sample (mM) was divided by its protein concentration (mM) to yield an average thiolBP substitution, i.e., the number of thiolBPs conjugated per fetuin. When necessary, thiolBP was also conjugated to bovine serum albumin (BSA) using the methodology described for fetuin ([SPDP] = 2 mM, [thiolBP] = 1 mM in this case).

HA Binding Assay

The mineral affinity of proteins was determined by using a HA binding assay as described previously [5]. Briefly, a 100 μL protein sample was diluted to 400 μL with a 100 mM phosphate buffer to give a buffer molarity of 75 mM (pH=7.0). The diluted samples were then added to microcentrifuge tubes containing 5 mg of HA in duplicate.

As a reference (i.e., 0% binding), the samples were incubated in microcentrifuge tubes without HA. All samples were shaken for 3 hours at room temperature and centrifuged, and the protein concentration in the supernatant was determined using the Bradford assay. HA binding (expressed as %binding) was calculated as follows: 100% x [(protein concentration without HA) – (protein concentration with HA)] ÷ (protein concentration without HA).

DTNB and TNBS Assays [19]

In some studies, DTNB and TNBS assays were used for assessment of thiol and amine concentration in solution, respectively. For the DTNB assay, 20 μL of a solution is added to a cuvette along with 970 μL of 100 mM phosphate buffer (pH=7.0) and 10 μL of 100 mM DTNB (dissolved in DMSO). The solution was allowed to incubate for 15 minutes, and then the absorbance was read at 412 nm. For the TNBS assay, 20 μL of test sample, 130 μL of 100 mM phosphate buffer (pH=7.0) and 850 μL of 1 mM TNBS in borate buffer (pH=9.4) were added to a cuvette. Then the samples were incubated for 1 hour at 37 ^{o}C, and the absorbance was read at 367 nm. Known concentrations of thiol and amine compounds served for the respective calibration curves.

Conjugate Cleavage with *L*-Cysteine, *DL*-Homocysteine and *L*-Glutathione

The cleavage of conjugates in solution was determined by dialyzing the proteins against 50 mM Tris buffer (pH=7.0) containing varying concentrations of *L*-cysteine, *DL*-homocysteine and *L*-glutathione. Disulfide cleavage was expected to release free BPs to be removed by dialysis, leading to a reduction in thiolBP substitution of the proteins.

Following dialysis against Tris buffer, the samples were dialyzed extensively against double distilled water (ddH_2O) to remove the cleaving thiols from the protein solutions. Cleavage of disulfide linkages was expressed as the changes in BP substitution (i.e., changes in number of thiolBP per fetuin). HA binding assay was further carried out on these samples and the %HA binding was determined as mentioned above.

For conjugate cleavage on HA surfaces, the fetuin-thiolBP conjugates were initially bound to HA by adding 100 μL of protein sample and 200 μL of 150 mM phosphate to microcentrifuge tubes containing 5 mg of HA, and shaking for 3 hours at room temperature. The conjugate stability while bound to HA was then investigated by adding 100 μL of various concentrations of *L*-cysteine, *DL*-homocysteine and *L*-glutathione (0-10 mM) dissolved in 100 mM phosphate buffer (pH=7.0). The incubation was at room temperature on an orbital shaker. At desired time points, the tubes were centrifuged, and aliquots of the supernatant were taken for protein concentrations to be assessed with the Bradford assay. The %HA binding was calculated based on the amount of protein released into the supernatant.

RESULTS

The extent of thiolBP substitution on fetuin was shown in **Figure 3-1A**, where the thiolBP concentration during the conjugation reaction was maintained at 2 mM and the SPDP concentration was changed. Increasing the concentration of SPDP during the process of conjugation led to a concentration-dependent increase in the number of thiolBPs attached onto fetuin. The conjugates had 3.3 thiolBP/fetuin at the highest concentration of SPDP used (5 mM). The control conjugate (i.e., fetuin reacted with 0

mM SPDP) had 0.4 thiolBP/fetuin, which presumably reflected the fraction of thiolBP that was not removed by dialysis. The HA binding of the conjugate was proportional to the extent of thiolBP substitution (**Figure 3-1B**). These results also corroborated the fact that HA binding was mediated by the conjugated thiolBP.

Next, we explored the changes in the extent of thiolBP substitution for the conjugates after incubation with thiols (**Figure 3-2**). The conjugates were incubated with the chosen thiols for 24 hours in solution, and then dialyzed extensively to remove cleaved BP and the thiols. Incubation with *L*-cysteine, *DL*-homocysteine and *L*-glutathione all reduced the extent of thiolBP substitution of the conjugates. The extent of thiolBP substitution decreased as the concentration of thiols increased (**Figure 3-2A**). In line with the decrease in thiolBP substitution, the %HA binding of the conjugates was also decreased (**Figure 3-2B**). Changes in the thiolBP substitution and %HA binding both pointed out that *DL*-homocysteine had the highest ability to cleave the conjugates among the three thiols. The correlation between the extent of thiolBP substitution and the %HA binding is shown in **Figure 3-2C**. A single correlation between the two variables was evident among the cleaved samples. The extent of thiolBP cleavage, and the nature of thiol used for conjugate cleavage did not seem to result in a different type of correlation.

The cleavage of the fetuin-thiolBP conjugates was then investigated after the conjugates were bound to HA (**Figure 3-3**). It was not possible to directly detect the changes in thiolBP substitution, since the binding medium contained a high concentration of phosphate (100 mM phosphate buffer). Changes in %HA binding were assessed after 0, 4 and 24 hours of thiol incubation. The %HA binding was decreased with the increase of

thiol incubation time. Comparing the cleavage among the three thiols, *DL*-homocysteine again appeared to exhibit the highest cleavage ability.

In a parallel experiment, the DTNB and TNBS assays were used to investigate the binding of the cleaving thiols to HA (all thiol compounds had both $-NH_2$ and –SH groups). This was performed to investigate the changes in the thiol concentration, if any, during the cleavage period of HA-bound fetuin-thiolBP conjugates. The thiols were incubated with the HA in the absence of proteins. There was no significant loss of $-NH_2$ and -SH groups in the supernatants of HA incubated with *L*-cysteine, *DL*-homocysteine and *L*-glutathione (**Figure 3-4**), suggesting that there was little binding of the compounds to HA.

A critical issue is the relative effectiveness of the thiols to cleave the conjugates in solution vs. on HA. To this end, cleavage after 24 hours of thiol incubation was compared based on %HA binding results, after normalizing the results with respect to the conjugates incubated without any thiols (**Figure 3-5**; data from **Figure 3-2** and **Figure 3-3**). There was no significant difference in the effectiveness of *L*-cysteine (**Figure 3-5A**) and *DL*-homocysteine (**Figure 3-5B**) to cleave the conjugates either in solution or on HA. *L*-Glutathione, on the other hand, gave a better cleavage of the conjugates on HA (**Figure 3-5C**) that was most evident at the highest concentration (3 mM) tested.

Finally, the cleavage of BSA-thiolBP conjugates was investigated to determine the cleavage of conjugated thiolBP anchored with a disulfide-linkage to a different protein. As with fetuin, (i) all three thiols reduced the thiolBP substitution in a concentration-dependent manner upon incubation of BSA-thiolBP conjugates with thiols in solution, and (ii) *DL*-homocysteine gave the most cleavage with the BSA-thiolBP conjugates

(**Figure 3-6**). %HA binding of these conjugates was correspondingly reduced (not shown). A comparison of the cleavage of BSA-thiolBP conjugates in solution vs. on HA was shown in **Figure 3-7**. Similar to the results summarized in **Figure 3-5**, the cleavage of BSA-thiolBP conjugates was expressed as a percentage of uncleaved samples (i.e., conjugates incubated with 0 mM thiol). For *L*-cysteine (**Figure 3-7A**) and *DL*-homocysteine (**Figure 3-7B**), there was no difference in the two modes of cleavage but *L*-Glutatahione (**Figure 3-7C**) gave a higher cleavage on HA surface that was most evident at the highest incubation concentration (at 3 mM).

DISCUSSION AND CONCLUSIONS

The main objective of this work was to investigate the cleavage of the disulfide-linked fetuin-thiolBP conjugates by three thiol compounds commonly found in the physiological milieu. These results are preparatory to further studies designed to evaluate the potential application of the cleavable fetuin conjugates *in vivo*. The fetuin conjugates prepared for the thiol cleavage had thiolBP substitutions of 3.3-4.9 thiolBP per protein. This extent of substitution was sufficient to impart a significant mineral affinity, as evident by strong (>70%) HA binding in this study. Previous studies also indicated this level of substitution to be sufficient for a significant mineral affinity when calcium/phosphate-based scaffold are implanted subcutaneously in a rat model [8]. The BSA-thiolBP conjugates had higher thiolBP substitutions than the fetuin-thiolBP conjugates, consistent with the larger size of this protein (~66 kDa vs. ~48 kDa, respectively) and availability of greater numbers of $-NH_2$ groups for the SPDP derivatization.

The stereo configurations of the thiol compounds are shown below:

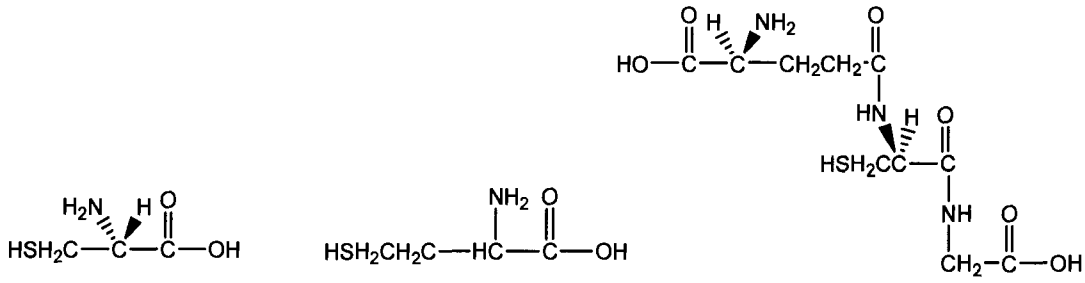

L-Cysteine

DL-Homocysteine

L-Glutathione (reduced)

The physiological concentration of *L*-cysteine in extracellular fluids such as plasma is 0.2-0.3 mM, at least 10-times higher than the other two thiol compounds used in this study (*DL*-homocysteine: ~0.01 mM; *L*-glutathione: ~0.01 mM) [20-22]. This makes *L*-cysteine most likely thiol for *in vivo* cleavage of disulfide-linked conjugates. Cysteinylglycine, another thiol with relatively high plasma concentration (0.03-0.06 mM), was not utilized in this study since we could not locate a commercial source of the compound. Many other thiol compounds, such as cysteamine, mycothiol, ergothioneine and ovothiol, are present in biological milieu but their concentrations are significantly lower than the thiol compounds employed in this study [23], and they are not expected to be significant participants in the disulfide cleavage. *L*-Glutathione is unique among the thiols in that it is the predominant low molecular-weight thiol (0.5-10mM) present intracellularly, but its extracellular concentration is relatively low (e.g. 0.002-0.02mM in plasma) [24]. Thus, *L*-glutathione may be the most significant participant in the intracellular cleavage of the disulfide-linked BP conjugates. This study did not address the cell-based cleavage of BP conjugates. Whereas *L*-glutathione was largest among the thiol compounds used in this study, the cysteine precursor *DL*-homocysteine contained a -SH group that was separated form the α-C with an extra methylene group. This makes

the –SH group of *DL*-homocysteine sterically less hindered. All three thiol compounds gave identical calibration curves (absorbance at 412 nm vs. molar concentration) by the DTNB assay (not shown), indicating that the compounds had equivalent thiol content per mol basis, and were not oxidized.

All three thiols cleaved the fetuin-thiolBP conjugates in a concentration-dependent manner, as evident by the reduction in thiolBP substitution, and loss of HA affinity. Significant cleavage was observed at thiol concentrations of ~0.3 mM (the physiological concentration of *L*-cysteine) but not at ~0.1 mM or less (the physiological concentrations of *DL*-homocysteine and *L*-glutathione). Based on the established mechanism of disulfide cleavage [25], the cleavage should occur by: (i) ionization of the attacking thiol ($R-SH \leftrightarrow R-S^{-}+H^{+}$); (ii) nucleophilic attack of the resultant thiolate on the disulfide ($Fetuin-S-S-BP+R-S^{-} \leftrightarrow Fetuin-S-S-R+^{-}S-BP$), and; (iii) protonation of the leaving thiolate group ($^{-}S-BP+H^{+} \leftrightarrow HS-BP$). The concentration dependent cleavage is consistent with the availability of increasing thiolate concentration in the reaction medium. Since the cleavage is performed with the thiolate anion (rather than unionized thiol), the extent of thiol ionization will determine the disulfide cleavage rate. The fractional dissociation (i.e., [RS^{-}]/[RSH]) of thiol compounds is dictated by their ionization constants (pKa), which are 8.37, 8.87 and 8.75 for *L*-cysteine, *DL*-homocysteine, and *L*-glutathione at 25 °C, respectively [26]. The fractional dissociation is given by $10^{-pKa}/(10^{-pKa} + 10^{-pH})$ [25]. Given the medium pH of 7.0 in our studies, the fractional dissociation of *L*-cysteine, *DL*-homocysteine, and *L*-glutathione was expected to be 0.041, 0.013 and 0.017, respectively. Assuming an equivalent reactivity of the thiolate anions (i.e., irrespective of the parent thiol compound), *L*-cysteine was expected

to give the highest cleavage rate, whereas *DL*-homocysteine was expected to give the lowest cleavage at a fixed thiol concentration. This was contrary to our observations, where *DL*-homocysteine yielded the highest extent of disulfide cleavage rate among the three thiols (see **Figures 3-2**, **3-3**, and **3-6**). Therefore, *DL*-homocysteine thiolate seems to be intrinsically more reactive towards the disulfide linkage, possibly due to less steric hindrance of the thiolate anion for the disulfide attack. The *L*-glutathione and *L*-cysteine had similar cleavage rates of the disulfide linkage, despite the expected lower extent of *L*-glutathione dissociation, and the larger size of the glutathione thiolate that will lead to more sterically hindered thiolate.

The established mechanism of disulfide cleavage also suggests the incorporation of the cleaving thiolate into conjugates. We were concerned that the HA affinity of the cleaved conjugate might have been differentially affected by the nature of the cleaving thiol in this case. **Figure 3-2C**, however, indicates that once the thiolBP is cleaved from the conjugate, the HA affinity was significantly diminished and that the final product, irrespective of the cleaving thiol compound, appeared to have a similar correlation between the extent of thiolBP substitution remaining and the resultant HA affinity. This was additionally supportive of the thiolBP to be primarily responsible for the exhibited HA affinity under our experimental conditions, rather than other functional groups on the proteins.

The cleavage experiments were also performed when the thiolBP-conjugates were already bound to HA. This was important to explore since, after the conjugates are delivered *in vivo*, the contact of proteins with circulating thiols might be obscured due to protein binding to the mineral matrix. Our earlier studies suggested a difference in the

rate of disulfide cleavage (cleaving species: *L*-cysteine) whether the conjugates were in solution or on HA [14]. The results in this study showed no significant difference in conjugate cleavage in solution and on HA surface when the cleaving species was *L*-cysteine and *DL*-homocysteine. This was the case for both fetuin and BSA conjugates with different extent of thiolBP substitutions. Interestingly, cleavage by *L*-glutathione was enhanced on HA surfaces for both fetuin and BSA conjugates. We initially thought that differences in the HA binding of thiols might lead to differential thiol concentration on HA surfaces (e.g., if *L*-glutathione had bound better to HA), and this might have explained better cleavage of HA-bound conjugates with *L*-glutathione. Our data, however, indicated no significant binding of any of the thiols to HA (see **Figure 3-4**). We also envisioned the possibility of differences in soluble thiol oxidation during the cleavage reaction, but data in **Figure 3-4** also argues against this possibility since insignificant loss of thiol was noted during the cleavage experiments. Therefore, the reason(s) for the better *L*-glutathione-mediated cleavage of conjugates on HA is not presently known.

Our future studies will focus on *in vivo* cleavage of the disulfide tethers in the thiolBP conjugates. Since the BP-conjugates could be used for systemic therapy after intravenous injection, or local therapy after implantation with mineral-based carriers, it will be critical to determine the cleavage rates once the conjugates reach to bones in the former case, or after the conjugates are implanted with matrices in the latter case. Conjugate cleavage *in vitro* did not seem to require any additional components apart from the cleaving thiol compounds, but it will be important to determine if this is the case *in vivo* as well, or if enzymatic components in plasma or bone environment will contribute to the conjugate cleavage as well.

In conclusion, the results of this study indicated that thiolBP conjugation to fetuin was controlled by varying the concentrations of the crosslinker SPDP. The extent of HA binding was proportional to the thiolBP substitution on the conjugates. The cleavage of the disulfide linkage in thiolBP-fetuin conjugates was explored by the physiological thiols *L*-cysteine, *DL*-homocysteine and *L*-glutathione, and all three thiols were found to be capable of cleaving the conjugates. *DL*-homocysteine exhibited the fastest cleavage of conjugates in solution, possibly due to less sterically hindered thiol in this compound. The %HA binding of the conjugates was decreased in line with the removal of thiolBP from the conjugates. Two ways of cleavage of protein-thiolBP conjugates, in solution and on HA surface, were performed, and our results showed no significant difference between these two cleavage methods for *L*-cysteine and *DL*-homocysteine, while *L*-glutathione cleaved the conjugates better after the proteins were bound to HA surfaces. Future studies will focus on *in vivo* delivery of the cleavage in order to assess cleavage kinetics of the disulfide-linked thiolBP conjugates under physiological conditions[#].

This disulfide cleavage of protein-BP conjugate was further evaluated *in vivo* with a subcutaneous implant model in rats, in comparison with the stable thioether linkages, and reported by our group (J.E.I. Wright et al., *Biomaterials*, 27 (2006) 769-784).

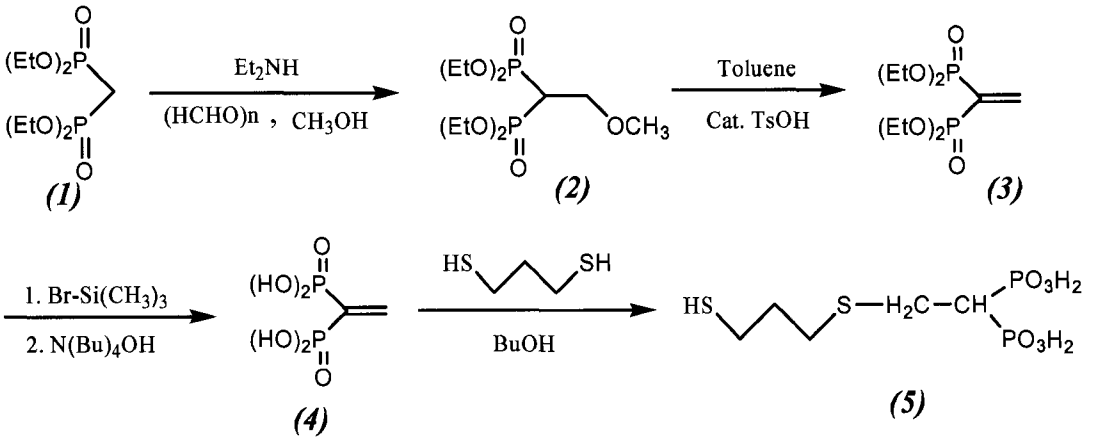

Scheme 3-1. Synthesis steps for the preparation of thiolBP (**5**) used in this study.

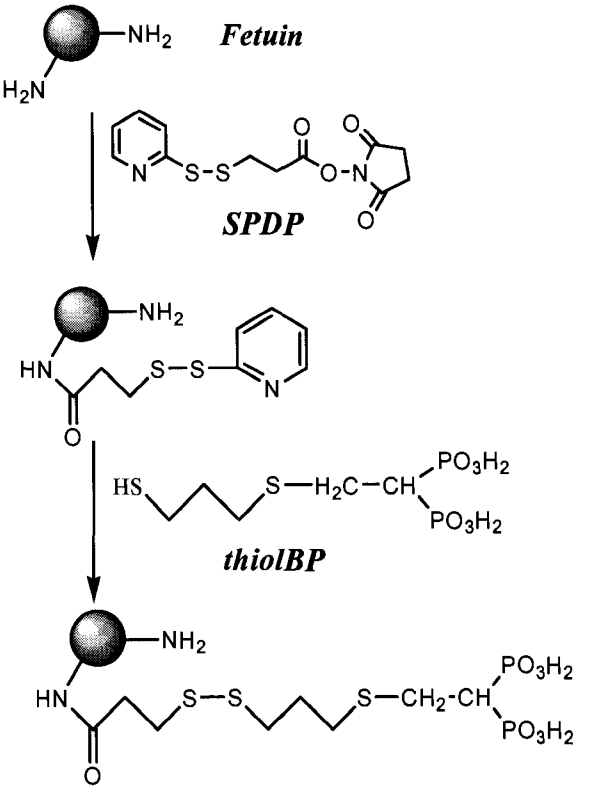

Scheme 3-2. Conjugation of thiolBP to fetuin in a two-step procedure by using the SPDP linker.

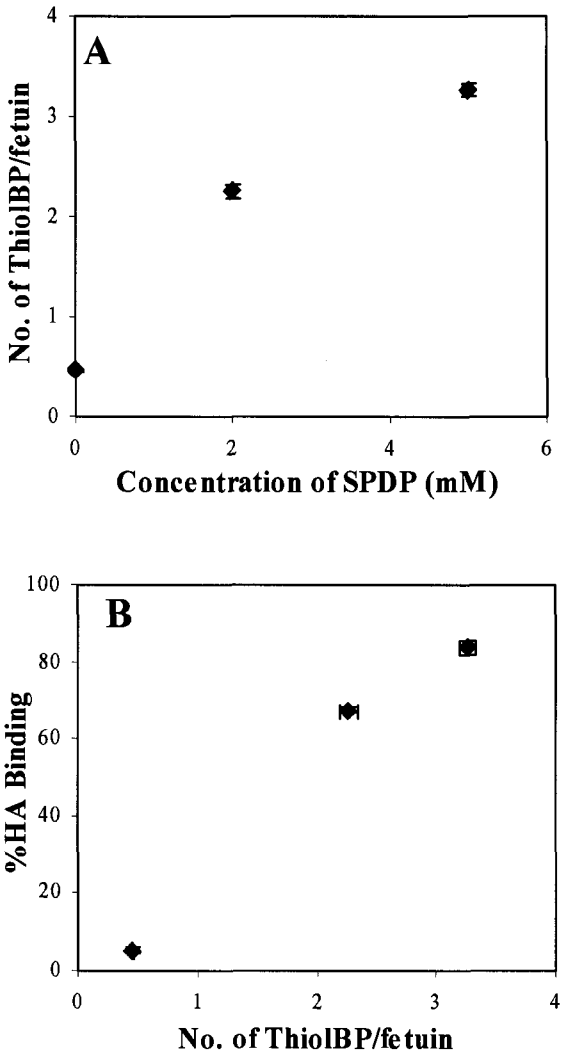

Figure 3-1. ThiolBP substitution on fetuin at various concentrations of SPDP (**A**) and %HA binding of the conjugates (**B**). The protein samples were first reacted with the indicated SPDP concentrations, then incubated with 2 mM thiolBP for 1 hour, and finally dialyzed to remove unreacted compounds. For control fetuin, there was a small extent of thiolBP remaining in the sample but no significant HA binding. The conjugates with >2 thiolBP/fetuin gave a strong %HA binding.

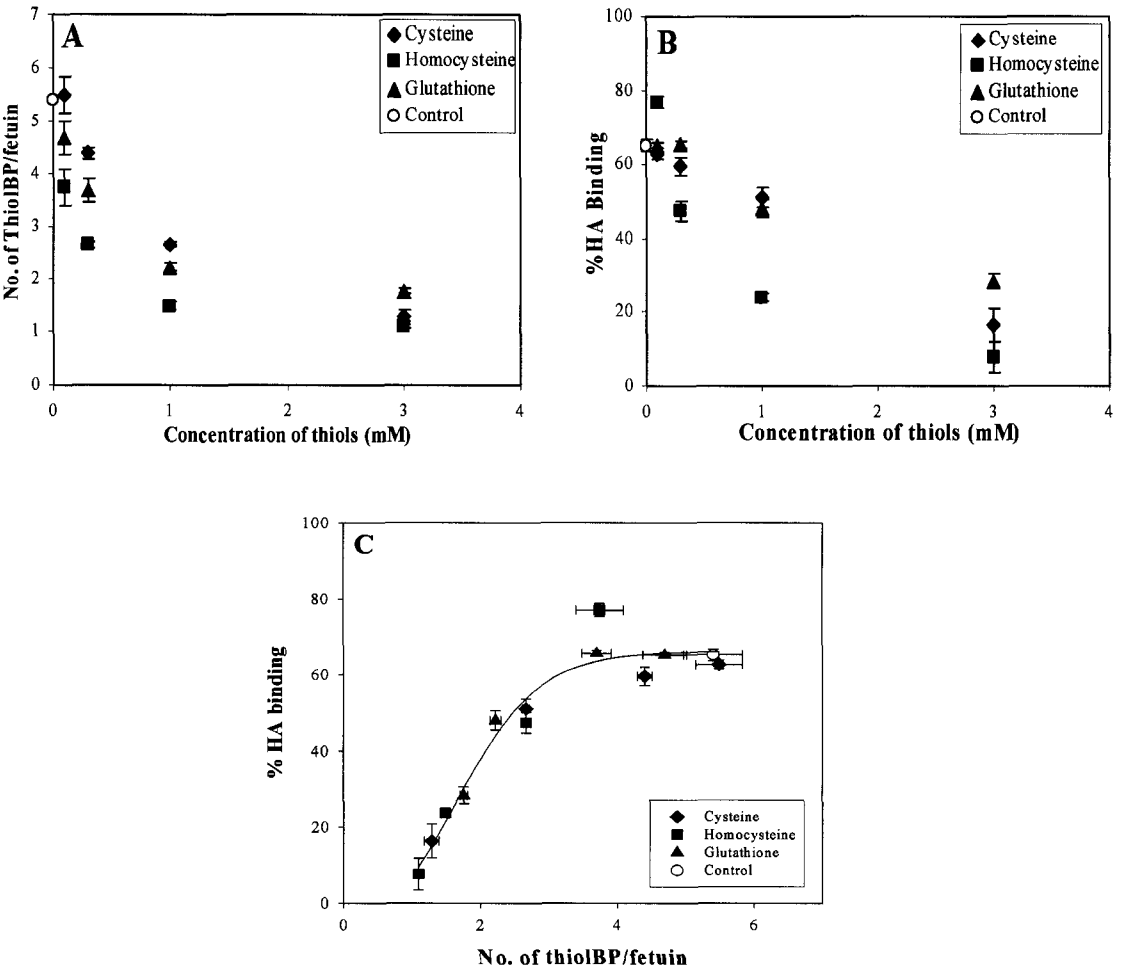

Figure 3-2. Changes in thiolBP substitution of the conjugates after incubation with 0 (control), 0.1, 0.3, 1 and 3 mM *L*-cysteine, *DL*-homocysteine and *L*-glutathione. Conjugates were incubated with the thiols for 24 hours, and the number of thiolBP/fetuin was determined for each sample after extensive dialysis. **A.** A decline in the thiolBP substitution was evident as the concentration of thiols was increased. **B.** %HA binding was also decreased for the conjugates incubated with all of the thiols. **C.** Correlation between %HA binding and thiolBP substitution of the conjugates (data from **A** and **B** were combined for this analysis). All results are mean ± SD of duplicate measurements. Based on **A** and **B**, *DL*-homocysteine appeared to exhibit the fastest cleavage rate among the three thiols.

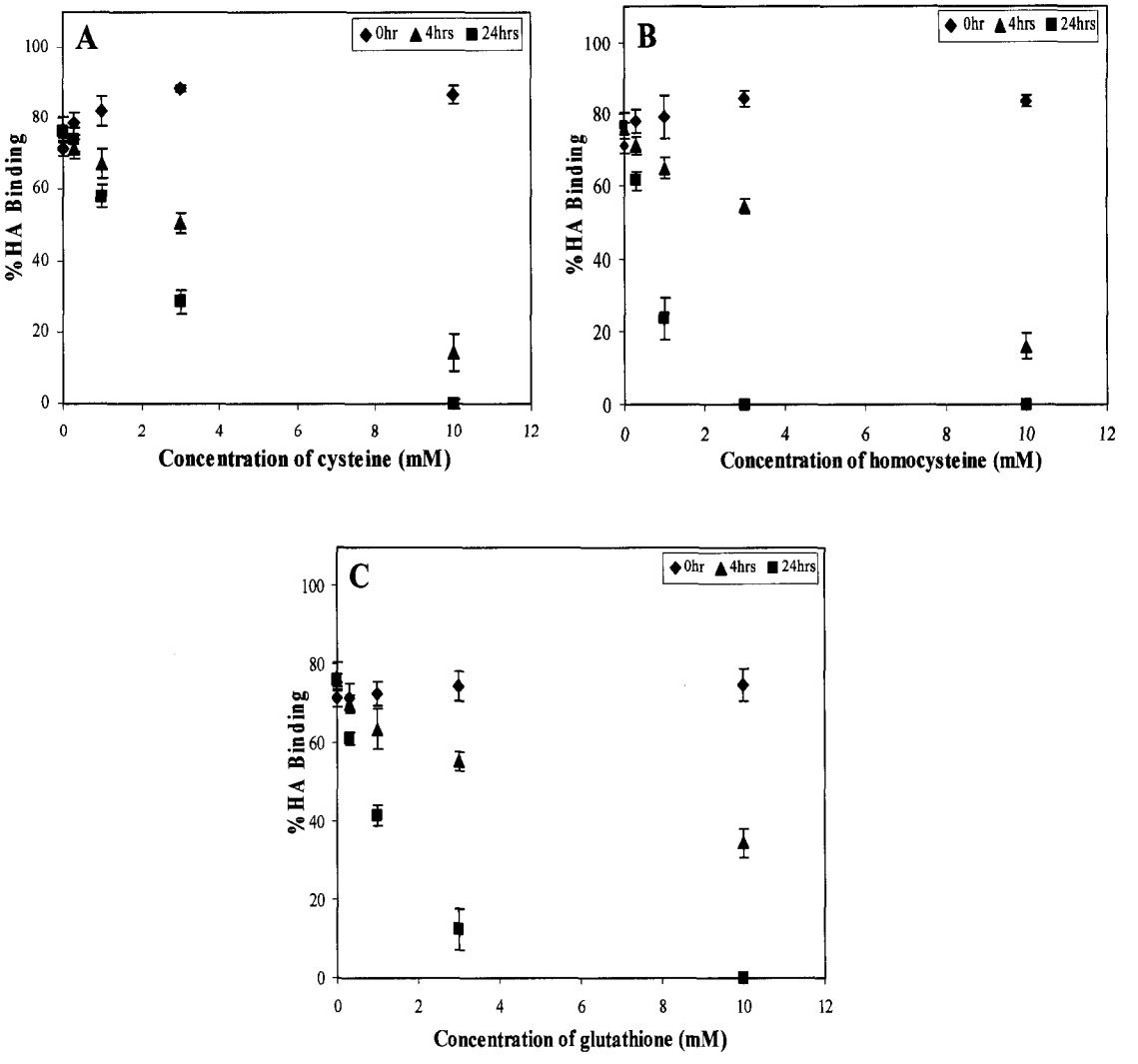

Figure 3-3. Changes in %HA binding of the conjugates after incubation of HA-bound conjugates with *L*-cysteine (**A**), *DL*-homocysteine (**B**) and *L*-glutathione (**C**). The conjugates were first allowed to bind to HA for 3 hours, followed by the addition of the thiols to the HA supernatants while on an orbital shaker. The protein concentrations in the supernatants were determined at 0, 4 and 24 hours to calculate %HA binding. The %HA binding decreased with (i) increasing incubation time, and (ii) increasing thiol concentration. A similar trend was observed for the three chosen thiols, and *DL*-homocysteine exhibited the most conjugate cleavage after 24 hours among the three thiols.

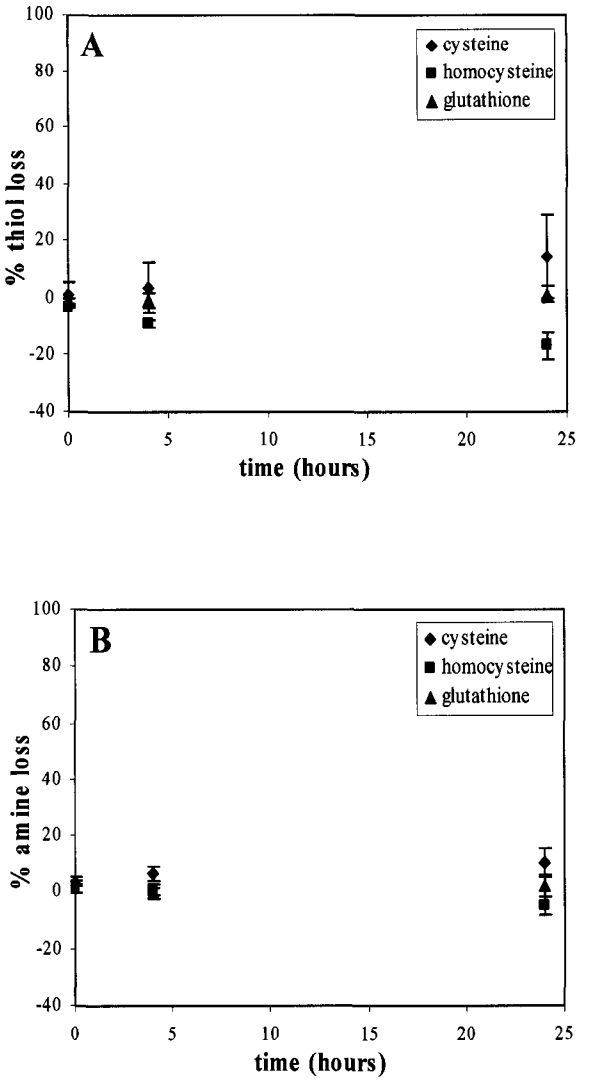

Figure 3-4. Changes in thiol and amine concentrations (mean ± SD) when the indicated thiols were incubated with HA in the absence of proteins. DTNB and TNBS assays were used for thiol and amine groups in solution, respectively. Both the thiol groups (**A**) and the amine groups (**B**) did not change significantly during the 24 hour incubation period, indicating little binding of the thiol compounds to the HA.

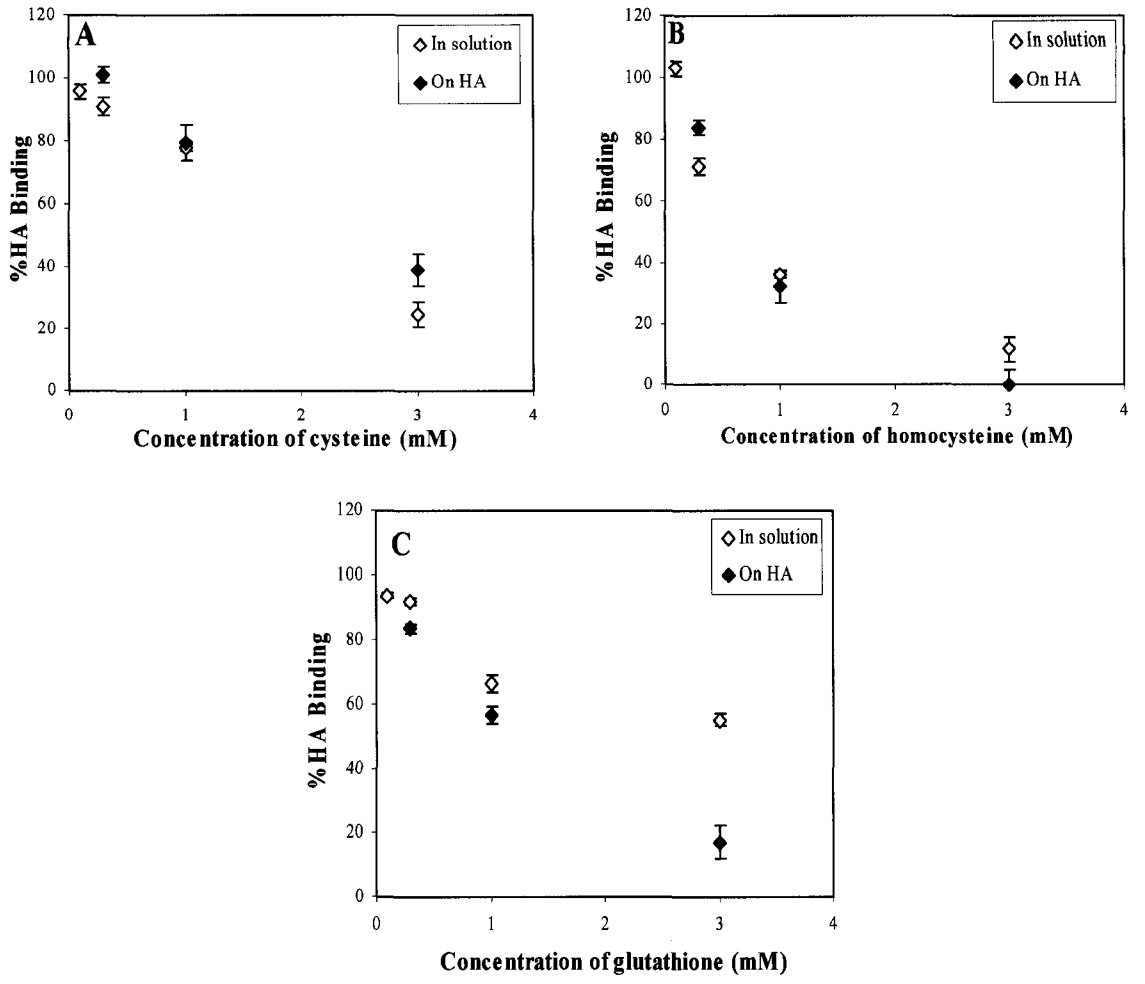

Figure 3-5. Comparison of the cleavage of fetuin-thiolBP conjugates in solution and bound to HA. The data from **Figure 3-2B** and **Figure 3-3** (only 24 hour time point) were normalized with respect to incubation with 0 mM thiol (control sample) to directly compare the two modes of cleavage. There was no difference in cleavage in solution or on HA when the conjugates were incubated with *L*-cysteine and *DL*-homocysteine, while *L*-glutathione cleaved the conjugates to a higher extent on HA surface (especially at the highest concentration used).

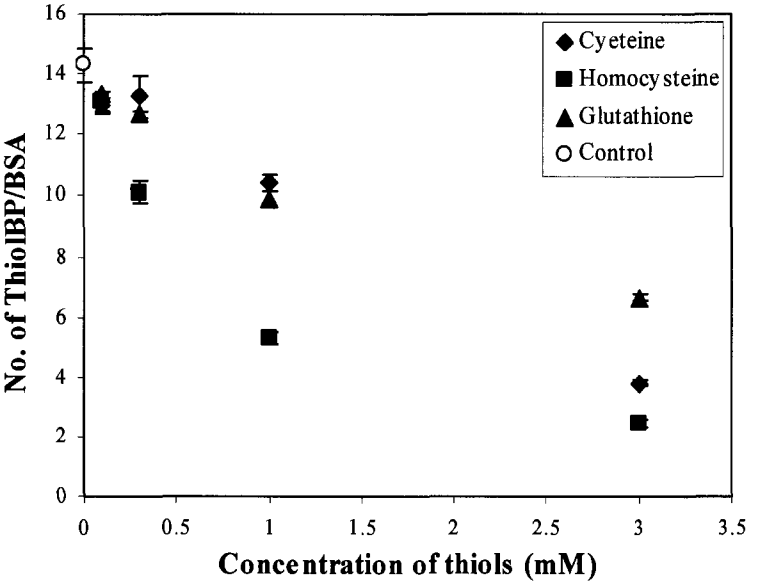

Figure 3-6. Changes in the thiolBP substitution for BSA-thiolBP conjugates in solution after incubation with *L*-cysteine, *DL*-homocysteine, and *L*-glutathione. The control refers to the conjugate sample incubated without any thiols (i.e., uncleaved). The thiolBP substitution was decreased with increasing thiol concentrations in solution and *DL*-homocysteine exhibited the highest cleavage ability among the three thiols.

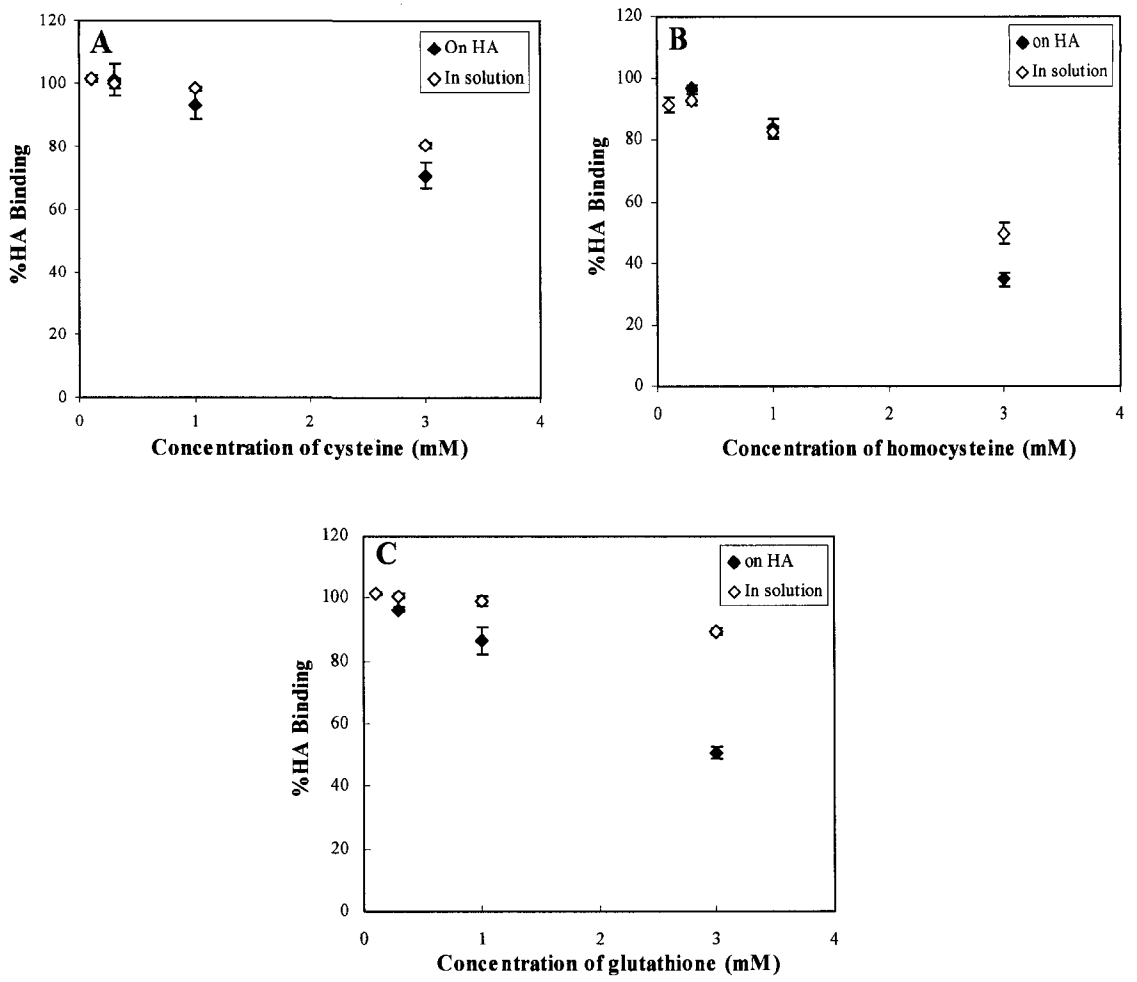

Figure 3-7. Comparison of the cleavage of BSA-thiolBP conjugates in solution and bound to HA. As in **Figure 3-5**, the data in this figure was obtained by normalizing the conjugate cleavages with respect to an uncleaved sample (i.e., sample incubation with 0 mM thiol) to directly compare the two modes of cleavage. The two modes of cleavage were similar for the samples incubated with *L*-cysteine and *DL*-homocysteine, while *L*-glutathione cleaved the conjugates to a higher extent on HA surface (especially at the highest concentration used).

References

[1] S. M. Kenny and M. Buggy, Bone cements and fillers: A review, *J. Mater. Sci. Mater. Med.*, 14 (2003) 923-938.

[2] M. J. Gorbunoff, The interaction of proteins with hydroxyapatite: I. Role of protein charge and structure, *Anal. Biochem.*, 136 (1984) 425-432.

[3] H. Uludağ, Bisphosphonates as a foundation of drug delivery to bone, *Curr. Pharm. Des.*, 8 (2002) 1929-1944.

[4] H. Uludağ, T. Gao, G. R. Wohl, D. Kantoci, and R. F. Zernicke, Bone affinity of a bisphosphonate-conjugated protein *in vivo*, *Biotechnol. Prog.*, 16 (2000) 1115-1118.

[5] H. Uludağ and J. Yang, Targeting systemically administered proteins to bone by bisphosphonate conjugation, *Biotechnol. Prog.*, 18 (2002) 604-611.

[6] H. Uludağ, N. Kousinioris, T. Gao, and D. Kantoci, Bisphosphonate conjugation to proteins as a means to impart bone affinity, *Biotechnol. Prog.*, 16 (2000) 258-267.

[7] G. Bansal, S. A. Gittens, and H. Uludağ, A di(bisphosphonic acid) for protein coupling and targeting to bone, *J. Pharm. Sci.*, 93 (2004) 2788-2799.

[8] S. A. Gittens, J. R. Matyas, R. F. Zernicke, and H. Uludağ, Imparting bone affinity to glycoproteins through the conjugation of bisphosphonates, *Pharm. Res.*, 20 (2003) 978-987.

[9] S. A. Gittens, P. Kitov, J. R. Matyas, R. Lobenberg, and H. Uludağ, Impact of tether length on bone mineral affinity of protein-bisphosphonate conjugates, *Pharm. Res.*, 21 (2004) 608-616.

[10] P. A. Price and J. E. Lim, The inhibition of calcium phosphate precipitation by fetuin is accompanied by the formation of a fetuin-mineral complex, *J. Biol. Chem.*, 278 (2003) 22144-22152.

[11] B. Jing, V. Janout, and S. L. Regen, Fully detachable molecular umbrellas as peptide delivery agents, *Bioconjug. Chem.*, 14 (2003) 1191-1196.

[12] F. Kratz, U. Beyer, and M. T. Schutte, Drug-polymer conjugates containing acid-cleavable bonds, *Crit. Rev. Ther. Drug Carrier Syst.*, 16 (1999) 245-288.

[13] G. Saito, J. A. Swanson, and K. D. Lee, Drug delivery strategy utilizing conjugation via reversible disulfide linkages: role and site of cellular reducing activities, *Adv. Drug Deliv. Rev.*, 55 (2003) 199-215.

[14] G. Bansal, J. E. I. Wright, S. Zhang, R. F. Zernicke, and H. Uludağ, Imparting mineral affinity to proteins with thiol-labile disulfide linkages, *J. Biomed. Mater. Res. Part A*, 74 (2005) 618-628.

[15] I. S. Alferiev, N. R. Vyavahare, C. X. Song, and R. J. Levy, Elastomeric polyurethanes modified with geminal bisphosphonate groups, *J. Polym. Sci. Part A: Polym. Chem.*, 39 (2001) 105-116.

[16] C. R. Degenhardt and D. C. Burdsall, Synthesis of ethenylidenebis(phosphonic acid) and its tetraalkyl esters, *J. Org. Chem.*, 51 (1986) 3488-3490.

[17] M. M. Bradford, A rapid and sensitive method for the quantitation of microgram quantities of protein utilizing the principle of protein-dye binding, *Anal. Biochem.*, 72 (1976) 248-254.

[18] B. N. Ames, Assay of inorganic phosphate, total phosphate and phosphatases, in: S. P. Colowick and N. Kaplan (Eds.), *Methods in Enzymology,* Academic Press, New York, 1966, pp. 115-118.

[19] J. Bullock, S. Chowdhury, A. Severdia, J. Sweeney, D. Johnston, and L. Pachla, Comparison of results of various methods used to determine the extent of modification of methoxy polyethylene glycol 5000-modified bovine cupri-Zinc superoxide dismutase, *Anal. Biochem.*, 254 (1997) 254-262.

[20] A. Pastore, R. Massoud, C. Motti, A. L. Russo, G. Fucci, C. Cortese, and G. Federici, Fully automated assay for total homocysteine, cysteine, cysteinylglycine, glutathione, cysteamine, and 2-mercaptopropionylglycine in plasma and urine, *Clin. Chem.*, 44 (1998) 825-832.

[21] A. Hernanz, E. Fernβndez-Vivancos, C. Montiel, J. J. Vazquez, and F. Arnalich, Changes in the intracellular homocysteine and glutathione content associated with aging, *Life Sci.*, 67 (2000) 1317-1324.

[22] D. W. Jacobsen, V. J. Gatautis, R. Green, K. Robinson, S. R. Savon, M. Secic, J. Ji, J. M. Otto, and L. M. Taylor, Jr., Rapid HPLC determination of total homocysteine and other thiols in serum and plasma: sex differences and correlation with cobalamin and folate concentrations in healthy subjects, *Clin. Chem.*, 40 (1994) 873-881.

[23] C. Bayle, E. Caussé, and F. Couderc, Determination of aminothiols in body fluids, cells, and tissues by capillary electrophoresis, Electrophoresis, 25 (2004) 1457-1472.

[24] G. Wu, Y. Z. Fang, S. Yang, J. R. Lupton, and N. D. Turner, Glutathione metabolism and its implications for health, *J. Nutr.*, 134 (2004) 489-492.

[25] J. Bai, B. Acan, A. Ghahary, B. Ritchie, V. Somayaji, and H. Uludağ, Poly(ethyleneimine)/arginine-glycine-aspartic acid conjugates prepared with N-succinimidyl 3-(2-pyridyldithio)propionate: An investigation of peptide coupling and conjugate stability, *J. Polym. Sci. Part A: Polym. Chem.*, 42 (2004) 6143-6156.

[26] R. M. C. Dawson, D. C. Elliott, W. H. Elliott, and K. M. Jones, *Data for Biochemical Research*, Clarendon Press, Oxford, 1986.

CHAPTER IV

The Interaction of Cationic Polymers and Their Bisphosphonate Derivatives with Hydroxyapatite[1]

[1]The contents of this chapter have been previously published in: S. Zhang, J.E.I. Wright, N. Özber and H. Uludağ. The interactions of cationic polymers and their bisphosphonate derivatives with hydroxyapatite, *Macromol. Biosci.*, 7 (2007) 656-670.

INTRODUCTION

Bisphosphonates (BPs) is a class of bone-seeking compounds due to the strong affinity of the spatially-optimized anionic phosphonates to bone mineral. BPs originated from the inorganic pyrophosphonate, which binds to bone mineral surface and prevents its dissolution. By replacing the P-O-P linkage in pyrophosphates with the P-C-P linkage, BPs become resistant to hydrolysis, and exhibit a prolonged persistence *in situ* [1]. A high percentage of administered BPs deposits to bones, and get concentrated at sites with a high metabolic turnover [2]. Because of this unique feature, much effort has been made to conjugate therapeutic agents with BPs to impart osteotropicity to the agents. Previous studies demonstrated that direct conjugation of BPs onto proteins is an effective means to enhance the mineral affinity of a wide-range of proteins, such as albumin (66 kDa), lysozyme (14 kDa) and Imunoglobulin G (150 kDa) [3-6]. Retaining bioactivity after conjugation is the central issue with the BP-derivatized proteins. In order to design bone-seeking proteins with minimal modification, dendritic BPs with two and four copies of BPs in a single molecule, were synthesized [6,7] with the purpose of introducing a high density of bisphosphonic acids on a single protein site. These multimeric BPs were advantageous over the conventional BPs for bone targeting, but did not exhibit a proportional increase in bone targeting efficiency as the BP content was increased. Presumably, a lack of flexibility in such compounds and possible steric hindrances to mineral access limited the ability of the compounds to impart a stronger mineral affinity to the conjugated molecules.

An alternative to such sterically constrained ligands is polymers incorporating multiple copies of BPs. Polymeric drug delivery systems are well-known for their ability

to provide a longer half-life of therapeutics in circulation, increasing drug solubility and stability, and improving the therapeutic efficiency for certain proteins and cancer therapies [8]. By employing polymers as an intermediate between a protein and BPs, multiple copies of BPs can be linked to proteins via a flexible linkage. This approach is preferable to directly conjugating several BPs onto proteins, in that a possible adverse effect on protein bioactivity could be minimized due to the need for minimal attachment site on proteins. The polymeric ligands for bone-targeting was initially reported by Kopeček group, based on N-(2-hydroxypropyl)methacrylamide (HPMA) polymers with bone-targeting alendronate ((4-amino-1-hydroxybutylidene)bisphosphonic acid) and poly-*D*-Aspartic acid moieties [9]. Wang et al [10] synthesized a poly(N-isopropylacrylamide)-based hydrogel with pamidronate ((3-amino-1-hydroxypropylidene)bisphosphonic acid), where pamidronate was incorporated into polymers with a monomeric BP suitable for polymerization.

We propose to construct polymeric bone-targeting ligands by conjugating a conventional BP, 2-(3-mercaptopropylsulfanyl)-ethyl-1,1-bisphosphonic acid (thiolBP), to poly(*L*-lysine) (PLL) and poly(ethylenimine) (PEI). PLL and PEI are two cationic polymers previously used for drug delivery; whereas PEI is a synthetic polymer, PLL is a polypeptide composed of the amino acid lysine. Ample primary amines are available in the polymers for chemical modification, so that multiple ligands can be introduced into the polymers, as was the case of chlorin *e6* conjugation to PLL in photodynamic therapy [11], and β-cyclodextrin conjugation to PEI in DNA delivery [12]. A critical issue in designing such linkers is the inherent affinity of the cationic polymers for HA. Cationic proteins, such as lysozyme, are known to bind to bone mineral [13], and polycations with

a high density of positive charges might exhibit a similar interaction. The HA, $Ca_{10}(PO_4)_6(OH)_2$, with its ensemble of oppositely charged ions [14], displays a slightly negative surface charge under physiological milieu since the point of zero charge of HA is ~7.3 [15], making it conducive for binding of cationic molecules.

This paper represents the first step in our efforts to construct bone-targeting technology based on polymeric-BP linkers. By utilizing two separate crosslinkers, *N*-hydroxysuccinimidyl polyethyleneglycol maleimide (NHS-PEG-MAL) for PLL and succinimidyl-4-(N-maleimidomethyl)-cyclohexane-1-carboxylate (SMCC) for PEI, polymer-BP conjugates were constructed. The mineral affinity of the conjugates was compared to the affinity of native polymers. The binding was assessed in the absence of competing ions (conditions conducive for molecular binding), as well as in high phosphate buffers, which compete effectively for binding of macromolecules to the mineral phase. In addition, binding in the presence of serum was assessed to mimic the *in situ* conditions. Finally, the mineral affinity of a select set of polymers was evaluated in a rat subcutaneous implant model using mineral-based carriers. Our results indicated that the chosen cationic polymers displayed a strong mineral affinity, and BP conjugation to the polymers did not impart any additional mineral affinity to the polymers.

MATERIALS AND METHODS

Materials

The synthesis of 2-(3-mercaptopropylsulfanyl)-ethyl-1,1-bisphosphonic acid (thiolBP) was described in Ref [16]. Branched PEIs (M_w ~25 kDa and M_w ~2 kDa), and triethylamine were obtained from Aldrich (Milwaukee, WI). HBr salt of PLL with

different MWs, acetic anhydride, picrylsulfonic acid solution (TNBS; 5% w/v), 1,3,4,6-tetrachloro-3α,6α-diphenylglycouril (TCDG), and N-succinimidyl-3-(4-hydroxy-phenyl) propionate (SHPP) were obtained from Sigma (St. Louis, MO). Fluorescein isothiocyanate (FITC) was obtained from PIERCE (Rockford, IL). $Na^{125}I$ (in 100 mM NaOH) was obtained from Perkin-Elmer (Wellesley, MA). SMCC was from Molecular Biosciences (Boulder, CO) and NHS-PEG-MAL (3.4 kDa) from NEKTAR (Huntsville, AL). The Spectra/Por dialysis tubing with 12–14 kDa cut-off was acquired from Spectrum Laboratories (Rancho Dominguez, CA). Distilled/de-ionized water (ddH_2O) used for buffer preparations were derived from a Milli-Q purification system. Serum used in binding studies were freshly prepared from Sprague-Dawley rats, after allowing the blood obtained by cardiac puncture to clot, and removing the clotted fraction by centrifugation (stored at -20 °C). The Skelite™ implants were obtained from Millenium Biologix Inc. (Mississauga, Ontario). Synthetic HA was prepared according to the method of Tiselius et al. [17], with modifications of Bernardi et al [18]. Briefly, 200 mL of 0.5 M $CaCl_2$ and 200 mL of 0.5 M Na_2HPO_4 were added to 20 mL of 1 M NaCl at a rate of 250 mL/hour under stirring. The precipitate was washed with ddH_2O, suspended in 400 mL dH_2O, and 10 mL of 40% (w/w) NaOH was added to the precipitate. The mixture was boiled for 1 hour under stirring, washed with ddH_2O, re-suspended in 400 mL of 10 mM sodium phosphate buffer (pH=6.8) and heated to just boiling. This was repeated once more with 1 mM sodium phosphate buffer and the mixture was boiled for 5 minutes. The HA crystals were blade-like (see Supplementary SEM image, **Figure S4-1**), as described in the original procedure.

ThiolBP Conjugation to Polymers (Scheme 4-1)

Conjugation of thiolBP to PLL. The PLL used in conjugations was labeled with FITC to better quantify the polymer amounts in samples at low polymer concentrations. The PLL was first dissolved in 100 mM phosphate buffer (pH=7.0), precipitated with excess ethanol, and washed with 100% ethanol to remove small amines that might have interfered with conjugation reactions. The PLL (2 mg/mL in 100 mM phosphate) was then incubated with 0.1 mM FITC (prepared as 10 mM stock solution in DMSO) for 2 hours, and precipitated by 100% ethanol and re-dissolved in phosphate buffer (100 mM, pH=7.0) before conjugations. The thiolBP was conjugated to FITC-labeled PLL by using NHS-PEG-MAL as the linker. The NHS-PEG-MAL and thiolBP was separately dissolved in 100 mM, pH=7.0 phosphate (5 and 10 mM, respectively), and mixed at equal volumes for 1 hour at room temperature (see Legends for exact concentrations). Then, FITC-PLL dissolved at 2 mg/mL in 100 mM phosphate (pH=7.0) was added to this solution at equal volume, and incubated for 2.5 hours at room temperature. To remove the unreacted linker and thiolBP, the samples were thoroughly dialyzed against 200 mM carbonate buffer (×3) followed by dialysis against ddH_2O (×2).

Conjugation of thiolBP to PEI. A series of SMCC solutions dissolved in DMF was mixed with equal volume of thiolBP solutions in 100 mM phosphate buffer (pH=7.0) for 1 hour at room temperature (see Legends for exact concentrations). The PEI solutions (3.2 mg/mL in 100 mM, pH=7.0 phosphate buffer; PEI purified by dialysis) were then added to the SMCC/thiolBP solutions at equal volumes, and incubated for 2.5 hours at room temperature. To remove the unreacted reagents, the samples were thoroughly

dialyzed against 200 mM carbonate buffer (×3) followed by ddH_2O dialysis (×2). Where indicated, the PEI conjugates were labeled with FITC after the conjugation reaction for binding studies. A stock solution of FITC (10 mM in DMSO) was added to the polymer samples for 2.5 hours to give a final concentration of 0.1 mM FITC, after which the samples were dialyzed against ddH2O (×2) to remove the unreacted FITC.

Modification of Primary Amines on PEI

One set of samples was prepared by reacting PEI (25 kDa) with different [NHS-PEG-MAL] without thiolBP addition. Briefly, the NHS-PEG-MAL was dissolved in 100 mM, pH=7.0 phosphate (see Legends for concentrations) and PEI solution (3.2 mg/mL in 100 mM phosphate, pH=7.0) was added to this solution at a volume ratio of 2:1 for PEI:NHS-PEG-MAL. The samples were incubated for 2.5 hours at room temperature, then dialyzed against 100 mM phosphate buffer (pH=5.0). Another set of samples was prepared by reacting PEI with different concentrations of acetic anhydride for different degree of acetylation [19]. The reactions were carried out in glass vials in anhydrous methanol at room temperature for 24 hours. Triethylamine (10% mole excess based on the amount of acetic anhydride) was added to quench the acetic acid formed as a side product during the reaction. The samples were dialyzed against 100 mM phosphate buffer (pH=8.0) and ddH_2O.

Biochemical Assays

TNBS Assay [20] The TNBS assay was used for assessment of [amine] in solution. 20 μL of a test sample, 130 μL of 100 mM phosphate buffer (pH=7.0) and 850 μL of 1 mM

TNBS in borate buffer (pH=9.4) were added to a cuvette, and the samples were incubated for 1 hour at 37 °C. The absorbance of the solutions was read at 367 nm. Serially diluted cysteine solutions typically served for the calibration curve.

Phosphate Assay [21] The [thiolBP] in conjugates was determined by measuring the total phosphate in the samples. 50 μL of sample was mixed with 30 μL of 10% $Mg(NO_3)_2$ in 95% ethanol in glass tubes and ashed over a flame. After boiling in 0.3 mL of 0.5 N HCl for 15 minutes, 0.6 mL of $(NH_4)_6Mo_7O_{24}{\cdot}4H_2O$ (0.42% w/v in 1 N H_2SO_4) and 0.1 mL of ascorbic acid (10% w/v) were added to the tubes and the samples were incubated at 37 °C for 1 hour. The absorbance was determined at 820 nm by a UV spectrophotometer (Pharmacia Biotech, Ultrospec@2000), and a calibration curve based on known concentrations of thiolBP was used. Where indicated, the [thiolBP] (in mM) generated here was divided by the [polymer] (in mM) in each sample to obtain an average thiolBP substitution; i.e., the number of thiolBPs per polymer molecule. The [polymer] was based on either TNBS assay (for PEI) or FITC fluorescence (for PLL) with the appropriate standard curves for each polymer preparation.

Copper (II)/PEI Complexation Assay [22,23] A spectroscopic method was additionally used for determining [PEI]. This was necessary to confirm that TNBS-based assay for [PEI] did not result in an underestimate due to amine modifications (i.e., since amine modification by various reactions might lead to lower TNBS signal, hence lower [PEI] – note that most reactions for this study utilized <10% amine modification). 100 μL of samples was added to 100 μL of 20 mM $Cu(SO_4)_2$ solution, and the mixture was diluted

to 500 μL with 100 mM acetate buffer (pH = 5.4). The absorbance was read at 630 nm. Known concentration of native PEI served as the calibration standards. Modification of primary amines of PEI with acetic anhydride was found not to affect the calibration curve (not shown), confirming that the assay was insensitive to primary amine modification.

Assessment of Mineral Affinity

The mineral affinity of the polymers was investigated by using HA and unprocessed bone matrix from rat femurs/tibiae [24]. In a typical HA binding assay, a 100 μL polymer sample was diluted with 300 μL of phosphate buffer (pH=7.0) to give 0 - 300 mM phosphate (see Legends for final [polymer] in the binding medium). The diluted samples were then added to microcentrifuge tubes containing 5 mg of HA in duplicate. As a reference (i.e., 0% of binding), the samples were incubated in tubes without HA. The tubes were incubated at room temperature on an orbital shaker for 3 hours, and centrifuged to separate the matrix from the supernatant. The ligand concentration in the supernatant was determined by either the TNBS assay or by fluorescence for FITC-labeled polymers. For the latter, a 200 μL of the aliquot was added to black 96-well plates (NUNC, Rochester, NY) and the fluorescence (λ_{ex}: 485 nm; λ_{em}: 527 nm) was determined with a multiwell plate reader (Thermo Labsystems, Franklin, MA). The [ligand] in supernatants were calculated based on appropriate calibration curves, and used to calculate %HA binding as: 100% × {([ligand] without HA) – ([ligand] with HA)} / ([ligand] without HA).

Modifications of this procedure were used to explore the effect of various parameters on binding. In some studies, fresh rat serum was added to the binding buffer

at 20-50% (v/v) to investigate the effect of serum on binding efficiency. In this case, only FITC-labeled polymers were utilized, and assay conditions were adjusted (20 μL sample + 180 μL of 100 mM phosphate buffer, pH=7.0) to ensure no interference of serum on the fluorescence measurements.

In one series of studies, HA was replaced with bone matrix (50 mg bone matrix with size range of 0.1–2 mm), and binding was assessed with FITC-labeled ligands as above. The bone matrix was prepared as described previously. [3] The bone matrices were washed with phosphate buffered saline (PBS, pH=7.2) (×3) with centrifugation between washes, and the fluorescence in the supernatant and washes were determined. Percent ligand binding was calculated as above.

Assessment of In Vivo Affinity in Rat Subcutaneous Implant Model

In vivo mineral affinity of the native PEI and a thiolBP-PEI conjugate was assessed by using ^{125}I-labeled polymers, and Skelite^{TM} matrices, according to the methodology described in a previous publication [24]. The extent of thiolBP substitution for the conjugates was determined prior to implantation. 8-week-old female Sprague-Dawley rats were purchased from Biosciences (Edmonton, Alberta). The rats were acclimated for 1 week under standard laboratory conditions (23°C, 12 hours of light/dark cycle) prior to the beginning of the study. While maintained in pairs in sterilized cages, rats were provided standard commercial rat chow, and tap water *ad libitum* for the duration of the study. All procedures involving the rats were approved by the Animal Welfare Committee at the University of Alberta (Edmonton, Alberta).

Preparation of Radiolabeled Polymer. Polymers were first conjugated to the unlabelled Bolton & Hunter reagent SHPP in 50 mM carbonate buffer (pH=9.4), followed by addition of ^{125}I to the tyrosine ring of SHPP [25]. Briefly, SHPP was dissolved in DMSO at 2.4 mg/mL and 4 μL of this solution was added to 600 μL of ~0.05 mg/mL (~30 μg) polymer solutions in 50 mM carbonate buffer (pH=9.4). The mixture was incubated for 30 min at room temperature and then dialyzed against PBS (pH=7.2, ×3). Microcentrifuge tubes were coated with TCDG (200 μL of 20 mg/mL TCDG in chloroform), and 10 μL of polymer solution was added to the coated tubes, along with 50 μL of PBS and 20 μL of 0.2 mCi of $Na^{125}I$. After reacting for 25 min, free ^{125}I was separated from the radiolabeled polymer by using a Sephadex G-25 column. After precipitating an aliquot of the purified samples with 20% trichloroacetic acid (TCA), the counts in the supernatant and the precipitate was determined with a γ-counter (Wizard 1470; Wallac, Turku, Finland), and it was confirmed that all iodinated samples contained <6% free ^{125}I.

Implantation. The Skelite™ implants (4×4×4 mm^3 cubes) were prepared by soaking 30 μL of ^{125}I-labeled polymer solutions into the implants. The exact counts in the added 30 μL solution was determined and used as the implanted polymer dose. 12 rats were utilized for implantation in total. Once rats were anesthetized with inhalational Metofane™ (methoxyflurane; Janssen Inc., Toronto, ON), two wet implants were implanted subcutaneously into bilateral ventral pouches in each rat. At indicated time points, 2 rats were euthanized with CO_2, the implants recovered, and the counts associated with the excised implants were quantified by using a γ-counter. Tissue

surrounding the implants were also recovered and counted. The amount of polymer retention, expressed as a percent of implanted dose, was calculated as follows: 100% × [(final counts in implant)/(initial counts in implant)]. The results are summarized as mean ± SD of %implant retention of polymers for 4 implants at each time point. Statistical differences between the group means were analyzed by the 2-sided *t*-test.

In Vitro Binding to Skelite™. The affinity of radiolabeled polymers for Skelite™ matrix was assessed *in vitro* as in HA binding assay. The binding was performed by incubating polymer-soaked Skelite™ matrices (prepared as above) in serum-containing PBS (pH=7.2, 50% v/v) for 2 hours. The matrices were then extensively washed with PBS (pH=7.2) to remove any fluid entrapped within the pores of the matrices. The Skelite™ matrices were separated from the supernatant by centrifugation, and the counts in the matrices and the supernatant were determined. The Skelite™ binding was calculated as follows: {(counts in matrix) ÷ (counts in supernatant + washes + matrix)} × 100%.

RESULTS AND DISCUSSION

This study was conducted as a first step towards our ultimate goal, namely to construct bone-seeking therapeutic agents with BP-incorporating polymeric targeting groups. Two sets of experiments were conducted towards this goal: (i) the mineral affinity of two cationic linkers (PLL and PEI) considered suitable for BP attachment was first determined; (ii) the thiolBP was subsequently conjugated to the chosen polymers, and the mineral affinity of the resultant thiolBP derivatives were compared to the

unmodified polymers. An *in vitro* HA binding assay as well as a rat subcutaneous implant model were used for assessment of the mineral affinity.

Interaction of Cationic Polymers with HA

PLL Interaction with HA. The HA affinity of unmodified PLL was first assessed with different MW PLLs (4, 9, and 25 kDa) in various [phosphate] (i.e. concentration of phosphate) (pH=7.0). The [PLL] in the supernatant of HA binding assay was determined by either TNBS assay, which is based on the quantitation of primary $-NH_2$ groups, and fluorescence measurements by using FITC-labeled PLL (**Figure 4-1A** and **4-1B,** respectively). For the 4 kDa PLL, a strong binding was obtained in 0 mM phosphate buffer by both assays, but the extent of binding was lower upon increasing the [phosphate] in the buffer. HA binding of 9 and 25 kDa PLLs was relatively stronger in all phosphate buffers. Assessment by FITC-labeled PLL gave a similar result, albeit the binding values obtained was relatively lower than the values from the TNBS assay, which was expected to be more accurate since it does not chemically modify the polymers, and cannot inadvertently influence the HA binding of the polymers. Our previous studies indicated that FITC-labeling underestimated HA binding when the [FITC] used for labeling was >0.1 mM [26]. Even though we used [FITC] of 0.1 mM, it is likely that we are slightly underestimating the HA affinity of PLL from this method. Nevertheless, we continued to utilize the FITC-labeled PLL, since certain binding conditions did not allow us to use the TNBS assay (see below).

The PLL will be positively charged during the binding assay, given the pK_a of ε-NH_2 in PLL (10.5) and our experimental pH (7.0). The reduction in binding with

increasing [phosphate] was most likely due to increased electrostatic shielding between the charged moieties of the PLL and the HA surface responsible for macromolecule adsorption to HA surfaces. With increased shielding at higher [phosphate], the strength of the point interactions between the PLLs and the HA was expected to be reduced. The 4 kDa PLL, which contained a relatively lower number of interacting species, was expected to be more significantly influenced as a result of increasing shielding, consistent with our results. The 9 and 25 kDa PLL contained more interacting species that presumably compensated for the shielding effect.

The effect of serum on binding was investigated next since *in vivo* bone binding is expected to take place in the presence of serum constituents capable of competing for mineral binding (e.g., serum proteins and other cations such as Ca^{2+}) [27]. The binding in the presence of serum was evaluated by the FITC-labeled PLL, since serum interfered with the TNBS assay (**Figure 4-2**). Both HA and bone particles were used in this assay to better mimic the *in vivo* binding substrate. In 0 mM phosphate buffer, the presence of serum (20% v/v) reduced PLL binding to HA by ~15% and by a more significant fraction of ~60% to bone particles. In 100 mM phosphate buffer, the presence of serum had unnoticeable effect on PLL binding to HA (~3% decrease), while reducing PLL binding to bone by ~20%. The binding pattern in 300 mM phosphate was similar to the one observed in 100 mM phosphate buffer. The more significant serum inhibition observed in 0 mM phosphate was presumably due to stronger binding of serum components to the mineralized matrices, which competed more effectively with the PLL adsorption to the mineral matrices. One competing species will be serum albumin, whose mineral binding is strong in the absence of phosphate, but loses mineral binding all together in 100 mM

phosphate in our HA binding assay [26]. This effect was more prominent for PLL binding to the bone particles. The synthetic HA should be composed of well hydrated particles, which is expected to present a greater surface area for adsorption, partially compensating for the increased competition of serum constituents. Nevertheless, these results indicated a strong affinity of the cationic PLL to both HA and bone particles in the presence of a significant quantity of competing serum components. The level of PLL binding seen in this highly standardized binding assay was equivalently to the binding of BPs previously reported by our group [26].

PEI Interaction with HA. PEI contains a combination of primary, secondary and tertiary amines with an isoelectric point of 10.8 [28]. Unlike the linear PLL, the branched PEI assumes a spherically symmetric, compact molecule in solution [29]. All of the PEI amines are expected to be charged under our experimental conditions since the pK_a are 10.63, 10.98 and 10.65 [30]. The HA binding of 2 commercially available PEI molecules (2 and 25 kDa) was assessed at 0-300 mM [phosphate], and in a [PEI] range of 0.1 to 1.0 mg/mL. For both 2 (**Figure 4-3A**) and 25 kDa (**Figure 4-3B**) PEI, %HA binding was decreased as a function of [PEI] in all phosphate buffers. The total amount of binding, however, was increased with increasing [PEI] in the medium (**Figure 4-3C**). Comparing the binding of 2 vs. 25 kDa PEIs, no significant differences appeared at the 0 mM phosphate buffer, but a difference was evident at 100 and 300 mM phosphate buffers (**Figure 4-3C**); the larger MW PEI gave a significantly higher adsorption at high [phosphate]. This is unlike the PLL binding, where higher [phosphate] reduced the polymer binding. A strong PEI binding to HA was also noted by others under

chromatographic conditions, where PEI removal from a HA column was not possible even with a 400 mM phosphate [31].

The non-electrostatic (i.e., hydrophobic) effects were likely the reason behind increased PEI binding with increasing [phosphate]. Van de Steeg et al. [32], who investigated the polyelectrolytes adsorption on oppositely charged surfaces based on a model by Böhmer et al. [33], proposed a transition region between the "screening-reduced adsorption regime" (i.e., increasing [salt] reducing polyelectrolyte adsorption) and "screening-enhanced adsorption regime" (i.e., increasing [salt] increasing polyelectrolyte adsorption). In the latter case, screening of repulsive forces among polyelectrolyte segments dominates the binding behavior. Whereas a purely electrostatic interaction is always attenuated as a result of increased ionic strength, the binding of a shielded polyelectrolyte may increase if additional attractive forces exist between the polyelectrolyte and the surface. PEI is known to display non-electrostatic interaction with charged surfaces [34]. Similar to our results, PEI adsorption on silica surfaces was observed to increase at higher ionic strengths, which was attributed to the presence of a significant non-electrostatic affinity of PEI to the surfaces. At pH=7.0, PEI is positively charged, and HA surface bears only slight negative charge density since its point of zero charge is ~7.3. In the absence of buffer salts (0 mM phosphate), the repulsive segment-segment interactions in PEI were expected to impede binding of other PEI molecules to HA surface. PEI is known to be flexible on surfaces and undergo significant conformational change to spread on surfaces [28,35]. The extent of PEI spreading (or compactness) was directly influenced by the packing density on surfaces [28]. Shielding

such interactions at higher [phosphate] will facilitate additional PEI binding to surfaces, and this mechanism appeared to be in effect for PEI binding on HA in our system.

The effect of serum on PEI binding to HA was evaluated by FITC-labeled PEI (25 kDa, **Figure 4-4**). In 0 mM phosphate, the presence of serum (20% v/v) reduced the binding by ~60%, and the higher serum percentage (50% v/v) continued to reduce the binding by a further ~6%. The binding in 100 and 300 mM phosphate buffers were similar: a ~10% decrease in binding from ~90% to ~80% in the presence of 20% v/v serum, and a further decrease of ~10% binding in 50% v/v serum. A stronger serum competition was again evident at 0 mM phosphate (as discussed in the case of PLL) and, as was the case with PLL, a strong HA affinity was retained by the 25 kDa PEI at higher [phosphate].

It is important to note that the extent of PEI binding to HA was similar or superior to the binding values of BP to HA reported by us [26]. Although one is tempted to compare the HA affinity of PLL and PEI, differences in binding conditions and molecular properties (such as MW) do not allow us to reach to a broad conclusion on this issue. Our experimental data does not indicate any obvious difference for the two polymers under a select set of conditions, where MW ~ 25 kDa, [polymer]: ~0.2 mg/mL, pH=7.0 and when TNBS assay was used for assessment of binding (since FITC labeling of polymers might differentially affect the HA binding).

ThiolBP Conjugation to Cationic Polymers and HA Affinity of the Conjugates

ThiolBP Conjugation to PLL. Our *in vitro* binding assay confirmed the strong affinity of amino-BPs to HA in previous studies [26]. Similar to cationic polymers, the amino

groups in such BPs might have contributed to strong HA adsorption. The thiolBP displayed a lower affinity to HA, but both BPs were equally potent in imparting a mineral affinity in their conjugate forms [26]. Due to the convenience of derivatizing –SH groups, we chose thiolBP for conjugation to polymers. Since both PLL and PEI already possessed high HA affinity, thiolBP conjugation was explored to determine whether the substituted polymers will display a further increase in mineral affinity.

Initial studies indicated the previously-used crosslinker SMCC [5] to be unsuitable for PLL modification, since it yielded insoluble products due to hydrophobicity of the SMCC. Although subsequent thiolBP conjugation to insoluble SMCC-derivatized PLL was explored to increase aqueous solubility, this strategy was not successful. The hydrophilic polyethyleneglycol (PEG) based heterofunctional linker NHS-PEG-MAL (3.4 kDa) was alternatively explored [36]. Unlike SMCC, NHS-PEG-MAL reaction with PLL gave readily soluble products in aqueous buffers, making it suitable for conjugations. To obtain conjugates with different thiolBP substitutions, PLL was reacted with different [NHS-PEG-MAL], which was first reacted with excess thiolBP before addition to PLL. FITC-labeled PLLs were used in preparing the conjugates, so as to estimate the PLL concentration from fluorescence measurements. The [PLL] and [thiolBP] in the recovered samples are shown in **Figure 4-5A** and **4-5B**, respectively. The results showed that the PLL reacted with higher [NHS-PEG-MAL] were retained in the samples to a higher extent after dialysis. The MW cut-off during dialysis was 12-14 kDa, and unreacted PLLs and PLLs with lower modifications were expected to be readily lost during this process (Though 25 kDa PLL showed higher HA binding in previous section, PLL MWs of 4 and 9 kDa were chosen for BP conjugation

since these MWs were less than the 12-14 kDa cut-off). This was by design since it was our intent to remove unreacted PLLs during the dialysis step. As expected, no thiolBP was recovered for the control samples where the thiolBP was omitted during the reaction of the PEG linker with PLL (**Figure 4-5B**). Based on the recovered thiolBP concentrations, the substitution efficiencies on the conjugates were estimated to be 3-4 thiolBP/PLL. This level of anionic thiolBP substitution was not expected to alter the net positive charge of the PLL under experimental condition (pH = 7.0), given the high degree of cationic repeating units in the polymer.

The binding of these conjugates were investigated in 100 mM phosphate (pH=7.0). With 4 kDa PLL, NHS-PEG-MAL reaction without thiolBP substitution completely abolished the mineral affinity of the polymer (**Figure 4-5C**). The NHS-PEG-MAL reacted with the 9 kDa PLL did not exhibit any loss in HA affinity at lower [NHS-PEG-MAL], but HA affinity was reduced when the polymer was reacted with higher [NHS-PEG-MAL]. The higher HA affinity of the native 9 kDa as compared to the native 4 kDa PLL presumably afforded the better HA affinity of the corresponding conjugates after NHS-PEG-MAL reaction. ThiolBP conjugation recovered the mineral affinity of the NHS-PEG-MAL-reacted PLLs of both MWs (**Figure 4-5C**).

The negative effect of PEG on surface adsorption is well appreciated [37], and PEG was previously shown to display no adsorption to HA [9]. It appears that PEG substitution caused a loss of HA affinity even for the strongly HA-adsorbing PLL if the MW is low (4 kDa). The larger PLL presumably retained sufficient cationic contacts with the surface for effective binding despite PEG substitution. The thiolBP conjugation did improve the mineral affinity of PLLs with reduced affinity but, in comparison to

unmodified PLL, the final thiolBP conjugates of PLL did not exhibit any superior affinity towards the HA. The situation was different with the HPMA polymer from the Kopeček group [9]. The HPMA polymer did not exhibit a mineral affinity on its own and, in that case, alendronate substitution on the polymer did impart the desired mineral affinity to the polymer. As an alternative to NHS-PEG-MAL, we attempted to use N-succinimidyl-3-(2-pyridyldithio) propionate (SPDP), which was previously used to add thiolBP to proteins via cleavable disulfide (-S-S-) linkage [38]. As in SMCC reaction, the resultant modification yielded insoluble conjugates (not shown). We therefore did not pursue PLL any further due to undesirable properties (insolubility) of the final BP-PLL conjugates.

ThiolBP Conjugation to PEI. Unlike the PLL, controlling the [SMCC] within a certain range ([SMCC]:[NH_2] < 1:4) led to water-soluble thiolBP-PEI conjugates after the reaction. The presence of additional charged moieties, in the form of secondary and tertiary amines in PEI, might have led to better solvation of this molecule after modification with the hydrophobic SMCC. Others have also reported soluble PEI conjugates after the polymer was modified with hydrophobic molecules, such as lauryl-groups or o,o'-dihydroxyazobenzene [39]. To control the extent of thiolBP substitution, the PEI (25 kDa) was reacted with varying [SMCC], and the extent of thiolBP substitution was calculated. Unlike PLL, PEI in all samples was recovered to an equivalent degree (not shown) and there was a good relationship between the [SMCC] and the extent of thiolBP substitution on PEI (**Figure 4-6A**). Up to ~20 thiolBP per PEI was obtained at the highest [SMCC] of 3 mM. The large SD for the PEI sample reacted with 3 mM SMCC was a result of the partial precipitation of the samples, indicating the

limit of solubility for this type of derivatization. The substitution pattern in **Figure 4-6A** was similar to many other proteins used for BP conjugation, such as albumin [3] and fetuin [5], and it was highly significant ($p<0.001$).

The HA binding (in 100 mM phosphate, pH=7.0) for thiolBP-PEI conjugates is shown in **Figure 4-6B**. The thiolBP conjugation to PEI did not seem to exhibit any enhancement of mineral affinity as compared with the unmodified PEI. On the contrary, a small decreasing trend in HA affinity was noted as a function of thiolBP substitution (**Figure 4-6B**, insert). Note that the dashed line in **Figure 4-6B** was not intended as a curve fit, but rather to guide the eye for a trend in this data set. The highest SMCC used in this reaction was 3 mM, while the amine concentration from the PEI was ~12 mM in the reaction medium. A significant fraction of amines was expected to be unmodified during this reaction.

The importance of primary amines in PEI binding to HA was further investigated by chemically modifying the amine groups of PEI. The NHS-PEG-MAL was used to determine if hydrophilic PEG substitution could prevent HA adsorption reminiscent of the PLL. Acetic anhydride was used to convert the cationic primary amines into neutral –NH-C(O)-CH_3 groups without attaching any bulky substituents on the amines. The HA affinity was significantly different depending on the type of modification (**Figure 4-7**); whereas PEG attachment gave a strong inhibition of HA binding, acetic anhydride modification did not affect HA binding to a significant degree even when ~70% of the amine groups were modified. Therefore, loss of HA affinity was considered to be due to PEG attachment *per se*, rather than actual modification of the amine groups. It appears that primary amine modification was not detrimental for binding in the case of PEI, and

that either (i) secondary and/or tertiary amines contributed to the overall mineral affinity, or (ii) a small percentage of unmodified primary amines (< 30%) was sufficient for strong HA binding. As with PLL, the strongly adsorbing nature of the PEI did not allow the thiolBP to manifest a beneficial mineral affinity on this macromolecule after substitution.

In Vivo Affinity of PEI and thiolBP-PEI Conjugate

In order to investigate if BP substitution will impart a superior mineral affinity to cationic polymers *in vivo*, mineral affinity of native PEI and a thiolBP-PEI conjugate (6.3 thiolBP/PEI) was determined in a rat subcutaneous implant model. Commercially available Skelite™, a multi-phase calcium phosphate matrix (67% Si-stabilized tricalcium phosphate and 33% HA), was used as an implant in this study. Skelite™ is a single-piece microporous scaffold used in clinical osteoconductive bone repair. Implanting particulate HA may cause difficulties for complete implant recovery [40], whereas Skelite™ can be conveniently recovered as a single piece. The *in vitro* affinity of ^{125}I-labeled polymers for Skelite™ was shown in **Figure 4-8A**. Since the polymers were suspended in saline for implantation, the binding was assessed in PBS with 50% v/v serum. The thiolBP-PEI conjugate displayed 43.3 ± 1.1% binding, while the unmodified PEI gave 57.6 ± 0.9% binding. As was the case with HA, no apparent benefit of the thiolBP substitution was evident in this *in vitro* binding assay using the Skelite™ matrices.

The retention of the polymers in implants as well as the surrounding tissue was shown in **Figure 4-8B**. After 1 day, Skelite™ retention of thiolBP-PEI conjugate and PEI were 38.2 ± 2.1% and 34.8 ± 11.8%, respectively. These values were somehow similar

(thiolBP-PEI) or lower (PEI) than the results form the *in vitro* binding assay. The binding of the polymers to the implants was similar at other time points and there was no significant differences of the implant retention between the two polymers at all explant times. The thiolBP-PEI conjugate exhibited a significant ($p<0.001$) loss during the 7-day implantation period, but this value was relatively small (~20% from days 1 to 7) as compared to the initial 24 hours loss (~60%). A similar loss was observed for the native PEI, but the loss of PEI was not significant ($p>0.05$) during the 7-day study period due to the large SD on day 1. The retention in surrounding tissues (**Figure 4-8B**, insert) was low (<3%) with no significant differences between the two types of polymers at each time point.

The collective results were indicative of the similar pharmacokinetics of the two polymers. The polymer loss during the 7-day implantation period (~20%) was lower than the burst release (>60%) in the first day. This observation was similar to the previous experiences with basic proteins, such as BMP-2 that possesses an isoelectric point of ~9.0 [41,42]. It appears that once bound, cationic polymers and proteins were retained on the mineral-based carriers for a prolonged time *in vivo*. More importantly, no apparent effect of the thiolBP substitution was seen on the implant pharmacokinetics of the PEI. This result is in line with the results from the *in vitro* binding studies, and indicated no additional factor(s) that have influenced the *in vivo* mineral affinity of the thiolBP-derivatized cationic polymer. ThiolBP derivatization of proteins [3-7] always resulted in better mineral affinities *in vitro*, and this translated into better *in vivo* mineral affinity for the proteins evaluated by implantation. The inherently high affinity of cationic polymers, perhaps due to repeating cationic units leading to a high charge density, seems to make

thiolBP substitution not necessary for a high mineral affinity. Both *in vitro* and *in vivo* observations in this study supported this conclusion.

CONCLUSIONS AND IMPLICATIONS

This study demonstrated the high affinity of cationic polymers towards HA. Our studies focused on the fundamentals of the adsorption process to better understand factors controlling the extent of adsorption. The cationic polymers were as effective as the well-studied BPs for HA binding and we intend to utilize the generated knowledge for designing superior delivery systems to target therapeutic agents to bones. We are particularly interested in utilizing cationic polymers in delivering proteins capable of stimulation bone tissue regeneration, since bone tissue is the only tissue containing HA under normal physiological conditions, and ligands with high affinity to HA (cationic polymers) have the potential to guide the therapeutic agents to bone.

Our results will also benefit attempts to tailor HA interfaces for cellular growth and differentiation. Cationic polymers have been used to facilitate cell attachment to non-HA surfaces. Glass slides are routinely coated with PLL by simple adsorption when one needs to grow cells for microscopic analysis. PLL coating on widely different substrates, such as polystyrene [43] and hyaluronic acid [44] have been successful in promoting cell attachment. HA has been used as a substrate for osteogenic cells, since it is the natural component of the bone tissue, and it can undergo remodeling via physiological mechanisms. Some efforts have been directed towards improving cell adhesive properties of HA, but this approach has typically relied on immobilization of the tripeptide arginine-glycine-aspartic acid (RGD) by using a poly(aspartic acid) tail that displays a high

affinity to HA [45-47]. PLL coating by a simple adsorption is a more convenient alternative to RGD immobilization given the robustness of PLL affinity to HA. The performance of immobilized peptides such as RGD may depend on the mode of immobilization (e.g., conjugation chemistry, nature of spacer between the surface and peptide, etc), but these issues should not be a concern when surfaces are coated with simple cationic polymers (it is worthwhile to mention that unlike RGD, PLL should not activate integrins). PEI was equally effective as PLL in HA binding in this study, making it an alternative reagent for creating cell-adhesive surfaces. Although relatively less number of studies reported a beneficial effect of PEI for cell attachment [48,49], the highly toxic nature of PEI might make it less attractive. Nevertheless, to the best of our knowledge, no attempts were made to coat HA surfaces with PLL or PEI for improved cell attachment, and our results provide merit of this approach.

The PLL and PEI can be also used to immobilize mitogenic (such as bFGF) or morphogenic ligands (such as BMP-2) on HA surfaces [50]. Acidic proteins with low isoelectric points [51], or proteins under optimal ionic strength environments [52] might naturally bind to cationic polymers, obviating the need for chemical immobilization. Alternatively, coupling of proteins to cationic polymers is relatively straightforward in solution (no steric hindrances as seen on surfaces), and such conjugates could decorate HA surfaces with physiological signals to modulate cell behavior. Especially controlling cell differentiation *in vitro* before implantation of tissue constructs will greatly accelerate the success of tissue engraftment. Cationic polymers, due to their inherent affinity to HA, could enable a unique approach for drug delivery to bone, while facilitating tissue engineering strategies involving HA as a scaffold.

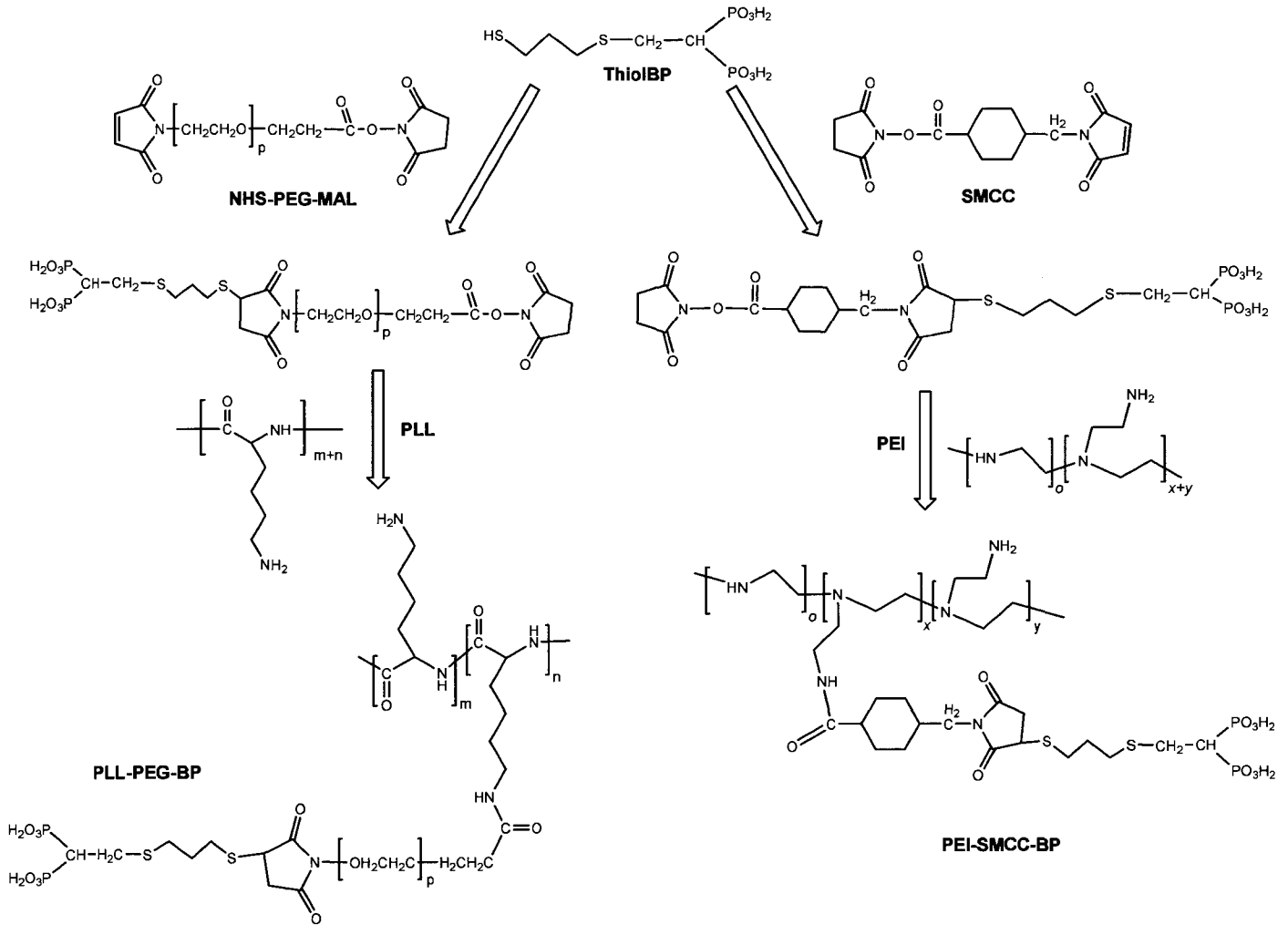

Scheme 4-1. Conjugation of thiolBP to PLL and PEI by using MAL-PEG-NHS and SMCC as linkers, respectively.

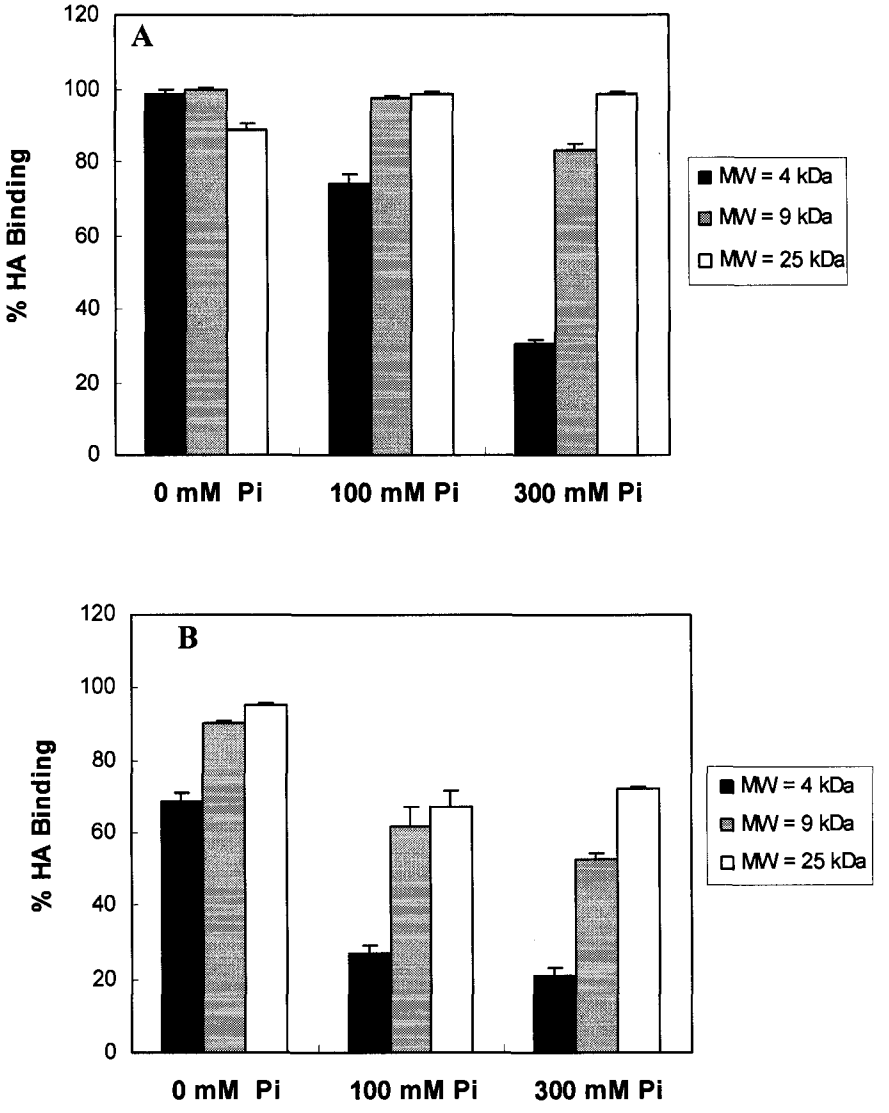

Figure 4-1. %HA binding of different MW PLLs (4, 9 and 25 kDa) at different phosphate buffers (0, 100 and 300 mM), as determined by the TNBS assay (**A**) and fluorescence measurements (**B**). The same concentration of PLL (0.17 mg/mL) was used for all binding studies. The 4 kDa PLL exhibited a strong binding in 0 mM phosphate buffer by both assays, but the extent of binding was lower upon increasing the [phosphate] in the buffer. Binding of higher MW PLLs was relatively stronger in all phosphate buffers. Data are shown as the mean ± SD from duplicate measurements.

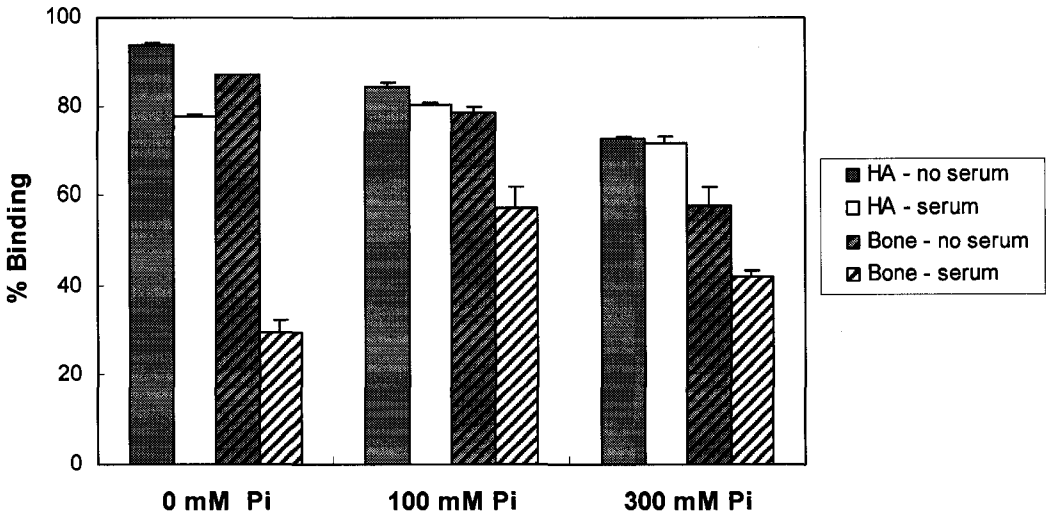

Figure 4-2. Effect of serum on PLL binding to HA and bone matrices evaluated by a FITC-labeled PLL (7.5 kDa) in different phosphate buffers (0, 100 and 300 mM). Rat serum was added to the binding buffer at 20% (v/v), where [PLL] was 0.17 mg/mL. The presence of serum reduced PLL binding to both HA and bone matrices at all phosphate buffers investigated, with a more significant effect on the bone binding of PLL than the HA binding. Binding of PLL at 0 mM buffer was more significantly affected by the presence of the serum as compared to binding in 100 mM and 300 mM phosphate buffers. Data are shown as the mean ± SD from duplicate measurements.

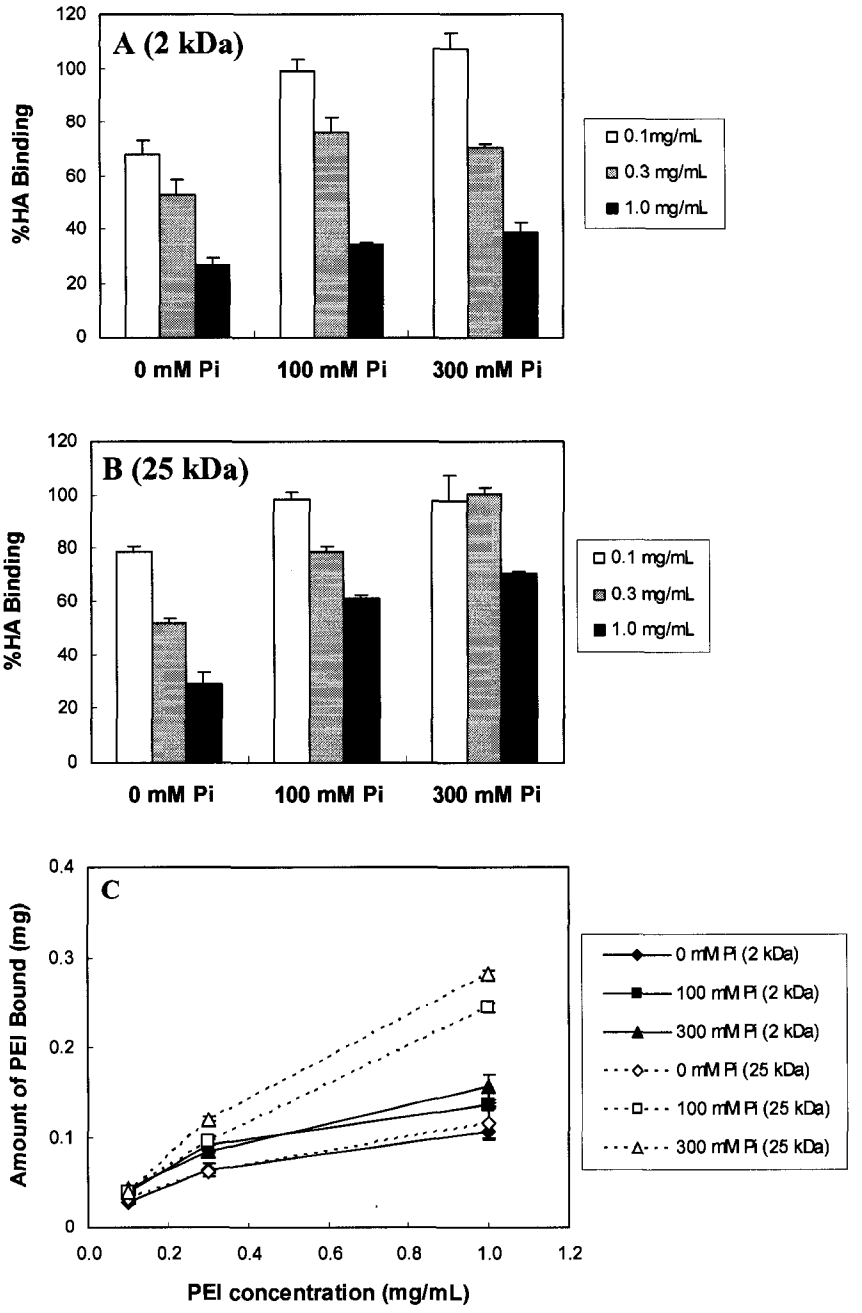

Figure 4-3. %HA binding of 2 kDa PEI (**A**) and 25 kDa PEI (**B**) at different phosphate buffers (0, 100 and 300 mM). The PEI concentrations were of 0.1, 0.3 and 1.0 mg/mL. Based on **A** and **B**, total amount of PEI bound to HA (mg) was calculated as a function of PEI concentration for both PEIs (**C**). For both 2 and 25 kDa PEI, %HA binding was decreased as a function of increasing [PEI] in all phosphate buffers. The total amount of binding, however, was increased with increasing [PEI] in the medium. No significant differences appeared at the 0 mM phosphate buffer between 2 and 25 kDa PEI. A difference was evident at 100 and 300 mM phosphate, the larger PEI giving a significantly higher adsorption at higher [phosphate]. Data are shown as the mean ± SD from duplicate measurements.

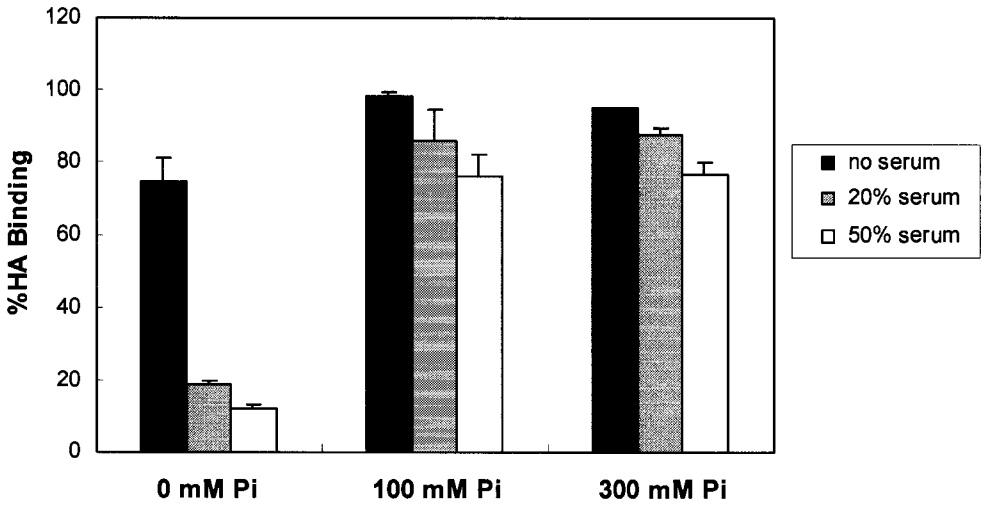

Figure 4-4. Effect of serum on PEI binding to HA, as evaluated by a FITC-labeled PEI (25 kDa). Rat serum was added to the binding buffer at 20% and 50% (v/v), and the [PEI] was 0.17 mg/mL. The presence of serum reduced PEI binding to HA at all phosphate buffers investigated. Binding of PEI at 0 mM phosphate buffer was more significantly affected by the presence of serum than the binding in 100 mM and 300 mM phosphate buffers. Data are shown as the mean ± SD from duplicate measurements.

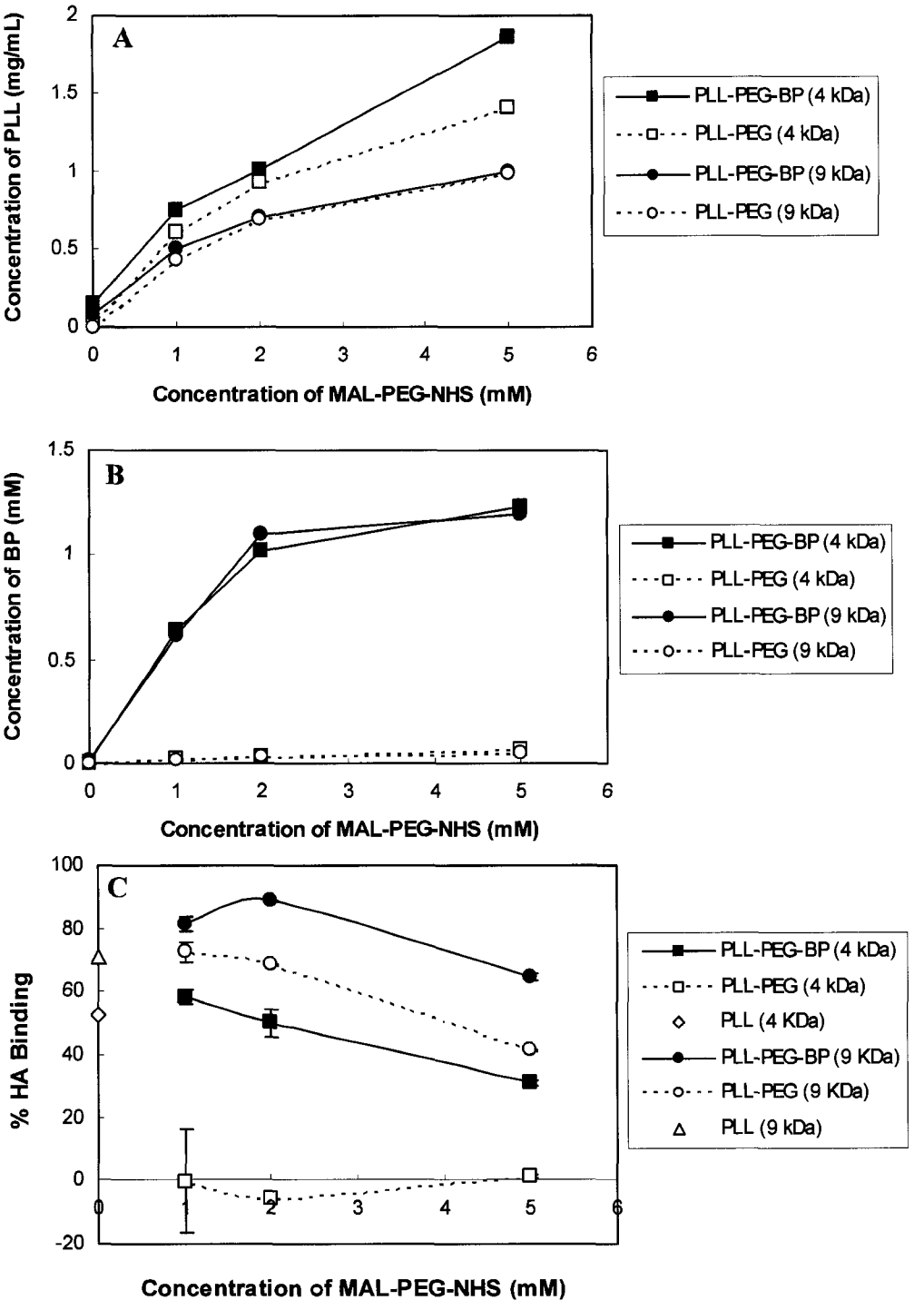

Figure 4-5. Quantitative analysis of PLL (**A**) and thiolBP (**B**) content of PLL samples (4 and 9 kDa) reacted with NHS-PEG-MAL. The results indicated that the PLL reacted with higher [NHS-PEG-MAL] were retained to a higher extent after dialysis (**A**), and thiolBP content increased at higher [NHS-PEG-MAL] (**B**). **C.** %HA binding of the same PLL samples in 100 mM phosphate buffer (pH=7.0). In comparison to corresponding native PLLs, the thiolBP conjugates did not exhibit any superior affinity to HA.

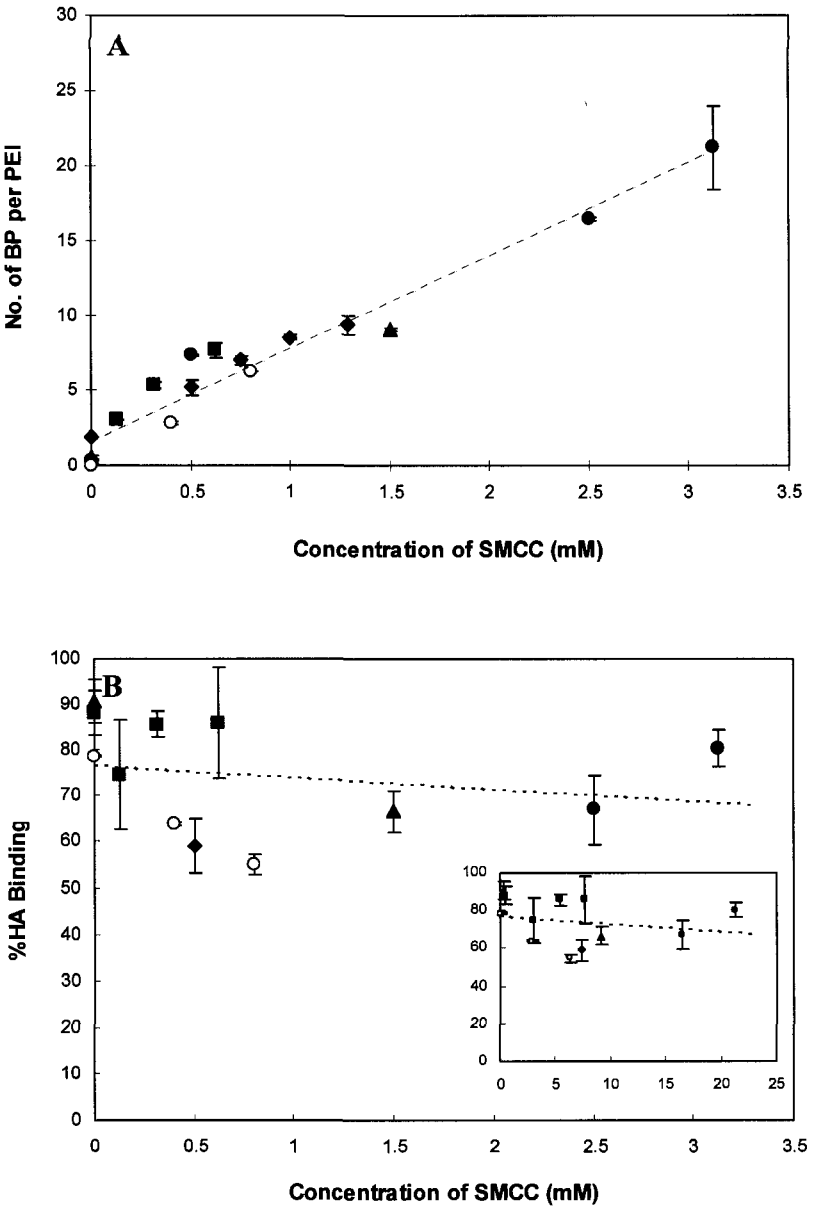

Figure 4-6. ThiolBP substitution on PEI (25 kDa) at various concentrations of SMCC (**A**) and %HA binding of the conjugates in 100 mM phosphate buffer (pH=7.0) (**B**). The %HA binding of the conjugates (y-axis) as a function of thiolBP substitution (x-axis) was shown in the insert of **B**. Different symbols in **A** indicates different sets of conjugation experiments (5 all together). The correlation between thiolBP substitution on PEI and [SMCC] was significant ($p<0.001$ by t-test). Solid symbols indicates %HA binding as determined by the TNBS assay, while open symbols were from the fluorescence measurements in **B**. The thiolBP conjugation to PEI did not seem to exhibit any enhancement in mineral affinity (note that the dashed line was not intended as a curve fit, but rather to guide the eye for a trend in this data set). Data are shown as the mean ± SD from duplicate measurements.

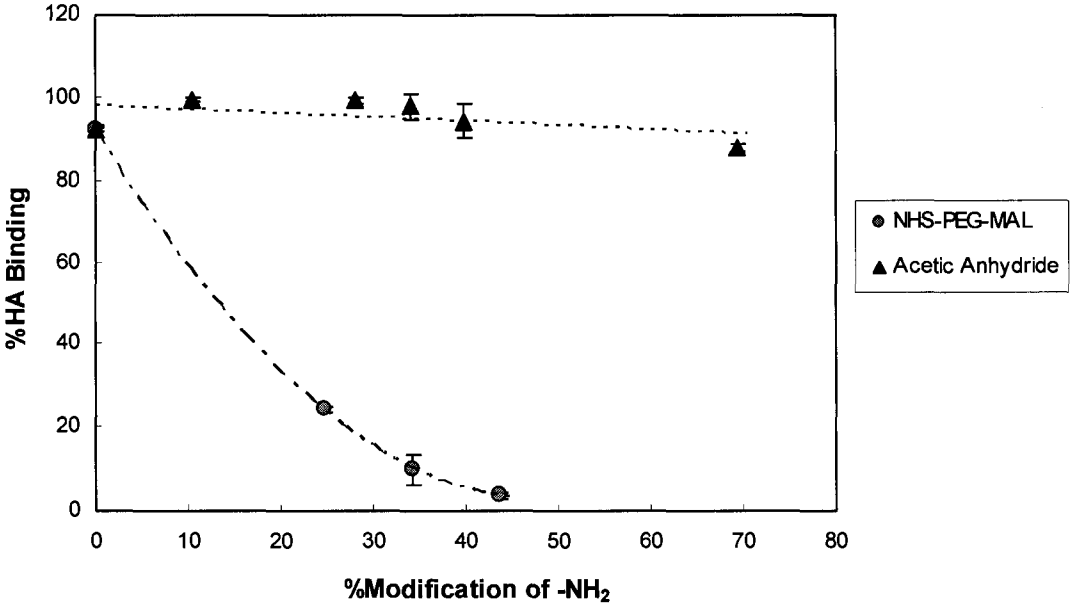

Figure 4-7. %HA binding of PEI (in 100 mM phosphate buffer, pH=7.0) with different degree of primary amines modification by NHS-PEG-MAL and acetic anhydride. The polymer concentration and amine content were determined by Cu (II)/PEI complexation and TNBS assay, respectively. The HA affinity was significantly different depending on the type of modification; whereas PEG attachment gave a strong inhibition of HA binding, acetic anhydride modification did not affect HA binding to a significant degree even when ~70% of the amine groups were modified. Data are shown as the mean ± SD from duplicate measurements.

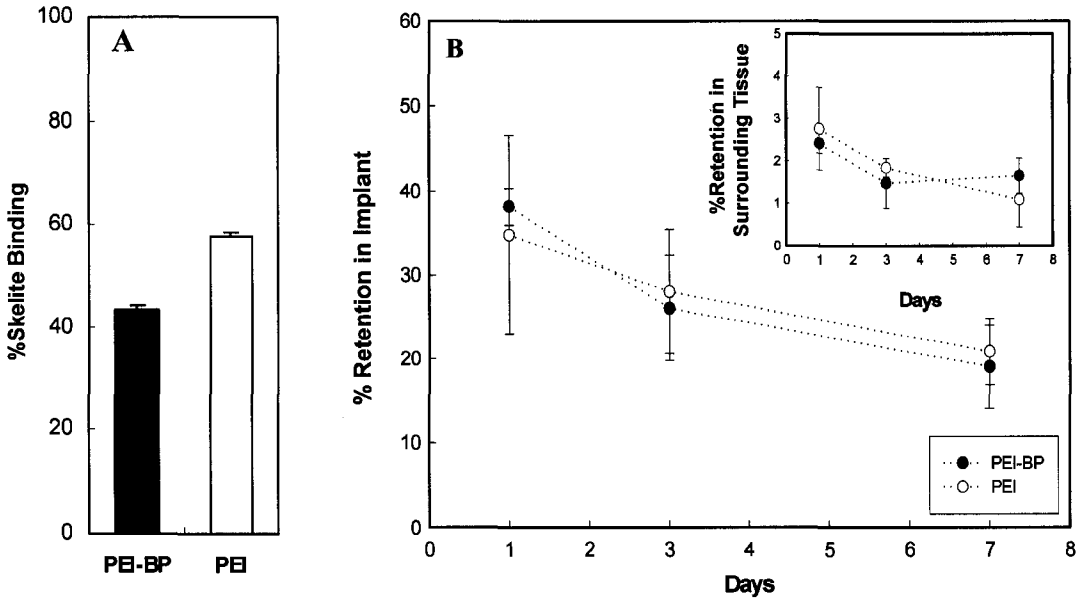

Figure 4-8. %Skelite^{TM} binding of thiolBP-PEI conjugate (6.3 thiolBP per PEI) and unmodified PEI by ^{125}I-labeled polymers (**A,** mean ± SD from triplicate measurements), and implant retention of thiolBP-PEI conjugate and unmodified PEI as a function of time (**B,** mean ± SD from quadruplicate measurements.). The retention of polymers in the surrounding tissues was shown in the insert of **B**. Unmodified PEI exhibited a higher affinity to the Skelite^{TM} matrix than the thiolBP-PEI conjugate *in vitro* (**A**). The thiolBP-PEI conjugate exhibited a significant ($p<0.001$) loss during the 7-day implantation period, however, the loss of PEI was not significant ($p>0.05$) during the 7-day study period due to large SD on day 1. There was no significant difference in implant retention between thiolBP-PEI conjugate and unmodified PEI at all explant times (**B**).

Supplementary Materials

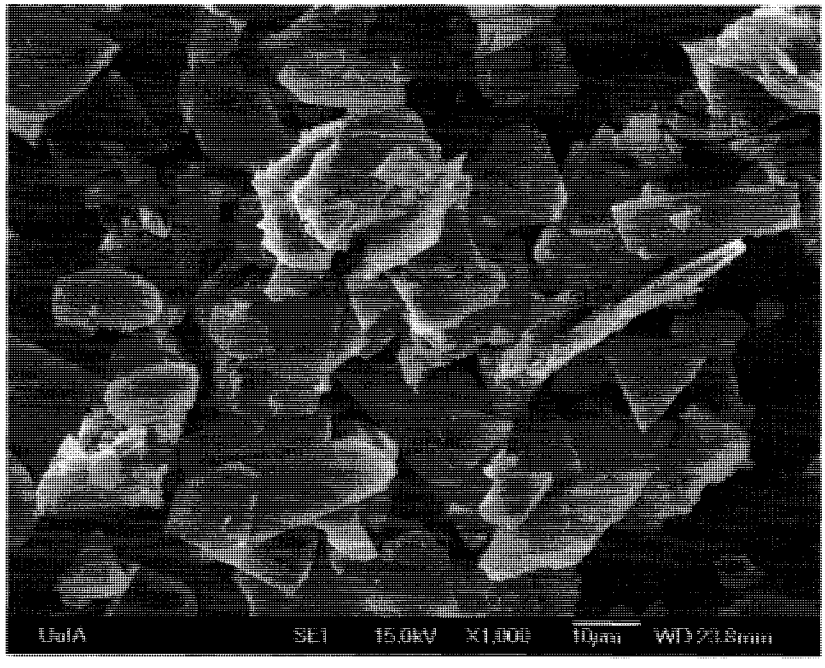

Figure S4-1. SEM image of synthesized HA crystals used in binding study. The crystals are blade-like and heterogeneous in size.

References

[1] H. Fleisch, R. G. G. Russell, and F. Straumann, Effect of pyrophosphate on hydroxyapatite and its implications in calcium homeostasis, *Nature*, 212 (1966) 901-903.

[2] J. H. Lin, Bisphosphonates: A review of their pharmacokinetic properties, *Bone*, 18 (1996) 75-85.

[3] H. Uludağ, N. Kousinioris, T. Gao, and D. Kantoci, Bisphosphonate conjugation to proteins as a means to impart bone affinity, *Biotechnol. Prog.*, 16 (2000) 258-267.

[4] H. Uludağ and J. Yang, Targeting systemically administered proteins to bone by bisphosphonate conjugation, *Biotechnol. Prog.*, 18 (2002) 604-611.

[5] S. A. Gittens, J. R. Matyas, R. F. Zernicke, and H. Uludağ, Imparting bone affinity to glycoproteins through the conjugation of bisphosphonates, *Pharm. Res.*, 20 (2003) 978-987.

[6] G. Bansal, S. A. Gittens, and H. Uludağ, A di(bisphosphonic acid) for protein coupling and targeting to bone, *J. Pharm. Sci.*, 93 (2004) 2788-2799.

[7] G. Bansal, J. E. I. Wright, C. Kucharski, and H. Uludağ, A dendritic tetra(bisphosphonic acid) for improved targeting of proteins to bone, *Angew. Chem. Int. Ed.*, 44 (2005) 3710-3714.

[8] R. Duncan, The dawning era of polymer therapeutics, *Nat. Rev. Drug Discov.*, 2 (2003) 347-360.

[9] D. Wang, S. C. Miller, P. Kopeckovβ, and J. Kopecek, Bone-targeting macromolecular therapeutics, *Adv. Drug Deliv. Rev.*, 57 (2005) 1049-1076.

[10] L. Wang, M. Zhang, Z. Yang, and B. Xu, The first pamidronate containing polymer and copolymer, *Chem. commun.*, 26, (2006) 2795-2797.

[11] N. S. Soukos, L. A. Ximenez-Fyvie, M. R. Hamblin, S. S. Socransky, and T. Hasan, Targeted antimicrobial photochemotherapy, *Antimicrob. Agents Chemother.*, 42 (1998) 2595-2601.

[12] M. E. Davis and N. C. Bellocq, Cyclodextrin-containing polymers for gene delivery, *J. Incl. Phenom. Macrocycl. Chem.*, 44 (2002) 17-22.

[13] M. J. Gorbunoff, The interaction of proteins with hydroxyapatite: I. Role of protein charge and structure, *Anal. Biochem.*, 136 (1984) 425-432.

[14] A. L. Boskey, The organic and inorganic matrices, in: J. O. Hollinger, T. A. Einhorn, B. A. Doll, and C. Sfeir (Eds.), *Bone Tissue Engineering*, CRC Press, Boca Raton, 2005, pp. 111-114.

[15] I. S. Harding, N. Rashid, and K. A. Hing, Surface charge and the effect of excess calcium ions on the hydroxyapatite surface, *Biomaterials*, 26 (2005) 6818-6826.

[16] G. Bansal, J. E. I. Wright, S. Zhang, R. F. Zernicke, and H. Uludağ, Imparting mineral affinity to proteins with thiol-labile disulfide linkages, *J. Biomed. Mater. Res. Part A*, 74 (2005) 618-628.

[17] A. Tiselius, S. Hjertén, and O. Levin, Protein chromatography on calcium phosphate columns, *Arch. Biochem. Biophys.*, 65 (1956) 132-155.

[18] G. Bernardi, Chromatography of nucleic acids on hydroxyapatite columns, *Meth. Enzymol.*, 21 (1971) 95-139.

[19] I. J. Majoros, B. Keszler, S. Woehler, T. Bull, and J. R. Baker, Acetylation of poly(amidoamine) dendrimers, *Macromolecules*, 36 (2003) 5526-5529.

[20] J. Bullock, S. Chowdhury, A. Severdia, J. Sweeney, D. Johnston, and L. Pachla, Comparison of results of various methods used to determine the extent of modification of methoxy polyethylene glycol 5000-modified bovine cupri-zinc superoxide dismutase, *Anal. Biochem.*, 254 (1997) 254-262.

[21] B. N. Ames, Assay of inorganic phosphate, total phosphate and phosphatases, in: S. P. Colowick and N. Kaplan (Eds.), *Methods in Enzymology,* Academic Press, New York, 1966, pp. 115-118.

[22] T. D. Perrine and W. R. Landis, Analysis of polyethylenimine by spectrophotometry of its copper chelate, *J. Polym. Sci. Part A-1: Polym. Chem.*, 5 (1967) 1993-2003.

[23] A. von Harpe, H. Petersen, Y. Li, and T. Kissel, Characterization of commercially available and synthesized polyethylenimines for gene delivery, *J. Control Release*, 69 (2000) 309-322.

[24] J. E. I. Wright, S. A. Gittens, G. Bansal, P. I. Kitov, D. Sindrey, C. Kucharski, and H. Uludağ, A comparison of mineral affinity of bisphosphonate-protein conjugates constructed with disulfide and thioether linkages, *Biomaterials*, 27 (2006) 769-784.

[25] M. V. Pimm, S. J. Gribben, K. Bogdβn, and F. Hudecz, The effect of charge on the biodistribution in mice of branched polypeptides with a poly(-lysine) backbone labelled with ^{125}I, ^{111}In or ^{51}Cr, *J. Control Release*, 37 (1995) 161-172.

[26] S. Zhang, G. Gangal, and H. Uludağ, Magic bullets for bone diseases: progress in rational design of bone-seeking medicinal agents, *Chem. Soc. Rev.*, 36 (2007) 507-531.

[27] P. T. Daley-Yates, J. C. Cal, A. Cockshott, M. Pongchaidecha, and K. Gilchrist, Plasma protein binding of APD: Role of calcium and transferrin, *Chem. Biol. Interact.*, 81 (1992) 79-89.

[28] T. Radeva and I. Petkanchin, Electric properties and conformation of polyethylenimine at the hematite-aqueous solution interface, *J. Colloid Interface Sci.*, 196 (1997) 87-91.

[29] G. M. Lindquist and R. A. Stratton, The role of polyelectrolyte charge density and molecular weight on the adsorption and flocculation of colloidal silica with polyethylenimine, *J. Colloid Interface Sci.*, 55 (1976) 45-59.

[30] H. K. Hall, Correlation of the base strengths of amines, *J. Am. Chem. Soc.*, 79 (1957) 5441-5444.

[31] R. Freitag and J. Breier, Displacement chromatography in biotechnological downstream processing, *J. Chromatogr.* A, 691 (1995) 101-112.

[32] H. G. M. Van de Steeg, M. A. Cohen Stuart, A. De Keizer, and B. H. Bijsterbosch, Polyelectrolyte adsorption: a subtle balance of forces, *Langmuir*, 8 (1992) 2538-2546.

[33] M. R. Böhmer, O. A. Evers, and J. M. H. M. Scheutjens, Weak polyelectrolytes between two surfaces: adsorption and stabilization, *Macromolecules*, 23 (1990) 2288-2301.

[34] R. Meszaros, L. Thompson, M. Bos, and P. de Groot, Adsorption and electrokinetic properties of polyethylenimine on silica surfaces, *Langmuir*, 18 (2002) 6164-6169.

[35] S. Akari, W. Schrepp, and D. Horn, Chemical imaging of single polyethylenimine polymers by chemical force microscopy, *Ber. Bunsenges. Phys. Chem.*, 100 (1996) 1014-1016.

[36] G. T. Hermanson, Modification with synthetic polymers, in *Bioconjugate Techniques,* Academic Press, San Diego, 1996, pp. 605-629.

[37] J. M. Harris and R. B. Chess, Effect of pegylation on pharmaceuticals, *Nat. Rev. Drug Discov.*, 2 (2003) 214-221.

[38] S. Zhang, J. E. I. Wright, G. Bansal, P. Cho, and H. Uludağ, Cleavage of disulfide-linked fetuin-bisphosphonate conjugates with three physiological thiols, *Biomacromolecules*, 6 (2005) 2800-2808.

[39] J. Suh, S. H. Lee, S. M. Kim, and S. S. Hah, Conformational flexibility of poly(ethylenimine) and its derivatives, *Bioorganic. Chem.*, 25 (1997) 221-231.

[40] S. A. Gittens, G. Bansal, C. Kucharski, M. Borden, and H. Uludağ, Imparting mineral affinity to fetuin by bisphosphonate conjugation: a comparison of three bisphosphonate conjugation schemes, *Mol. Pharmaceutics*, 2 (2005) 392-406.

[41] H. Uludağ, D. D'Augusta, R. Palmer, G. Timony, and J. Wozney, Characterization of rhBMP-2 pharmacokinetics implanted with biomaterial carriers in the rat ectopic model, *J. Biomed. Mater. Res.*, 46 (1999) 193-202.

[42] H. Uludağ, D. 'Augusta, J. Golden, J. Li, G. Timony, R. Riedel, and J. M. Wozney, Implantation of recombinant human bone morphogenetic proteins with biomaterial carriers: A correlation between protein pharmacokinetics and osteoinduction in the rat ectopic model, *J. Biomed. Mater. Res.*, 50 (2000) 227-238.

[43] A. K. Vogt, L. Lauer, W. Knoll, and A. Offenhausser, Micropatterned substrates for the growth of functional neuronal networks of defined geometry, *Biotechnol. Prog.*, 19 (2003) 1562-1568.

[44] M. Hu, E. E. Sabelman, C. Tsai, J. Tan, and V. R. Hentz, Improvement of Schwann cell attachment and proliferation on modified hyaluronic acid strands by polylysine, *Tissue Eng.*, 6 (2000) 585-593.

[45] M. C. Durrieu, S. Pallu, F. Guillemot, R. Bareille, J. Amédée, C. Baquey, C. Labrugère, and M. Dard, Grafting RGD containing peptides onto hydroxyapatite to promote osteoblastic cells adhesion, *J. Mater. Sci. Mater. Med.*, 15 (2004) 779-786.

[46] D. Itoh, S. Yoneda, S. Kuroda, H. Kondo, A. Umezawa, K. Ohya, T. Ohyama, and S. Kasugai, Enhancement of osteogenesis on hydroxyapatite surface coated with synthetic peptide (EEEEEEEPRGDT) *in vitro*, *J. Biomed. Mater. Res.*, 62 (2002) 292-298.

[47] A. A. Sawyer, D. M. Weeks, S. S. Kelpke, M. S. McCracken, and S. L. Bellis, The effect of the addition of a polyglutamate motif to RGD on peptide tethering to hydroxyapatite and the promotion of mesenchymal stem cell adhesion, *Biomaterials*, 26 (2005) 7046-7056.

[48] C. P. Ong, R. P÷rtner, H. MΣrkl, Y. Yamazaki, K. Yasuda, and M. Matsumura, High density cultivation of hybridoma in charged porous carriers, *J. Biotechnol.*, 34 (1994) 259-268.

[49] H. M. Aydin, M. Türk, A. Calimli, and E. Piskin, Attachment and growth of fibroblasts on poly(L-lactide/epsilon-caprolactone) scaffolds prepared in supercritical CO2 and modified by polyethylenimine grafting with ethylene diamine-plasma in a glow-discharge apparatus, *Int. J. Artif. Organs.*, 29 (2006) 873-880.

[50] M. Varkey, C. Kucharski, T. Haque, W. Sebald, and H. Uludağ, *In vitro* osteogenic response of rat bone marrow cells to bFGF and BMP-2 treatments, *Clin. Orthop. Relat. Res.*, 443 (2006) 113-123.

[51] M. Müller, B. Kessler, N. Houbenov, K. Bohata, Z. Pientka, and E. Brynda, pH Dependence and protein selectivity of poly(ethyleneimine)/poly(acrylic acid)

multilayers studied by in situ ATR-FTIR spectroscopy, *Biomacromolecules*, 7 (2006) 1285-1294.

[52] B. C. C. Pessela, L. Betancor, F. Lopez-Gallego, R. Torres, G. M. Dellamora-Ortiz, N. Alonso-Morales, M. Fuentes, R. Fernández-Lafuente, J. M. Guisán, and C. Mateo, Increasing the binding strength of proteins to PEI coated supports by immobilizing at high ionic strength, *Enzyme Microb. Technol.*, 37 (2005) 295-299.

CHAPTER V

Polyethylenimine-Coated Albumin Nanoparticles for BMP-2 Delivery[1]

[1]The contents of this chapter have been previously published in: S. Zhang, G. Wang, X. Lin, M. Chatzinikolaidou, H. P. Jennissen, M. Laub and H. Uludağ, Polyethylenimine-coated albumin nanoparticles for BMP-2 delivery, *Biotechnol. Prog.*, 24 (2008) 945-956.

INTRODUCTION

Bone-inducing growth factor, Bone Morphogenetic Protein-2 (BMP-2), plays a critical role in bone healing by means of its ability to stimulate differentiation of mesenchymal cells to an osteochondroblastic lineage [1]. After Wozney et al. reported the nucleotide sequence of first bone morphogenetic proteins in 1988 [2], various BMPs were produced in abundance with the use of recombinant gene technology. The therapeutic applications involving the recombinant BMPs demonstrated robust efficacy in the treatment of bone diseases. For example, BMP-2 showed good ability to heal critical size defects in rat, rabbit, sheep, dog, and primate models [3-7] and it has become part of a new treatment modality in orthopaedic practice [8]. Unlike the traditional surgical repair that necessitates the use of autografts, stimulation of local bone healing via the delivery of BMPs can fulfill the aim of bone repair without morbidity associated with the surgical techniques. However, BMP-2 is a 32-kDa molecular weight peptide [9] and it exhibits a short *in vivo* half-life. The clinical BMP-2 administration was focused on local delivery by incorporating the protein into a carrier matrix to provide a slow delivery formulation [10]. The delivery mechanism has relied on adsorption of the protein in collagenous biomaterials; slow protein desorption from the implanted biomaterial has provided the necessary concentration at the local site. The collagen sponge appeared to be the most effective matrix in animal studies, and it remains the only FDA-approved recombinant human BMP-2 carrier in clinical practice [11, 12].

A better way to control the BMP-2 delivery is to encapsulate the protein in nanoparticles (NPs) so that the physicochemical properties of the particles can control the BMP-2 release more precisely. Nanoparticulate drug delivery system may provide a

promising mechanism, not only for local application, but also for targeted bone stimulation via intravascular injection. The colloidal micro/nanoparticles were originally explored for delivery of other cytokines. For example, erythropoietin, NGF and IL-2 were formulated in poly(lactic acid)/poly(*D,L*-lactic-*co*-glycolic acid) (PLA/PLGA) particles for delivery [13]. Drawbacks of these materials include low encapsulation efficiency and rapid initial release of proteins, as well as the need for special formulations to maintain protein stability [14]. Current techniques often produce NPs by employing harsh organic solvents, synthetic polymers, or surfactants having high toxicity or immunological activity [15]. More recently, BMP-2 was encapsulated in 20-40 μm particles of dextranglycidyl-methacrylate/poly(ethylene glycol) [16]. BMP-2 was shown to remain bioactive after *in vitro* release, which displayed a burst release for all particles prepared. Another study investigated the BMP-2 nanospheres prepared by a coacervation-co-precipitation method [17], with the use of polysaccharide/N,N-diethylaminoethyl dextran/BSA to form particles stabilized by phosphatidyl-choline. The size of the particles ranged from 160 to 250 nm, but BMP-2 release from these particles was not investigated in that study.

NPs based on natural biopolymers will be more advantageous over particles made of synthetic materials. Bovine serum albumin (BSA) is a physiological protein that was widely used for NP preparation by different techniques [18-21]. BSA NPs are considered suitable for drug delivery since they are naturally biodegradable, non-toxic and non-antigenic. The BSA NPs can be easily prepared under mild conditions by coacervation, or controlled desolvation processes [22-24]. To improve NP stability, BSA NPs is typically cross-linked by glutaraldehyde [25-27]. The glutaraldehyde reacts with free amines on

BSA, and possibly with any amines on the encapsulated drug, which could adversely affect the drug integrity. The potential toxicity of glutaraldehyde is also a concern for *in vivo* delivery. As an alternative to glutaraldehyde, we considered the possibility of stabilizing BSA NPs with polyethylenimine (PEI). Branched PEI, due to its high density of positive charges, was expected to readily adsorb to the surface of BSA particles. The PEI coating could provide a means of controlling release rate of the encapsulated BMP-2. In this study, we explored the feasibility of such an approach by entrapping BMP-2 in BSA NPs and coating the particles with PEI. The results indicated that BMP-2 encapsulated in BSA NPs retained its bioactivity, and was released from the NPs as a function of PEI coating on the particles.

MATERIALS AND METHODS

Materials

Bovine serum albumin (BSA), 3-(4,5-dimethylthiazol-2-yl)-2,5-diphenyltetrazolium bromide (MTT), the ALP substrate p-nitrophenol phosphate (p-NPP), 1,3,4,6-tetrachloro-3a,6a-diphenylglycouril (TCDG), and branched PEI (M_w ~25,000 by LS, M_n ~10,000 by GPC) were obtained from Sigma-Aldrich (St. Louis, MO, USA). Recombinant human Bone Morphogenetic Protein-2 (BMP-2, from *E.coli.*) was prepared as described before [28]. Fluorescein isothiocyanate (FITC) was obtained from Pierce (Rockford, IL, USA). $Na^{125}I$ (in 0.1M NaOH) was obtained from GE Healthcare (Piscataway, NJ, USA). Dulbecco's Modified Eagle Medium (DMEM), Hank's Balanced Salt Solution (HBSS), penicillin (10,000 U/mL solution) and streptomycin (10,000 μg/mL solution) were from Invitrogen (Carlsbad, CA, USA). Fetal bovine serum (FBS)

was from Atlanta Biologics (Atlanta, GA, USA). All tissue culture plasticware was from Corning (Corning, NY, USA). The Spectra/Por dialysis tubings with 12-14 kDa and 100 kDa cut-off were acquired from Spectrum Laboratories (Rancho Dominguez, CA, USA). Distilled/de-ionized water (ddH_2O) used for buffer preparations were derived from a Milli-Q purification system.

Preparation of BMP-2 Encapsulated, PEI-Coated BSA NPs

BSA NPs were prepared by a coacervation method, or desolvation, as described previously [29-31], except the cross-linker glutaraldehyde was eliminated in this process. Briefly, 250 μL of 10 mg/mL BSA solution (50 mg of BSA dissolved in 5 mL ddH_2O) was added to 250 μL of 10 mM NaCl solution (pH=7.0) in a glass vessel under constant stirring (600 rpm) at room temperature. The stirring was allowed to proceed for 15 min. Then, 72 μL of 0.5 mg/mL BMP-2 in ddH_2O was added into the above solution. This aqueous phase was then desolvated with dropwise addition of 3.0 mL of ethanol after 2 h of incubation. The mixture was stirred (600 rpm) under room temperature for 3 h. The BMP-2 encapsulated BSA NPs so formed were coated with different PEI concentrations (see Legends for exact concentrations). Specially, different concentrations of PEI in 0.5 mM NaCl solution were added to the above NPs solution by a volume ratio of 1.25 to 1. The coating was allowed to proceed for 1 or 4 h under stirring. The coated NPs were extensively dialyzed (MWCO: 12-14 kDa) against phosphate buffered saline (pH=7.3, ×3) and, for the bioactivity studies, then against DMEM with 1% penicillin/streptomycin (×1). The dialyzed buffer was exchanged every 3 h. All solutions used for NP preparation were sterilized by passing through 0.20 μm sterile filter (SARSTEDT, Aktiengesellschaft &

Co., Germany) before use, and the manufacture process was carried out under sterile conditions.

For the determination of the percentage of BSA transformed into NPs before coating, the NPs were separated from the supernatant by centrifugation at 10,000 rpm for 10 min at room temperature. The amount of BSA in the supernatant was determined by the Bradford protein assay [32]. To 50 μL of the supernatant, 1 mL of the protein reagent was added, and the samples were analyzed spectrophotometrically at 595nm. A calibration curve was based on known concentrations of BSA standards. The yield of BSA in the NPs was calculated as: 100% × {(initial amount of BSA – BSA amount in the supernatant)/(initial amount of BSA)}.

Particle Size and Zeta Potential

The mean particle size and polydispersity index of the PEI-coated and uncoated BSA NPs were determined by dynamic light scattering at 25°C with a Zetasizer 3000 HS (Malvern Instruments Ltd., UK) using a 633 nm He-Ne laser at a scattering angle of 90°. The surface charge of the coated and uncoated BSA NPs were investigated by measuring the electrophoretic mobility of the particles using the zeta potential modus of the same instrument at 25°C. The samples for measurement were prepared after appropriate dilution and suspended in 1 mM NaCl solution. Both particle size and zeta potential measurements were measured for three batches of particles, each measurement being the average of 3 runs.

Scanning Electron Microscopy (SEM)

Scanning electron microscopy was used to study the morphology of the NPs. The samples were first dialyzed (MWCO: 100 kDa) against ddH_2O (×3), then centrifuged at 8000 rpm for 10 min (×3) to remove any free BSA and PEI. The pellet was then re-dispersed in ddH_2O. 3 μL of the sample was added onto a clean silica surface, and dried under room temperature with natural convection. The prepared samples were, then, scanned on a JOEL Jamp-9500F SEM.

Atomic Force Microscopy (AFM)

MFP-3D AFM (Asylum Research, Santa Barbara, CA, USA) was used for the AFM studies of PEI-coated BSA nanoparticles. AC240TS cantilever was used throughout all AFM measurements. The oscillation amplitude of the scanning tip was registered at 0.6 V and the frequency of the oscillation was in the range of 60-70 kHz. All AFM imaging was under conventional ambient tapping mode AFM. The scan rate was typically 0.5-1.0 Hz, and the sample size was 512×512 pixels. Images were processed and analyzed by the Igor Pro imaging software (version 5.04B). The NP samples were sonificated for 5 min and then 1.5 μL of the sample was dropped onto the mica surface (PELCO^R Mica Discs; TED PELLA, Inc.; Redding, CA, USA), and imaged after drying under room temperature.

Coating Efficiency with FITC-PEI

In one study, the amount of FITC-PEI coated on BSA NPs was determined by fluorescence measurements. To obtain the labeled polymer, a stock solution of FITC (10 mM in DMSO) was added to PEI solution (10 mg/mL in ddH_2O) for 2.5 h to give a final

concentration of 0.1 mM FITC, after which the samples were dialyzed (MWCO: 12-14 kDa) against ddH_2O (×3) to remove the unreacted FITC [33]. Different concentrations of FITC-PEI were used to coat BSA NPs. The PEI-coated NPs (1 h and 4 h coating) were first dialyzed (MWCO: 100 kDa) against ddH_2O (×3), centrifuged (×3) for 10 min at 8000 rpm to remove ethanol, free BSA and uncoated PEI, and then re-dispersed in ddH_2O. A 200 μL of the aliquot in duplicate was then added to black 96-well plates (NUNC, Rochester, NY, USA) and the fluorescence (λ_{ex}: 485 nm; λ_{em}: 527 nm) was determined with a multiwell plate reader (Thermo Labsystems, Franklin, MA, USA). The amount of FITC-PEI coated on the BSA NPs was calculated based on a calibration curve generated by using the FITC-PEI in ddH_2O. The calibration curve was also generated in a mixture of FITC-PEI and BSA solution (0.5 and 1.0 mg/mL of BSA, respectively), and the results showed that they were comparable to the calibration curve generated in ddH_2O (data not shown). The coating efficiency of FITC-PEI was calculated as: 100% × {(final FITC-PEI of the pellet)/(initial FITC-PEI for coating)}.

Encapsulation Efficiency and *In Vitro* Release of BMP-2

To determine the encapsulation efficiency and *in vitro* release of BMP-2, BMP-2 was labeled with ^{125}I by using the Iodo-Gen procedure [34]. Microcentrifuge tubes were coated with TCDG (200 μL of 20 μg/mL TCDG in chloroform), and 20 μL of BMP-2 solution (10 μg of BMP-2) was added to the coated tubes, along with 50 μL of 0.1 M phosphate buffer (pH=4.5) and 20 μL of 0.2 mCi of $Na^{125}I$. After reacting for 25 min, free ^{125}I was separated from the radiolabeled BMP-2 by using a Sephadex G-25 column. After precipitating an aliquot of the purified samples with 20% trichloroacetic acid

(TCA), the counts in the supernatant and the pellet was determined with a γ-counter (Wizard 1470; Wallac, Turku, Finland), and it was confirmed that the iodinated samples contained < 4% free ^{125}I. To determine the encapsulation efficiency, ^{125}I-labeled BMP-2 was first diluted by ddH_2O (1:5), and then mixed with BSA solution as described above to prepare the NPs. 500 μL of ^{125}I-labeled BMP-2 encapsulated BSA NPs, uncoated and coated with different concentrations of PEI, were then added into the microcentrifuge tubes in triplicate. The samples were centrifuged at high speed for 10 min (BHG Hermle Z230 M Centrifuge). The counts in the supernatant and pellet were determined by a γ-counter, and the encapsulation efficiency (EE) was calculated as: EE = 100% × {(counts in the pellet)/ (counts in the pellet + counts in the supernatant)}.

The NPs containing ^{125}I-labeled BMP-2 was used to measure the release rate of BMP-2 *in vitro*. The NPs were coated with PEI concentrations of 0.6, 0.3, 0.1 and 0 mg/mL for 1 h for this study. The release experiment was performed by incubating the NPs (in triplicate) in 1 mL DMEM with 1% penicillin/streptomycin at 37±1°C and under constant shaking. At indicated time points, the samples were centrifuged at high speed for 10 min (BHG Hermle Z230 M Centrifuge). The counts in the supernatant and the pellet were determined separately by a γ-counter. 1 mL of fresh release medium was added back to the pellet to maintain a constant volume during release period. To test for free iodine in the supernatant, an aliquot of the purified samples was precipitated with 20% TCA after each centrifugation. The counts in the TCA supernatant and the pellet were determined by a γ-counter, and ^{125}I-labeled BMP-2 released to the supernatant was calculated accordingly.

Toxicity of BSA NPs by MTT assay

The MTT dye reduction assay [35] was used to assess the cytotoxicity of PEI-coated NPs. Various concentrations of PEI were coated on BMP-2 encapsulated BSA NPs for 1 h. After coating, the samples were first dialyzed (MWCO: 12-14 kDa) against phosphate buffered saline (pH=7.3; ×3), followed by dialysis against DMEM with 1% penicillin/streptomycin (×1). The samples were then centrifuged at 8000 rpm for 10 min, and the supernatant was removed. The same volume of fresh DMEM with 1% penicillin/streptomycin was added to the pellet, which was sonicated for 20 min. An aliquot of the supernatant and the suspended pellet was incubated with human C2C12 cells grown on 48-well plates (in triplicate). After 48 h incubation, 100 μL of sterile filtered 5.0 mg/mL MTT solution in HBSS were added to 0.5 mL cell culture medium in each well. The plates were incubated in the dark for 2 h, the supernatant was aspirated, and 0.5 mL DMSO was added to each well. Then the plates were incubated for 5 min and mixed to dissolve the crystals. The optical density of the crystals was measured by an ELISA reader at 570 nm. The untreated cells served as the reference. The mean optical density was used as a measurement of cell number/well.

BMP-2 Bioactivity by Kinetic ALP assay

A kinetic ALP assay was performed to determine the bioactivity of encapsulated BMP-2 [36]. Human C2C12 cells, grown in 48-well plates, were first incubated with the NPs (supernatant and suspended pellet), which were processed as described in the MTT assay. After 72 h of incubation, the C2C12 cells were washed with HBSS (×2) and lysed with 200 μL ALP buffer (0.5 M 2-amino-2-methylpropan-1-ol and 0.1% (v/v) Triton-X;

pH=10.5). After 1 h of lysis, 200 μL of 1.0 mg/mL ALP substrate (p-nitrophenol phosphate) was added to the lysed cells. The changes in optical density ($\lambda_{absorbance}$: 405 nm) were determined in a multiwell plate reader at an intervals of 1.5 min for 8 cycles. The kinetic ALP activity was expressed as the change in optical density of the wells per unit time (mAbs/minute). All results were expressed as mean ± standard deviation (SD) of triplicate wells.

Data Analysis

All data shown in Figures are summarized as mean ± SD of the specified number of replicates. The number of independent experiments (n) was specified for each Figure in the legends. Where indicated, statistical differences between group means were analyzed by the two-sided Student's *t*-test or single factor analysis of variance (ANOVA, Microsoft Office Excel 2003).

RESULTS AND DISSCUSSION

A new formulation of BMP-2 in NPs was pursued by first eliminating the glutaraldehyde used in a typical BSA NP fabrication process. The reason for this was the possibility of glutaraldehyde cross-linking the protein amines to the BSA matrix, producing a protein-conjugate, which could affect the protein release and bioactivity. This was noted for the encapsulation of recombinant IFN-γ, a cytokine of the Th1-type cellular immune response, with albumin NPs. The IFN-γ inside the BSA matrix completely abrogated its bioactivity, whereas the adsorbed IFN-γ on the glutaraldehyde cross-linked NPs retained its bioactivity [26]. A previous study performed by the same

group [27], in which no release of IFN-γ was observed from the glutaraldehyde cross-linked BSA NPs, also highlighted the need to eliminate glutaraldehyde in the BSA NP fabrication process. In addition to proteins, glutaraldehyde cross-linking was also problematic for the small molecular drug doxorubicin, which gave only ~8% free drug release in a 3-day study period due to drug conjugation to the BSA matrix [25]. This incomplete release of drug was also reported by another group studying the glutaraldehyde cross-linked albumin microspheres for the release of adriamycin [37]. We, therefore, turned to branched PEI, which is known to display exceptional affinity to anionic surfaces. This physical interaction between PEI and BSA matrix should not affect the BMP-2 integrity during encapsulation and at the same time control the release of BMP-2 through the network of BSA-PEI matrix formed on the NP surface (**Scheme 5-1**). The properties of NPs formed from such a process were first investigated, followed by the BMP-2 release kinetics and bioactivity *in vitro*.

Characterization of PEI-Coated BSA NPs.

In order to examine the influence of PEI coating, BSA NPs were prepared by changing the PEI concentration during the coating process as well as the contact time between the NPs and the PEI. Using PEI concentrations of 0.1, 0.3, 0.6 and 1.0 mg/mL, the size of the NPs was observed to gradually increase as the PEI coating concentration was increased; from 150 nm for the uncoated NPs, to ~230, ~280, ~330, and ~400 nm for 0.1, 0.3, 0.6 and 1.0 mg/mL PEI, respectively (**Figure 5-1A**). A coating time of 1 or 4 h did not seem to make a difference in the size of the particles (**Figure 5-1A**). With higher PEI concentration, the availability of more PEI presumably facilitated the formation of a

thicker and more intensive layer of a PEI-BSA network on NP surfaces [38]. The coating appeared to be rapid, since it seemed to be complete within 1 hour of contact between the NPs and the PEI. The extent of PEI coating controlling the size of NPs was also reported for a preparation of PLA/PLGA NPs, where PEI was used to reduce the interfacial surface energy between the particle surface and the aqueous media [39]. Coating by using 1.0 mg/mL PEI led to relatively significant variations in the NP size (see large SDs in **Figure 5-1A**), probably due to higher aggregation of the BSA NPs with the availability of abundant PEI capable of forming linkages among the particles. The polydispersities of the NPs are summarized in **Figure 5-1B** for three independent batches of NPs. The relatively high polydispersity of NPs was attributed to two possible reasons: (1) the manual performance of the desolvation process by adding the desolvating agent, ethanol, to the protein solution drop by drop as mentioned by other groups before [29]; (2) some aggregation of particles formed for PEI coated NPs, or unstable particles disassociated for uncoated NPs during the dialysis process. There was no significant difference in the polydispersity of NPs from different PEI concentrations used for coating (ANOVA).

The zeta-potential of the particles increased significantly as a result of PEI coating (**Figure 5-1C**), from -10 mV for uncoated NPs to +21-29 mV for the PEI coated NPs. A slight increase from +21 to +29 mV was exhibited for coated NPs as the PEI concentration was increased from 0.1 mg/mL to 1.0 mg/mL. This was indicative of increased PEI adsorption with increased concentration, an observation consistent with increasing particle size in this concentration range. There was a small increase of the zeta potential as the coating time was increased from 1 to 4 h, but this was not significant and it paralleled the effect of coating time on particle size.

Using the Bradford protein assay, we obtained >90% BSA transformation into the NPs after ethanol desolvation. This was in agreement with earlier results of Langer and Weber et al [29, 40]. The amount of PEI adsorption on BSA NPs was directly quantified by using a FITC-labeled PEI polymer and measuring the extent of adsorbed fluorescence on NPs. The results were summarized as PEI amount (μg) adsorbed on NPs (**Figure 5-2A**). As the PEI concentration was increased, the amount of adsorbed PEI was increased as expected. There was no difference in the adsorbed PEI between 1 and 4 h for PEI coating concentration of 0.1 mg/mL, but a difference was noted for other PEI concentrations. Between the lowest and highest PEI concentrations used in this study, ~2-fold and ~3-fold increase in PEI coating were seen for 1 h and 4 h coating time, respectively. The effect of such an increase did not have a corresponding consequence in size and/or charge of the NPs. The PEI coating efficiency (**Figure 5-2B**) was dependent on the PEI concentration; as expected, coating with 0.1 mg/mL PEI demonstrated the highest coating efficiency (~45%) among all PEI concentrations. The coating efficiency was increased by 4-6% as the coating time was increased from 1 to 4 h for other PEI concentrations. The highest coating efficiency obtained with the lowest PEI concentration was consistent with our previous results of PEI adsorption to hydroxyapatite: the percentage of hydroxyapatite adsorption was decreased as the PEI concentration increased; the total amount of binding, however, increased with the increasing PEI concentration in the medium [33]. It was interesting to note that FITC-labeled PEI continued to adsorb to BSA NPs from 1 to 4 h, even though this was not immediately clear from size and charge measurements. It is likely the adsorbed PEI was penetrating

into the interior of the NPs during this time without affecting the size or surface properties.

As shown in **Figure 5-3,** the NPs generally possessed spherical shapes and smooth surface characteristics after analysis by SEM and AFM. **Figures 5-3A** and **5-3B** are SEM images for particles coated with 1.0 and 0.1 mg/mL PEI, respectively. Whereas more uniform particles were evident for coating with the lower PEI concentration, coating with higher PEI concentration resulted in some non-spherical particles, typically appearing as elongated particles. Presumably this resulted from fusion of two separate spherical particles. This might also be the underlying mechanism for increased sizes of the particles measured by the dynamic light scattering. **Figures 5-3C** and **5-3D** are height-mode AFM images for 1.0 and 0.1 mg/mL PEI coating, respectively. Larger particles for coating with 1.0 mg/mL PEI were also evident in comparing these two images. **Figure 5-3E** is the amplitude-mode AFM image for 0.1 mg/mL PEI coated BSA NPs with BMP-2 encapsulated (14.4 μg/mg bulk BSA). Encapsulating BMP-2 in the NPs did not increase the size of the particles (**Figure 5-3E**).

The particle size and surface charge are two main properties that can influence biodistribution of colloidal carriers upon administration [41]. This is not likely to be a critical issue when NPs are used for local delivery of proteins after implantation, but it will be a significant issue when NPs are injected systemically. A positive surface charge of the NPs is regarded beneficial for penetrating plasma membrane [42]; however, it is a major disadvantage after systemic administration since cationic NPs can bind nonspecifically to cell surfaces and activate the complement system [43]. In addition, particulates are rapidly opsonized with serum proteins [44], leading to preferential uptake

of particles by the cells of the reticuloendothelial system (RES) and rapid clearance. These adverse effects associated with the use of cationic NPs *in vivo* can be reduced with smaller NPs [45, 46] and lower surface charges [44]. It was reported that the extent of opsonization decreased as the size of the particles decreased from 800 to 200 nm, and no enhancement of phagocytic uptake was recorded at particle sizes below 200 nm [41]. However, particles below 100 nm were able to cross the fenestration in the hepatic sinusoidal endothelium, leading to a hepatic accumulation instead of long circulation times. Though deformity of particles was considered to be a factor for crossing endothelial fenestration [47], the albumin-based particles are regarded as a solid particle matrix. One study investigated *in vivo* distribution of surface-modified albumin NPs in rats, and observed no differences in blood circulation times and organ accumulation among positive, negative and neutral surface charged nanoparticles [48]. Evaluating *in vivo* biodistribution of the PEI-coated BSA NPs was beyond the scope of this study, but it appears that BSA NPs coated with lower PEI concentrations might be more desirable for systemic administration due to reduced size, reducing the chances of opsonization. It remains to be seen whether *in vivo* biodistribution will be unaffected by the extent of PEI coating, as suggested in [48], or whether PEI will impart a unique biodistribution pattern to the BSA NPs.

Encapsulation Efficiency and BMP-2 Release.

The encapsulation efficiency and *in vitro* release of BMP-2 was assessed by using ^{125}I-labeled BMP-2 in BSA NPs. The BMP-2 encapsulation efficiency was typically >90% for all NPs prepared (**Table 1**), and it was even higher after PEI coating of the NPs.

A significant effect of PEI coating was readily observed on the BMP-2 release kinetics, analyzed by assessing the BMP-2 amount in the tissue culture release medium (**Figure 5-4A**) or the BMP-2 amount retained in the NPs (**Figure 5-4B**). A burst release of BMP-2 was readily evident for uncoated NPs, where >70% of the BMP-2 content was released into the medium within the first day. When NPs were treated with PEI, a pronounced decrease in the BMP-2 burst release (<15% in 1 day) was seen, while the release period was extended over the 10-day study period (**Figure 5-4**). Increasing the PEI concentration used for coating NPs decreased the extent of BMP-2 release; the cumulative release at the end of the 10 days was 51%, 42% and 29% for NPs coated with 0.1, 0.3 and 0.6 mg/mL PEI, respectively (**Figure 5-4A**). The differences in accumulative release between 0.6 and 0.3 mg/mL, and 0.6 and 0.1 mg/mL PEI coating were significant ($p<0.05$), whereas the difference between 0.3 and 0.1 mg/mL PEI coating was not. Taken together, an effective layer of PEI appeared to be formed around the NP surfaces to control the BMP-2 release, and treatment with higher PEI concentration allowed slower release of BMP-2 with a minimal burst release. It is likely that the effect of PEI coating was mediated by two mechanisms, one in which the PEI coating physically reduced the BMP-2 diffusion through the NP surface, and one in which the PEI stabilized the particles, preventing pre-mature disintegration of the BSA NPs. In this case, microscopy study of uncoated NPs labeled with fluorescence over time will be useful in the investigation of NP disintegration. Nevertheless, the relative contribution of each mechanism remains to be determined.

The 10-day, 29-51% cumulative BMP-2 release obtained with the current PEI-coated BSA NPs was less than the VEGF release obtained from NPs formed by VEGF-

bound dextran and PEI (~50% encapsulation efficiency with >10 days of ~75% cumulative release) [49]. The ionic interaction between anionic dextran sulfate and cationic PEI built up the NPs in that system and effectively controlled the release of VEGF. Chitosan and poly-L-lysine were also investigated in that study as alternative polycations, but they all showed similar VEGF release trends. However, the influence of PEI concentration on particles formation and VEGF release was not examined in that study. Similar approach for protein delivery was also employed for the delivery of insulin and amphotericin B [50, 51], where 40-100% release were observed in the study period depending on the ionic strength and the nature of the release medium. BMP-2 is not readily soluble at the physiological pH, and this may explain the lower amount of BMP-2 release in our system. A lower release, however, may be advantageous for *in vivo* application where increased retention at implant site may give a more robust bone induction [52].

Toxicity of PEI-Coated BSA NPs

The MTT assay was employed to determine the cytotoxicity of the PEI-coated BSA NPs. Among the components of the prepared NPs, only PEI was expected to display cytotoxicity since cationic polymers strongly interact with anionic cellular surfaces and might compromise the integrity of cellular membranes [53]. PEI is known to induce cytotoxicity due to its unique architecture and an increased toxicity was noted with high molecular weight and branching [54]. Initial studies indeed showed a strong toxicity of the prepared NPs on C2C12 cells, especially for particles coated with high PEI concentrations (not shown). To elucidate the source of the toxicity, BSA NPs were

separated into two fractions by centrifugation; a supernatant containing soluble BSA and PEI molecules, and a pellet containing the NPs, and the cytotoxicity of these two fractions was evaluated separately. The supernatant of the BSA NPs displayed differential cytotoxicity as a function of PEI concentration used for coating (**Figure 5-5A**). A clear toxicity was evident for the two higher PEI concentrations (1.0 and 0.6 mg/mL) while the toxicity of 0.3 mg/mL PEI coating was dependent on the volume of the supernatant added to the cells. The lowest concentration of the PEI (0.1 mg/mL) did not indicate any additional toxicity as compared to the uncoated NPs. In contrast, the pellet containing the NPs from different preparations did not reduce the viability of the cells, based on the relatively similar MTT absorbance for all PEI concentrations used for coating (**Figure 5-5B**). Two additional batches of NP preparations were evaluated in the similar manners, and both batches gave similar results as above (not shown).

These results were indicative of free PEI being present in the NP preparations. The dialysis procedure used for removing free PEI apparently did not lead to complete removal of the PEI, but a centrifugation process was successful to prepare the NPs with no/little cytotoxicity. This was important in further bioactivity testing of the NP preparations, since any toxicity of NPs might lead to underestimation of the BMP-2 bioactivity retained in the NPs. The PEI immobilized on the BSA NPs was apparently not toxic, either due to its low concentration or its immobilized state which prevented its association with cellular surfaces. An independent study on PEI based DNA-polyplexes, reported a significant proportion of the polymer utilized remained in free form; this was in part responsible for cell dysfunction and cytotoxicity. After purification of the PEI/DNA complex, the particles demonstrated reduced toxicity [55], which suggested

that the purification of the NPs could reduce the toxicity of the PEI coating. It might be necessary to replace PEI in future studies with more biocompatible cationic polymers, but for the purposes of this study, PEI-coated NPs was further tested to investigate whether BMP-2 activity was retained in the NP formulations.

BMP-2 Activity in PEI-Coated BSA NPs.

ALP is an early marker of osteoblast differentiation [56]. We used the BMP-2 induced ALP induction in C2C12 cells *in vitro* as a measure of BMP-2 activity. We first measured the ALP induction by four groups: (i) BSA NPs without BMP-2, (ii) BSA/BMP-2 solution that was subjected to NP formation process without the addition of ethanol so that no NPs was formed, (iii) BSA NPs with encapsulated BMP-2, and (iv) PEI (1.0 mg/mL)-coated BSA NPs with encapsulated BMP-2 (**Figure 5-6**). The BMP-2 loading in the above samples was 14.4 μg BMP-2/mg bulk BSA. The samples were analyzed without centrifugal purification. An equivalent BMP-2 activity was evident in two samples, the BMP-2/BSA mixture and the BMP-2 entrapped in BSA NPs (**Figure 5-6**). For the other two groups, BSA NPs without BMP-2 and PEI-coated BSA NPs with encapsulated BMP-2, there was no detectable activity. This was expected for the former group in the absence of BMP-2, as well as the latter due to excessive toxicity of PEI at this coating concentration (see **Figure 5-5A**). This study confirmed the retention of BMP-2 activity as a result of entrapment in BSA NPs. The fact that a similar activity was seen with and without NP formation suggests an equivalent level of BMP-2 retention in these samples. We expected almost complete entrapment of the BMP-2 in NPs based on the obtained encapsulation efficiencies (see **Table 5-1**); We also expected to retain a high

amount of BMP-2 in the BSA solution after processing, since (i) the dialysis tubing used for NP purification had a MW cut-off (12-14 kDa) smaller than the MW of BMP-2 (~32 kDa), and (ii) the presence of abundant BSA (~100-fold higher) should stabilize BMP-2 in solution and prevent its loss due to adsorption to the dialysis apparatus.

A subsequent study was performed by using BMP-2 containing NPs that were coated with lower PEI concentrations. The NP preparations were additionally fractionated into a supernatant containing the soluble molecules and a pellet containing the NPs before the bioactivity testing. The ALP induction is shown in **Figure 5-7A** for the NPs before fractionation, in **Figure 5-7B** for the pellet after fractionation and in **Figure 5-7C** for the supernatant after fractionation. For the unfractionated NPs, the ALP activity was induced as a function of NP volume added for uncoated BSA NPs and BSA NPs coated with 0.1 mg/mL PEI. No significant difference was evident between these two groups, indicating no adverse effects of the 0.1 mg/mL PEI coating. For BSA NPs coated with 0.6 and 0.3 mg/mL PEI, however, the induced ALP activity decreased as the volume of NPs increased, presumably due to the toxicity of the higher amount of PEI in the medium. Upon fractionation, free PEI was expected to be removed from the preparation, so that bioactivity could be tested in the absence of toxicity issues associated with the PEI. In this case (**Figure 5-7B**), all PEI-coated NPs containing BMP-2 gave significant activity in the pellet and the level of ALP induction of BSA NPs coated with 0.1 mg/mL PEI was significantly higher than 0.6 and 0.3 mg/mL PEI coating ($p<0.05$) at the highest volume (100 μL) of suspended pellet added. For the samples coated with the higher PEI concentration (0.6 and 0.3 mg/mL), there was still a decline in ALP activity at the higher volumes of samples added, indicating continued toxicity even for the pellet

fraction. It is possible that a high concentration of PEI adsorbed onto the NPs might directly damage the cells or be released into the medium to manifest its toxic effect. The NPs with the lowest PEI coating (0.1 mg/mL) gave a dose-response curve in the ALP induction assay without any sign of toxicity. BMP-2 entrapped in uncoated BSA NPs gave a little activity in the pellet fraction. This was presumably due to rapid release of BMP-2 into the supernatant of NP preparations, which suggested that the uncoated NPs are stable in ethanol, but relatively unstable during the dialysis procedure. The ALP activity was demonstrated when the supernatants of the same samples were analyzed in the bioassay; the uncoated BSA NPs gave a significant BMP-2 activity whereas the 0.6 and 0.3 mg/mL PEI-coated NPs gave nearly no BMP-2 activity and 0.1 mg/mL PEI-coated NPs gave some activity. Presumably, there was little release of BMP-2 for the 0.6 and 0.3 mg/mL PEI-coated NPs samples. It is possible that the lack of BMP-2 activity is obscured by the toxicity of 0.3 and 0.6 mg/mL PEI samples (from **Figure 5-5A**), but this was not valid for the 0.1 mg/mL PEI-coated sample since toxicity of the original preparation was minimal, if any, with this sample. In this case, some release of BMP-2 might have been achieved during the 4-day C2C12 cell incubation study, so that the BMP-2 was available during this time for the ALP induction.

The results from the bioactivity studies indicated that BSA NPs coated with 0.1 mg/mL PEI was the preferred formulation. Such NPs provided a release formulation that was compatible with the mammalian cells *in vitro*. The BMP-2 entrapped in such NP formulations was bioactive based on the ALP induction assay with C2C12 cells. The bioactivity studies also provided supportive evidence for the slower release of the BMP-2 from these formulations, unlike uncoated BSA NPs, which displayed the most BMP-2

activity in the supernatant and not in the pellet containing the NPs. The fact that little BMP-2 was recovered from the supernatant of NP formulations is encouraging for developing an aqueous-based process for NP fabrication, since protein loss due to release from NPs will be minimized during the fabrication process. It remains to be seen whether this is true for other bioactive proteins; BMP-2 is usually not soluble under physiological conditions (i.e., ionic strength and pH) and this might have helped with improved encapsulation efficiency and a more-sustained release profile. More-readily soluble proteins might behave differently in this respect. We are aware that C2C12 cells are myogenic origin and more studies will be needed to assess the bioactivity of the proposed BMP-2 formulations with more relevant cellular phenotypes. For example, cells derived from bone marrow cavity [36] or osteoblastic cell lines such as mouse calvarial MC3T3-E1 cells [28] will need to be further explored to better extrapolate the bioactivity results to physiological responses.

CONCLUSIONS

The bone-inducing growth factor BMP-2 was encapsulated in albumin NPs, which were coated with the cationic polymer, polyethylenimine, for better control of BMP-2 delivery kinetics. The electrostatic interaction between the anionic albumin and cationic PEI was sufficient to create an effective PEI coating on the NPs. The size of spherical nanoparticles ranged from ~150 nm for uncoated BSA NPs, and significantly increased up to 400 nm as a function of PEI concentration used for coating the particles. The zeta-potential of the particles similarly increased significantly as a result of PEI coating. The encapsulation efficiency was typically >90% in all NP preparations. *In vitro*

release of encapsulated BMP-2 was controlled by the PEI coating of the NPs, providing a gradual reduction of BMP-2 release as the PEI concentration for coating was increased. The cytotoxicity was a significant issue for NPs coated with high concentrations of PEI, but it was possible to minimize the toxic effect of PEI by using lower PEI concentration during coating process. The overall results indicated that BMP-2 encapsulated BSA NPs coated with 0.1 mg/mL PEI gave tolerable toxicity, retained a robust ALP induction activity in C2C12 cells, and efficiently slowed the release of BMP-2 from the BSA NPs. These studies established the foundation for testing NP formulations for BMP-2 in animal models, and in particular evaluating the effect of sustained-release formulations on BMP-2 induced bone formation.

TABLES

PEI concentration (mg/mL)	Encapsulation Efficiency	
	Before coating	After coating
0.6	-	96.53 ± 0.08
0.3	-	96.88 ± 0.15
0.1	-	96.20 ± 0.27
0	90.10 ± 0.38	-

Table 5-1. Encapsulation efficiency obtained by using ^{125}I-labeled BMP-2 (in triplicate). The coating time for all preparations was 1 h (n=2).

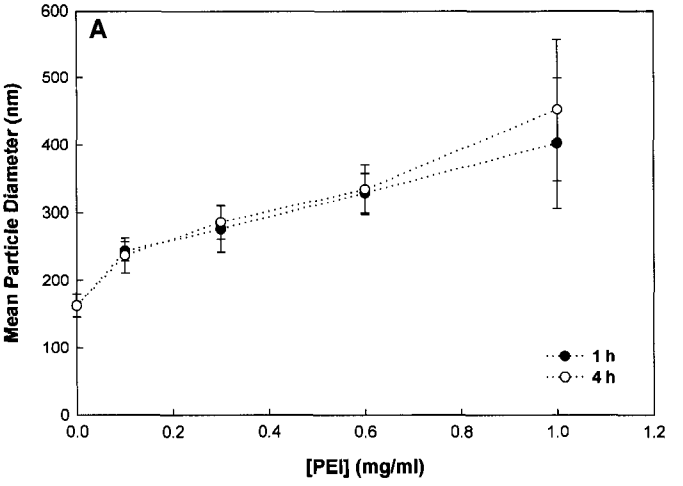

B. Polydispersity

1 h	Mean ± SD	4 h	Mean ± SD
1	0.42 ± 0.21	1	0.26 ± 0.23
0.6	0.47 ± 0.12	0.6	0.44 ± 0.06
0.3	0.20 ± 0.05	0.3	0.24 ± 0.17
0.1	0.32 ± 0.17	0.1	0.27 ± 0.16
0	0.44 ± 0.16	0	0.44 ± 0.16

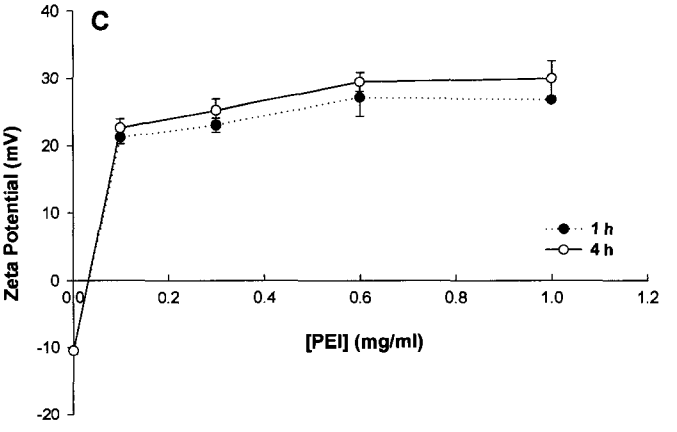

Figure 5-1. The mean particle diameter (**A**), polydispersity index (**B**), and zeta potential (**C**) of BSA NPs coated with different PEI concentrations (n=3). Three independent batches for each coating concentration were used for measurements, and each measurement was performed in 3 runs. The mean particle diameter increased from ~150 nm for uncoated BSA NPs to ~400 nm for the highest PEI coating concentration (1.0 mg/mL). The zeta potential of the coated NPs increased dramatically as compared to uncoated NPs, and slightly increased as PEI concentration was increased from 0.1 to 1.0 mg/mL for both 1 and 4 h coating times.

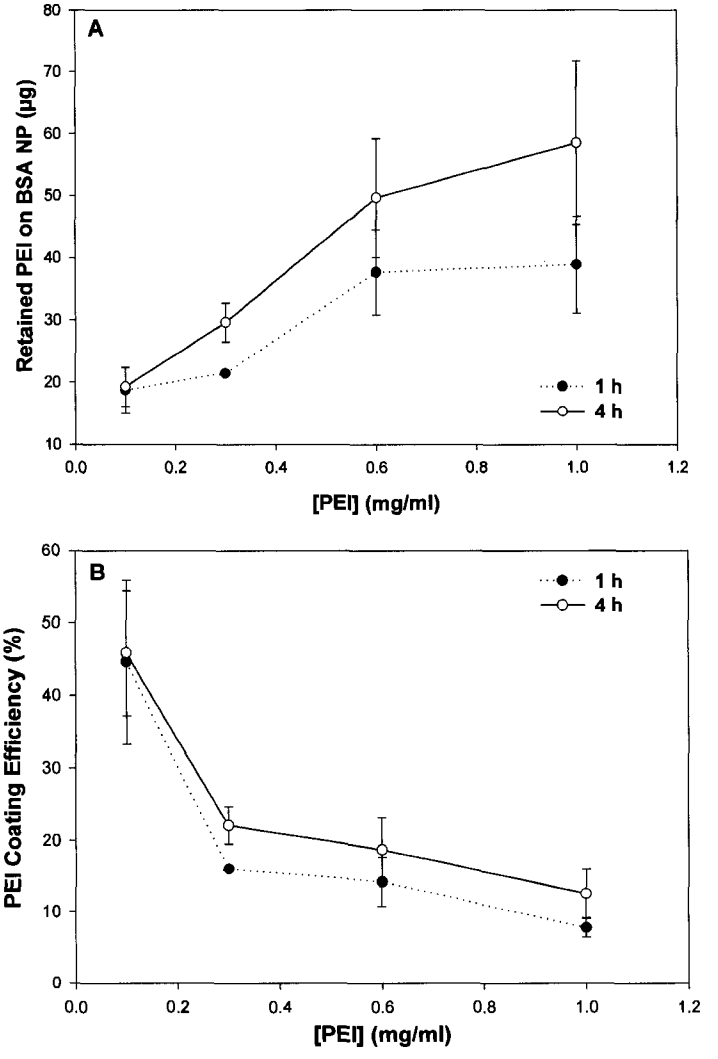

Figure 5-2. The quantification of PEI coating on BSA NPs, as measured by adsorption of FITC-labeled PEI (n=3). The fluorescence of the PEI adsorbed on BSA NPs was measured as a function of PEI coating concentration, and converted to mass (µg) of PEI adsorbed (**A**) based on FITC-PEI calibration curve. The amount of PEI adsorbed on the NPs was increased with the PEI concentration and the coating time. The coating efficiency on BSA NPs was calculated from the adsorbed PEI and the initial PEI in solution (**B**). Note that coating concentration of 0.1 mg/mL PEI gave the highest coating efficiency among the PEI concentrations used.

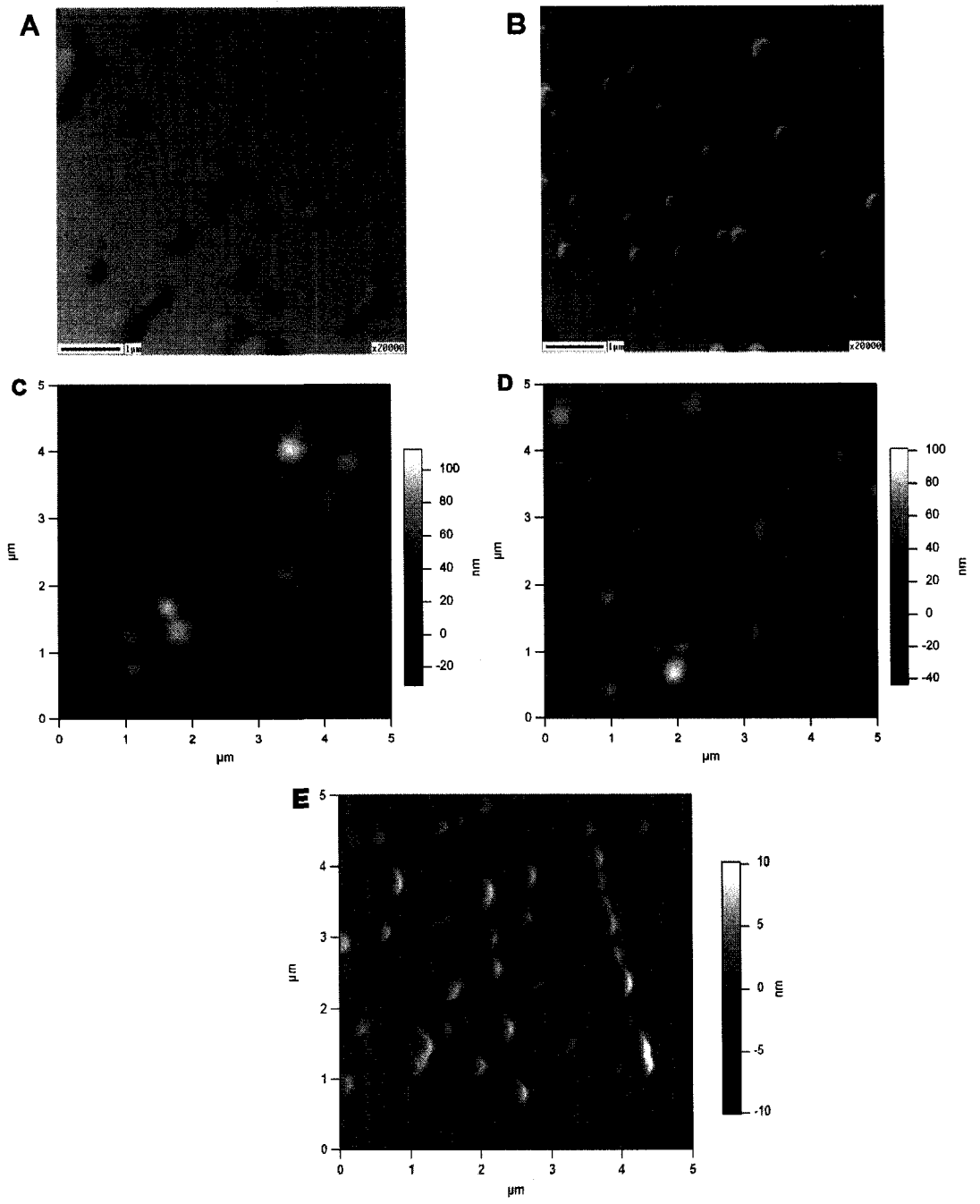

Figure 5-3. SEM images of BSA NPs coated with 1.0 mg/mL PEI (**A**) and 0.1 mg/mL PEI (**B**). AFM images (height-mode) of BSA NPs coated with 1.0 mg/mL PEI (**C**), 0.1 mg/mL PEI (**D**) and an amplitude-mode image of PEI (0.1 mg/mL)-coated BSA NPs with BMP-2 encapsulated (**E**). Larger diameter NPs were evident in the samples coated with the higher PEI concentration.

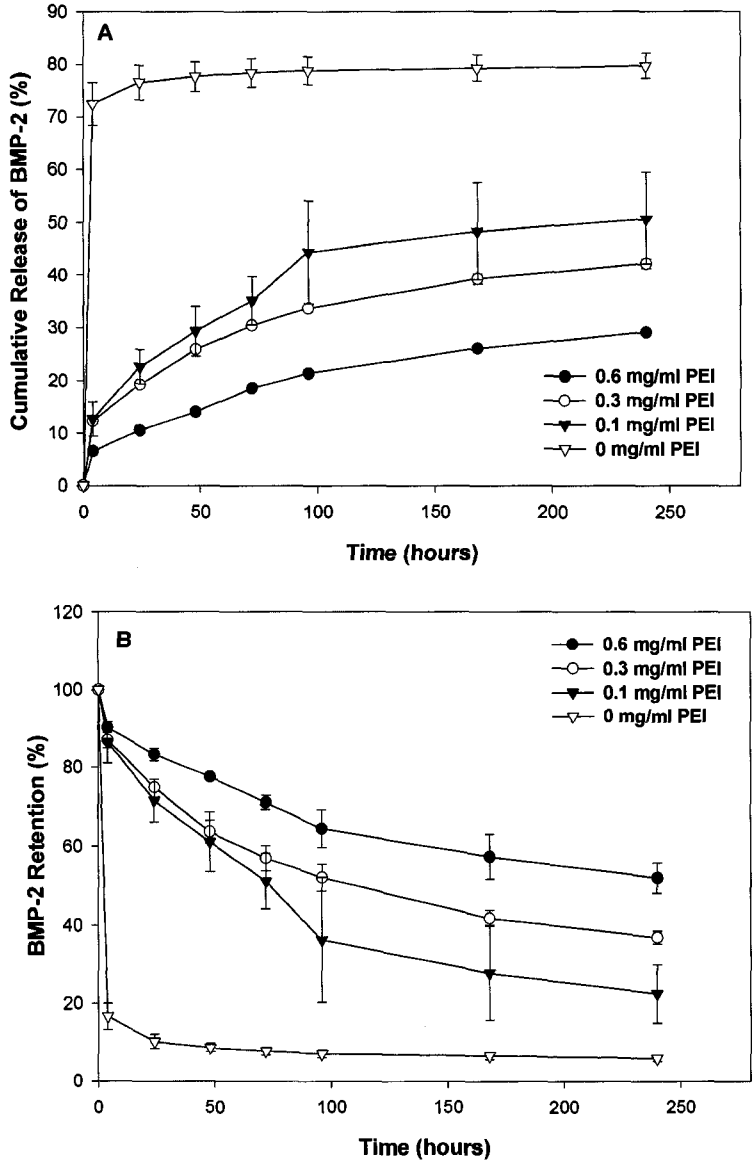

Figure 5-4. The release profile of BMP-2 from the PEI-coated BSA NPs with different PEI coating concentrations. The release was performed after encapsulating ^{125}I-labeled BMP-2 in BSA NPs and using a release medium of DMEM containing 1% penicillin/streptomycin at 37±1°C (**A**). PEI coating time was 1 h and the results were expressed as the mean ± SD (triplicate) percentage of BMP-2 loaded in NPs. At each time point, the amount of BMP-2 in the supernatant (**A**) and the pellet (**B**) was determined after separating the supernatant from the NPs by centrifugation. There was a burst release of BMP-2 for uncoated BSA NPs within hours of incubating the NPs in the release medium. The burst release was effectively suppressed by PEI coating. Note that the gradual reduction of BMP-2 release as the PEI coating concentration was increased from 0.1 to 0.6 mg/mL. In case where SDs are not seen, they are smaller than the symbols and this study was repeated once more with similar results (n=2).

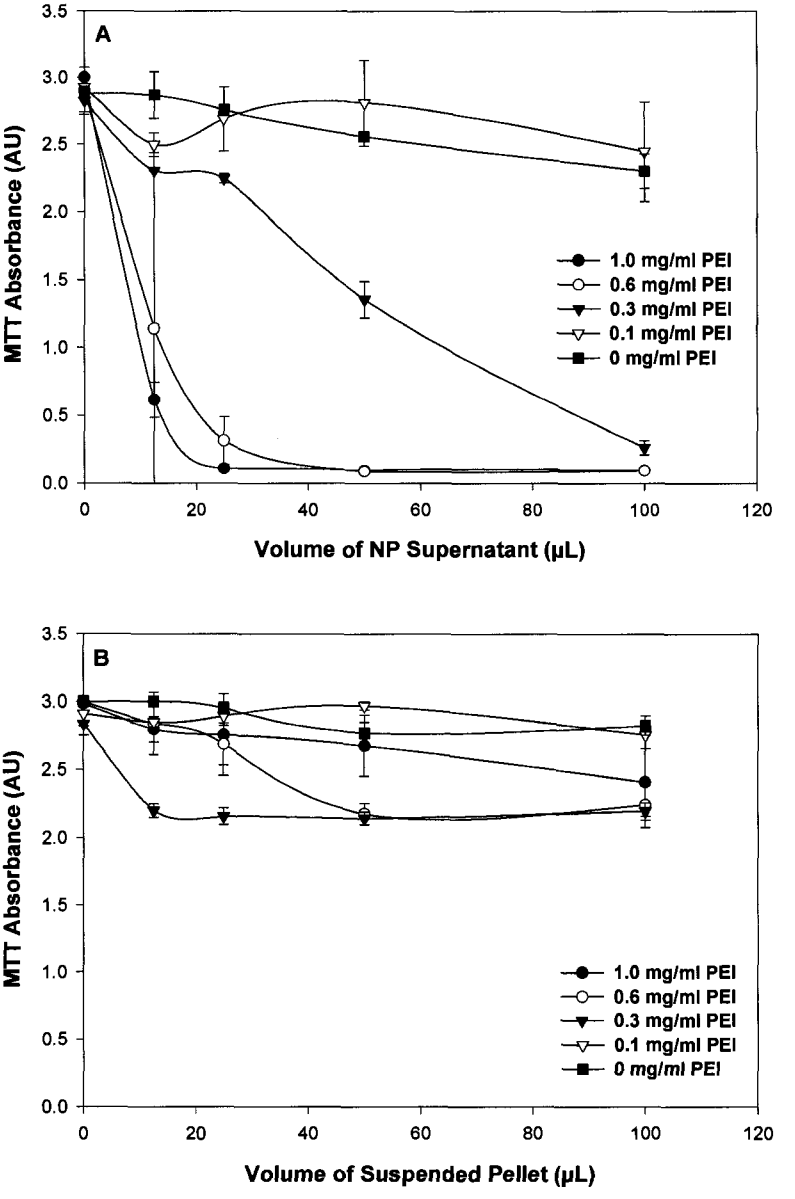

Figure 5-5. Cytotoxicity of BSA NPs coated with different PEI concentrations. The cell viability by the MTT assay was determined by using C2C12 cells incubated with the supernatant (**A**) and the suspended pellet (**B**) after separating the two fractions by centrifugation. Cells were grown in 48-well plates (in triplicate) and incubated with the samples for 48 h. Note that the observed toxicity was dependent on the PEI concentrations. In the supernatant, no toxicity was observed with uncoated BSA NPs but significant toxicity was evident for PEI coating concentration >0.3 mg/mL. The pellet separated from the supernatant, on the other hand, gave no clear toxicity for all PEI concentrations. Two additional batches of NP preparations were evaluated in the similar manners, and both batches gave similar results as above (n=3).

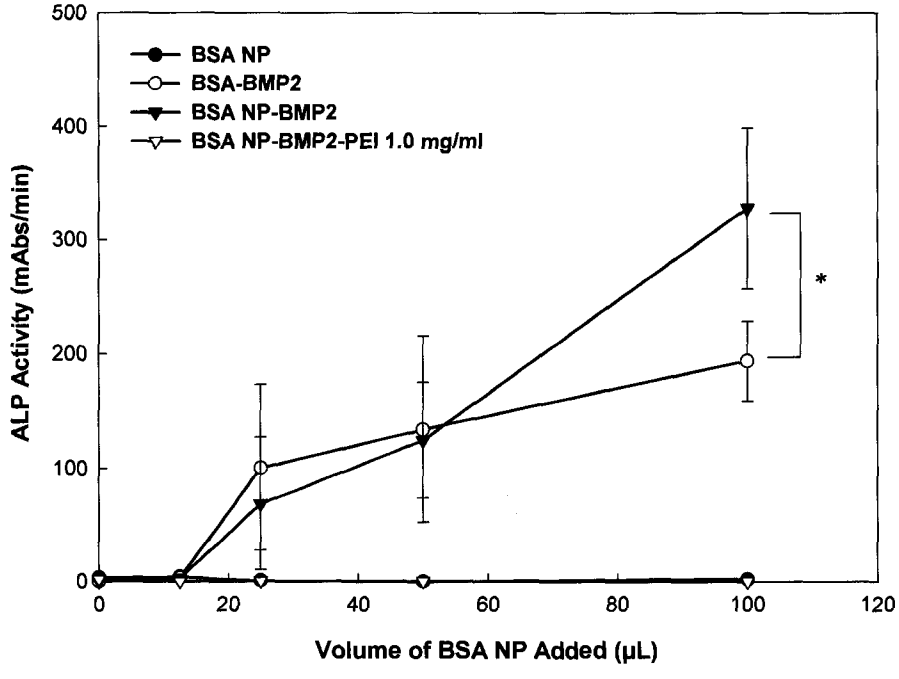

Figure 5-6. The BMP-2 activity in different NP formulations, as measured by ALP induction assay with C2C12 cells (in triplicate). The formulations used were a mixture of BSA and BMP-2 solution without NP formation (i.e., no ethanol addition), BSA NPs without any BMP-2, BMP-2 encapsulated in uncoated BSA NPs, and BMP-2 encapsulated in BSA NPs coated with 1.0 mg/mL PEI. The bioactivities of BMP-2 in BSA solution or in BSA NPs were comparable. No activity was seen in BSA NPs in the absence of BMP-2, and BMP-2 in NPs coated with 1.0 mg/mL PEI gave no activity, presumably due to toxicity of this formulation. *$p<0.05$ at this volume added.

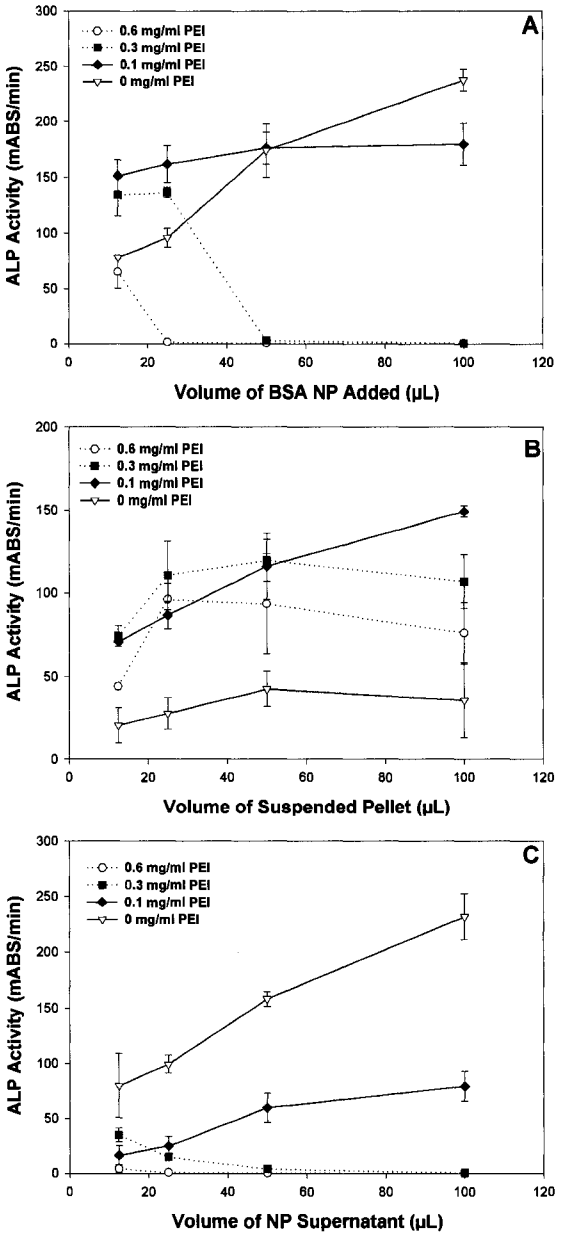

Figure 5-7. The BMP-2 activity in different PEI coated NP formulations, as measured by ALP induction assay with C2C12 cells (in triplicate). The formulations were tested without purification (**A**), or after centrifugation to separate the pellet containing the NPs (**B**) and the supernatant containing the soluble molecules (**C**). In the original NP formulation (**A**), uncoated and 0.1 mg/mL PEI coated BSA NPs retained the BMP-2 activity to an equivalent degree, while the NPs coated with 0.6 and 0.3 mg/mL PEI gave a decreasing BMP-2 activity as higher volumes added. In the pellet with NPs (**B**), NPs coated with all three PEI concentrations displayed an ALP induction activity higher than the uncoated BSA NPs, which showed no activity. In the supernatant (**C**), The uncoated BSA NPs induced ALP activity, while the supernatant from the PEI-coated NPs did not yield any BMP-2 activity except some ALP activity was observed for 0.1 mg/mL PEI coated NPs. This study was repeated twice more with similar results (n=3).

References

[1] J. R.Lieberman, A. Daluiski, and T. A. Einhorn, The role of growth factors in the repair of bone: biology and clinical applications, *J. Bone Joint Surg. Am.*, 84 (2002)1032-1044.

[2] J. M. Wozney, V. Rosen, A. J. Celeste, L. M. Mitsock, M. J. Whitters, R. W. Kriz, R. M. Hewick, and E. A. Wang, Novel regulators of bone formation: molecular clones and activities, *Science*, 242 (1988) 1528-1534.

[3] A. W. Yasko, J. M. Lane, E. J. Fellinger, V. Rosen, J. M. Wozney, and E. A. Wang, The healing of segmental bone defects, induced by recombinant human bone morphogenetic protein (rhBMP-2). A radiographic, histological, and biomechanical study in rats, *J. Bone Joint Surg. Am.*, 74 (1992) 659–670.

[4] M. Bostrom, J. M. Lane, E. Tomin, M. Browne, W. Berberian, T. Turek, J. Smith, J. Wozney, and T. Schildhauer, Use of bone morphogenetic protein-2 in the rabbit ulnar nonunion model, *Clin. Orthop.*, 327 (1996) 272–282.

[5] T. N. Gerhart, C. A. Kirker-Head, M. J. Kriz, M. E. Holtrop, G. E. Hennig, J. Hipp, S. H. Schelling, and E. Wang, Healing segmental femoral defects in sheep using recombinant human bone morphogenetic protein, *Clin. Orthop.*, 293 (1993) 317–326.

[6] M. F. Sciadini, and K. D. Johnson, Evaluation of recombinant human bone morphogenetic protein-2 as a bone-graft substitute in a canine segmental defect model, *J. Orthop. Res.* **2000**, *18,* 289–302.

[7] A. H. Reddi, Bone morphogenetic proteins: an unconventional approach to isolation of first mammalian morphogens, *Cytokine Growth Factor Rev.*, 8 (1997)11-20.

[8] A. L. Jones, R. W. Bucholz, M. J. Bosse, S. K. Mirza, T. R. Lyon, L. X. Webb, A. N. Pollak, J. D. Golden, and A. Valentin-Opran, Recombinant human BMP-2 and allograft compared with autogenous bone graft for reconstruction of diaphyseal tibial fractures with cortical defects. A randomized, controlled trial, *J. Bone Joint Surg.*, 88 (2006) 1431-1441.

[9] S. N. Khan, M. P. G. Bostrom, and J. M. Lane, Bone growth factors, *Orthop. Clin. North Am.*, 31 (2000) 1-14.

[10] V. Luginbuehl, L. Meinel, H. P. Merkle, and B. Gander, Localized delivery of growth factors for bone repair, *Euro. J. Pharm. Biopharm.*, 58 (2004) 197–208.

[11] H. Maeda, A. Sano, and K. Fujioka, Controlled release of rhBMP-2 from collagen minipellet and the relationship between release profile and ectopic bone formation, *Int. J. Pharm.*, 275 (2004) 109–122.

[12] M. Geiger, R. H. Li, and W. Friess, Collagen sponges for bone regeneration with rhBMP-2, *Adv. Drug Deliv. Rev.*, 55 (2003) 1613–1629.

[13] S. Putney, and P. Burke, Improving protein therapeutics with sustained-release formulations, *Nature Biotech.*, 16 (1998) 153-157.

[14] J. L. Cleland, E. T. Duenas, A. Park, A. Daugherty, J. Kahn, J. Kowalski, and A. Cuthbertson, Development of poly-(*D,L*-lactide-co-glycolide) microsphere formulations containing recombinant human vascular endothelial growth factor to promote local angiogenesis, *J. Control Release*, 72 (2001) 13-24.

[15] I. Bala, S. Hariharan, and M. N. Kumar, PLGA nanoparticles in drug delivery: the state of the art, *Crit. Rev. Ther. Drug Carrier Syst.*, 21 (2004) 387-422.

[16] F. Chen, Z. Wu, H. Sun, H. Wu, S. Xin, Q. Wang, G. Dong, Z. Ma, S. Huang, Y. Zhang, and Y. Jin, Release of bioactive BMP from dextran-derived microspheres: a novel delivery concept, *Int. J. Pharm.*, 307 (2006) 23-32.

[17] B. Jiang, C. Gao, L. Hu, and J. Shen, Water-dispersed bone morphogenetic protein nanospheres prepared by co-precipitation method, *Zhejiang Univ. SCI.*, 5 (2004) 936-940.

[18] R. Arshady, Albumin microspheres and microcapsules: methodology of manufacturing techniques, *J. Control Release*, 14 (1990) 111-131.

[19] Y. Morimoto, and S. Fujimoto, Albumin microspheres as drug carriers, *Crit. Rev. Ther. Drug Carrier Syst.*, 2 (1985) 19-63.

[20] B. A. Rhodes, I. Zolle, J. W. Buchanan, and H. N. Wagner Jr., Radioactive albumin microspheres for studies of the pulmonary circulation, *Radiology*, 92 (1969) 1453-1460.

[21] B. Praveen Reddy, A. K. Dorle, and D. R. Krishna, Albumin microspheres: effect of process variables on size distribution and in-vitro release, *Drug Dev. Ind. Pharm.*, 16 (1990) 1791-1803.

[22] S. Das, R. Banerjee, and B. Jayesh, Aspirin loaded albumin nanoparticles by coacervation: implications in drug delivery, *Trends Biomater. Artif. Organs*, 18 (2005) 203- 212.

[23] W. Lin, A. G. A. Coombes, M. C. Davies, S. S. Davis, and L. Illum, Preparation of sub-100 nm human serum albumin nanoshperes using a pH-coacervation method, *J. Drug Targeting*, 1 (1993) 237-243.

[24] M. Merodio, A. Arnedo, M. J. Renedo, and J. M. Irache, Ganciclovir-loaded albumin nanoparticles: characterization and in vitro release properties, *Euro. J. Pharm. Sci.*, 12 (2001) 251-259.

[25] E. Leo, M. A. Vandelli, R. Cameroni, and F. Forni, Doxorubicin-loaded gelatin nanoparticles stabilized by glutaraldehyde: involvement of the drug in the cross-linking process, *Int. J. Pharm.*, 155 (1997) 75-82.

[26] S. Segura, C. Gamazo, J. M. Irache, and E. Espuelas, Gamma interferon loaded onto albumin nanoparticles: in vitro and in vivo activities against *Brucella abortus*, *Antimicrob. Agents Chemother.*, 51 (2007) 1310-1314.

[27] S. Segura, S. Espuelas, M. J. Renedo, and J. M. Irache, Potential of albumin nanoparticles as carriers for interferon gamma, *Drug Dev. Ind. Pharm.*, 31 (2005) 271-280.

[28] M. Chatzinikolaidou, T. Zumbrink, and H. P. Jennissen, Stability of surface-enhanced ultrahydrophilic metals as a basis for bioactive rhBMP-2 surfaces, *Materialwiss. Werkstofftech.*, 34 (2003) 1106–1112.

[29] K. Langer, S. Balthasar, V. Vogel, N. Dinauer, H. Von Briesen, and D. Schubert, Optimization of the preparation process for human serum albumin nanoparticles, *Int. J. Pharm.*, 257 (2003) 169-180.

[30] W. Lin, M. Garnett, M. C. Davies, F. Bignotti, P. Ferruti, S. S. Davis, and L. Illum, Preparation of surface-modified albumin nanospheres, *Biomaterials*, 18 (1997) 559-565.

[31] M. Rahimnejad, M. Jahanshahi, and G. D. Najafpour, Production of biological nanoparticles from bovine serum albumin for drug delivery, *Afr. J. Biotechnol.*, 5 (2006) 1918-1923.

[32] M. M. Bradford, A rapid and sensitive method for the quantitation of microgram quantities of protein utilizing the principle of protein-dye binding, *Anal. Biochem.*, 72 (1976) 248-254.

[33] S. Zhang, J. E. I. Wright, N. Özber, and H. Uludağ, The interaction of cationic polymers and their bisphosphonate derivatives with hydroxyapatite, *Macromol. Biosci.*, 7 (2007) 656-670.

[34] S. A. Gittens, G. Bansal, C. Kucharski, M. Borden, and H. Uludağ, Imparting mineral affinity to fetuin by bisphosphonate conjugation: a comparison of three bisphosphonate conjugation schemes, *Mol. Pharm.*, 2 (2005) 392-406.

[35] T. Mosmann, Rapid colorimetric assay for cellular growth and survival: application to proliferation and cytotoxicity assays, *J. Immunol. Methods.*, 65 (1983) 55-63.

[36] M. Varkey, C. Kucharski, H. Takrima, W. Sebald, and H. Uludağ, *In vitro* osteogenic response of rat bone marrow cells to bFGF and BMP-2 treatments, *Clin. Orthop. Relat. Res.*, 443 (2006) 113-123.

[37] N. Willmott, J. Cummings, and A. T. Florence, *In vitro* release of adriamycin from drug-loaded albumin and haemoglobin microspheres, *J. Microencapsulation*, 2 (1985) 293-304.

[38] T. G. Park, S. Cohen, and R. Langer, Controlled protein release from polyethyleneimine-coated poly(L-lactic Acid)/pluronic blend matrices, *Pharm. Res.*, 9 (1992) 37-39.

[39] I. S. Kim, S. K. Lee, Y. M. Park, Y. B. Lee, S. C. Shin, K. C. Lee, and I. J. Oh, Physico-chemical characterization of poly(*L*-lactic acid) and poly(*D,L*-lactide-*co*-glycolide) nanoparticles with polyethylenimine as gene delivery carrier, *Int. J. Pharm.*, 298 (2005) 255-262.

[40] C. Weber, C. Coester, J. Kreuter, and K. Langer, Desolvation process and surface characterisation of protein nanoparticles, *Int. J. Pharm.*, 194 (2000) 91-102.

[41] S. M. Moghimi, A. C. Hunter, and J. C. Murray, Long-circulating and target-specific nano-particles: theory to practice, *Pharmacol. Rev.*, 53 (2001) 283-318.

[42] D. Thassu, M. Deleers, and Y. Pathak, In *Nanoparticulate drug delivery systems*, Informa Healthcare, New York, 2007, 51-99.

[43] C. Plank, K. Mechtler, F. C. Szoka Jr., and E. Wagner, Activation of the complement system by synthetic DNA complexes: a potential barrier for intravenous gene delivery, *Hum. Gene Ther.*, 7 (1996) 1437-1446.

[44] D. E. Owens III, and N. A. Peppas, Opsonization, biodistribution, and pharmacokinetics of polymeric nanoparticles, *Int. J. Pharm.*, 307 (2006) 93-102.

[45] D. V. Devine, K. Wong, K. Serrano, A. Chonn, and P. R. Cullis, Liposome complement inter-actions in rat serum: implications for liposome survival studies, *Biochim. Biophys. Acta*, 1191 (1994) 43–51.

[46] H. Harashima, K. Sakata, K. Funato, and H. Kiwada, Enhanced hepatic uptake of liposomes through complement activation depending on the size of liposomes, *Pharm. Res.*, 11 (1994) 402–406.

[47] E. L. Romero, M. J. Morilla, J. Regts, G. A. Koning, and G. L. Scherphof, On the mechanism of hepatic transendothelial passage of large liposomes, *FEBS Lett.*, 448 (1999) 193-196.

[48] M. Roser, D. Fidher, and T. Kissel, Surface-modified biodegradable albumin nano- and microspheres. II: effect of surface charges on in vitro phagocytosis and biodistribution in rats, *Euro. J. Pharm. Biopharm.*, 46 (1998) 255-263.

[49] M. Huang, S. N. Vitharana, L. J. Peek, T. Coop, and C. Berkland, Polyelectro-lyte complexes stabilize and controllably release vascular endothelial growth factor, *Biomacromolecules*, 8 (2007) 1607-1614.

[50] W. Tiyaboonchai, J. Woiszwillo, R. C. Sims, and C. R. Middaugh, Insulin containing poly-ethylenimine-dextran sulfate nanoparticles, *Int. J. Pharm.*, 25 (2003) 139-151.

[51] W. Tiyaboonchai, J. Woiszwillo, and C. R. Middaugh, Formulation and characterization of amphotericin B-polyethylenimine-dextran sulfate nanoparticles, *J. Pharm. Sci.*, 90 (2001) 902-914.

[52] H. Uludag, D. D'Augusta, J. Golden, J. Li, G. Timony, R. Riedel, and J. M. Wozney, Implantation of recombinant human bone morphogenetic proteins with biomaterial carriers: A correlation between protein pharmacokinetics and osteoinduction in the rat ectopic model, *J. Biomed. Mater. Res.*, 50 (2000) 227–238.

[53] S. Rhaese, H. Von Briesen, H. Rübsamen-Waigmann, J. Kreuter, and K. Langer, Human serum albumin–polyethylenimine nanoparticles for gene delivery, *J. Control Release*, 92 (2003) 199-208.

[54] A. C. Hunter, Molecular hurdles in polyfectin design and mechanistic background to polycation induced cytotoxicity, *Adv. Drug Deliv. Rev.*, 58 (2006) 1523-1531.

[55] S. Boeckle, K. Von Gersdorff, S. Van der Piepen, C. Culmsee, E. Wanger, and M. Ogris, Purification of polyethylenimine polyplexes highlights the role of free polycations in gene transfer, *J. Gene Med.*, 6 (2004) 1102–1111.

[56] D. J. Rickard, T. A. Sullivan, B. J. Shenker, P. S. Leboy, and I. Kazhdan, Induction of rapid osteoblast differentiation in rat bone marrow stromal cell cultures by dexamethasone and BMP-2, *Dev. Biol.*, 161 (1994) 218–228.

CHAPTER VI

Assessing the Pharmacokinetics and Ectopic Bone Formation by Polyethylenimine-Coated Albumin Nanoparticles Containing BMP-2

INTRODUCTION

The bone morphogenetic proteins (BMPs) are a group of secreted proteins that belong to the transforming growth factor-β (TGF-β) superfamily [1]. BMPs exert an osteoinductive effect by acting on the non-committed progenitor cells and causing cell differentiation into bone-depositing osteoblast phenotypes. BMP-2 has been shown to induce osteogenesis at various sites in many animal species [2-7]. The potency of BMP-2 to successfully stimulate bone formation at the implantation site makes it an alternative for the autogenous bone graft in bone healing process, which required the grafting procedure associated with the donor-site morbidity and potentially limited supply of suitable autogenous bone from patients [8-10]. Currently BMP-2 is clinically used for treatment of fractures and spinal fusion procedure [11,12]. The clinical administration of BMP-2 was focused on local BMP-2 delivery. Studies showed that BMP induces bone induction only locally at the site of implantation, and bone induction is limited temporally only to the time when the BMP is present [13]. Because BMP-2 diffuse rapidly from the site of administration when applied without a carrier, it has been widely accepted that BMP-2 needs a carrier in order to maximize the osteogenic effect. The carrier maintains BMP-2 at the treatment site, optimizing the release profile of BMP-2, and restricts BMP-2 to the site of application to prevent extraneous bone formation [14,15].

BMP-2 has been studied in different carriers for ectopic and orthotopic bone regeneration, including inorganic materials (e.g. hydroxyapatite [16], tricalcium phosphate [17] and calcium phosphate-based cements [18]), synthetic polymers (e.g. polylactide[19], polyglycolide [20], and poly (*D,L*-lactide)-co-glycolide [21]), natural polymers (e.g. collagen [22] and hyaluronans [23]) and the composites of the above three

materials [24-27]. The disadvantages associated with inorganic and synthetic carriers for BMP-2 were the poor biodegradability and the possible inflammatory response, respectively [28]. Currently one of the most effective carriers for BMP-2 delivery proved to be the Type I bovine absorbable collagen sponge (ACS) [15]. As a natural polymer, it is recognized as a suitable biomaterial that can be transformed into a porous structure with excellent operational properties, and good biocompatibility with tissues [29,30]. The carrier properties of ACS have been extensively studied [31-33]. Although the achievement of BMP-2 delivered in collagen-based matrices is encouraging, this system has some inherent problems in controlling the release rate of BMP-2, often resulting in a high initial burst release, and consequently unable to provide a long-term BMP-2 release [26,34].

Polymer-based nanoparticle (NP) for drug delivery and targeting system was developed since early 1980s [35,36]. The NPs are colloidal system with a size of submicron. Polymer nanosphere is one type of NPs, which are matrix systems where the drug is dispersed within the polymer throughout the particle. In this way, the polymers protect the active drugs inside with a better retention of drug bioactivity, and after local or systemic administration, potentially target and then release the drug in a controlled, predictable manner. During the development of NPs, there are generally three generations of nanoparticles with increased targeting ability to desired tissues (**Scheme 6-1**). NPs possess the potential of eliminating problems associated with drug non-specific distribution, and rapid break-down and/or clearance *in vivo*. By encapsulating the drug in a protective environment, NPs increase the drug's bioavailability and provide a sustained release of the drug [35], which is not only beneficial for local application, but also

promising for bone targeting via intravascular injection. NPs made from natural or synthetic materials have been explored for protein delivery [37]. Previously, we reported that a coacervation method followed by surface coating process demonstrated the ability to fabricate BMP-2 encapsulated, polyethylenimine-coated albumin NPs with controlled size and slow release profile, and capable of inducing the alkaline phosphatase activity in human C2C12 cells [38]. This nanoparticle was prepared without any chemical modification of the ingredients, primarily the glutaraldehyde was eliminated form the fabrication process, and the bone-inducing protein, BMP-2, was encapsulated in the NPs. The encapsulation efficiency of BMP-2 in the albumin NPs was typically greater than 90%. The surface coating with cationic polymer, polyethylenimine, effectively controlled the release of BMP-2 from the NPs **(Chapter V)**. In this work, by using the PEI-coated, BMP-2 encapsulated albumin NPs, studies were carried out with two main goals: i) to examine the pharmacokinetics of BMP-2 release *in vivo* by implantation of the NPs subcutaneously into rats; ii) to assess the ability of the released BMP-2 from the NPs to induce bone formation in an ectopic rat model. The implantation was performed by loading the BMP-2 encapsulated NPs into ACS, and then subcutaneously implanted into rats. In the pharmacokinetics study, the local BMP-2 concentration was determined by using ^{125}I-labeled BMP-2. The rat ectopic assay was chosen for osteoinduction study because of its robustness and, also, it is routinely used in numerous studies to investigate bioactive factors for bone formation.

MATERIALS AND METHODS

Materials

Bovine serum albumin (BSA), branched PEI (M_w ~25,000 by light scattering (LS), M_n ~10,000 by gel permeation chromatography(GPC)), ALP substrate p-nitrophenol phosphate (p-NPP), 1,3,4,6-tetrachloro-3α,6α-diphenylglycouril (TCDG), *o*-cresolphthalein, 8-hydroxyquinoline, trichloroacetic acid (TCA) and Calcium assay standards (Sigma diagnostic®) were obtained from Sigma-Aldrich (St. Louis, MO, USA). Recombinant Human Bone Morphogenetic Protein-2 (BMP-2, from *E.coli*) was prepared as described before [39]. $Na^{125}I$ (in 0.1 M NaOH) was obtained from GE Healthcare (Piscataway, NJ, USA). Metofane™ (methoxyflurane) was obtained from Janssen Inc. (Toronto, ON, Canada). Saline used for implantation (0.9% sodium chloride, sterile, non-pyrogenic) was obtained from Baxter Corporation (Toronto, ON, Canada). Absorbable collagen Hemostatic sponge (ACS, Helistat®, sterile, non-pyrogenic) was obtained from Integra Life sciences Corporation (Plainsboro, NJ, USA). Triton X-100 (rein-pure octylphenol-polyethyleneglycol ether) was obtained from Feinbiochemica (Heidelburg, NY, USA). Dulbecco's Modified Eagle Medium (DMEM), Hank's Balanced Salt Solution (HBSS), penicillin (10,000 U/mL solution) and streptomycin (10,000 μg/mL solution) were from Invitrogen (Carlsbad, CA, USA). 2-amino-2-methyl-propan-1-ol (AMP) was obtained from Aldrich chemicals (Milwaukee, WI, USA). Hydrochloric acid (HCl) and concentrated sulfuric acid (H_2SO_4) were obtained from Fisher scientific Inc. (Nepean, ON, Canada). The chemicals were used as received, without any further purification. All tissue culture plasticware was from Corning (Corning, NY, USA).Where

indicated, in-house prepared distilled/de-ionized water (ddH_2O) for buffer preparations and dialysis was derived from a Milli-Q purification system.

Pharmacokinetics Study

Preparation of ^{125}I-labeled BMP-2 Encapsulated BSA NPs: The characterization of BMP-2 encapsulated, PEI-coated BSA NPs *in vitro* was reported by our group previously [38]. In this *in vivo* study, BMP-2 was labeled with the radioisotope ^{125}I [40], to determine the retention of BMP-2 encapsulated in the NPs. Microcentrifuge tubes were coated with TCDG (200 μL of 20 μg/mL TCDG in chloroform), and 20 μL of BMP-2 solution (containing of 10 μg of BMP-2) was added to the coated tubes, along with 50 μL of 0.1 M phosphate buffer (pH = 4.5) and 20 μL of 0.2 mCi of $Na^{125}I$ in 0.1 M of NaOH. After reacting for 25 min, free ^{125}I was separated from the radiolabeled BMP-2 by using a Sephadex G-25 column. After precipitating an aliquot of the purified samples with 20% (w/v) trichloroacetic acid (TCA), the counts in the supernatant and the pellet was determined with a γ-counter (Wizard 1470; Wallac, Turku, Finland), and it was confirmed that the iodinated sample contained < 5% free ^{125}I. After iodination, 10 μL of ^{125}I-labeled BMP-2 was first diluted by 40 μL of ddH_2O (volume ration of 1:5), and then mixed with BSA solution as described previously to prepare the NPs [38]. Briefly, 250 μL of 10 mg/mL BSA solution (50 mg of BSA dissolved in 5 mL ddH_2O) was added to 250 μL of 10 mM NaCl solution (pH=7.0) in a glass vessel under constant stirring (600 rpm) at room temperature. The stirring was allowed to proceed for 15 min. Then, 50 μL of ^{125}I-labeled BMP-2 in ddH_2O was added into the above solution. This aqueous phase was desolvated with dropwise addition of 3.0 mL of ethanol after 2 h of mixing. The

mixture was then stirred (600 rpm) under room temperature for 3 h. The ^{125}I-labeled BMP-2 encapsulated BSA NPs so formed were coated with different 0.1 and 0.6 mg/mL PEI, respectively. PEI dissolved in 0.5 mM NaCl solution was added to the above NPs solution by a volume ratio of 1.25 to 1. The coating was allowed to proceed for 1 h under stirring.

Implantation and *in vivo* Retention: 6~8-week-old female Sprague-Dawley rats were purchased from Biosciences (Edmonton, Alberta). The rats were acclimated for 1 week under standard laboratory conditions (23°C, 12 hours of light/dark cycle) prior to the beginning of the study. While maintained in pairs in sterilized cages, rats were provided standard commercial rat chow, and tap water *ad libitum* for the duration of the study. All procedures involving the rats were approved by the Animal Welfare Committee at the University of Alberta (Edmonton, Alberta). The NPs containing ^{125}I-labeled BMP-2 were coated with 0.6, 0.1 and 0 mg/mL PEI for 1 h in this study (See details in **Table 6-1**). 675 μL of samples (prepared from 300 μL of NPs and 375 μL of PEI solution) were centrifuged at high speed for 5 minutes (BHG Hermle Z230 M Centrifuge) to remove the supernatant containing ethanol, NaCl and free BMP-2, BSA and PEI. Then the pellet was re-dispersed into 675 μL of saline for implantation. The absorbable collagen sponge (ACS) used for implantation was 1 cm × 1 cm square cut from a 7.5 cm ×10 cm ACS (5.0 mm thickness). The dry sponge square cut was then soaked with 50 μL of ^{125}I-labeled NPs sample for 15 minutes prior to implantation. The exact counts in the added 50 μL sample were determined by a γ-counter prior to implantation, and used as the total implanted ^{125}I-labeled BMP-2 dose. Once rats were anesthetized with inhalational

Metofane™, two implants (duplicates of the same type) were implanted subcutaneously into bilateral ventral pouches in each rat. There were 24 rats in total utilized for implantation, with 3 rats in each study group (with an exception of the first time point, where 2 rats in each group). At indicated time points, the rats were euthanized with CO_2, the implants were recovered, and the counts associated with the excised implants were quantified by using a γ-counter. The amount of BMP-2 retention, expressed as a percentage of implanted dose, was calculated as: 100% × [(recovered counts in the implant)/(initial counts in the implant)]. The results were summarized as mean ± SD of %implant retention of BMP-2 for six implants (or four implants for the first time point) at each time point.

Ectopic Bone Formation in Rat Subcutaneous Implant model

Preparation of Implants and Implantation into Rats: Four groups of implants were investigated in this study, including the control saline (G1), free BMP-2 solution (G2), uncoated BMP-2/BSA NPs (G3) and 0.6 mg/mL PEI coated BMP-2/BSA NPs (G4). The BMP-2 encapsulated BSA NPs were prepared as described previously for bioactivity study [38]. The NPs were centrifuged, and then the pellet was concentrated in saline to obtain 50 μL of NPs re-dispersion containing 3 μg of BMP-2 [41]. Free BMP-2 solution was prepared by using 50 μL of 0.06 μg/μL BMP-2 solutions for each implant to be in accordance with this requirement. 50 μL of sample from each group was soaked into a piece of ACS, with a dimension of 1 cm × 1cm × 5 mm for 10 min prior to implantation. For control group, 50 μL of saline was absorbed into ACS pieces (See details in **Table 6-2**). Once rats were anesthetized with inhalational Metofane™, two implants (duplicates

of the same type) were implanted subcutaneously into bilateral ventral pouches in each rat. The implants were recovered at two time points, day 10 and day 16. At indicated time points, rats were euthanized with CO_2, the implants were recovered, the weight was weighed, and ALP assay and calcium assay were carried out for the recovered implants. The results were summarized as mean ± SD for 6 implants at each time point.

In a follow-up study, free BMP-2 solution was added to each group as initiator for bone formation together with the NPs. There were seven groups being investigated in this study: (1) control saline (G1); (2) uncoated BMP-2/BSA NPs (G21); (3) uncoated BMP-2/BSA NPs with 3 μg of free BMP-2 solution (G22); (4) 0.6 mg/mL PEI coated BMP-2/BSA NPs (G31); (5) 0.6 mg/mL PEI coated BMP-2/BSA NPs with 3 μg of free BMP-2 solution (G32); (6) 0.1 mg/mL PEI coated BMP-2/BSA NPs (G41); and (7) 0.1 mg/mL PEI coated BMP-2/BSA NPs with 3 μg of free BMP-2 solution (G42). The implants were prepared as described above except that G22, G32 and G42 were supplemented with 3 μg of free BMP-2 solution additionally before implantation (See details in **Table 6-3**). The ACS sponge for loading samples had dimensions of 1 cm × 1cm × 5 mm, and it was absorbed with 50 μL of desired sample volumes for 10 minutes, and then implanted subcutaneously into rats. There were 42 rats in total used in this study, and two time points, day 14 and day 21 post-implantation were tested. The results were summarized as mean ± SD for 6 implants at each time point.

ALP Activity in Implants [42]: At day 10 and day 16 post-implantation, the rats were sacrificed, and implants were recovered. The wet weight of explants was determined before further investigation. After weighing, the explants were incubated in 2.0 mL of

PBS (1×) at 4 °C (in 24- well-plate) overnight with gentle shaking to remove any serum contaminant. The explants were then transferred into 1.0 mL of 25 mM of $NaHCO_3$ (pH = 7.4) containing 0.01% Triton X-100 for a 72 h incubation at 4 °C with gentle shaking. After 72 h of incubation, 200 µL of the sample solution (in duplicate) from each well were placed into a 48-well-plate, and then 200 µL of p-NPP in ALP buffer (pH = 10.5, containing 0.1 % of Triton X-100) was added to each extraction solution. A kinetic ALP assay was performed to determine the bioactivity of BMP-2 [43]. The changes in optical density ($\lambda_{absorbance}$: 405 nm) were determined in a multi-well plate reader at an intervals of 1.5 min for 8 cycles. The kinetic ALP activity was expressed as the change in optical density of the wells per unit time (mABS/minute). All results were expressed as mean ± SD of duplicate wells for each recovered implant.

Calcium Deposition in Implants: After extraction for the measurement of ALP activity, the explants were first washed with 2.0 mL of PBS ×1, and then transferred to a new 24-well-plate with 1.0 mL of 0.5 N HCl per well. Then the explants were immersed in the HCl solution and left standing at + 4 °C with gentle shaking for 24 h to extract the calcium deposited in the sponge. The exacted concentration of calcium was quantified by a calcification assay with calcium standards (Sigma diagnostic® ($\lambda_{absorbance}$: 574 nm)) to yield the amount of calcium formed. Briefly, 20 µL of the dissolved calcium solution was added to 50 µL of a solution containing 28 mM of 8-hydroxyquinoline and 0.5% (v/v) sulfuric acid, as well as 0.5 mL of solution containing 0.37 mM of *o*-cresolphthalein and 1.5% (v/v) of AMP (2-amino-2-methyl-propan-1-ol). A calcium standard curve based on the standards was used to convert the absorbance into concentration of calcium. The level

of calcification was summarized as the mean concentration of calcium (mg/dL) ± SD of duplicate wells for each implant.

Osteocalcin Deposition in Implants: To determine the osteocalcin content in the well, the remaining cell lysis solution were frozen in –80 °C freezer, thawed at a suitable time, and analyzed with a sandwich ELISA Kit specific for rat osteocalcin (Rat osteocalcin EIA Kit, Biomedical Technologies Inc., Stoughton, MA, USA, Lot#121107). The assay was performed with a 96-well plate. A monoclonal antibody directed against the N-terminal region of osteocalcin was first bound to the polystyrene wells for sample capture. Manufacturer supplied standards of highly purified rat osteocalcin are used to generate a standard curve along with the explant lysis solutions. 100 μL of sample buffer (blank), standards, controls and tested samples were added into designated duplicate wells. The plate was incubate at 37 °C for 2.5 h, and then the wells were aspirated completely and washed three times with 0.3 mL PBS (1×). 100 μL of the osteocalcin antiserum was added to each well and incubated at 37 °C for 1 h. The plate was washed again as described in last step. 100 μL of the diluted Donkey anti-Goat IgG Peroxidase was added to each well and incubated at room temperature for 1 h. The plate was washed again after the incubation as in last step. 100 μL of the mixture of Peroxidase substrate TMB (3,3',5,5'-tetramethyl benzidine) solution and Hydrogen Peroxide solution (volume ratio = 1:1) was added to all wells and incubate at room temperature in the dark for 30 minutes. 100 μL of Stop solution was added to all wells, swirl and measure absorbance at 450nm. Based on the obtained calibration curve, the concentration of osteocalcin in explants was summarized as mean ± SD of duplicate wells.

Micro Computer Tomography (micro-CT) Imaging for Explants: Before decalcified, the recovered implants were scanned on a micro-CT scanner (Skyscan-1076, Skyscan, Belgium). The recovered implants were taken out from ALP lysis buffer which stored at 4 °C, and then placed into a 1.5 mL microcentrifuge tube, scanning together with a micro-CT standard. The scanning process was typically ~23 minutes per sample (Voltage: 48kV; Current: 100 μA; Filter: Titanium 0.025mm; Rotation step: 0.35 degree; Imaging pixel size: 18 μm; Frame Averaging: 3). The scanned images were reconstructed into 3D image with NRecon Reconstruction software (version 1.5.1).

In vitro ALP Activity for NPs with Implant Formulation

To determine the *in vitro* ALP activity for the implant formulations, the NP samples were produced by the same method as for the implant, with 50 μL of sample containing 3 μg of BMP-2. Four PEI coating concentrations were tested in this study, 0.01, 0.03, 0.1 and 0.6 mg/mL PEI, as well as two control groups, free BMP-2 solution and the uncoated BMP-2/BSA NPs. The NPs solution was fractionated into supernatant and pellet by centrifugation at 8000 rpm for 10 min. The supernatant was discarded, and the pellet was re-dispersed into DMEM containing 1% of penicillin/streptomycin. The re-dispersion was centrifuged again to obtain the supernatant and the pellet for ALP assay. The two fractions were incubated with human C2C12 cells for 72 h, and a kinetic ALP procedure was described before [38].

In vitro ALP Activity for NPs with Different BMP-2 Loading

In order to investigate the effect of encapsulated BMP-2 dosage on the *in vitro* ALP activity, NPs was prepared with different BMP-2 dosages. Three dosages of NP, 3.6, 7.2 and 14.4 μg per batch (7.2, 14.4 and 28.8 μL of 0.5 mg/mL BMP-2) were encapsulated into BSA NPs. The final mass ratio of BMP-2 to BSA in the NPs increased from 1.44%, 2.88% to 5.76%, respectively. The NPs was then coated with 0.01, 0.03 and 0.1 mg/mL PEI, with the uncoated BMP-2/BSA NPs serving as a control. The NPs were produced by the same method as for the implant formulation. After coating, samples were first centrifuged to remove the supernatant containing ethanol, NaCl and free polymer. The pellet was then re-dissolved in DMEM containing 1% penicillin/streptomycin. This re-dispersion was centrifuged again, to separate the supernatant and pellet for a kinetic ALP assay. There were two volumes of the pellet dispersion incubated with C2C12 cells for each BMP-2 dosage, giving an estimated concentration of 1.0 and 0.5 μg/mL of BMP-2 in the final medium. For the supernatant fraction, the same volumes as of the pellet dispersion were added to cells. The kinetic ALP assay procedure was described as before [38].

Long-term (28 days) *in vitro* ALP Study of the Encapsulated BMP-2 Bioactivity

The long term bioactivity of BMP-2 released from NPs was assessed *in vitro* by determining its ability to stimulate the ALP activity in human C2C12 cells. There were five groups examined in this study: (1) BSA NPs without any BMP-2 encapsulated; (2) free BMP-2; (3) uncoated BMP-2/BSA NPs; (4) 0.1 mg/mL and (5) 0.6 mg/mL PEI coated BMP-2/BSA NPs. The final BMP-2 concentration in the culture medium was 1.0 μg/mL in all groups except the blank BSA NPs. The free BMP-2 group was prepared by

dilution of the stock 0.5 mg/mL of BMP-2 solution to a final concentration of 1.0 μg/mL, with the use of BSA and NaCl mixture that of the same ratio for making NPs. The NPs were fabricated by the same procedure as described before [38], with a mass ratio of BMP-2 to BSA of 1.44% (wt). For the coating, 300 μL of NPs were mixed with 375 μL of 0.6 or 0.1 mg/mL PEI solution for 1 h, respectively; while for the uncoated BMP-2/BSA NPs, 300 μL of NPs were mixed with 375 μL of 0.5 mM of NaCl solution. BMP-2 encapsulation efficiency was assumed to be 100%, and the NPs were added to cell culture medium to give the desired 1.0 μg/mL concentration. There were six of such aliquots prepared for each sample for the 6 time points to be examined. These aliquots were placed on an orbital shaker, and incubated at 37 °C with 5% of CO_2 under gentle shaking. At each time point (1, 5, 8, 14, 22 and 28 days), one aliquot of each sample was taken out, centrifuged (6000 rpm for 3 min and then 8000 rpm for 2 min), the supernatant and the pellet were separated, and then the pellets were re-dissolved in 675 μL of DMEM with 1% of penicillin/streptomycin. Human C2C12 cells were seeded in 48-well-plates, and used after 24 h of seeding. Samples were added to the cells at volumes of 100, 50 and 25 and 0 μL, with the final volume per well of 0.5 mL. A kinetic ALP assay was performed to determine the bioactivity of encapsulated BMP-2 as described before [38].

Statistical Analysis

All quantitative data were expressed as the mean ± standard deviation (SD). In the pharmacokinetics study, statistical analysis was performed by unpaired Student's *t*-test. In the ectopic bone formation study, statistical analysis was performed by the non-parametric Mann-Whitney-Wilcoxon test. Where indicated, statistical differences

between group means were analyzed by single factor analysis of variance (ANOVA) or Kruskal-Wallis one-way analysis of variance (for non-parametric test). A value of $p<0.05$ was considered statistically significant.

RESULTS

Long-term (28 days) *in vitro* ALP Study of the Encapsulated BMP-2 Bioactivity

A 28-day *in vitro* study was used to examine the bioactivity of BMP-2 retained in NPs **(Figure 6-1)**. The well-established C2C12 cells were used for this purpose and our intention was to determine the preservation of BMP-2 activity in a 4-week time period, in order to better understand *in vivo* bone induction by NP formulations of BMP-2. Free BMP-2 demonstrated the highest ALP activity in the supernatant as expected at all time points, except day 5 and day 8 where some ALP activity appeared in the pellet of free BMP-2. This might be due to some precipitation of BMP-2 protein. Due to the unstable nature of the uncoated BMP-2/BSA NPs, the ALP activity was mainly in the supernatant instead of the pellet because of a fast release of BMP-2 into the supernatant for the study period. For 0.1 mg/mL PEI coated NPs, the ALP activity was mainly in the pellet during the study period. The ALP activity in the supernatant initially increased (day 1 to day 5) and later decreased (day 14 to day 28) for these NPs. For the 0.6 mg/mL PEI coated NPs, the ALP activity in the pellet was lower than 0.1 mg/mL PEI coated NPs until day 8, after which they were equivalent. The ALP activity in the supernatant of 0.6 mg/mL PEI coated NPs was not as evident as the 0.1 mg/mL PEI coated NPs. The results from the NPs containing no BMP-2 were not included in the figure, since the ALP activity in both the pellet and supernatant was close to zero at all time points. This long term study

indicated that BMP-2 encapsulated in PEI-coated BSA NPs was released over a prolonged period and it remained in a bioactive form both in the supernatant as well as in the pellet. We then proceeded to implant studies in the chosen animal model.

Pharmacokinetics of BMP-2 in NPs

The *in vivo* BMP-2 retention in PEI-coated and uncoated NPs is shown in **Figure 6-2**. After 1 day post-implantation, the burst release was more significant for the uncoated NPs, with only 22% of the implanted dosage remaining in the ACS. A reduced BMP-2 burst release was observed for both 0.6 and 0.1 mg/mL PEI coated NPs, with 83% and 67% of BMP-2 implanted dosage remaining in the implants, respectively. At 4 and 7 days post-implantation, the BMP-2 retention percentage for 0.6 and 0.1 mg/mL PEI coated BMP-2/BSA NPs were 51% and 33%, and 47% and 30%, respectively. For the uncoated BMP-2/BSA NPs, the BMP-2 retention percentage was 12% and 10% for day 4 and day 7 post-implantation, respectively. There was no significant difference in the BMP-2 retention percentage between 0.6 and 0.1 mg/mL PEI coated NPs; on the other hand, the differences between the uncoated NPs and PEI coated NPs were significant at all time points ($p < 0.03$ by ANOVA). The pharmacokinetics results indicated that slow release of BMP-2 was achieved by PEI coating on NPs compared with the uncoated NPs.

Ectopic Bone Formation

To assess the therapeutic potential of nanoparticulate BMP-2 delivery system, the BMP-2 encapsulated NPs were subcutaneously implanted into rats. We used an implant dose of 3 μg BMP-2 per 50 μL of NP solution and, to achieve this, the NPs were

concentrated by centrifugation. The rats were sacrificed at day 10 and day 16 post-implantation. The wet weight of the recovered implants at the time points was determined **(Figure 6-3A)**. To compensate for the weight loss, the ALP activity and calcium deposition were normalized against the weight of the recovered implants. The results of ALP assay showed a higher ALP activity in the uncoated BMP-2/BSA NPs and free BMP-2 solution, compared to the control and 0.6 mg/mL PEI coated BMP-2/BSA NPs, which did not demonstrate any significant signal of ALP activity at both time points **(Figure 6-3B)**. The relatively large error bars is typical of this *in vivo* bioassay, where the response usually follows non-normal distribution among the study groups. The calcification assay for the recovered implants also showed that calcium deposition was evident on day 16 in both the uncoated BMP-2/BSA NPs and free BMP-2, but not detected in the control and 0.6 mg/mL PEI coated BMP-2/BSA NPs **(Figure 6-3C)**. Comparing the two time points, there was an increased ALP activity at day 16 than day 10, so did the calcification assay for both the uncoated BMP-2/BSA NPs and free BMP-2. The correlation between the ALP activity and calcium deposition of all the recovered implants was shown in **Figure 6-3D**. A significant linear relationship tested by Pearson correlation was observed between ALP activity and calcification for day 10 ($p<0.0001$, two-tailed), and day 16 ($p<0.0001$, two-tailed) post-implantation.

Next, an ELISA assay was performed for the osteocalcin level in the recovered implants **(Figure 6-4)**. Osteocalcin is a non-collagenous matrix protein that is synthesized by mature osteoblasts. It is a good marker of bone deposition since osteocalcin is not present at early calcification stages, but is expressed in concert with calcification deposits [44]. The results showed that the free BMP-2 and BMP-2/BSA NPs groups demonstrated

significantly higher osteocalcin level compared with the control group and 0.6 mg/mL PEI coated BMP-2/BSA NPs at both day 10 and day 16 ($p < 0.05$). The osteocalcin level obtained for free BMP-2 and BMP-2/BSA NPs group was increased from day 10 to day 16 significantly ($p < 0.02$ for both groups). There was no evident ostaocalcin deposition in PEI-coated BMP-2/BSA NPs, since there was no significant difference between the control and PEI-coated BMP-2/BSA NPs for both time points ($p > 0.70$).

In order to further investigate the ectopic bone formation by PEI-coated BMP-2/BSA NPs, a follow-up study was conducted with two changes: (1) a lower concentration of PEI (0.1 mg/mL) was additionally used for NP coating, and (2) free BMP-2 was added to the study groups in order to ensure osteoinduction in the implants. In this way, any detrimental effect of relatively high concentration of PEI could be explored. The investigated time points were day 14 and day 21. There was a significant weight loss, ~50 to 80%, for all the recovered implants from day 14 to day 21 **(Figure 6-5A)**. There was no ALP activity or calcification in the blank control group (G1) at both time points. The uncoated BMP-2/BSA NPs, with and without free BMP-2 addition (G21 and G22), showed higher ALP activity than all other groups at both day 14 and day 21 **(Figure 6-5B)**. At day 14, the uncoated BMP-2/BSA NPs with free BMP-2 (G22) demonstrated the highest ALP activity among all groups, while at day 21 it exhibited equivalent ALP activity with the uncoated BMP-2/BSA NPs without additional free BMP-2 (G21). On the other hand, both PEI (0.6 and 0.1 mg/mL) coated NPs, with or without free BMP-2 addition, did not demonstrate any significant ALP activity compared to control, even at day 21 ($p > 0.31$). The calcium deposition results exhibited similar trend as to the ALP activity, except the uncoated BMP-2/BSA NPs with free BMP-2 addition

deposited much more calcium than the NPs without free BMP-2 at day 21 **(Figure 6-5C)**. The ALP activity initiated by BMP-2 increased and saturated at 3 weeks while the calcium deposition augmented steadily with time was also observed in other studies [45,46]. This was considered in accordance with the course of bone formation in the subcutaneous tissue. The PEI-coated NPs, with and without free BMP-2 addition, did not display any evident calcium deposition compared to control at both time points ($p>0.24$ and $p>0.32$ for day 14 and day 21, respectively). The overall results suggested an undesired effect of PEI on osteoinductive activity for PEI-coated BMP-2/BSA NPs. The correlation between ALP activity and calcification was significant for day 14 explants ($p<0.0001$, two-tailed), but not quite evident for day 21 explants ($p < 0.01$, two-tailed) **(Figure 6-5D)**. The micro-CT images for recovered implants at day 14 visually demonstrated the calcium deposition inside the implanted sponge **(Figure 6-6)**, which were in accordance with the ALP assay and calcification results. Based on micro-CT, only group G22 (free BMP-2 + BMP-2/BSA NP) gave a strong osteoinduction and adding free BMP-2 to PEI-coated NPs did not give an increase in calcification.

In vitro ALP Activity for NPs Used for Implantation

The *in vitro* ALP activity was performed by using NPs that were produced under identical conditions to implantation formulations **(Figure 6-7)**. The NPs were concentrated before they were separated into pellet and supernatant, and then incubated separately with C2C12 cells. The expected final BMP-2 concentration in culture medium was 1.0 and 0.5 μg/mL for the two different volumes added. The results showed that the pellet fraction of NP coated with 0.6 and 0.1 mg/mL PEI did not induce any ALP

activity. Incubation with the aforementioned pellet caused cell death after visual inspection of the incubated cells under microscope. No evident ALP activity was induced by the pellet fraction even for the 0.03 mg/mL PEI coated NPs. Only the pellet fraction of 0.01 mg/mL PEI coated NPs showed induced ALP activity, and it was higher than the pellet of uncoated NPs. In the supernatant, free BMP-2 was used as a positive control, which showed the highest ALP activity. However, all other samples did not give evident ALP activity except the 0.01 mg/mL PEI coated NPs. This was indicative of toxicity of the concentrated NP formulations that was used for implantation.

In vitro ALP Activity for NPs with Different BMP-2 Loading

Higher BMP-2 loading in NPs were investigated in order to reduce the PEI packing on NPs by decreasing the extent of NP "concentration". 3.6, 7.2 and 14.4 μg of BMP-2 were the three encapsulated dosages used in this study. The lowest encapsulated dosage, 3.6 μg of BMP-2, was the dosage used throughout previous studies. The PEI coating concentration was between 0.1 and 0.01 mg/mL in this study. The final BMP-2 concentrations to be used were 1.0 and 0.5 μg/mL in the culture medium, and to achieve these, the pellets were concentrated at different times **(Figure 6-8A)**, with 13.5, 6.75 and 3.38 times for 3.6, 7.2 and 14.4 μg of BMP-2 dosage, respectively. In the pellet fraction, the ALP activity of different BMP-2 loadings showed that the 3.6 μg of BMP-2 dosage did not induce any ALP activity at both BMP-2 concentrations tested for 0.1 mg/mL PEI coated NPs; however, the 7.2 μg of BMP-2 dosage, showed some ALP activity, and the 14.4 μg of BMP-2 dosage exhibited a dose-respondent ALP activity for 0.1 mg/mL PEI coated NPs. For 0.03 and 0.01 mg/mL PEI coated NPs, the pellet fraction of all three

BMP-2 dosages showed induced ALP activity, and it was dose-respondent **(Figure 6-8B, C)**. In the supernatant, no significant ALP activity was observed for all formulations tested, except the 0.01 mg/mL PEI coated NPs, which showed the highest ALP activity with the 3.6 μg of BMP-2 dosage, and as BMP-2 encapsulated dosage increased, the ALP activity decreased **(Figure 6-8D, E)**. Overall speaking, the ALP activity of PEI-coated NPs demonstrated an increasing tendency as the PEI coating concentration decreased from 0.1 to 0.01 mg/mL. In the pellet fraction, the ALP activity increased as the BMP-2 loading amount increased, while in the supernatant the ALP activity decreased as the BMP-2 loading amount increased.

DISCUSSION

BMP-2 is a potent stimulant of bone formation as it induces the differentiation of mesenchymal stem cells into bone-depositing osteoblast cells [47]. The necessity of a carrier for BMP-2 delivery is due to the short biological half-life of BMP-2 at implant site; moreover, safety issues arising from uncontrolled outflow of free BMP-2 solution after implantation makes the use of a carrier necessary. In order to develop an effective and safe approach for BMP-2 delivery, we previously reported a BMP-2 delivery system based on PEI-coated BSA NPs [38]. The previous *in vitro* BMP-2 release study suggested that the release of BMP-2 from the NPs can be controlled by the PEI concentration used for coating the NPs [38]. In this study, we first evaluate if the BMP-2 bioactivity is lost in a 4-week time period in the NP formulations, since it is imperative to maintain BMP-2 bioactivity over a long period in delivery formulations. Our 28-day *in vitro* ALP study suggested that BMP-2 remained bioactive over the entire time period for both the

uncoated and PEI-coated NPs (0.1 and 0.6 mg/mL PEI for coating). Compared to the uncoated NPs, PEI-coated NPs exhibited enhanced ALP activity in the pellet, which suggested that PEI coating effectively controlled BMP-2 released from NPs. This was consistent with the previous *in vitro* release study [38]. The controllable release pattern was also observed for other PEI coating systems for drug release [48-50]. Moreover, stabilization of BSA NPs by PEI coating eliminates the exposure of BMP-2 to chemical cross-linking agent, usually glutaraldehyde, during the fabrication process, thus enabling better integrity of BMP-2 biological activity. We then continued to examine this BMP-2 delivery system by evaluating the *in vivo* pharmacokinetics of BMP-2 and the osteoinduction activity of the BMP-2 delivered by NPs in a rat ectopic model. It was our intention to explore a relationship between local retention of BMP-2 in implants and the osteoinductivity of encapsulated BMP-2.

Pharmacokinetics of BMP-2 Delivery

The pharmacokinetics of BMP-2 in different carriers, such as ACS, demineralized bone matrix and bone mineral, has been studied thoroughly [31,32,41]. Previous studies suggested that BMP loss from the implanted matrix-based carriers occurred in two phases: an initial burst release and a gradual protein loss afterwards [41]. BMP implant concentration did not affect the *in vivo* pharmacokinetics [31]. It was shown that BMP-2 retention was ~10% in ACS after 7 days by subcutaneous implantation [41]. In this study, with the same methodology [41], a similar retention was achieved for the uncoated BMP-2/BSA NPs. This study also showed more than 30% of BMP-2 was retained in the ACS with the presence of PEI coated BMP-2/BSA NPs at 7 days post-implantation. It clearly

indicated that PEI coating on BSA NPs can effectively reduce the initial burst release of BMP-2 from ACS for both 0.6 and 0.1 mg/mL PEI coating. The BMP-2 retention at implant site is expected to depend on several factors, including diffusion of BMP-2 and/or NPs, the degradation rate of NPs, the degradation rate of collagen, and the interactions among BMP-2, BSA, PEI and collagen. The NP size should also play a role in BMP-2 release, but this issue was not explored in this study. The uncoated BSA NPs demonstrated an initial burst release of BMP-2. This was not surprised since the BSA NPs without a PEI coating will be unstable [38], facilitating degradation of BSA *in vivo*. After coating, the interaction of PEI with BSA NPs might delay this process, since the PEI coating layer forms a barrier that better maintains the integrity of BSA NPs. Although this study did not investigate the degradation pattern of BSA NPs, Lin et al. studied the degradation of albumin NPs in rat serum *in vitro* [51]. The results indicated 17% of albumin NPs were degraded after 4 days at 37 °C. However, the albumin NPs tested in that study was cross-linked with glutaraldehyde, which was not used in our NPs. It's also not known if *in vivo* degradation is impeded or facilitated as compared to the *in vitro* condition. In our hands, one *in vivo* pharmacokinetics study by subcutaneous implantation in rats showed similar release pattern of free BMP-2 and BMP-2 entrapped in BSA NPs (data not shown). This suggested that BSA NPs without coating is not very stable *in vivo*. A more precise way to investigate the degradation rate of BSA NPs is to fabricate the NPs with ^{125}I-labeled BSA, and then implant them for pharmacokinetics analysis.

Though *in vivo* pharmacokinetics of BMP-2 release was studied in numerous delivery systems, there were few studies on BMP-2 release from the NP delivery system.

Hosseinkhani et al. investigated the *in vivo* release of BMP-2 from a gel-like nano-scaffold, which was constructed by self-assembled peptide amphiphile (PA) nanofibers [45]. By injecting the ^{125}I-labeled BMP-2 incorporated nano-scaffold subcutaneously into the back of rats, the results showed no initial burst release of BMP-2 at day 1, and 30~40% of BMP-2 remained in the nano-scaffold at day 7. This retention percentage was comparable to our results of BMP-2 retention in PEI-coated NPs. Based on the degradation profile of PA nanofibers by using ^{125}I-labeled PA, the mechanism for BMP-2 release was proposed as a combination of diffusion and degradation of PA nanofibers. Another study conducted by Ruhe et al. investigated the *in vivo* release of BMP-2 from PLGA (poly(*D,L*-lactic-co-glycolic acid)) microparticles (40-50 μm)/calcium phosphate (Ca-P) composites [52]. ^{131}I-labeled BMP-2 was entrapped into the PLGA particle made from two different molecular weights (MW) of PLGAs. The results showed that the release of entrapped BMP-2 from low MW PLGA/Ca-P composites was faster than high MW PLGA. The faster degradation of low MW PLGA than high MW was suggested as the reason for this different release pattern. The PLGA/Ca-P exhibited relatively high retention of BMP-2, with 50~70% at day 28, was attributed to the released BMP-2 binding to Ca-P cement. Yamamoto et al. investigated BMP-2 release from glutaraldehyde cross-linked gelatin hydrogels with different water contents [46]. The finding showed that the longer retention of BMP-2 was achieved by the lower water content of the hydrogel. Since BMP-2 release was governed by the degradation of the hydrogel carrier, the water content in the hydrogel was proposed as the likely determinant of BMP-2 release, via its effect on hydrogel degradation.

Ectopic Bone Formation

Implantation of BMP-2 at osseous or extraosseous site results in new bone formation. The BMP-2 concentration required for bone induction depends on the type of the defect, and the state of the organism in the evolutionary scale, with larger amount of BMP-2 being needed for higher organisms [53]. It is thought that large animals may have a smaller pool of available responsive stem cells from the bone and soft tissue envelopes than small animals [14]. It was suggested that 2 μg of BMP-2 at the implantation site is minimal for the osteoinduction in a rat ectopic model [41], but this is expected to depend on the choice of carrier. Our *in vitro* NP formulation is designed to provide 3 μg of BMP-2 in 675 μL of NP solution. It was our intention to implant NPs containing 3 μg of BMP-2 for the *in vivo* bone formation study. This was achieved by "concentrating" the 675 μL of NP solution containing 3 μg of BMP-2 by centrifugation, into a 50 μL volume, and then this 50 μL volume per implant was implanted into rat. In this way, the NPs were concentrated by 13.5 times.

Reports on the initiation of BMP-2 induced bone formation after implantation provide different times, ranging from day 5 to day 10 [54-56]. We evaluated bone formation at 10 days and 16 days after implantation for the first study. Free BMP-2 loaded ACS implants and the uncoated BMP-2/BSA NPs loaded in ACS induced robust bone formation, based on all investigated markers of bone formation. In contrast, the NPs coated with 0.6 mg/mL PEI did not demonstrate any osteoinduction. This was not consistent with the BMP-2 pharmacokinetics, since higher amount of BMP-2 was retained in PEI-coated NPs than the uncoated NPs at the implant site. Since BMP-2 functions only locally, the more retention of BMP-2 in the carrier, the more bone

formation should have been observed. Takita et al. reported that the slow release of BMP-2 from a carrier can give a late response of bone formation [57]. However, it might not apply to this condition since the bone formation was evaluated at a relatively late phase of 16 days post-implantation. Therefore, two possible reasons were attributed to this phenomena: (i) the lack of the initial burst release of BMP-2 could not recruit enough responsive cells in the surrounding to initiate the bone formation process, and the relatively slow release afterwards could not accumulate the BMP-2 at a critical threshold concentration at the implantation site to induce the bone formation, as suggested in the studies of Saito et al [58] and Yamamoto et al [46]; (ii) the cytotoxicity of PEI dissociated from the NPs surface is detrimental, which might abolish BMP-2 bioactivity. Either one or a combination of these two reasons could impede bone formation.

We first tested the necessity of initial burst release of BMP-2, by delivering free BMP-2 along with the NP formulations. With the uncoated NPs, the addition of free BMP-2 greatly increased the bone formation as compared to NPs without additional BMP-2. With regard to PEI-coated NPs, there was little sign of bone formation in the recovered implants, even with the addition of free BMP-2. Two recovered implants in the 0.6 mg/mL PEI-coated groups was an exception (both from the same rat), which showed good osteoinduction. This might be due to uneven re-dispersion of the concentrated pellet, which contained less PEI but relatively more BMP-2 for these two implants. Therefore, the collective observations point out to cytotoxicity of PEI, which abolished the BMP-2 bioactivity even with free BMP-2. Since previous result showed that the pellet of PEI-coated NPs (0.1 and 0.6 mg/mL PEI) induced ALP activity *in vitro* in the original formulation [38], which was before the "concentration" process to obtain 3 μg/50 μL of

BMP-2 in NPs solution for the implantation, the abolishment of BMP-2 activity should be due to the NP "concentration" process. The effect of this process was an increase in BSA amount, but such a high concentration of BSA seemed to be compatible with the osteoinductive process. We previously identified PEI to be the most toxic component in our system [38] and it looks like this "concentration" process was too excessive for PEI. The cytotoxicity of PEI was well-documented when PEI concentration above a certain level, since cationic polymers strongly interact with anionic cellular surfaces, which might compromise the integrity of cellular membranes, and inhibit normal cellular process [59,60].

In order to test if the "concentration" process was detrimental to BMP-2 activity, ALP assay was performed *in vitro* by using NP formulation identical to implant formulations. The results clearly manifested that no ALP activity was detected for the 0.6, 0.1 and even 0.03 mg/mL PEI coated NPs; only 0.01 mg/mL PEI coated NPs demonstrated ALP activity after NP "concentration". Cell death was visually observed after cells incubated with 0.6 and 0.1 mg/mL PEI coated NPs. Since the "concentration" process concentrated NPs 13.5 times (from 675 μL to 50 μL), PEI coating concentration became 8.10, 1.35, 0.40, 0.14 mg/mL PEI for 0.6, 0.1, 0.03 and 0.01 mg/mL PEI coating, respectively. Previously, *in vitro* ALP study showed that PEI coating concentration on BSA NPs higher than 1.0 mg/mL totally demolished any ALP activity with C2C12 cells [38]. With regard to the implants containing PEI-coated NPs, the concentrated PEI reached ~31.9 μg and ~16.7 μg PEI per implant (calculated from PEI concentration and coating efficiency [38]) for 0.6 and 0.1 mg/mL PEI coating, respectively. When adding this 50 μL of implantation formulation into the culture medium, the final PEI

concentration was 63.8 and 33.4 μg/mL for 0.6 and 0.1 mg/mL PEI coating, respectively. Since the toxicity of PEI is usually displayed at > 3.0 μg/mL, these concentrated samples from the implantation formulation clearly abolished the BMP-2 activity. Based on the above results, the absence of bone formation for implants containing PEI-coated BMP-2/BSA NPs should be attributed to the "concentration" process that accumulated excessive PEI.

One way to reduce PEI "concentration" is to increase BMP-2 loading in NPs. Three BMP-2 dosages, 3.6, 7.2 and 14.4 μg of BMP-2 were utilized in this study. For example, for 3.6 μg of BMP-2 NP formulation, after the "concentration" process, the PEI concentration was equivalent to 1.35 mg/mL PEI coating for 0.1 mg/mL PEI coating. For 7.2 and 14.4 μg of BMP-2 used, the PEI concentration became 0.68 and 0.34 mg/mL, respectively, after "concentration" **(Figure 6-8A)**. By this approach, the BMP-2 amount contained in NPs is in the practical implant range while the amount of PEI is reduced. The results clearly manifested that the ALP activity was retained for high BMP-2 dosage with low PEI "concentration" extent, but not for the low BMP-2 dosage with high extent of concentrated PEI. These results point out a way for new formulations with PEI-coated BMP-2/BSA NPs – use higher BMP-2 encapsulated amount. This is the objective we will investigate in the next study.

The concentration and retention time of BMP-2 at the implant site play an important role in inducing new bone formation [61]. The optimal condition is not clear at present. To clarify the optimal conditions, the cellular and biochemical studies are required to evaluate the effect of BMP-2 release kinetics on the proliferation and differentiation of osteoprogenitor cells in the body. In consideration of clinical

application of BMP-2, reducing the dose of BMP-2 for successful bone regeneration and diminishing the potential side effects elicited by BMP-2 at extraskeletal sites is a critical issue. A controlled and localized delivery system to deliver the appropriate amount of BMP-2 and efficiently retain BMP-2 at the site for bone regeneration remains a goal to tackle. NP could be important in this respect, since they can be engineered for precise release rates. Future studies are directed towards this goal.

CONCLUSIONS

We designed and tested the pharmacokinetics and osteoinduction of a BMP-2 delivery system based on PEI-coated BSA NPs by using a rat subcutaneous implant model. The results of pharmacokinetics study suggested that PEI coating on BSA NPs effectively reduced the initial burst release of BMP-2 from the NPs. The PEI concentrations for coating, 0.6 and 0.1 mg/mL, did not make a significant difference in BMP-2 retention *in vivo.* In the case of osteoinduction study, our findings indicated that the uncoated BMP-2/BSA NPs was capable of inducing new bone formation after implantation. However, the PEI-coated BMP-2/BSA NPs did not demonstrate new bone formation at both the 0.6 and 0.1 mg/mL PEI coating concentrations. Presumably the "concentration" process of NP preparation, which was necessary for osteoinduction, also increased the toxicity of coated PEI. This was confirmed by the outcome of *in vitro* ALP activity assay with the "concentration" preparations. Our future studies are designed to reduce the toxicity of PEI coating on NPs by lowering the PEI concentrations, or chemically modified PEI with ligand, for example, poly(ethylenglycol), to reduce the cytotoxicity, in order to keep BMP-2 bioactive for the induced bone formation.

TABLES

Table 6-1. Study groups for pharmacokinetics assessment

Implant set	Group	Amount per implant (μL)	no. of rats (implants)	Harvest (days)	Evaluation
1	ACS + BMP-2/BSA NP	50	2 (4), 3 (6), 3 (6)	1, 4, 7	Counts
2	ACS + BMP-2/BSA NP coated with PEI (0.1 mg/mL)	50	2 (4), 3 (6), 3 (6)	1, 4, 7	Counts
3	ACS + BMP-2/BSA NP coated with PEI (0.6 mg/mL)	50	2 (4), 3 (6), 3 (6)	1, 4, 7	Counts

Table 6-2. Study groups in ectopic bone formation at the rat subcutaneous model

Implant set	Group	BMP-2 dose per implant(ug)	BSA dose (mg)	no. of rats (implants)	Harvest (days)	Evaluation
G1	ACS	0	0	3 (6), 3 (6)	10, 16	weight, Ca^{2+}, ALP
G2	ACS + BMP-2/free	3	0	3 (6), 3 (6)	10, 16	weight, Ca^{2+}, ALP
G3	ACS + BMP-2/BSA NP	3	0.2	3 (6), 3 (6)	10, 16	weight, Ca^{2+}, ALP
G4	ACS + BMP-2/BSA NP coated with PEI (0.6 mg/mL)	3	0.2	3 (6), 3 (6)	10, 16	weight, Ca^{2+}, ALP

Table 6-3. Study groups in ectopic bone formation with additional free BMP-2 at the rat subcutaneous model

Implant set	Group	BMP-2 dose per implant (μg)	no. of rats (implants)	Harvest (days)	Evaluation
G1	ACS	0	3 (6), 3 (6)	14, 21	weight, Ca^{2+}, ALP, Micro-CT
G21	ACS + BMP-2/BSA NP	3 + 0	3 (6), 3 (6)	14, 21	weight, Ca^{2+}, ALP Micro-CT
G22		3 + 3	3 (6), 3 (6)		
G31	ACS + BMP-2/BSA NP coated with PEI (0.6 mg/mL)	3 + 0	3 (6), 3 (6)	14, 21	weight, Ca^{2+}, ALP Micro-CT
G32		3 + 3	3 (6), 3 (6)		
G41	ACS + BMP-2/BSA NP coated with PEI (0.1 mg/mL)	3 + 0	3 (6), 3 (6)	14, 21	weight, Ca^{2+}, ALP Micro-CT
G42		3 + 3	3 (6), 3 (6)		

SCHEMES

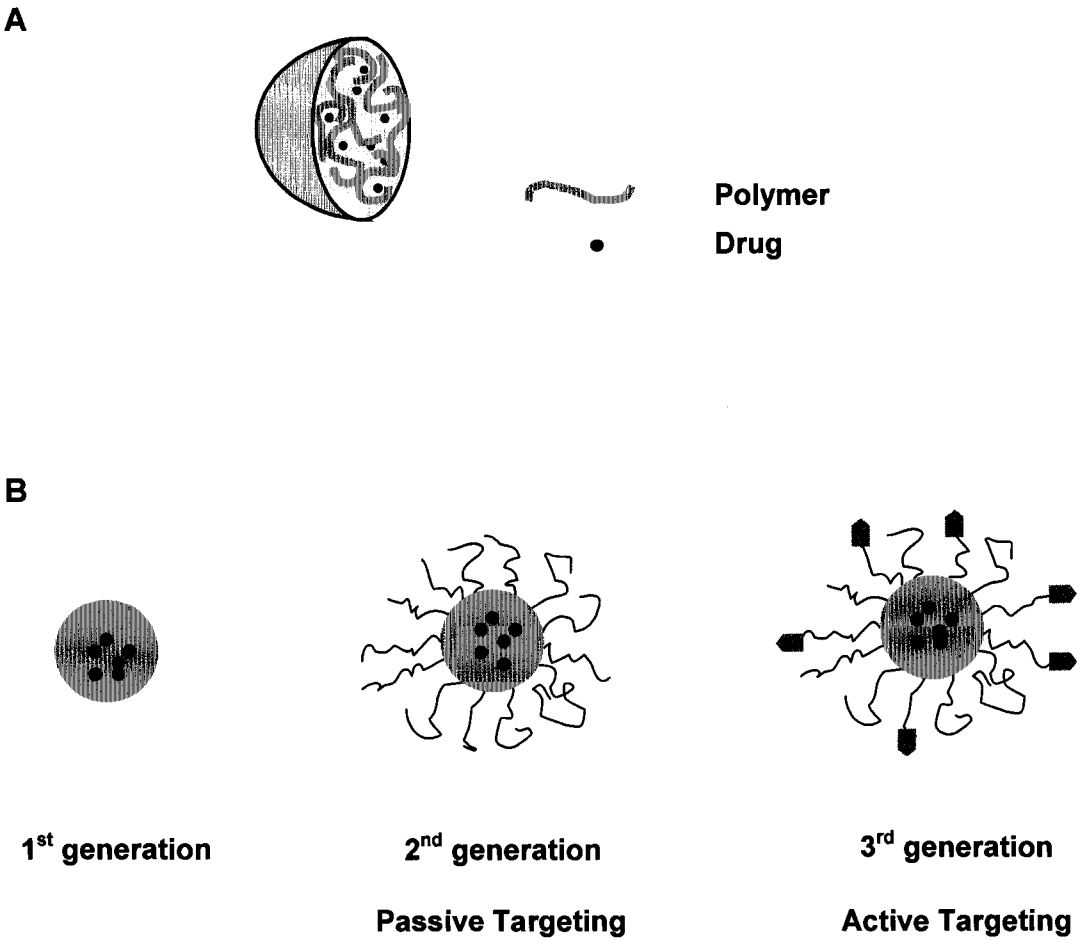

Scheme 6-1. Schematic representation of polymer nanospheres and the three generations of NPs. (**A**) Polymer nanospheres are matrix systems where drugs are dispersed within the polymer throughout the particle; (**B**) The development of three generations of NPs. The 1st generation is the unmodified NPs; the 2nd generation of NPs is surface-modified with polyethylene glycol (PEG) for passive targeting; and the 3rd generation of NPs is surface decorated with molecules that are able to recognize a biological target for active targeting (adapted from ref [36]).

	Free BMP-2	BMP-2/BSA NPs	0.1 mg/mL PEI coated BMP-2/BSA NPs	0.6 mg/mL PEI coated BMP-2/BSA NPs
Day 1	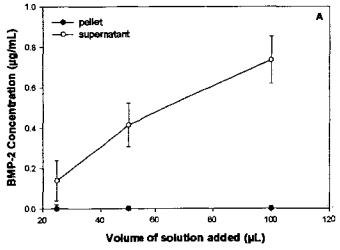	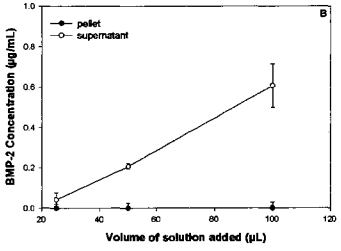	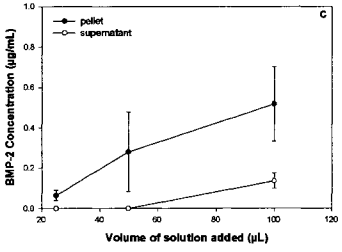	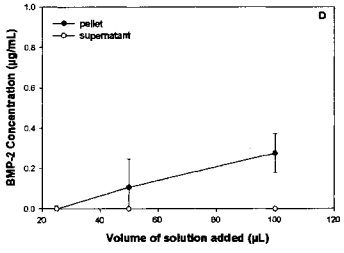
Day 5	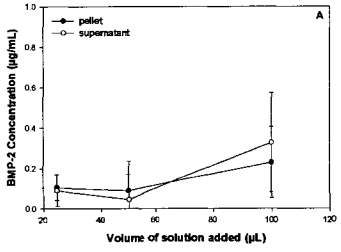	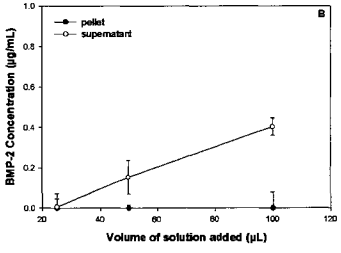	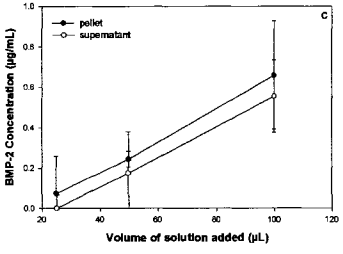	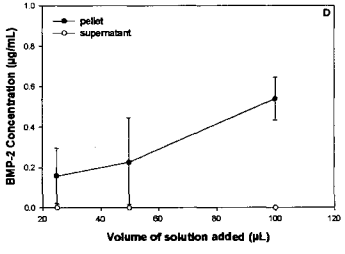
Day 8	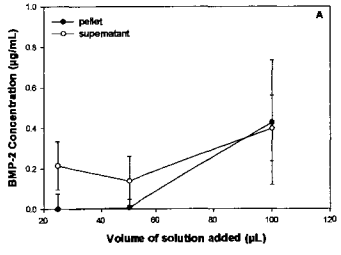	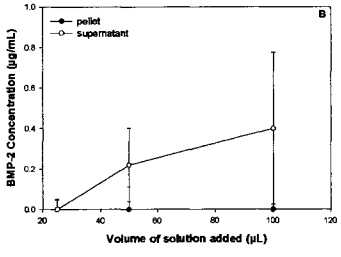	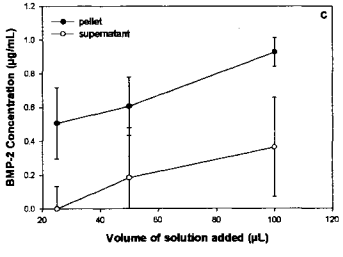	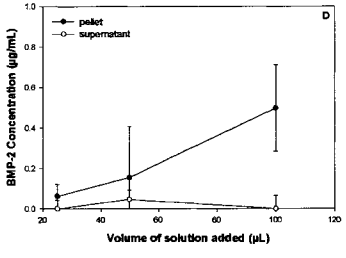

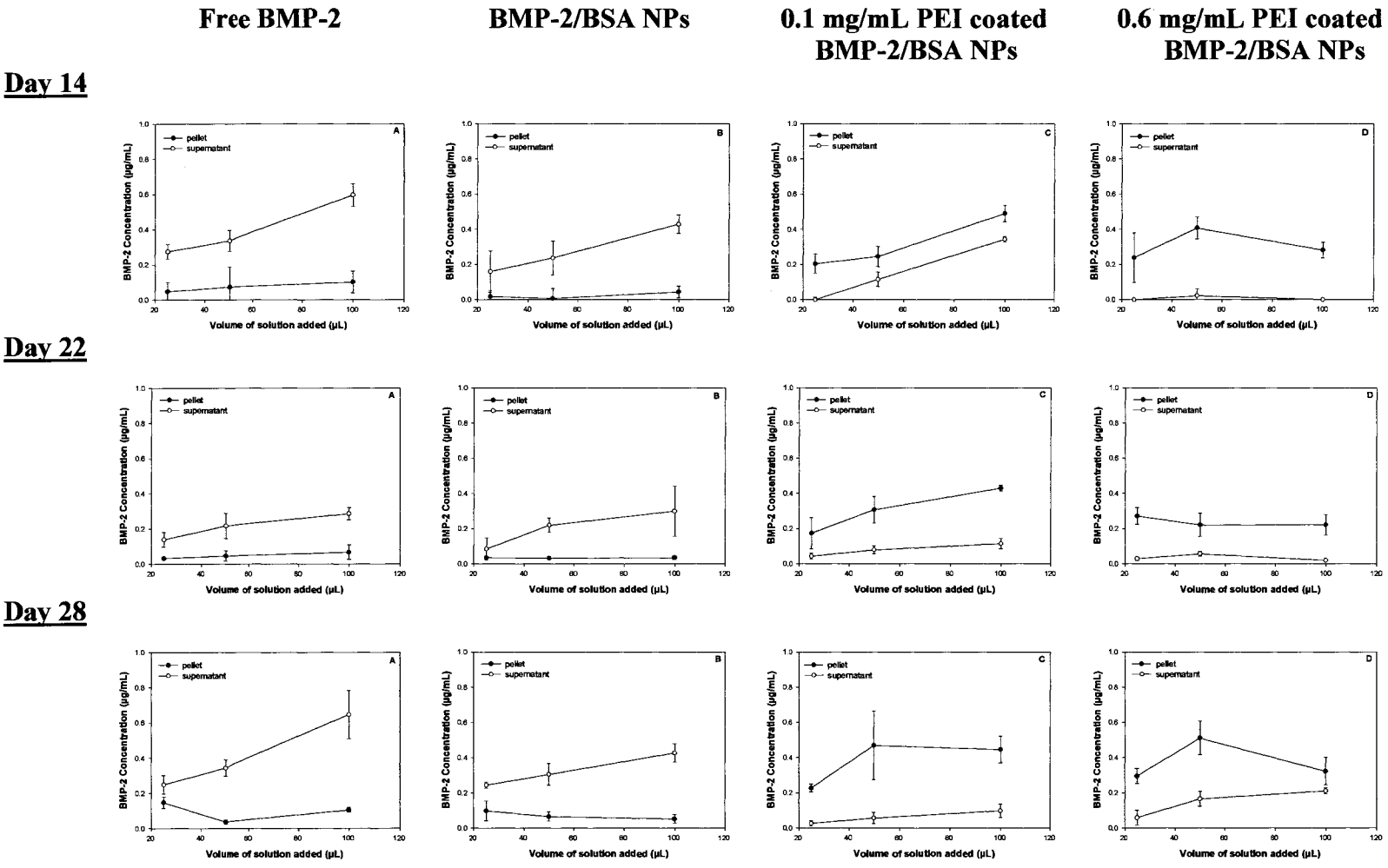

Figure 6-1. The long term ALP activity study of BMP-2 in BSA NPs. **A.** free BMP-2; **B.** Uncoated BMP-2/BSA NPs; **C.** 0.1 mg/mL PEI coated BMP-2/BSA NPs; **D.** 0.6 mg/mL PEI coated BMP-2/BSA NPs. BMP-2 retained its bioactivity for at least 28 days in this delivery system.

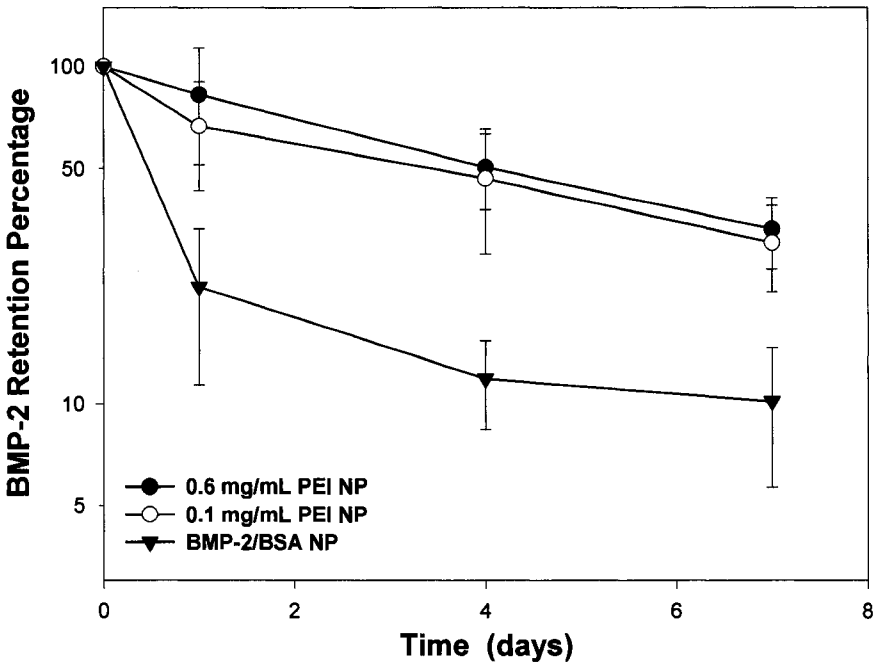

Figure 6-2. Pharmacokinetics study of BMP-2 retention in BSA NPs investigated by ^{125}I-labeled BMP-2 in the rat ectopic assay (logarithmic scale). The results were summarized as the percent retention of the implanted BMP-2 dose as a function of time. Both 0.6 and 0.1 mg/mL PEI coated BMP-2/BSA NPs gave significantly higher BMP-2 retention at all time points than the uncoated BMP-2/BSA NPs ($p<0.03$ by ANOVA).

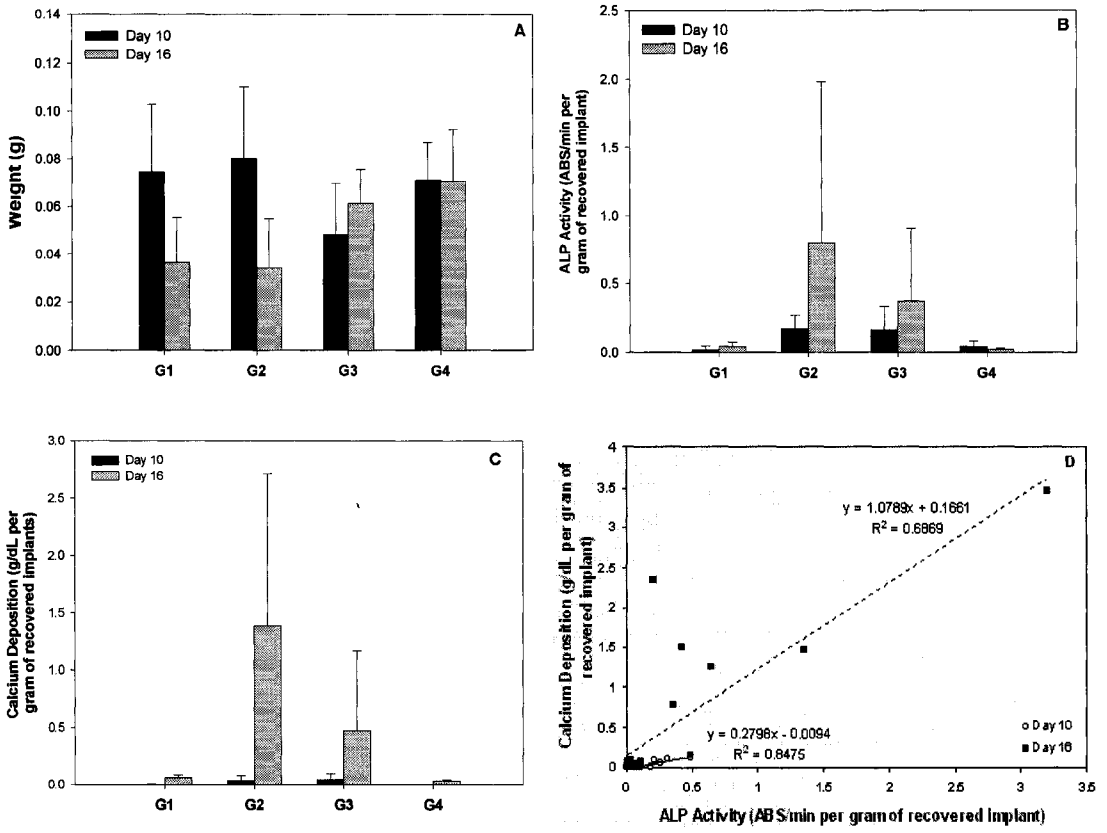

Figure 6-3. *In vivo* investigation of the osteoinductive effect with different NP formulations. G1: ACS alone; G2: ACS loaded with free BMP-2 solution; G3: ACS loaded with uncoated BMP-2/BSA NPs; G4: ACS loaded with BMP-2/BSA NPs coated with 0.6 mg/mL PEI. In all the tested groups, the amount of BMP-2 is 3 μg except the control group without any BMP-2. **A.** Wet weight of recovered implants at day 10 and day 16; **B.** Normalized ALP activity of different study groups at day 10 and day 16; **C.** Normalized calcium deposition of different study groups at day 10 and day 16; **D.** Correlation between calcium deposition and ALP activity of the recovered implants at day 10 and day 16.

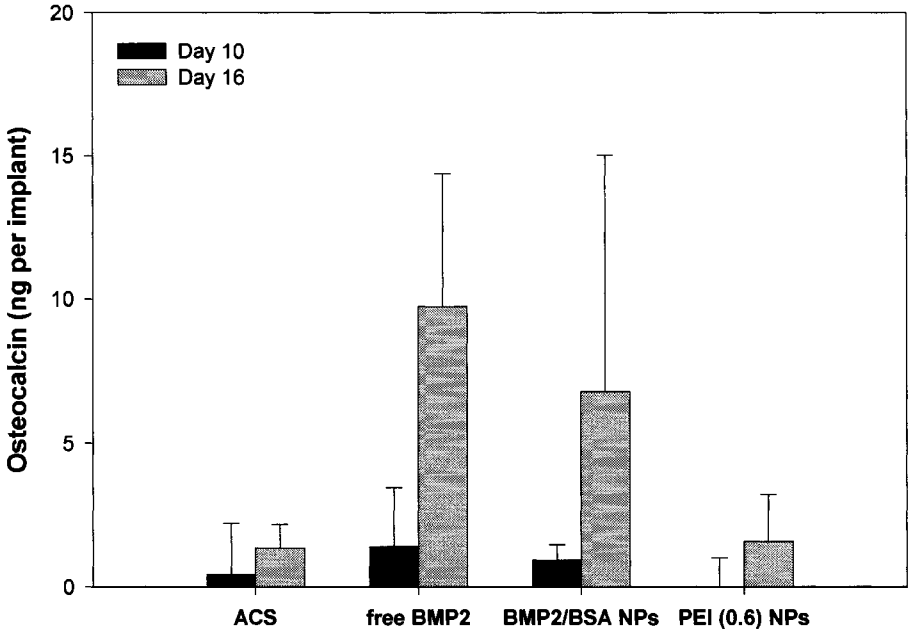

Figure 6-4. Osteocalcin deposition in implants at day 10 and day 16. The osteocalcin level in free BMP-2 and the uncoated BMP-2/BSA NPs was significantly higher than the control and 0.6 mg/mL PEI coated BMP-2/BSA NPs at both day 10 and day 16 ($p<0.05$). PEI-coated BMP-2/BSA NPs did not demonstrate any osteocalcin content at both time points, with no significant difference from the control ACS group ($p>0.70$).

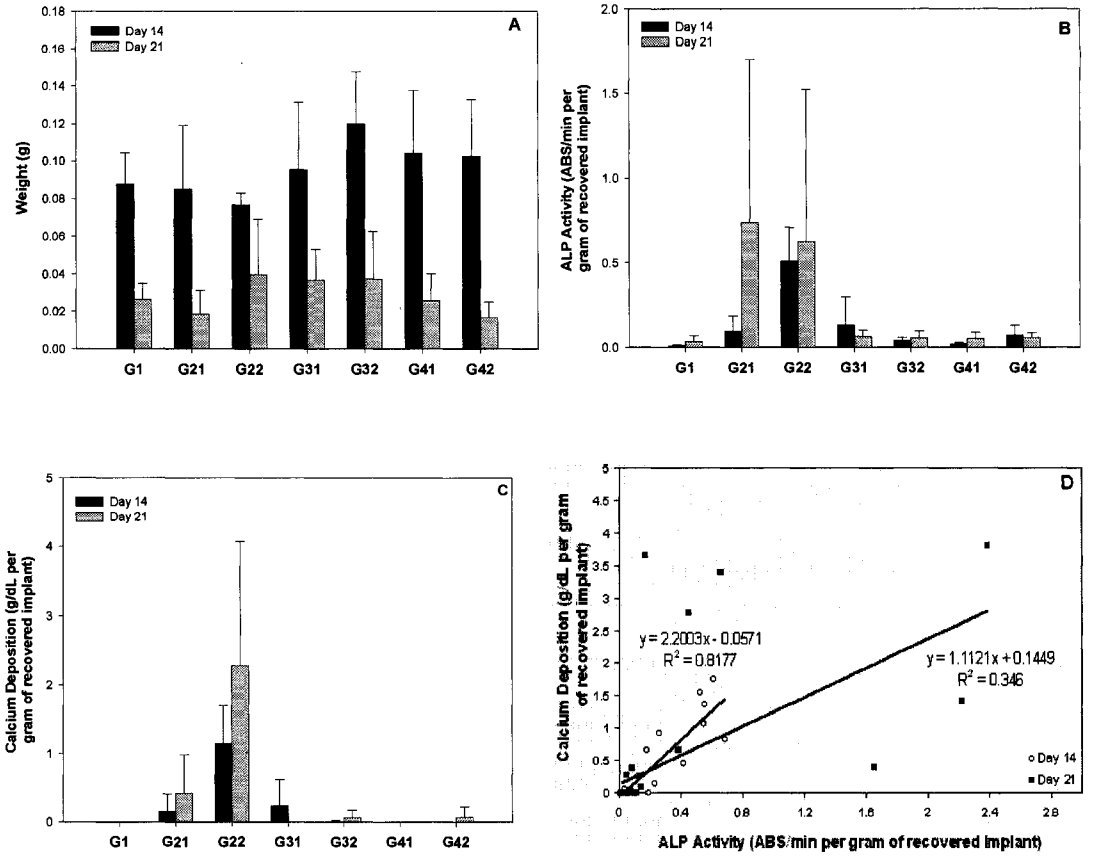

Figure 6-5. *In vivo* investigation of osteoinductive effect by using free BMP-2 to initiate bone formation. G1: ACS alone (0 μg of BMP-2 in this group); G21: ACS loaded with uncoated BMP-2/BSA NPs (3 μg of BMP-2 in this group); G22: ACS loaded with uncoated BMP-2/BSA NPs addition with 3 μg of free BMP-2 (6 μg of BMP-2 in this group); G31: ACS loaded with BMP-2/BSA NPs coated with 0.6 mg/mL PEI (3 μg of BMP-2 in this group); G32: ACS loaded with BMP-2/BSA NPs coated with 0.6 mg/mL PEI addition with 3 μg of free BMP-2 (6 μg of BMP-2 in this group); G41: ACS loaded with BMP-2/BSA NPs coated with 0.1 mg/mL PEI (3 μg of BMP-2 in this group); G42: ACS loaded with BMP-2/BSA NPs coated with 0.1 mg/mL PEI addition with 3 μg of free BMP-2 (6 μg of BMP-2 in this group). **A.** Wet weight of recovered implants at day 10 and day 16; **B.** Normalized ALP activity of different study groups at day 14 and day 21; **C.** Normalized calcium deposition of different study groups at day 14 and day 21; **D.** Correlation between calcium deposition and ALP activity of the recovered implants at day 14 and day 21.

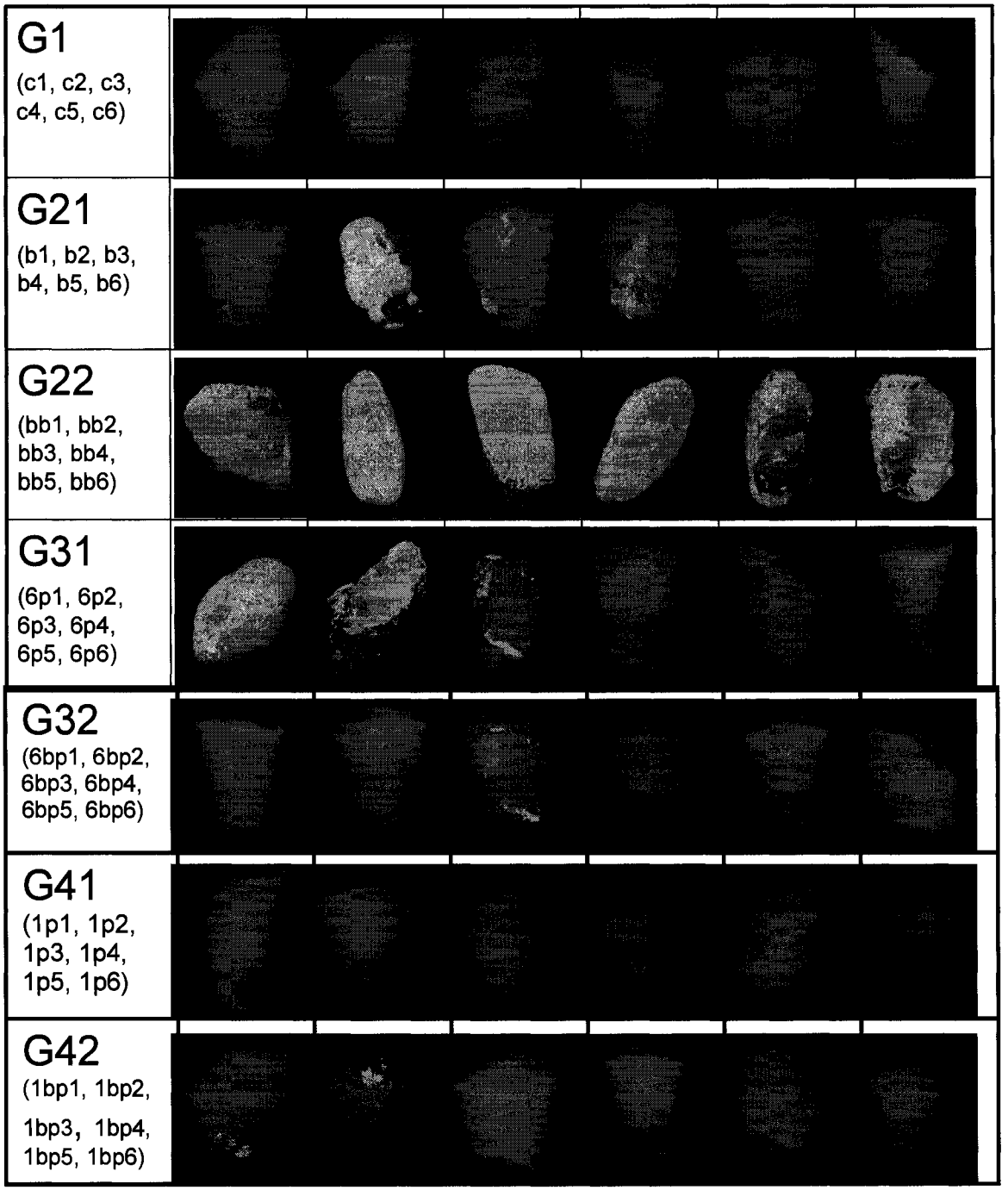

Figure 6-6. Micro-CT images of the bone formation study with free BMP-2 addition. The implants were recovered at day 14 post-implantation. The groups in the study were as following: G1: ACS loaded with saline; G21: ACS loaded with BMP-2/BSA NPs; G22: ACS loaded with BMP-2/BSA NPs + 3 μg of free BMP-2; G31: ACS loaded with BMP-2/BSA NPs coated with 0.6 mg/mL PEI; G32: ACS loaded with BMP-2/BSA NPs coated with 0.6 mg/mL PEI + 3 μg of free BMP-2; G41: ACS loaded with BMP-2/BSA NPs coated with 0.1 mg/mL PEI; G42: ACS loaded with BMP-2/BSA NPs coated with 0.1 mg/mL PEI + 3μg of free BMP-2.

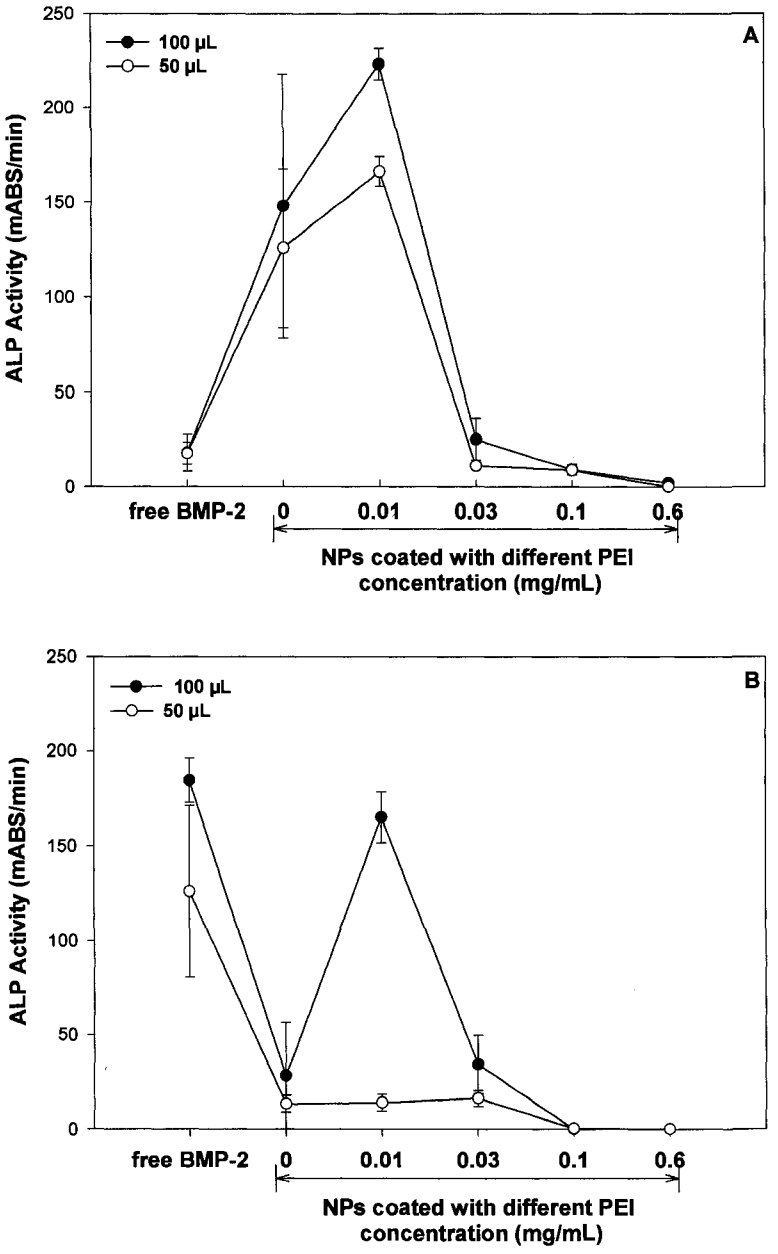

Figure 6-7. *In vitro* ALP activity for NPs produced by "concentration" reminiscent of implant conditions. The NPs were centrifuged for 13.5-fold concentration, and ALP assay was performed with both the pellet (**A**) and supernatant (**B**). No significant ALP activity was observed for both the pellet and supernatant of PEI coating concentration above 0.01 mg/mL. The excessive PEI after the "concentration" process appeared to be detrimental to the bioactivity of BMP-2.

A. Summary of final PEI concentrations after "concentrating" NPs to mimic implantation procedure

BMP-2 dose (μg)	Effect of "Concentration"	PEI coating concentration (mg/mL)				NP volume added to medium (μL)	Final [BMP-2] in medium (μg/mL)
		0.1	0.03	0.01	0		
3.6	Extent of concentration (fold)	13.5	13.5	13.5	13.5	100	1.0
	Final PEI concentration (mg/mL)	1.35	0.40	0.14	0	50	0.5
7.2	Extent of concentration (fold)	6.75	6.75	6.75	6.75	50	1.0
	Final PEI concentration (mg/mL)	0.68	0.20	0.068	0	25	0.5
14.4	Extent of concentration (fold)	3.38	3.38	3.38	3.38	25	1.0
	Final PEI concentration (mg/mL)	0.34	0.10	0.034	0	12.5	0.5

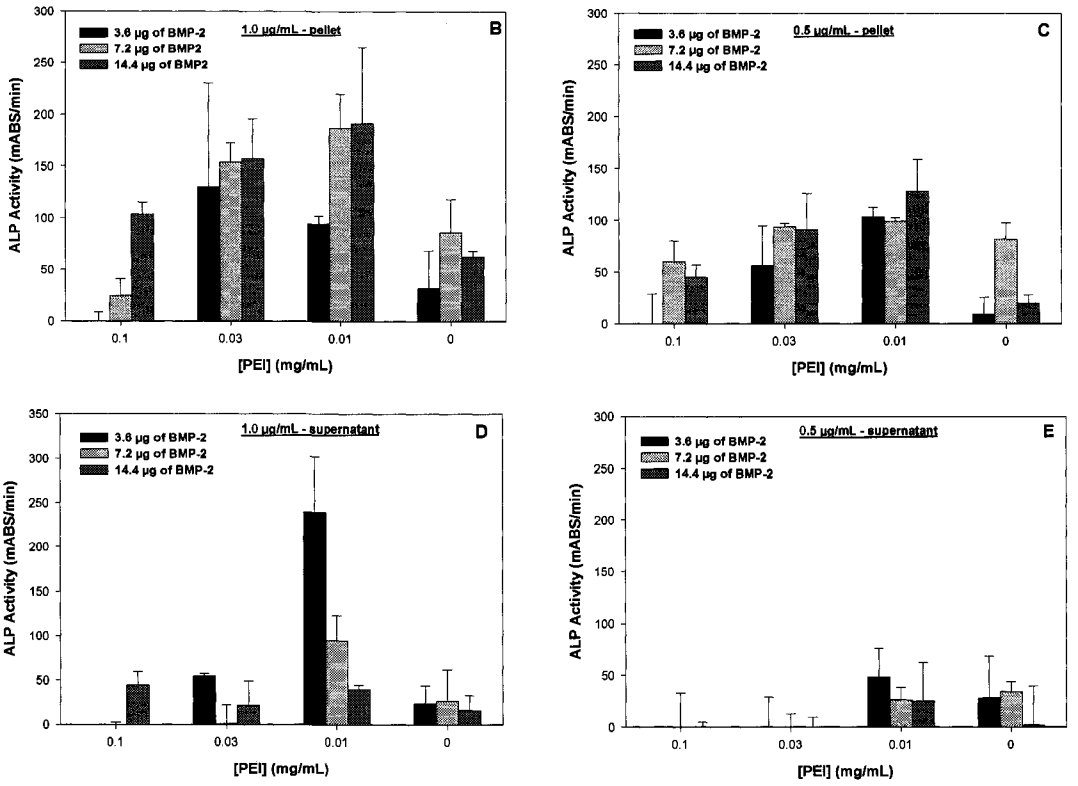

Figure 6-8. *In vitro* ALP assay for NPs with different BMP-2 encapsulated dosages. According to the different BMP-2 loading dosage, different extent of "concentration" process was performed to prepare NPs for ALP assay (**Figure 6-8A**). **B** and **D** are the ALP activity of pellet and supernatant fractions from NPs containing 1.0 μg/mL of BMP-2 in the culture medium. **C** and **E** are the ALP activity of pellet and supernatant fractions from NPs containing 0.5 μg/mL of BMP-2 in the culture medium. This was achieved by adding different volumes of NP solution to the culture medium. PEI concentration of 0.01, 0.03 and 0.1 mg/mL were used for coating. The result showed that the "concentration" process indeed affects the bioactivity of BMP-2, and the higher extent of "concentration", the more detrimental effect of PEI to BMP-2 activity.

References

[1] J. M. Wozney, V. Rosen, A. J. Celeste, L. M. Mitsock, M. J. Whitters, R. W. Kriz, R. M. Hewick, and E. A. Wang, Novel regulators of bone formation: molecular clones and activities., *Science*, 242 (1988) 1528-1534.

[2] P. J. Boyne, Application of bone morphogenetic proteins in the treatment of clinical oral and maxillofacial osseous defects, *J. Bone Joint Surg. Am.*, 83 (2001) S146-S150.

[3] B. Chen, H. Lin, J. Wang, Y. Zhao, B. Wang, W. Zhao, W. Sun, and J. Dai, Homogeneous osteogenesis and bone regeneration by demineralized bone matrix loading with collagen-targeting bone morphogenetic protein-2, *Biomaterials*, 28 (2007) 1027-1035.

[4] J. Levine, J. Bradley, A. E. Turk, J. L. Ricci, J. J. Benedict, G. Steiner, M. T. Longaker, and J. G. McCarthy, Bone morphogenetic protein promotes vascularization and osteoinduction in preformed hydroxyapatite in the rabbit, *Ann. Plast. Surg.*, 39 (1997) 158-168.

[5] H. Maeda, A. Sano, and K. Fujioka, Controlled release of rhBMP-2 from collagen minipellet and the relationship between release profile and ectopic bone formation, *Int. J. Pharm.*, 275 (2004) 109-122.

[6] U. Ripamonti, L. N. Ramoshebi, T. Matsaba, J. Tasker, J. Crooks, and J. Teare, Bone induction by BMPs/OPs and related family members in primates : the critical role of delivery systems, *J. Bone Joint Surg. Am.*, 83 (2001) S116-S127.

[7] H. S. M. Sandhu and S. N. M. Khan, Animal models for preclinical assessment of bone morphogenetic proteins in the spine, *Spine*, 27 (2002) S32-S38.

[8] M. Szpalski and R. Gunzburg, Recombinant human bone morphogenetic protein-2: a novel osteoinductive alternative to autogenous bone graft?, *Acta orthop. Belg.*, 71 (2005) 133-148.

[9] A. L. Jones, R. W. Bucholz, M. J. Bosse, S. K. Mirza, T. R. Lyon, L. X. Webb, A. N. Pollak, J. D. Golden, and A. Valentin-Opran, Recombinant human BMP-2 and allograft compared with autogenous bone graft for reconstruction of diaphyseal tibial fractures with cortical defects. a randomized, controlled trial, *J. Bone Joint Surg.*, 88 (2006) 1431-1441.

[10] A. R. M. Poynton and J. M. M. Lane, Safety profile for the clinical use of bone morphogenetic proteins in the spine, *Spine*, 27 (2002) S40-S48.

[11] S. D. Boden, T. A. Zdeblick, H. S. Sandhu, and S. E. Heim, The use of rhBMP-2 in interbody fusion cages, *Spine*, 25 (2000) 376-381.

[12] G. E. Riedel and A. Valentin-Opran, Clinical evaluation of rhBMP-2/ACS in orthopedic trauma: a progress report, *Orthopedics*, 22 (1999) 663-665.

[13] S. Ebara and K. Nakayama, Mechanism for the action of bone morphogenetic proteins and regulation of their activity, *Spine*, 27 (2002) S10-S15.

[14] H. Seeherman, The influence of delivery vehicles and their properties on the repair of segmental defects and fractures with osteogenic factors, *J. Bone Joint Surg. Am.*, 83 (2001) S79-S81.

[15] B. McKay and H. S. Sandhu, Use of recombinant human bone morphogenetic protein-2 in spinal fusion applications, *Spine*, 27 (2002) S66-S85.

[16] K. Yoshida, K. Bessho, K. Fujimura, Y. Konishi, K. Kusumoto, Y. Ogawa, and T. Iizuka, Enhancement by recombinant human bone morphogenetic protein-2 of bone formation by means of porous hydroxyapatite in mandibular bone defects, *J. Dent. Res.*, 78 (1999) 1505-1510.

[17] S. D. Boden, G. J. J. Martin, M. A. Morone, J. L. Ugbo, and P. A. Moskovitz, Posterolateral lumbar intertransverse process spine arthrodesis with recombinant human bone morphogenetic protein-2/hydroxyapatite-tricalcium phosphate after laminectomy in the nonhuman primate, *Spine*, 24 (1999) 1179.

[18] J. W. M. Vehof, J. Mahmood, H. Takita, M. A. van't Hof, Y. Kuboki, P. H. M. Spauwen, and J. A. Jansen, Ectopic bone formation in titanium mesh loaded with bone morphogenetic protein and coated with calcium phosphate, *Plast. Reconstr. Surg.*, 108 (2001) 434-443.

[19] N. Saito, T. Okada, H. Horiuchi, N. Murakami, J. Takahashi, M. Nawata, H. Ota, S. Miyamoto, K. Nozaki, and K. Takaoka, Biodegradable poly-D,L-lactic acid-polyethylene glycol block copolymers as a BMP delivery system for inducing bone, *J. Bone Joint Surg. Am.*, 83 (2001) 92-98.

[20] K. Whang, D. C. Tsai, E. K. Nam, M. Aitken, S. M. Sprague, P. K. Patel, and K. E. Healy, Ectopic bone formation via rhBMP-2 delivery from porous bioabsorbable polymer scaffolds, *J. Biomed. Mater. Res.*, 42 (1998) 491-499.

[21] M. Isobe, T. Amagasa, S. Oida, Y. Yamazaki, K. Ishihara, and N. Nakabayashi, Bone morphogenetic protein encapsulated with a biodegradable and biocompatible polymer, *J. Biomed. Mater. Res.*, 32 (1996) 433-438.

[22] M. Murata, B. Z. Huang, T. Shibata, S. Imai, N. Nagal, and M. Arisue, Bone augmentation by recombinant human BMP-2 and collagen on adult rat parietal bone, *Int. J. Oral Maxillofac. Surg.*, 28 (1999) 232-237.

[23] H. D. Kim and R. F. Valentini, Retention and activity of BMP-2 in hyaluronic acid-based scaffolds in vitro, *J. Biomed. Mater. Res.*, 59 (2002) 573-584.

[24] M. Murata, M. Arisue, D. Sato, T. Sasaki, T. Shibata, and Y. Kuboki, Bone induction in subcutaneous tissue in rats by a newly developed DNA-coated atelocollagen and bone morphogenetic protein, *Br. J. Oral Maxillofac. Surg.*, 40 (2002) 131-135.

[25] P. Q. Ruhe, E. L. Hedberg, N. T. Padron, P. H. M. Spauwen, J. A. Jansen, and A. G. Mikos, rhBMP-2 release from injectable poly(DL-lactic-co-glycolic Acid)/calcium-phosphate cement composites, *J. Bone Joint Surg. Am.*, 85 (2003) 75-81.

[26] Y. Takahashi, M. Yamamoto, and Y. Tabata, Enhanced osteoinduction by controlled release of bone morphogenetic protein-2 from biodegradable sponge composed of gelatin and [beta]-tricalcium phosphate, *Biomaterials*, 26 (2005) 4856-4865.

[27] T. van den Bos and W. Beertsen, Mineralization of alkaline phosphatase-complexed collagenous implants in the rat: Relation with age, sex, and site of implantation, *J. Biomed. Mater. Res.*, 28 (2008) 1295-1301.

[28] H. P. Seeherman, V, J. P. Wozney, and R. P. Li, Bone morphogenetic protein delivery systems, *Spine*, 27 (2002) S16-S23.

[29] T. Miyata, T. Taira, and Y. Noishiki, Collagen engineering for biomaterial use, *Clin. Mater.*, 9 (1992) 139-148.

[30] K. H. Stenzel, T. Miyata, and A. L. Rubin, Collagen as a biomaterial, *Annu. Rev. Biophys. Bioeng.*, 3 (1974) 231-253.

[31] H. Uludağ, D. D'Augusta, R. Palmer, G. Timony, and J. Wozney, Characterization of rhBMP-2 pharmacokinetics implanted with biomaterial carriers in the rat ectopic model, *J. Biomed. Mater. Res.*, 46 (1999) 193-202.

[32] H. Uludağ, T. Gao, T. J. Porter, W. Friess, and J. M. Wozney, Delivery systems for BMPs: factors contributing to protein retention at an application site, *J. Bone Joint Surg. Am.*, 83 (2001) S128-S135.

[33] W. Friess, H. Uludağ, S. Foskett, and R. Biron, Bone regeneration with recombinant human bone morphogenetic protein-2 (rhBMP-2) using absorbable collagen sponges (ACS): influence of processing on ACS characteristics and formulation, *Pharm. Dev. Technol.*, 4 (1999) 387-396.

[34] G. A. Helm, J. M. Sheehan, J. P. Sheehan, J. A. Jane, C. G. Dipierro, N. E. Simmons, G. T. Gillies, D. F. Kallmes, and T. M. Sweeney, Utilization of type I collagen gel, demineralized bone matrix, and bone morphogenetic protein-2 to enhance autologous bone lumbar spinal fusion, *J. Neurosurg.*, 86 (1997) 93-100.

[35] S. S. Chakravarthi, D. H. Robinson, and S. De, in *Nanoparticulate Drug Delivery System*, edited by D. Thassu, M. Deleers, and Y. Pathak, Informa Healthcare, New York, 2007, pp. 51-61.

[36] H. Hillaireau and P. Couvreur, in *Polymers in Drug Delivery*, edited by I. F. Uchegbu and A. G. Schätzlein, CRC Press, Boca Raton, 2006, pp. 101-111.

[37] S. D. Putney and P. A. Burke, Improving protein therapeutics with sustained-release formulations, *Nat. Biotech.*, 16 (1998) 153-157.

[38] S. Zhang, G. Wang, X. Lin, M. Chatzinikolaidou, H. Jennissen, M. Laub, and H. Uludağ, Polyethylenimine-coated albumin nanoparticles for BMP-2 delivery, *Biotechnol. Prog.*, 24 (2008) 945-956.

[39] M. Chatzinikolaidou, T. Zumbrink, and H. P. Jennissen, Stability of surface-enhanced ultrahydrophilic metals as a basis for bioactive rhBMP-2 surfaces., *Materialwiss. Werkstofftech.*, 34 (2003) 1106-1112.

[40] S. A. Gittens, G. Bansal, C. Kucharski, M. Borden, and H. Uludağ, Imparting mineral affinity to fetuin by bisphosphonate conjugation: a comparison of three bisphosphonate conjugation schemes, *Mol. Pharm.*, 2 (2005) 392-406.

[41] H. Uludağ, D. 'Augusta, J. Golden, J. Li, G. Timony, R. Riedel, and J. M. Wozney, Implantation of recombinant human bone morphogenetic proteins with biomaterial carriers: a correlation between protein pharmacokinetics and osteoinduction in the rat ectopic model, *J. Biomed. Mater. Res.*, 50 (2000) 227-238.

[42] M. Varkey, C. Kucharski, T. Haque, W. Sebald, and H. Uludağ, *In vitro* osteogenic response of rat bone marrow cells to bFGF and BMP-2 treatments, *Clin. Orthop. Relat. Res.*, 443 (2006) 113-123.

[43] K. Makino, T. Mizorogi, S. Ando, T. Tsukamoto, and H. Ohshima, Sonochemically prepared bovine serum albumin microcapsules: factors affecting the size

distribution and the microencapsulation yield, *Colloids Surf. B Biointerfaces*, 22 (2001) 251-255.

[44] A. P. Gadeau, H. Chaulet, D. Daret, M. Kockx, J. M. niel-Lamaziere, and C. Desgranges, Time course of osteopontin, osteocalcin, and osteonectin accumulation and calcification after acute vessel wall injury, *J. Histochem. Cytochem.*, 49 (2001) 79-86.

[45] H. Hosseinkhani, M. Hosseinkhani, A. Khademhosseini, and H. Kobayashi, Bone regeneration through controlled release of bone morphogenetic protein-2 from 3-D tissue engineered nano-scaffold, *J. Control Release*, 117 (2007) 380-386.

[46] M. Yamamoto, Y. Takahashi, and Y. Tabata, Controlled release by biodegradable hydrogels enhances the ectopic bone formation of bone morphogenetic protein, *Biomaterials*, 24 (2003) 4375-4383.

[47] A. Yamaguchi, T. Komori, and T. Suda, Regulation of osteoblast differentiation mediated by bone morphogenetic proteins, hedgehogs, and Cbfa1, *Endocr. Rev.*, 21 (2000) 393-411.

[48] M. Huang, S. N. Vitharana, L. J. Peek, T. Coop, and C. Berkland, Polyelectrolyte complexes stabilize and controllably release vascular endothelial growth factor, *Biomacromolecules*, 8 (2007) 1607-1614.

[49] I. Messai, S. Munier, Y. Ataman-önal, B. Verrier, and T. Delair, Elaboration of poly(ethyleneimine) coated poly(,-lactic acid) particles: effect of ionic strength on the surface properties and DNA binding capabilities, *Colloids Surf. B Biointerfaces*, 32 (2003) 293-305.

[50] T. G. Park, S. Cohen, and R. Langer, Controlled protein release from polyethyleneimine-coated poly(L-lactic acid)/pluronic blend matrices, *Pharm. Res.*, 9 (1992) 37-39.

[51] W. Lin, A. G. A. Coombes, M. C. Davies, S. S. Davis, and L. Illum, Preparation of sub-100 nm human serum albumin nanospheres using a pH-coacervation method, *J. Drug Target.*, 1 (1993) 237-243.

[52] P. Q. Ruhe, O. C. Boerman, F. G. M. Russel, P. H. M. Spauwen, A. G. Mikos, and J. A. Jansen, Controlled release of rhBMP-2 loaded poly(dl-lactic-co-glycolic acid)/calcium phosphate cement composites *in vivo*, *J. Control Release*, 106 (2005) 162-171.

[53] S. S. Rengachary, Bone morphogenetic proteins: basic concepts, *Neurosurg. focus*, 13 (2002) 1-6.

[54] E. A. Wang, V. Rosen, J. S. D'Alessandro, M. Bauduy, P. Cordes, T. Harada, D. I. Israel, R. M. Hewick, K. M. Kerns, and P. LaPan, Recombinant human bone morphogenetic protein induces bone formation, *Proc. Natl. Acad. Sci. U. S. A.*, 87 (1990) 2220-2224.

[55] Y. Okamoto, Y. Horisaka, N. Matsumoto, K. Yoshida, J. Kawada, K. Yamashita, and T. Takagi, Muscle tissue reactions to implantation of bone matrix gelatin, *Clin. Orthop. Relat. Res.*, 263 (1991) 242-253.

[56] Y. Horisaka, Y. Okamoto, N. Matsumoto, Y. Yoshimura, A. Hirano, M. Nishida, J. Kawada, K. Yamashita, and T. Takagi, Histological changes of implanted collagen material during bone induction, *J. Biomed. Mater. Res.*, 28 (1994) 97-103.

[57] H. Takita, J. W. M. Vehof, J. A. Jansen, M. Yamamoto, Y. Tabata, M. Tamura, and Y. Kuboki, Carrier dependent cell differentiation of bone morphogenetic protein-2 induced osteogenesis and chondrogenesis during the early implantation stage in rats, *J. Biomed. Mater. Res.*, 71 A (2004) 181-189.

[58] N. Saito, T. Okada, H. Horiuchi, N. Murakami, J. Takahashi, M. Nawata, H. Ota, K. Nozaki, and K. Takaoka, A biodegradable polymer as a cytokine delivery system for inducing bone formation, *Nat. Biotechnol.*, 19 (2001) 332-335.

[59] A. C. Hunter, Molecular hurdles in polyfectin design and mechanistic background to polycation induced cytotoxicity, *Adv. Drug Deliv. Rev.*, 58 (2006) 1523-1531.

[60] H. Lv, S. Zhang, B. Wang, S. Cui, and J. Yan, Toxicity of cationic lipids and cationic polymers in gene delivery, *J. Control Release*, 114 (2006) 100-109.

[61] M. Yamamoto, Y. Takahashi, and Y. Tabata, Controlled release by biodegradable hydrogels enhances the ectopic bone formation of bone morphogenetic protein, *Biomaterials*, 24 (2003) 4375-4383.

CHAPTER VII

In Vitro and *In Vivo* Assessment of PEG-modified Polyethylenimine-Coated Albumin Nanoparticles for BMP-2 Delivery

INTRODUCTION

Bone morphogenetic proteins (BMPs) play an essential role in bone formation and healing, and they were demonstrated to elicit new bone formation both at ectopic and orthotopic sites in various animal models [1-8]. Due to the limitations of biologically derived grafts in repair of bone defects, an alternative approach to stimulate new bone formation is becoming increasingly more prevalent by the utilization of BMPs. Numerous studies have examined the effects of implant treatment for osseous defect with BMPs. With the validation of efficacy and safety for bone repair [9-12], BMP-2 has been recently approved by FDA for spinal fusion in humans (InFUSE® Bone Graft). Since the rapid diffusion of BMP-2 away from the application site and the loss of bioactivity, exogenous administration of BMP-2 in buffer solution does not yield satisfactory new bone induction, especially in higher mammals [13,14]. A controlled and localized delivery system for BMP-2 would be appropriate for effective bone regeneration. Studies have demonstrated a correlation between the osteoinductivity of BMP-2 and its retention in various carriers *in vivo* [15-17]. Based on these observations, it was suggested that the enhancement of protein retention in the carrier can potentially improve the performance of BMP-2 function at the implantation site.

Currently delivery of BMP-2 in collagen matrices, though successful in preclinical and human clinical trials, demonstrated some drawbacks [18]. Initial burst release is a concern when BMP-2 simply absorbed onto/into the carrier, which will result in less retention time period for BMP-2. By entrapment or covalent binding of BMP-2 to the carrier, the initial burst release could be suppressed, and a prolonged retention time is expected. However, the difficulty in retaining the protein biological activity limited the

utilization of covalent binding to the carrier. Alternatively, bone growth factors have been physically entrapped into micro/nanoparticles (MPs/NPs), liposomes, hydrogels, foams or bone cements [19]. As an efficient and simple delivery system developed in 1980s, NPs delivery system holds promise for BMP-2 delivery for bone regeneration. This system provides methods for releasing drug in very defined regions over a prolonged time, and preserves the drug's bioactivity, which can be beneficial for local application, as well as targeted delivery via intravascular injection [20]. We previously reported that BMP-2 can be encapsulated in PEI-coated BSA NPs with encapsulation efficiency above 90%, and retained its bioactivity after *in vitro* release. The release of BMP-2 from NPs can be controlled by the PEI coating concentrations [21]. The PEI-coated, BMP-2 encapsulated BSA NPs was also examined in a rat ectopic model by subcutaneous implantation for osteoinduction activity **(Chapter VI)**. However, the osteoinductive effect was not achieved by the NPs at all PEI coating concentrations examined, presumably because the NP formulation for implantation increased the toxicity of coated PEI, which consequently abolished the bioactivity of BMP-2.

PEGylation of polymers is an established method for increasing polymer biocompatibility, as well as minimizing aggregation of particulates by providing steric stabilization and a prolonged circulation time after systemic injection [22,23]. The ample primary amine groups on PEI facilitate PEG modification. In this report, we designed a new approach for BSA NPs coating, by utilization of PEGylated PEI, in order to reduce the toxicity of PEI coating on NP and increase the biocompatibility of this delivery system. N-hydroxysuccinimidyl-poly(ethyleneglycol)-maleimide (NHS-PEG-MAL) was employed as a linker to attach PEG fraction onto PEI [24]. The BMP-2 encapsulated

BSA NPs coated with PEI-PEG was evaluated for the osteoinduction activity of released BMP-2 in a rat ectopic model by subcutaneous implantation, and this BMP-2 delivery system successfully induced new bone formation.

MATERIALS AND METHODS

Materials

Bovine serum albumin (BSA), branched PEI (M_w ~25,000 by LS, M_n ~10,000 by GPC), 3-(4,5-dimethylthiazol-2-yl)-2,5-diphenyltetrazolium bromide (MTT), the ALP substrate p-nitrophenol phosphate (p-NPP), *o*-cresolphthalein, 8-hydroxy-quinoline, dimethyl sulfoxide (DMSO) and picrylsulfonic acid solution (TNBS; 5% w/v) were obtained from Sigma-Aldrich (St. Louis, MO, USA). Recombinant Human Bone Morphogenetic Protein-2 (BMP-2, from *E.coli.*) was prepared as described before [25]. Fluorescein isothiocyanate (FITC) was obtained from PIERCE (Rockford, IL, USA). N-hydroxysuccinimidyl-polyethylene glycol-maleimide (NHS-PEG-MAL, 3400 Da) was obtained from NEKTAR (Huntsville, AL, USA). Dulbecco's Modified Eagle Medium (DMEM), Hank's Balanced Salt Solution (HBSS), penicillin (10,000 U/mL solution) and streptomycin (10,000 μg/mL solution) were from Invitrogen (Carlsbad, CA, USA). 2-amino-2-methyl-propan-1-ol (AMP) was obtained from Aldrich chemicals (Milwaukee, WI, USA). Triton X-100 (rein-pure octylphenol-polyethyleneglycol ether) was obtained from Feinbiochemica (Heidelburg, NY, USA). Fetal bovine serum (FBS) was from Atlanta Biologics (Atlanta, GA, USA). The chemicals were used as received, without any further purification. The Spectra/Por dialysis tubing with 12–14 kDa and 100 kDa cut-off was acquired from Spectrum Laboratories (Rancho Dominguez, CA, USA). All tissue

culture plasticware was from Corning (Corning, NY, USA). Distilled/de-ionized water (ddH_2O) used for buffer preparations were derived from a Milli-Q purification system.

Preparation of PEI-PEG Conjugate [24]

The PEI-PEG conjugates were prepared by reacting PEI (branched, 25 kDa) with different concentrations of NHS-PEG-MAL. Briefly, the NHS-PEG-MAL was dissolved in 100 mM, pH =7.0 phosphate buffer (see Legends for exact concentrations), and PEI solution (3.6 mg/mL in 100 mM phosphate buffer, pH = 7.0) was added to this solution at a volume ratio of 1:1. The samples were incubated for 2.5 hours at room temperature, then dialyzed against 100 mM phosphate buffer (pH = 5.0) (×2), and subsequently dialyzed against ddH_2O (×2). The remained PEI content in PEI-PEG conjugate was determined by TNBS assay to quantify the primary amine groups. The substitution percentage of PEG on PEI was determined by the reduction of primary amine concentration on PEI, and calculated as: 100% × [(initial amine concentration) – (final amine concentration)]/(initial amine concentration).

Preparation of BMP-2 Encapsulated, PEI-PEG Coated BSA NPs

Briefly, 250 μL of 10 mg/mL BSA solution (50 mg of BSA dissolved in 5 mL ddH_2O) was added to 250 μL of 10 mM NaCl solution (pH = 7.0) in a glass vial under constant stirring (600 rpm) at room temperature. The mixing was allowed to proceed for 15 min. Then, 72 μL of 0.5 mg/mL BMP-2 solution (in ddH_2O) was added into the above solution. This aqueous phase was then desolvated with dropwise addition of 3.0 mL of ethanol after 2 h of incubation. The mixture was stirred (600 rpm) under room

temperature for another 3 h. The BMP-2 encapsulated BSA NPs so formed were coated with different PEI-PEG concentrations (see Legends for exact concentrations). Different concentrations of PEI-PEG in 0.5 mM NaCl solution were added to the above NPs solution by a volume ratio of 1.25 to 1 (polymer to NPs). The coating was allowed to proceed for 1 h on an orbital shaker (450 rpm). The coated NPs were extensively dialyzed (MWCO: 12-14 kDa) against phosphate buffered saline (pH=7.3, ×3) and, for the bioactivity studies, then against DMEM with 1% penicillin/streptomycin (×1). The dialyzed buffer was exchanged every 3 h. All solutions used for NP preparation were sterilized by passing through 0.20 μm sterile filter (SARSTEDT, Aktiengesellschaft & Co., Germany) before use, and the manufacture process was carried out under sterile conditions.

Characterization of PEI-PEG Coated BSA NPs

The mean particle size and polydispersity index of the PEI-coated and uncoated BSA NPs were determined by dynamic light scattering at 25°C with a Zetasizer 3000 HS (Malvern Instruments Ltd., UK) using a 633 nm He-Ne laser at a scattering angle of 90°. The surface charge of the coated and uncoated BSA NPs were investigated by measuring the electrophoretic mobility of the particles using the zeta potential modus of the same instrument at 25°C. The samples for measurement were prepared after appropriate dilution and suspended in 1 mM NaCl solution. The particle size measurement was the average of 3 runs, with each run containing 10 sub-runs. The zeta potential measurements were the automatic mode, being the average of 3 runs.

Samples were also dialyzed against ddH_2O for AFM (atomic force microscopy) images. The NP sample was sonificated for 5 min and then 1.5 μL of the sample was dropped onto the mica surface (PELCO^R Mica Discs; TED PELLA, Inc.; Redding, CA, USA), and imaged after drying under room temperature [21]. MFP-3D AFM (Asylum Research, Santa Barbara, CA, USA) was used for the AFM studies of PEI-PEG coated BSA NPs. Images were processed and analyzed by the Igor Pro imaging software (version 5.04B).

Coating Efficiency with FITC-PEI-PEG and FITC-PEI

The amount of FITC-PEI-PEG coated on BSA NPs was determined by fluorescence measurements. To obtain the labeled polymer, PEI (10 mg/mL) was first reacted with FITC as described before [21]. The obtained FITC-PEI was then reacted with different concentrations of MAL-PEG-NHS (see Legends for exact concentrations). The FITC-PEI-PEG conjugates so formed were dialyzed (MWCO: 12-14 kDa) against 100 mM phosphate buffer (pH = 5.0) (2×), and subsequently dialyzed against ddH_2O (2×) to remove the unreacted MAL-PEG-NHS. Different concentrations of FITC-PEI-PEG and FITC-PEI were used to coat BSA NPs. The coating time was 1 h. The coated NPs were dialyzed (MWCO: 100 kDa) against ddH_2O (3×), centrifuged for 30 min at high speed (BHG Hermle Z230 M Centrifuge) to remove ethanol, free BSA and uncoated polymer, and then re-dispersed in ddH_2O. A 200 μL of the aliquot in duplicate was then added to black 96-well plates (NUNC, Rochester, NY, USA) and the fluorescence (λ_{ex}: 485 nm; λ_{em}: 527 nm) was determined with a multiwell plate reader (Thermo Labsystems, Franklin, MA, USA). The amount of FITC-PEI-PEG or FITC-PEI coated on the BSA

NPs was calculated based on a calibration curve generated by using the FITC-PEI-PEG or FITC-PEI in ddH_2O. The coating efficiency of polymer was calculated as: 100% × {(final FITC-polymer of the pellet)/(initial FITC-polymer for coating)}.

Cytotoxicity of PEI-PEG and PEI

The cytotoxicity of PEI-PEG and PEI was assessed by MTT dye reduction assay [21]. Two different PEG modified PEI, 3 mM and 1 mM (expressed as PEI-PEG-3mM and PEI-PEG-1mM, respectively) was examined in this study. Sample concentrations, both the unmodified PEI and PEI-PEG, were quantified in terms of PEI content. Various concentrations of PEI and PEI-PEG in ddH_2O solutions (See Legends for details) were added to human C2C12 cells grown on 48-well plates with 0.5 mL DMEM (10 % FBS and 1% penicillin/streptomycin) in triplicate. After 48 h incubation, the MTT assay was performed as described before [21]. In order to determine the cytotoxicity of PEI-PEG or PEI coated BSA NPs, MTT assay was carried out for NPs. The NPs were prepared as described above, and then coated with 0.03, 0.1 and 0.3 mg/mL PEI or PEI-PEG for 1 h on an orbital shaker. PEI-PEG concentration was quantified in terms of PEI content. After coating, samples were dialyzed against PBS (pH = 7.4) (2×), and then DMEM with 1% penicillin/streptomycin (1×). Human C2C12 cells grown on 48-well plates were incubated with various concentrations of PEI and PEI-PEG in triplicate for 48 h. After 48 h incubation, MTT assay was performed as described before [21].

ALP Assay for PEI-PEG and PEI Coated NPs

As a parallel study to the above MTT assay for NPs, the bioactivity of BMP-2 encapsulated in PEI-PEG or PEI coated BSA NPs was studied by ALP assay. The NPs were prepared the same way as in the MTT assay aforementioned. Different volumes of NPs solutions were added to the C2C12 cells. The final BMP-2 concentrations in the culture medium were 0.5, 0.25, 0.125 and 0.0625 μg/mL by adding 50, 25, 12.5 and 6.25 μL NPs solutions to the wells, respectively. Human C2C12 cells, grown in 48-well plates, were incubated with NPs solutions for 72 h. After 72 h of incubation, the ALP assay was performed as described before [21].

***In vitro* Assessment for NPs of Implant Formulation**

Prior to *in vivo* ectopic bone formation study, the NPs formulation was tested *in vitro* for cytotoxicity and ALP activity determination. Briefly, 120 μL of 1.0 mg/mL BMP-2 in ddH_2O was added to the mixture of 125 μL of 10 mg/mL of BSA solution and 12.5 μL of 100 mM of NaCl solution in a glass vessel (9.6% wt BMP-2 in BSA). The mixture was stirred at 600rpm for 1 h under room temperature. Then 1.0 mL of 100% ethanol was added dropwise to the mixture, and stirred for 3 h at 600rpm to form BMP-2 encapsulated BSA NPs. The so formed NPs were then coated with 0.1 mg/mL PEI or 0.1 mg/mL PEI-PEG-3mM, which were dissolved in 0.5 mM NaCl solution. The volume ratio for NPs to polymer for coating was 1:1. The coating was allowed to proceed for 1 h on an orbital shaker. The uncoated sample was processed the same way as the coated samples, except by adding 0.5 mM of NaCl solution to the NPs. Then samples were dialyzed against PBS (pH = 7.4) (2×) and DMEM (1% of penicillin/streptomycin) (1×). Different volumes of NPs solution were incubated with human C2C12 cells grown on 48-

well plate. The final BMP-2 concentrations in the culture medium were 1.0, 0.5, 0.25 and 0.125 μg/mL by adding different volumes of NPs solution to cells (See Legend for details). The wells without any NPs solution served as control. After 48 h incubation, the medium was aspirated, and 0.5 mL of fresh DMEM (1% of penicillin/streptomycin and 10% of fetal bovine serum) was added per well. MTT assay was then performed as described before [21]. The ALP activity was assessed after NP solutions incubated with cells for 72 h, and the kinetic ALP procedure was described as before [21].

Ectopic Bone Formation with PEI Coated and PEI-PEG Coated NPs

Preparation of Implants and Implantation into Rats: The BMP-2 encapsulated BSA NPs formulations were prepared as described aforementioned in the *in vitro* assessment section. This NP preparation ensured that 3 μg/50 μL BMP-2 in NP solution after dialysis (assuming the encapsulation efficiency is ~100% [21]) without further concentrating the NPs. There were four groups examined in this study: (1) ACS alone; (2) ACS loaded with the uncoated BMP-2/BSA NPs; (3) ACS loaded with 0.1 mg/mL PEI-PEG coated BMP-2/BSA NPs and (4) ACS loaded with 0.1 mg/mL PEI coated BMP-2/BSA NPs. Samples were dialyzed against PBS (pH = 7.4, 2×). The ACS was cut into 1 cm × 1 cm × 0.5 cm piece, to absorb 50 μL of sample for each piece. For the unloaded ACS, 50 μL of PBS (pH = 7.4) was absorbed into ACS (See details in **Table 1**), and allowed to soak for ~15 minutes before implantation. 6~8-week-old female Sprague-Dawley rats (average weight: 240 g) were purchased from Biosciences (Edmonton, Alberta). The rats were acclimated for 1 week under standard laboratory conditions (23°C, 12 hours of light/dark cycle) prior to the beginning of the study. While maintained in pairs in sterilized cages, rats were

provided standard commercial rat chow, and tap water *ad libitum* for the duration of the study. All procedures involving the rats were approved by the Animal Welfare Committee at the University of Alberta (Edmonton, Alberta). Once rats were anesthetized with inhalational Metofane^{TM}, two implants (duplicates of the same type) were implanted subcutaneously into bilateral ventral pouches in each rat. The pouches were closed with staples. There were 24 rats utilized in this study, with each group containing 3 rats at designated time point (10 and 16 days). Rats were euthanized with CO_2 at indicated time points, the implants were recovered, weighed before further investigation. ALP assay and calcium assay were carried out for the recovered implants. The results were summarized as mean ± SD for 6 implants at each time point.

Kinetic ALP Assay for Recovered Implants: At day 10 and day 16 post-implantation, the rats were sacrificed, and implants were recovered. After weight determination, the explants were incubated in 2.0 mL of PBS (1×) at 4 °C (in 24-well-plate) overnight with gentle shaking, to remove any serum contaminants. The explants were then transferred into 1.0 mL of 25 mM of $NaHCO_3$ (pH = 7.4) containing 0.01% Triton X-100 for a 72 h incubation at 4 °C with gentle shaking. After 72 h incubation, 200 μL of the lysis solution (in duplicate) from each well were placed into a 48-well-plate. Then 200 μL of p-NPP in ALP buffer (pH = 10.5, containing 0.1 % of Triton X-100) was added to the lysis solution. A kinetic ALP assay was performed to determine the bioactivity of BMP-2 [21]. The changes in optical density ($\lambda_{absorbance}$: 405 nm) were determined in a multi-well plate reader at an intervals of 1.5 min for 8 cycles. The ALP activity was expressed as the change in optical density of the wells per unit time (mABS/minute).

Micro Computer Tomography (micro-CT) Imaging for Explants: Before decalcification, the recovered implants were scanned on a micro-CT scanner (Skyscan-1076, Skyscan, Belgium) for both day 10 and day 16 post-implantation. The recovered implants were in ALP lysis buffer, which stored at 4 °C, and then placed into a 1.5 mL microcentrifuge tube, scanned together with a micro-CT phantom standard. The scanning process was typically 23~30 minutes (Voltage: 48kV; Current: 100 μA; Filter: Titanium 0.025mm; Rotation step: 0.35 degree; Imaging pixel size: 18 μm; Frame Averaging: 3). The scanned images were reconstructed into 3D image with NRecon software (version 1.5.1). The bone volume formed in the sponge was automated measured by the micro-CT scan with a unit of mm^3.

Calcium Deposition into Implants: After micro-CT scan, the recovered implants were first washed with 2.0 mL of PBS (1×), and then transferred to a new 24-well-plate, immersed in 1.0 mL of 0.5 M HCl at 4°C for 24 h to extract the calcium deposited in the sponge. The extraction process was under gentle shaking on an orbital shaker. The concentration of calcium in this solution was quantified by a calcification assay with calcium standards (Sigma diagnostic® ($\lambda_{absorbance}$: 574 nm)) to yield the amount of calcium formed. Briefly, 20 μL of the dissolved calcium solution was added to 50 μL of a solution containing 0.028 M of 8-hydroxyquinoline and 0.5% (v/v) sulfuric acid, as well as 500 μL of a solution containing 3.7×10^{-4} M of *o*-cresolphthalein and 1.5% (v/v) AMP. A calcium standard curve based on the standards was used to convert the absorbance into concentration of calcium. The level of calcification was summarized as the concentration of calcium (mg/dL) per well.

Statistics Analysis

All quantitative data were expressed as the mean ± standard deviation (SD). In the *in vitro* study, statistical analysis was performed by Student's *t*-test. In the ectopic bone formation study, statistical analysis was performed by the non-parametric Mann-Whitney-Wilcoxon test. Where indicated, statistical differences between group means were analyzed by single factor analysis of variance (ANOVA) or Kruskal-Wallis one-way analysis of variance (for non-parametric test). A value of $p<0.05$ was considered statistically significant.

RESULTS

PEI-PEG Conjugation and Cytotoxicity of PEI-PEG

PEGylation is a well-established modification in order to increase the hydrophilicity and reduce the surface charge of polymers [26]. By reacting the primary amines on PEI with the NHS functional group in NHS-PEG-MAL [24], a serial of cationic copolymers were synthesized by grafting linear 3.4 kDa PEG to the amino group of 25 kDa branched PEI **(Scheme 7-1)**. The substitution extent of PEG onto PEI was expected to be controlled by the ratio of NHS-PEG-MAL to PEI. In this study, three different concentrations of NHS-PEG-MAL, 3, 1, and 0.3 mM, were used, and the ratios of NHS-PEG-MAL to PEI were 42:1, 14:1 and 4.2:1, respectively. The resultant PEG substitutions on PEI were 20.0, 11.1 and 4.2 PEG per PEI.

After the conjugation, the cytotoxicity of different PEI-PEG conjugates, along with the unmodified PEI was determined with human C2C12 cells **(Figure 7-1)**. The PEI with the lowest substitution of PEG did not significantly improve the cytotoxicity.

Highest degree of PEGylation (20.0 PEG/PEI), reduced PEI-induced cell death significantly, with 78.6% cell viability at the highest concentration of 20 μg/mL tested. The moderately modified PEI (11.1 PEG/PEI), gave some improvement in PEI toxicity. The IC_{50} values, i.e. the polymer concentration at which 50% cell viability was obtained, are listed in **Table 7-2**. The IC_{50} was found to be 6.3, 6.3, 10.2 μg/mL and > 20 μg/mL for 0, 4.2, 11.1 and 20.0 PEG/PEI, respectively. It was thus clear that PEG substitution greatly reduced the toxicity of PEI. Since the 4.2 PEG modified PEI behaved similar to the unmodified PEI, this PEG-modified PEI was eliminated from the following studies.

Characterization of PEI-PEG Coated NPs

Next, we explored the feasibility of PEI-PEG coating on BSA NPs. The two PEI-PEG conjugates utilized in this study were the 3mM (PEI-PEG-3mM) and 1mM (PEI-PEG-1mM) PEG modified PEI. Three polymer concentrations were used for coating, 0.03, 0.1 and 0.3 mg/Ml (based on PEI content). We first measured the size and zeta potential of the coated NPs (**Figure 7-2A** and **7-2C**, respectively). For 0.03 mg/mL PEI coating, large aggregates were produced after coating, presumably due to the bridging flocculation among the formed particles [27]. However, PEI-PEG-3mM coating at this concentration effectively protected particles from aggregation but not PEI-PEG-1Mm. The size of 0.03 mg/mL PEI-PEG-1mM and PEI-PEG-3mM coated BSA NPs were 634.6 ± 88.6 nm and 154.5 ±1.3 nm, respectively. For 0.1 mg/mL polymer coating, the size of the NPs was 136.8 ± 6.1 nm, 175.1 ± 3.2 nm and 215.2 ± 5.2 nm for PEI-PEG-3mM, PEI-PEG-1mM and PEI coating, respectively. The polydispersity indices for the NPs were 0.23, 0.26 and 0.27, respectively. For 0.3 mg/mL, the size of the coated NPs was

131.8 ± 4.7 nm, 148.1 ± 2.4 nm and 204.9 ± 88.6 nm for PEI-PEG-3mM, PEI-PEG-1mM and PEI coated NPs, respectively ($p>0.2$ for the size difference at 0.3 mg/mL polymer coating by ANOVA). The polydispersity indices for NPs were 0.08, 0.13 and 1.0, respectively **(figure 7-2B)**. A typical AFM image **(Figure 7-3)** showed the morphology of 0.3 mg/mL PEI-PEG coated BSA NPs. They are general spherical in shape, and the size was around 100 -180 nm.

The zeta potential of the coated NPs increased significantly from ~ -16 mV to >> 10 mV. At 0.3 mg/mL concentration, PEI coating produced the highest zeta potential among all the groups, 29.7 mV; while the zeta potential of PEI-PEG-1mM and PEI-PEG-3mM were significantly reduced to 25.2 and 18.6 mV, respectively ($p<0.001$ by ANOVA). The reduction in zeta potential, as compared with PEI coating, indicated that PEI-PEG coating effectively reduced the surface charge of the NPs, and the higher the PEG substitution, the lower the surface charge was. These trends were seen in an additional independent batch of NPs. The collective results revealed that PEGylated PEI coating on NPs dramatically decreased the size of NPs, as well as the polydispersity index and the zeta potential.

The amount of PEI and PEI-PEG adsorption on BSA NPs was investigated in two independent batches of NPs by direct fluorescence measurements. The results were summarized as polymer amount (μg) adsorbed on NPs **(Figure 7-4A)**. As the polymer concentration was increased, the amount of adsorbed polymer was increased, with PEI coating showed evident increase while PEI-PEG showed relative slight increase. The two PEGylated PEI, PEI-PEG-1mM and PEI-PEG-3mM, demonstrated similar retained amount on BSA NPs. A ~5.2, ~4.8 and ~2.5-fold increase in retained polymer amount

were seen for PEI coating compared to PEI-PEG coating at 0.3, 0.1 and 0.03 mg/mL coating concentrations, respectively. The coating efficiency of polymers **(Figure 7-4B)** was dependent on the polymer concentration; as expected, the coating efficiency of polymers decreased as the polymer concentration for coating increased. This was consistent with previous studies of PEI coating on BSA NPs [21] and PEI adsorbed to hydroxyapatite [24]. The PEI demonstrated higher coating efficiency than the PEI-PEG polymers at the three coating concentrations. The results suggested the charge density on PEI backbone might be responsible for the coating, with reduced charge densities, the PEI-PEG produced less coating than the unmodified PEI.

Toxicity of Polymer Coated BSA NPs

In order to examine the cytotoxicity of the PEI-PEG coated NPs, MTT assay was performed for coated NPs incubated with C2C12 cells **(Figure 7-5)**. Two different PEGs, PEI-PEG-3mM and PEI-PEG-1mM, along with the unmodified PEI, were used for NP coating. The polymer concentrations tested for coating were 0, 0.03, 0.1 and 0.3 mg/mL. Different volumes of NP solutions (50, 25, 12.5 and 6.25 μL) were incubated with C2C12 cells. The results showed that the PEI-PEG coated NPs exhibited significantly reduced toxicity compared with the PEI-coated NPs at 50 μL of NP solutions of 0.3 mg/mL polymer coating ($p<0.001$): with 7% cell viability for PEI coating; while 12% and 45% cell viability for PEI-PEG-1mM and PEI-PEG-3mM coating, respectively. No significant difference in toxicity was observed for NPs when NP solutions were $\leq$ 12.5 μL at 0.3 mg/mL polymer coating, with $\geq$ 70% cell viability for all polymers coating. At 0.1 and 0.03 mg/mL polymer coating, there were no significant difference in cell viability

between the NPs coated with PEI and PEI-PEG at the NP volumes evaluated, with ≥ 70% cell viability demonstrated by all preparations. These results suggested that PEI-PEG coating reduced the cytotoxicity of coated NPs when polymer concentration for coating was higher than 0.1 mg/mL.

Bioactivity of BMP-2 in Polymer Coated NPs

A parallel study was conducted to test the ALP induction activity of BMP-2 encapsulated in the polymer coated NPs **(Figure 7-6)**. PEI-PEG-3mM and PEI-PEG-1mM, along with the unmodified PEI, were used for NP coating. The polymer concentrations for coating were 0.03, 0.1 and 0.3 mg/mL. NP solutions of 50, 25, 12.5 and 6.25 μL were incubated with C2C12 cells. The results showed that at 0.3 mg/mL polymer coating, no ALP activity was observed for unmodified PEI at all NP volumes tested, and ALP activity was significant for PEI-PEG-1mM coating at 12.5 and 6.25 μL of NP solutions, but not higher volumes; however, some ALP activity was exhibited for PEI-PEG-3mM coating even at 50 μL of NP solution tested. This was consistent with the cytotoxicity result, where PEI-PEG coating decreased the toxicity. PEI-PEG coated NPs generally possessed much higher ALP activity than PEI-coated NPs under the same conditions tested, except a nearly comparable ALP activity was seen for PEI and PEI-PEG coating at 0.1 mg/mL polymer concentration. The uncoated NPs showed relatively low ALP activity in this study, which was probably due to batch difference that a much faster disassociation of NPs during the dialysis resulting in BMP-2 loss.

NPs Implantation and *in vivo* Ectopic Bone Formation

The subcutaneous implantation of polymer coated NPs, along with the uncoated NPs, was performed in a rat ectopic model. A parallel study investigated the toxicity and ALP induction by the NP formulations *in vitro* **(Figure 7-7)**. Since the unacceptable level of toxicity was expected at 0.3 mg/mL polymer coating concentration, and the large aggregation observed at 0.03 mg/mL coating concentration, 0.1 mg/mL polymer concentration was chosen for NPs coating. The NPs formulations investigated in this study were the uncoated BMP-2/BSA NPs, BMP-2/BSA NPs coated with 0.1 mg/mL PEI-EPG-3mM and 0.1 mg/mL PEI. No cell death was observed under microscope after polymer-coated NPs incubated with C2C12 cells for 48 h. The MTT results showed that the uncoated NPs and 0.1 mg/mL PEI coated NPs demonstrated above 100% cell viability, and PEI-PEG coated NPs showed > 80% cell viability **(Figure 7-7A)**. The over 100% cell viability was probably due to the increased cell numbers during the 48 h incubation, and/or the change in the mitochondrial reductase enzymes activity by the NP formulations. PEI-PEG coated NPs seemed to activate less enzyme activities and/or less increased cell numbers than PEI coated NPs and the uncoated NPs. Overall, there is no significant cytotoxicity of the polymer coated NPs for C2C12 cells. Dose-respondent ALP activity was observed for all groups tested, and PEI-PEG coated NPs exhibited the highest ALP activity, while PEI coated NPs showed the lowest ALP activity among all the groups **(Figure 7-7B)**.

The NPs with 3 μg BMP-2/50 μL was then used for implantation. The ACS implants loaded with four groups: (1) PBS (×1, pH = 7.4) as control; (2) the uncoated BMP-2/BSA NPs; (3) BMP-2/BSA NPs coated with 0.1 mg/mL PEI-EPG-3mM, and (4)

BMP-2/BSA NPs coated with 0.1 mg/mL PEI. The implants were recovered at 10 and 16 days post-implantation **(Table 7-1)**, and wet weights were similar among the study groups. A typical ~20% to ~40% weight reduction from day 10 to day 16 post-implantation was observed for all the recovered implants **(Figure 7-8A)**. Due to the relatively similar weight range for all the recovered implants at both time points, the ALP and calcium assay results were compared at the obtained data without normalization. The ALP activity is an indicator of surrounding cells commitment towards the osteogenic differentiation [28]. There was significant difference in ALP activity for the four tested groups at both day 10 and day 16 (Kruskal-Wallis, $p<0.008$ for day 10 and $p<0.002$ for day 16) **(Figure 7-8B)**. No evident ALP activity was displayed by the control (ACS) group. The uncoated NPs and NPs coated with PEI-PEG coated NPs demonstrated a significant ALP activity at both day 10 and day 16. The implant with PEI coated NPs demonstrated marginal ALP activity. There was no significant difference in ALP activity between PEI-PEG coated NPs and the uncoated NPs implantation at both time points ($p>0.60$ for day 10 and $p>0.40$ for day 16). However, the difference between PEI-PEG coated NPs and PEI coated NPs implantation was significant at day 16 ($p<0.01$). Both PEI-PEG coated NPs and PEI-coated NPs implants achieved significant increased ALP activity from day 10 to day 16 ($p<0.05$ and $p<0.007$, respectively), but not the uncoated NPs ($p>0.05$).

There was significant difference in calcium deposition for the four tested groups at day 16 ($p<0.0001$) but not day 10 ($p>0.05$, Kruskal-Wallis) **(Figure 7-8C)**. At day 10, the uncoated NPs implant exhibited the highest calcification among all the groups, with a significant difference from the control ($p<0.03$). The calcification in other groups, on the

other hand, was not significant. At day 16, however, the calcification in PEI-PEG coated NPs implant was the highest among all the groups, with a significant difference from the control and PEI coated NPs implants ($p<0.006$), but not from the uncoated NPs implant and ($p>0.34$). A significant calcification was achieved by PEI-coated NPs at day 16 compared to control ($p<0.005$). A significant increase in calcification from day 10 to day 16 was obtained for all three BMP-2 encapsulated groups ($p<0.005$). The correlation between the ALP activity and calcium deposition was significant at day 16 ($p<0.0001$, 2-tailed by Pearson correlation), but not quite evident at day 10 ($p>0.05$, 2-tailed) **(Figure 7-8D)**. The collective ALP activity and calcium deposition results revealed that PEI-PEG coated NPs implant successfully demonstrated ectopic bone formation, and was able to induce higher ALP activity and deposit more calcium compared to the uncoated NPs and PEI coated NPs implants.

The micro-CT images for all the recovered implants at day 10 and day 16 were shown in **Figure 7-9A** and **Figure 7-10A**, respectively. The control group did not induce any new bone formation at both time points. At day 10, the uncoated NPs induced new bone formation first as compared to other groups where sporadic calcification in PEI-PEG coated NPs was observed. However, at day 16, PEI-PEG coated NPs produced more extensively bone formation. The deposited bone volume (mm^3) in each recovered implant was measured by the micro-CT scan (**Figure 7-9B** for day 10 and **Figure 7-10B** for day 16, respectively). The non-parametric statistical analysis on the formed bone volume showed similar results to the calcification assay. The micro-CT images were consistent with the ALP and calcium assay results, visually displayed the calcium deposited in the recovered implants.

DISCUSSION

As one of the most important growth factors in bone formation and healing, BMP-2 has been extensively studied during recent decades, and carriers made from different materials and geometries were employed for BMP-2 delivery [29-31]. The main role of a local delivery system for BMP-2 is to retain the growth factor at the site of implantation for a prolonged time frame, protect the integrity of BMP-2 activity against the undesired side effects of extraneous bone formation. In order to overcome the initial burst release and consequently low retention time associated with BMP-2, we previously reported that BMP-2 was encapsulated in PEI-coated BSA NPs, where the release of BMP-2 can be controlled by the PEI coating [21]. However, the PEI-coated BMP-2/BSA NPs failed to elicit bone formation when examined in the rat ectopic model. The reason was the toxicity of the PEI coating, which consequently abolished the bioactivity of BMP-2 **(Chapter VI)**. In this report, we aimed to reduce the toxicity of PEI coating on NPs by developing a new approach with PEGylated PEI **(Scheme 7-2)**, since PEGylation of polymers is an established method for markedly decreasing the toxicity and increasing the polymer biocompatibility [22]. By utilizing PEI-PEG for BMP-2/BSA NPs coating, successful ectopic bone formation was achieved after subcutaneous implantation in rats.

The nature of PEI with ample primary amines facilitates the introduction of PEG onto PEI to lower its cytotoxicity. The NHS group in NHS-PEG-MAL ensures reaction with primary amines on PEI to form a conjugate with amide linkage. Moreover, the MAL group could be further modified for functional targeting for example, by reacting it with a thiol-containing bisphosphonates [24]. The PEGylated PEI demonstrated reduced cytotoxicity compared to the unmodified PEI, which was also observed when PEI-PEG

was incubated with different cell lines in independent studies [32,33]. Furthermore, the PEGylation of PEI not only changed the toxicity profile of PEI, but also influenced the physicochemical property of the coated NPs. The reduced NPs size and zeta potential after PEI-PEG coating on BSA NPs was consistent with other reports when PEI-PEG was utilized to form DNA [32-34] or ODNs complex [35]. Note that the particle formation in the latter case was by polyelectrolyte complexation via electrostatic interactions. Presumably, the PEG modification minimized the aggregation of the formed particulates due to the increased hydrophilicity of the particles formed. Therefore, smaller NPs and lower zeta potential can be achieved. The reduced binding of the PEI-PEG polymers was also confirmed by the polymer coating efficiency, where PEI-PEG exhibited lower coating efficiency than PEI. Owing to the dramatically reduced size and zeta potential, this approach of PEGylated PEI for NPs coating holds the potential of intravascular injection; in addition, the PEGylation also tailored the *in vivo* fate of the NPs as PEG is well recognized for its "stealth" effect – reduce reticuloendothelial system uptake and prolong the circulation time [36-38].

Since the physiochemical parameters of NPs is expected to have a decisive impact on the interaction of NPs with cells, it is not surprising that PEI-PEG coated BMP-2/BSA NPs generally displayed higher ALP activity than PEI coated NPs, which could be a result of improved biocompatibility of PEI-PEG and elevated cellular uptake of smaller NPs by PEI-PEG coating [39,40]. Furthermore, the steric stabilization by PEI-PEG coating can effectively prevent aggregation of particles into larger structures [41,42]. The remnants of NPs used for implantation were stored in the + 4 °C fridge and the sizes of different formulations were examined 3 weeks after the implantation. They were

208.3±137.1, 224.5±1.9 and 407.3±613.8 nm for the uncoated BMP-2/BSA NPs, PEI-PEG coated and PEI-coated NPs, respectively. The polydispersity indices were 0.954±0.079, 0.159±0.024 and 0.921±0.136, respectively. The unstable nature of the uncoated NPs and the PEI-coated NPs without a hydrophilic coating has contributed to increased polydisperisty indices for these formulations.

BMP-2 is able to induce both ectopic and orthotropic bone regeneration; therefore, the localization of the delivered growth factor is of great importance. In this study, we have chosen to load BMP-2 encapsulated NPs into ACS for the osteoinduction study of BMP-2. ACS is one of the most extensively studied BMP-2 carriers, with the appropriate porous structure that allows vascularization and bone formation. However, the control over release kinetics was limited and initial burst release of BMP-2 is an inherent problem associated with this carrier, since BMP-2 was simply adsorbed into ACS [43-45]. Loading with BMP-2 encapsulated into NPs, the control over BMP-2 release from NPs is expected to reduce the initial burst release of BMP-2 from ACS and provide a sustained release. This would allow the surrounding tissues to be exposed to BMP-2 at a higher concentration for a long period.

In the implantation study, 0.1 mg/mL was chosen to coat the BMP-2/BSA NPs for implantation, as this polymer concentration coated NPs demonstrated little toxicity and high ALP activity *in vitro* **(Figures 7-5 and 7-6)**. The encapsulated amount of BMP-2 in NPs was increased as compared to previous studies **(Chapter VI)**, so that the implantation dose of BMP-2 can be achieved without concentrating the NPs. The ectopic bone formation results suggested that PEI-PEG coated NPs induced higher ALP activity and calcification than the PEI-coated NPs. There were several factors that could

contribute to this outcome: (1) the improved biocompatibility of PEGylated PEI compared to the unmodified PEI, causing less toxicity in the surrounding tissue; (2) PEI-PEG coating on BSA NPs produced smaller particles than PEI, resulting in a larger surface area than PEI-coated NPs [35]. In this way, a relatively faster release of BMP-2 could be achieved for local bone formation; (3) the weaker polyelectrolyte interactions between PEI-PEG coating and BSA might produce less intensive polymer network on NP surface for BMP-2 release. As a result of these factors, BMP-2 release from PEI-PEG coated NPs could be faster in this study. It was remained unknown that the relatively low bone formation from PEI-coated NPs was simply due to (1) slow release of BMP-2 from coated NPs, which takes longer time to reach the suitable local concentration of BMP-2 for bone formation or (2) PEI was not compatible with the biological activity of BMP-2 *in vivo*, even though no toxic effect was seen *in vitro*. Whether this elicited bone formation will keep increase in this implant needs to be examined in a longer term *in vivo* study.

The uncoated BMP-2/BSA NPs demonstrated an initial burst release, which was investigated in previous studies (**Chapter VI** and [21]). This burst release can provide a high local concentration of BMP-2 initially; therefore, it was not surprising to see that the uncoated NPs to be the first to induce new bone formation at day 10 **(Figure 7-9A)**. Though the release kinetics of BMP-2 from PEI-PEG coated NPs was not investigated in this study, previously studies showed that PEI-coated BMP-2/BSA NPs reduced the BMP-2 initial burst release (**Chapter VI** and [21]), and provided a sustained release of BMP-2. Others showed that it was possible to achieve NP modification with PEG without affecting the release pattern of the drugs, as suggested by one study about drug delivery

to brain with albumin NPs [46]. This was also implied by PEI-PEG coated NPs demonstrated higher ALP activity and more extensively calcium deposition than the uncoated NPs at day 16, which indicated that not only the initial level of BMP-2 but also the local retention of BMP-2 is important for achieving adequate bone formation, as also suggested by Maeda et al. [47]. Nevertheless, the release kinetics of BMP-2 from PEGylated-PEI coated BSA NPs should be assessed in the future studies.

The ALP activity and calcification in the recovered implants was compared with previous 16-day implantation study where implants were prepared with concentrating the NPs **(Chapter VI)**. This comparison was possible since the uncoated NPs group was examined in both studies. For uncoated NPs, 2-fold higher ALP activity and 4~5 fold higher calcification was obtained for the NPs preparation without the "concentration" process **(Table 7-3)**. This was probably due to the BMP-2 loss during concentrating NPs. Since the free BMP-2 solution was directly diluted from stock solution for implantation, it would be possible to compare it with the groups from this study. Similar ALP activity and calcification of free BMP-2 and the uncoated NPs in this study was obtained at day 10 post-implantation. However, at day 16, the uncoated NPs in this study exhibited 2-fold higher ALP activity and almost 3-fold higher calcification than free BMP-2 group. The PEI-PEG coated NPs displayed 3-fold higher ALP activity and almost 5-fold higher calcification than free BMP-2 group. This comparison indicated that a high BMP-2 encapsulation dosage that eliminated the need to concentrate NPs, as 9.6%wt compared to previously 1.44%wt BMP-2 in BSA, could be beneficial for the BMP-2 activity in the NPs.

PEI was reported to exhibit strong affinity to hydroxyapatite, which is comparable to the well-recognized bisphosphonates [24]. Previously, in the consideration of delivering proteins to bone, PEI was chosen for coating BSA NPs, not only to stabilize the NPs, but also to serve as a ligand to guide the NPs to bone. In this study, PEI was modified by less than 25% primary amines substituted by PEG. This was based on the concern of polymer coating to BSA NPs afterwards, since PEGylation weakens the polyelectrolyte interactions between PEI and BSA NPs as a result of less charge density and the increased hydrodynamic PEG layer [23]. In addition, the high amount of PEG on PEI might interfere with the affinity to bone of the PEI ligand on the coated NPs [24]. The modification degree of PEG on PEI should be a balance between decrease of PEI toxicity, retention of PEI coating ability on NPs, as well as the affinity of PEI to bone mineral. To examine the HA affinity of the coated NPs and investigate the systemic delivery to bone of the PEI coated NPs should be a future goal.

It is difficult to compare different drug carriers for BMP-2 due to the variations in animal species, age and implantation sites reported in the literatures [48], as well as the geometry size of carriers, different loading of BMP-2 and explantation time. Similar approach by using the NPs for BMP-2 delivery was conducted by Chung et al, where BMP-2 loaded heparin-functionalized PLGA NPs in fibrin hydrogel on the rat calvarial critical size defect model was investigated [49]. Heparin was entrapped onto the surface of PLGA NPs with the purpose of specific complexation with BMP-2, and then these BMP-2 loaded NPs were incorporated into fibrin gel. Significantly higher bone formation was found in the BMP-2 loaded NP-fibrin gel complex, compared to the BMP-2 loaded fibrin gel without functionalized NPs at 4 weeks, which suggested that a more controlled

release of BMP-2 was achieved in the former carrier. Another study by Wei et al. investigated the BMP-7 encapsulated into PLGA nanospheres which were then post-seeded into PLLA scaffold in rat ectopic model [45]. This scaffold induced significant bone formation while passive adsorption of BMP-7 into PLLA scaffold failed to generate bone at 6 weeks. The suggested reason was the BMP-7 nanosphere-scaffold delivery system released and localized BMP-7 for a desired duration at the implantation site, while simple adsorption of BMP-7 into the scaffold likely gave a bolus or pulse release of BMP-7 with substantial loss of bioactivity, leading to the failure of bone formation. Encapsulation of growth factors into NP then combined with different matrix or scaffold as hybrid carrier for bone defect replacement has been demonstrated to be a successful strategy to achieve prolonged release of bioactive growth factors [45,49-51]. The release of protein from the carrier can be tailored by the modification of NPs. This is also a versatile approach that can be expanded to many bioactive molecules.

It has been estimated that normal bone contains approximately 2 μg of BMP-2 per kilogram of pulverized bone [52]. Since BMP-2 has a very short half life *in vivo*, about ~7-16 min [53], and is rapidly degraded *in vivo*, a controlled and localized delivery system for a small amount of BMP-2 would be appropriate for effective bone regeneration. Currently the BMP-2 concentrations in use (micrograms to milligrams) are supraphysiological, compared to nanogram ranges of BMP-2 *in vivo* [52]. In addition to the danger of excess bone formation, possible overflow of BMP-2 from the implant may upregulate the BMP-2 inhibitors such as noggin or sclerotin, and interfere with the bone induction process [54]. The delivery system that release BMP-2 at the right dose and

kinetics can be advantageous for the growth factor therapy, and broadly emerge for the benefit in treatment of bone diseases.

CONCLUSIONS

In this study, we demonstrated that PEGylated PEI effectively reduced the toxicity of PEI, and the PEI-PEG employed for BSA NPs coating dramatically reduced the size and zeta potential of NPs, compared with NPs coated with PEI. The higher extent of PEGylation of PEI displayed a more pronounced effect in the reduction of NP size and zeta potential. The PEI-PEG coated BMP-2/BSA NPs was then examined in a rat ectopic model for osteoinduction activity. Effective bone formation was achieved by the BMP-2 in BSA NPs coated with 0.1 mg/mL PEI-PEG-3mM, as determined by ALP assay, calcification and micro-CT scan. The BMP-2/BSA NPs coated with 0.1 mg/mL PEI gave less bone formation than the PEI-PEG coated NPs. The advantage of PEGylated PEI coated BMP-2/BSA NPs for bone formation presumably attributed to the ameliorated biocompatibility and beneficial physiochemical properties of coated NPs. Based on the characteristics of this NP formulation, this system can be favorable not only for local application, but also promising for targeted bone stimulation via intravascular injection. Moreover, NP formulation can be also combined with other matrix or scaffold for the application to a large orthotopic defect site.

TABLES

Table 7-1. Study groups in ectopic bone formation at the rat subcutaneous model

Implant set	Group	BMP-2 dose per implant(ug)	Implant volume (μL)	no. of rats (implants)	Harvest (days)	Evaluation
G1	ACS	0	50	3 (6), 3 (6)	10, 16	weight, ALP, Ca^{2+}, Micro-CT
G2	ACS + BMP-2/BSA NP	3	50	3 (6), 3 (6)	10, 16	weight, ALP, Ca^{2+}, Micro-CT
G3	ACS + BMP-2/BSA NP coated with PEI-PEG (0.1 mg/mL)	3	50	3 (6), 3 (6)	10, 16	weight, ALP, Ca^{2+}, Micro-CT
G4	ACS + BMP-2/BSA NP coated with PEI (0.1 mg/mL)	3	50	3 (6), 3 (6)	10, 16	weight, ALP, Ca^{2+}, Micro-CT

Table 7-2. IC_{50} values (in equivalent μg/mL) of C2C12 cells cultured with polymers

Incubation time (h)	IC_{50} (μg/mL)			
	PEI	PEI-PEG-0.3mM	PEI-PEG-1mM	PEI-PEG-3mM
48	6.3	6.3	10.2	> 20.0

Table 7-3. Comparison of the ALP activity and Calcification in two implantation studies

Study groups	Study Set	ALP activity (mABS/min)		Calcium deposition (mg/dL)	
		Day 10	Day 16	Day 10	Day 16
ACS + free BMP-2	#1	14.14 ± 10.50	21.75 ± 24.86	2.78 ± 4.09	30.05 ± 28.50
ACS + uncoated BMP-2/BSA NPs	#1 (concentrating process)	6.40 ± 6.78	20.21 ± 24.41	1.36 ± 1.90	17.37 ± 27.39
	#2 (direct use)	15.46 ± 11.25	43.94 ± 45.60	2.78 ± 5.38	85.48 ± 78.72
ACS + PEI-PEG coated BMP-2/BSA NPs (0.1 mg/mL)	#2	31.23 ± 40.59	62.68 ± 45.83	0.66 ± 1.13	135.01 ± 112.68
ACS + PEI coated BMP-2/BSA NPs (0.1 mg/mL)	#2	3.45 ± 2.29	10.24 ± 6.76	0.01 ± 0.03	11.69 ± 12.61

SCHEMES

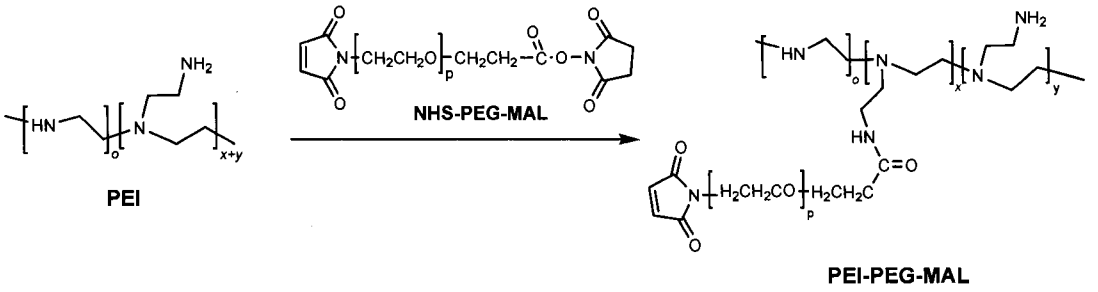

Scheme 7-1. Reaction Scheme for PEI-PEG conjugate (*o, x, y* and *p* are arbitrary numbers). PEG segment was linked to the PEI backbone through the NHS functional group on NHS-PEG-MAL. The PEI-PEG conjugate was purified by sufficient dialysis against phosphate buffer (pH = 5, 2×), and then ddH_2O (2×).

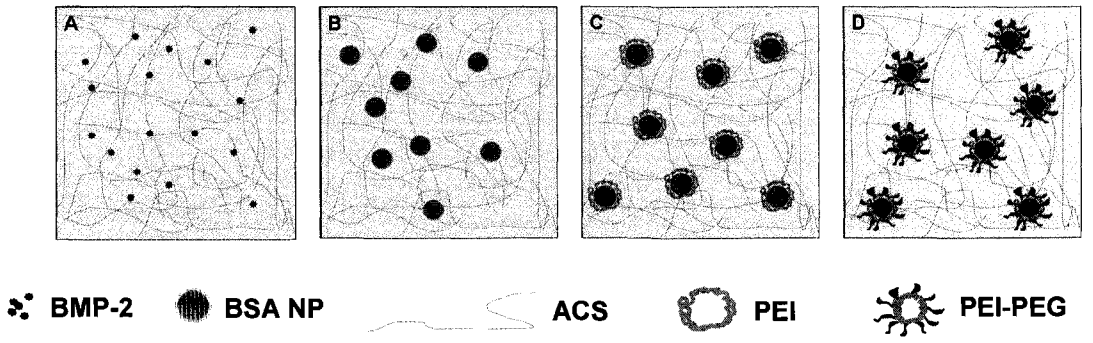

Scheme 7-2. Schematic representation of different BMP-2 release: (**A**) free BMP-2 aqueous solution loaded in ACS (clinical BMP-2 device); (**B**) uncoated BMP-2/BSA NPs; (**C**) PEI-coated BMP-2/BSA NPs; (**D**) PEI-PEG coated BMP-2/BSA NPs.

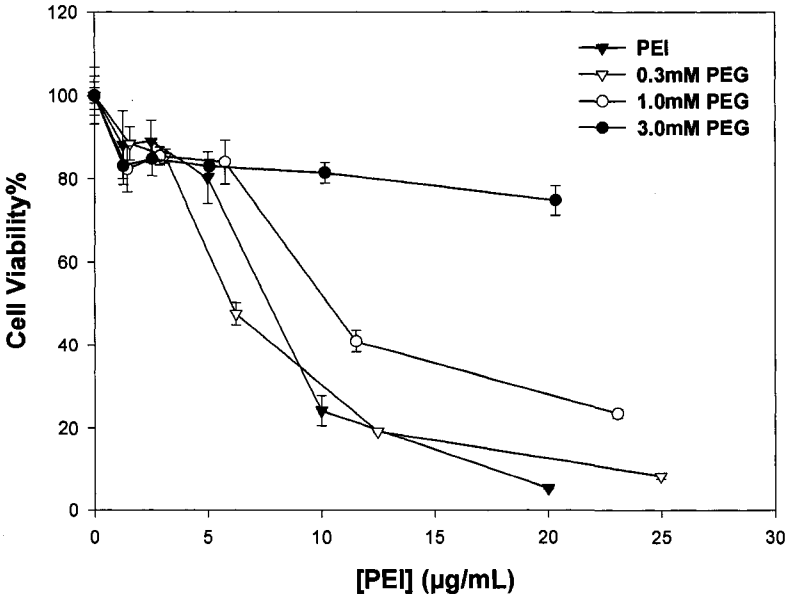

Figure 7-1. Cytotoxicity of different PEI-PEG conjugates, along with the unmodified PEI after incubation with C2C12 cells. PEI showed evident cytotoxicity at > 5 μg/mL, with only 5% cell viability being retained at 20 μg/mL. However, the PEI-PEG conjugates exhibited reduced cytotoxicity as the PEG substitution in the conjugate increased. The highest PEG concentration used for modification, 3 mM PEG, showed 75% cell viability at 20 μg/mL of polymer concentration.

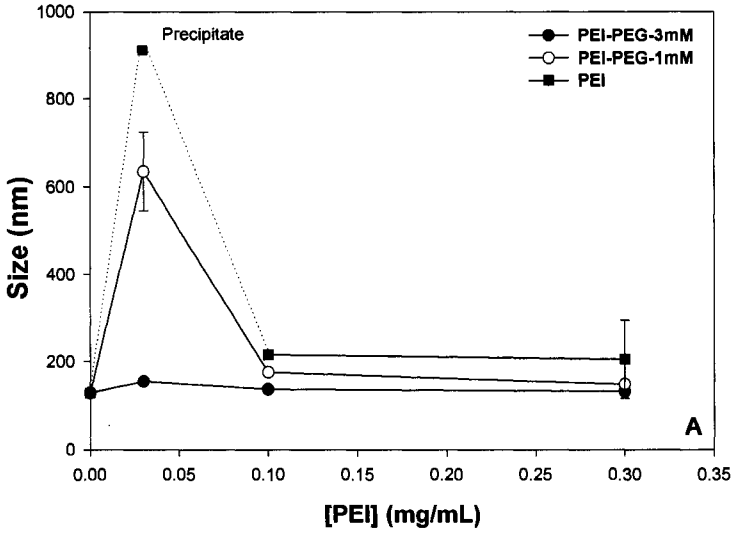

B. Polydispersity Index

PEI (mg/mL)	PEI-PEG-3mM	PEI-PEG-1mM	PEI
0.03	0.13 ± 0.02	1.0	N/A
0.1	0.23 ± 0.10	0.26 ± 0.03	0.27 ± 0.06
0.3	0.08 ± 0.01	0.13 ± 0.06	1.0
0	0.20 ± 0.02		

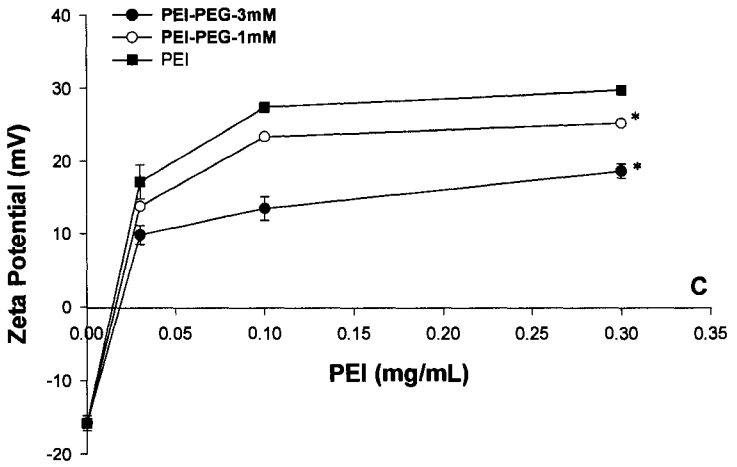

Figure 7-2. The mean particle diameter (**A**), polydispersity index (**B**) and zeta potential (**C**) of PEI-PEG and unmodified PEI coated BSA NPs. Two independent batches for each coating concentration were prepared for measurements, and each measurement was performed in 3 runs. PEI-PEG coated BSA NPs exhibited reduced size compared with the unmodified PEI coated BSA NPs at the same concentration used for coating. The zeta potential of PEI-PEG coated NPs decreased correspondingly compared with the unmodified PEI coated NPs (* indicated significant difference between the values, $p<0.001$. Only 0.3 mg/mL polymer coating samples were performed with statistical analysis).

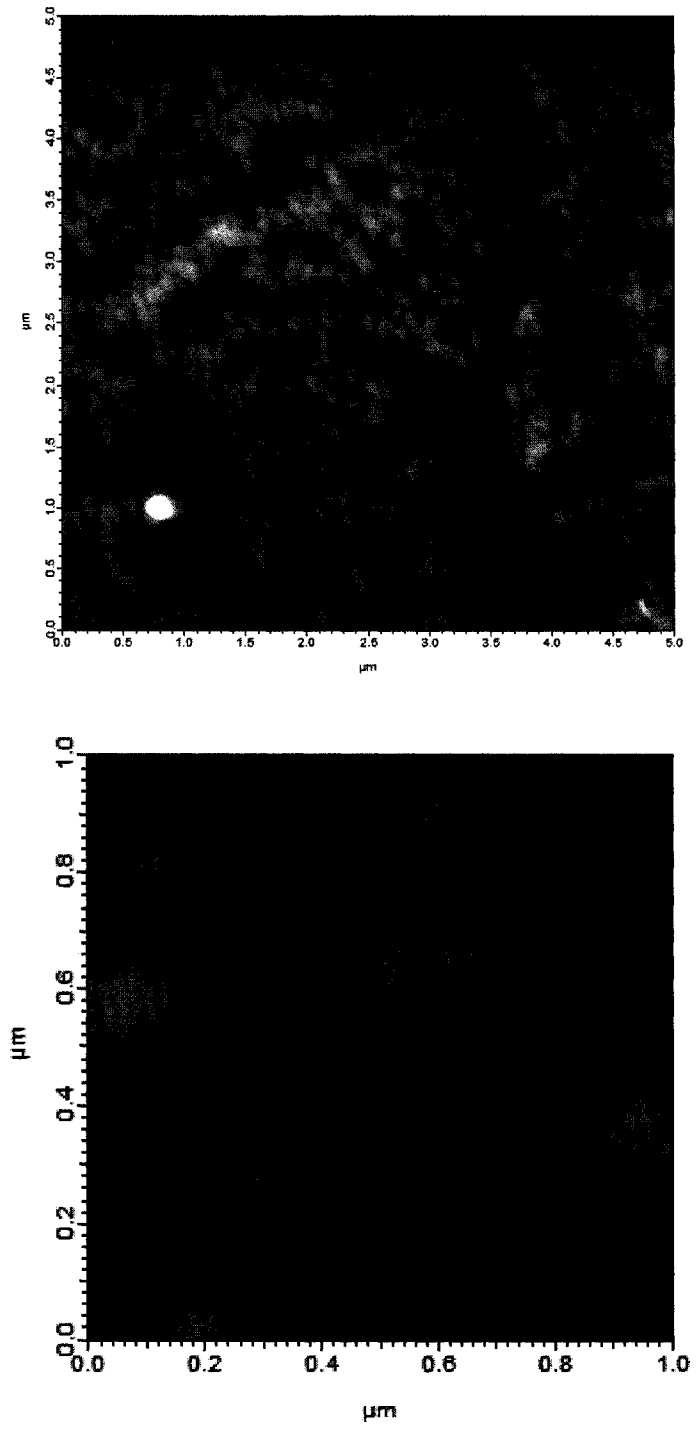

Figure 7-3. AFM images of PEI-PEG-3mM coated NPs at (**A**) 5.0 µm scale and (**B**) 1.0 µm scale. The polymer concentration for coating was 0.3 mg/mL.

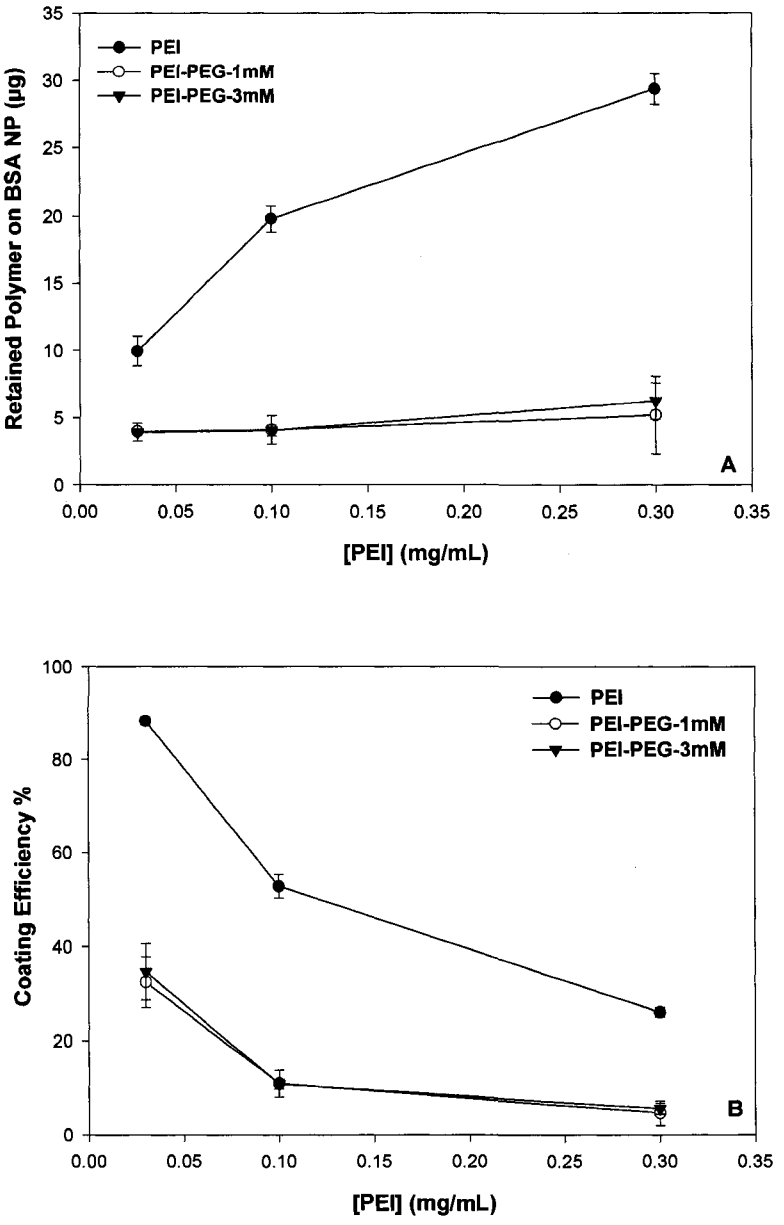

Figure 7-4. The quantification of polymer coating on BSA NPs, as measured by adsorption of FITC-labeled polymers (n=2). The PEG was conjugated to FITC-PEI at different concentrations (1 and 3 mM). The fluorescence of the polymer adsorbed on BSA NPs was measured as a function of polymer coating concentration, and converted to mass (µg) of polymer adsorbed (**A**) based on the polymer calibration curve. The amount of PEI adsorbed on the NPs was increased with the PEI concentration increased, while PEI-PEG showed relatively slight increase as the coating concentration increased. The coating efficiency on NPs was calculated from the adsorbed polymer and the initial polymer in solution (**B**). The efficiency of polymer coating was decreased as the polymer concentration increased. PEI demonstrated higher coating efficiency than PEI-PEG polymers at each concentration tested.

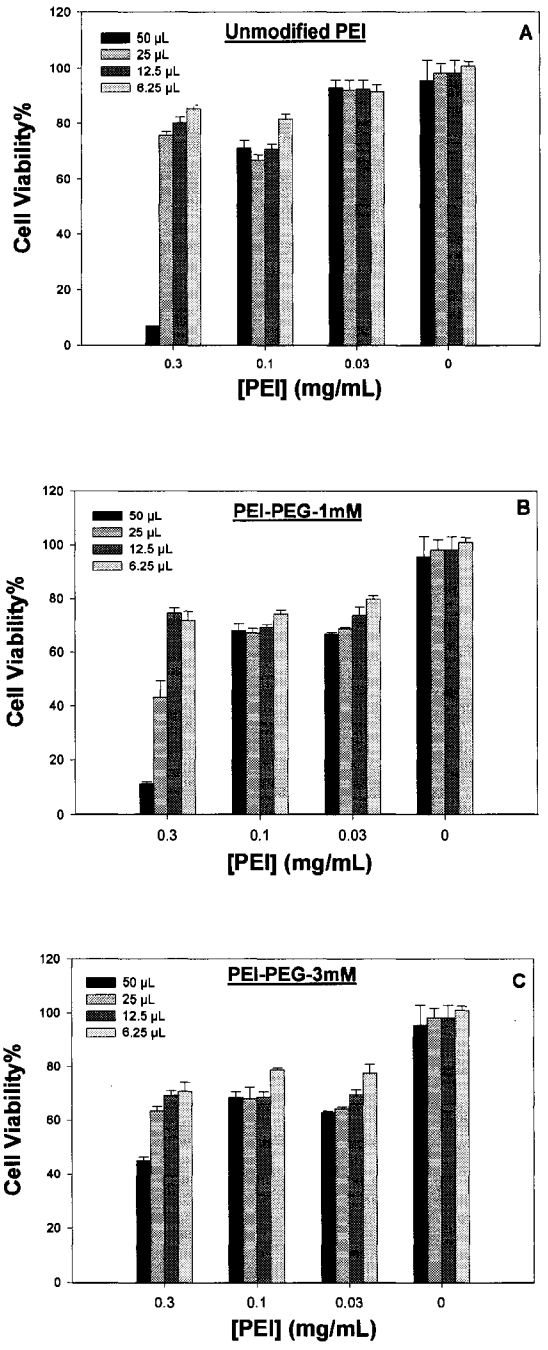

Figure 7-5. Cytotoxicity of PEI-PEG and PEI coated BSA NPs. Two different PEGs, PEI-PEG-3mM (**C**) and PEI-PEG-1mM (**B**), along with the unmodified PEI (**A**), were examined for NP coating. The polymer concentrations tested for coating were 0, 0.03, 0.1 and 0.3 mg/mL. Different volumes of NP solutions (6.25, 12.5, 25, and 50 µL) were incubated with C2C12 cells. The PEI-PEG coated NPs demonstrated significantly reduced toxicity than the PEI coated NPs at the highest volume tested of 0.3 mg/mL polymer coating ($p<0.001$). There was $\geq$ 70% cell viability at other polymer coating concentrations.

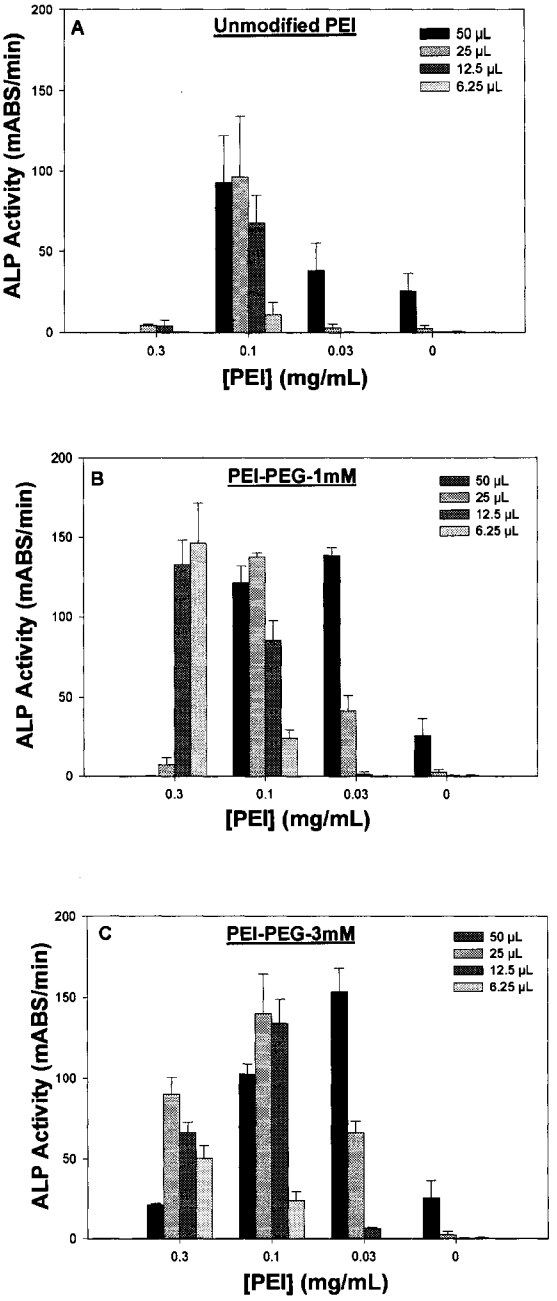

Figure 7-6. ALP activity assay of PEI-EPG and PEI coated BSA NPs. Two different PEGs, PEI-PEG-3mM (**C**) and PEI-PEG-1mM (**B**), along with the unmodified PEI (**A**), were examined. The polymer coating concentrations tested were 0, 0.03, 0.1 and 0.3 mg/mL. Different volumes of the NP solutions (6.25, 12.5, 25, and 50 µL) were incubated with C2C12 cells. The PEI-PEG coated NPs generally possessed higher ALP activity than PEI coated NPs under the same conditions tested, except a nearly comparable ALP activity for PEI and PEI-PEG coating at 0.1 mg/mL polymer concentration.

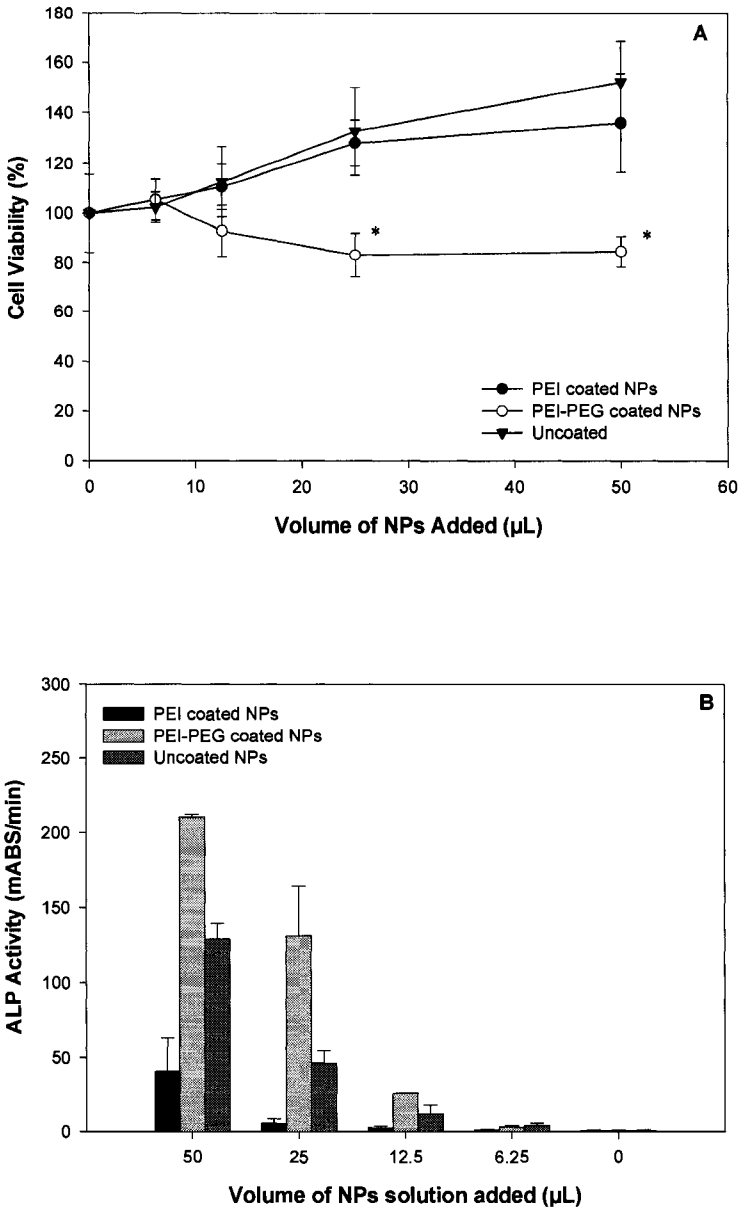

Figure 7-7. *In vitro* tests for the implantation formulation of NPs: (**A**) MTT assay and (**B**) ALP assay. There was no evident cytotoxicity exhibited by the three groups investigated, with > 80% cell viability at all volumes examined (* indicated significant difference between PEI-PEG and PEI coated NPs, $p<0.01$). PEI-PEG coated NPs demonstrated the highest ALP activity among the three groups, and a dose-respondent ALP induction was observed for all groups.

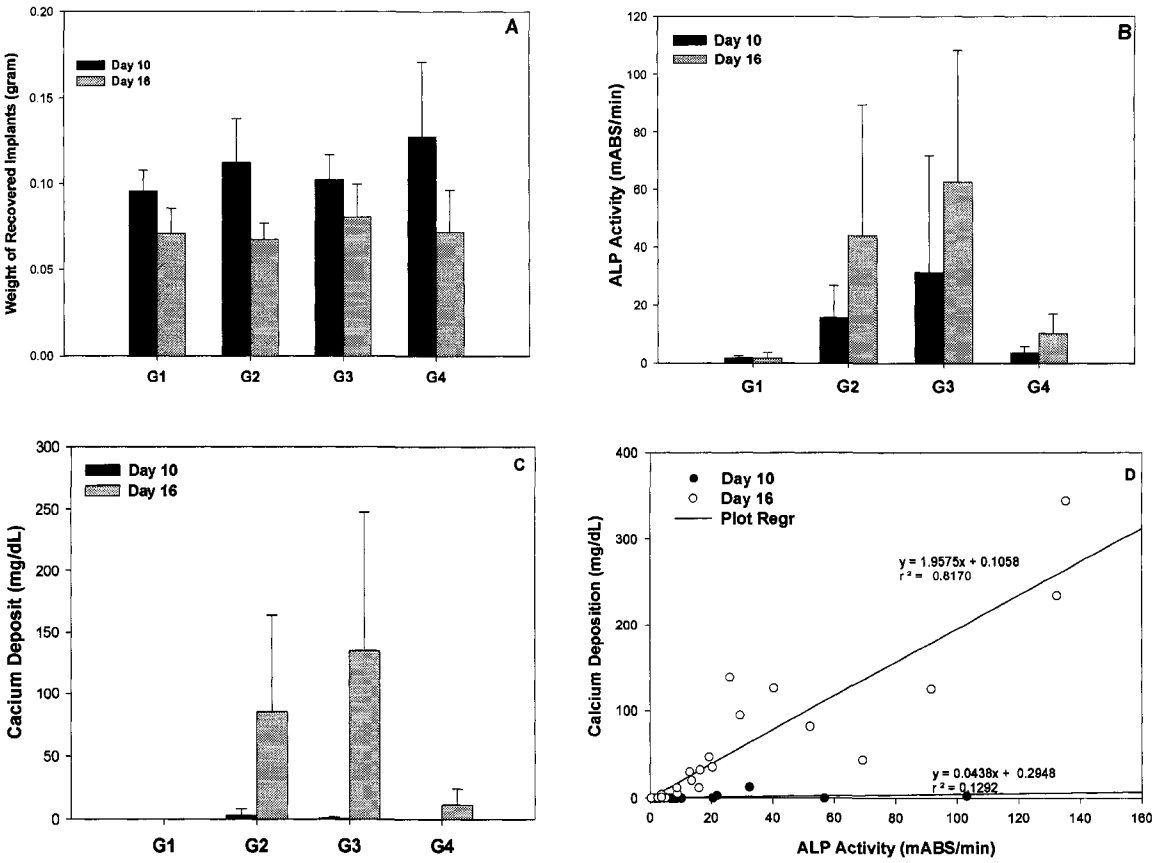

Figure 7-8. *In vivo* investigation of the osteoinductive effect with different study groups. G1: ACS alone; G2: ACS loaded with uncoated BMP-2/BSA NPs; G3: ACS loaded with BMP-2/BSA NPs coated with 0.1 mg/mL PEI-PEG (3mM PEG); G4: ACS loaded with BMP-2/BSA NPs coated with 0.1 mg/mL PEI. In all the study groups, the amount of BMP-2 was 3 μg except the control group without any BMP-2. (**A**) Wet weight of recovered implants at day 10 and day 16; (**B**) ALP activity at day 10 and day 16; (**C**) Calcium deposition at day 10 and day 16; (**D**) Correlation between calcium deposition and ALP activity of the recovered implants at day 10 and day 16.

A

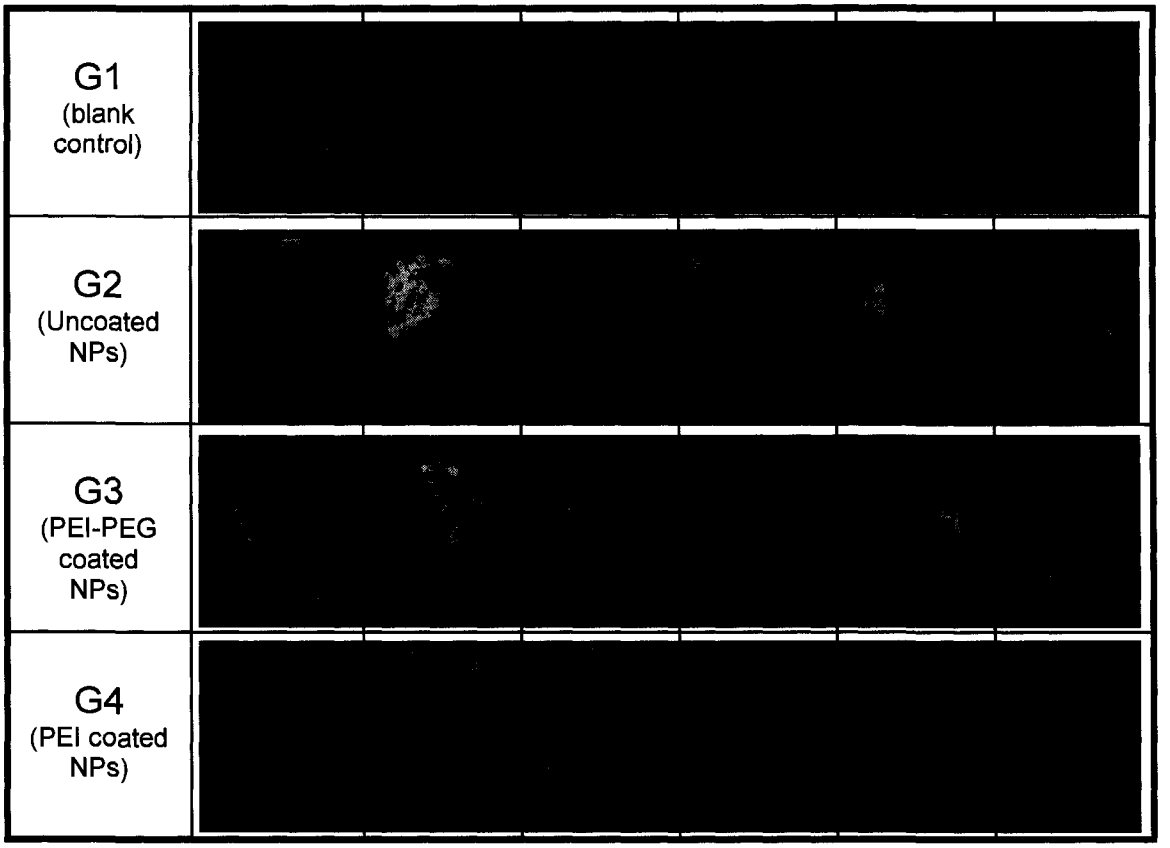

B

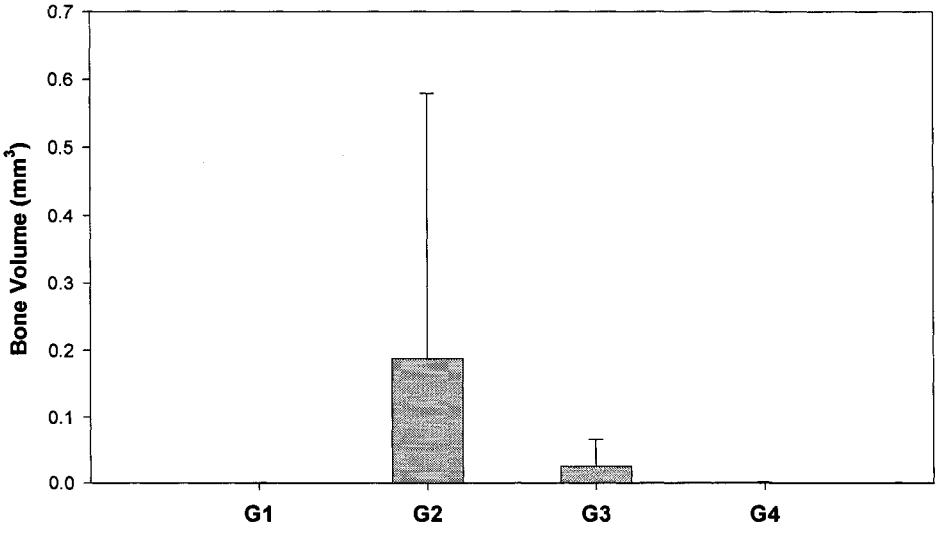

Figure 7-9. Micro-CT images (**A**) and bone volume analysis (**B**) of the osteoinductive effect of NPs at day 10 post-implantation.

A

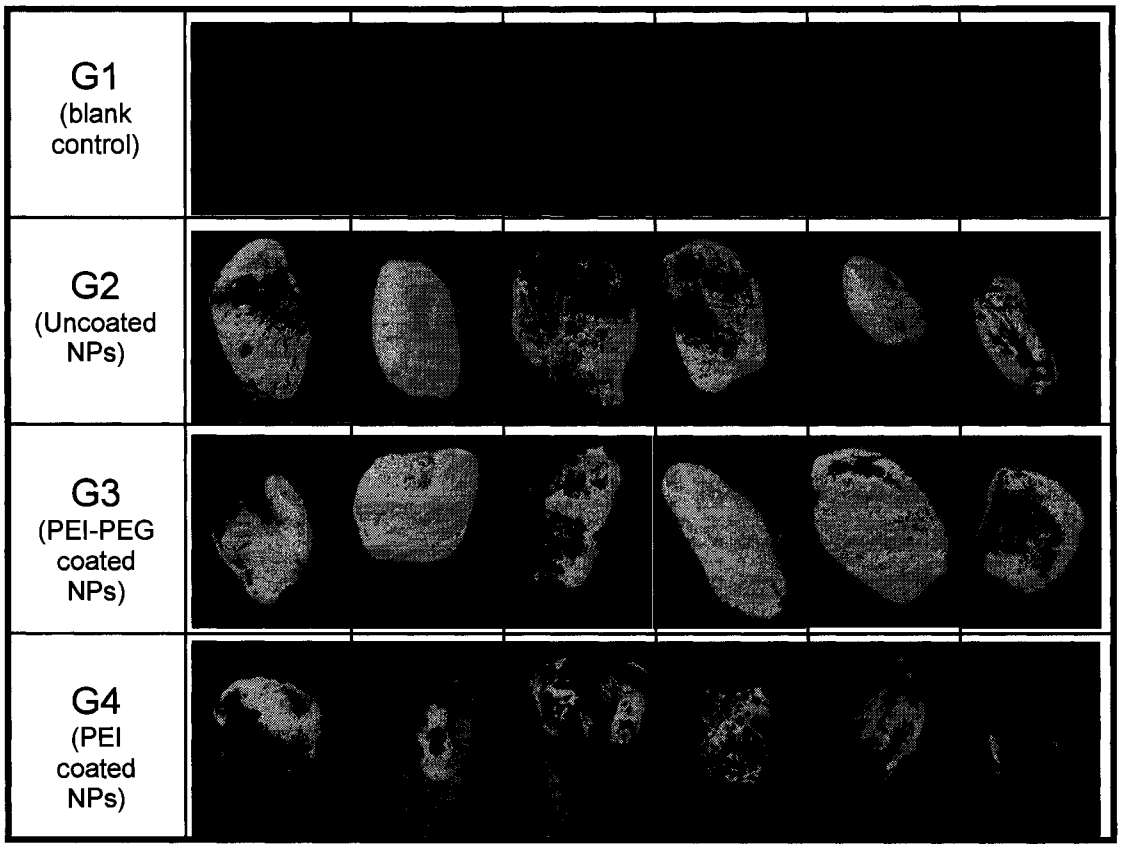

B

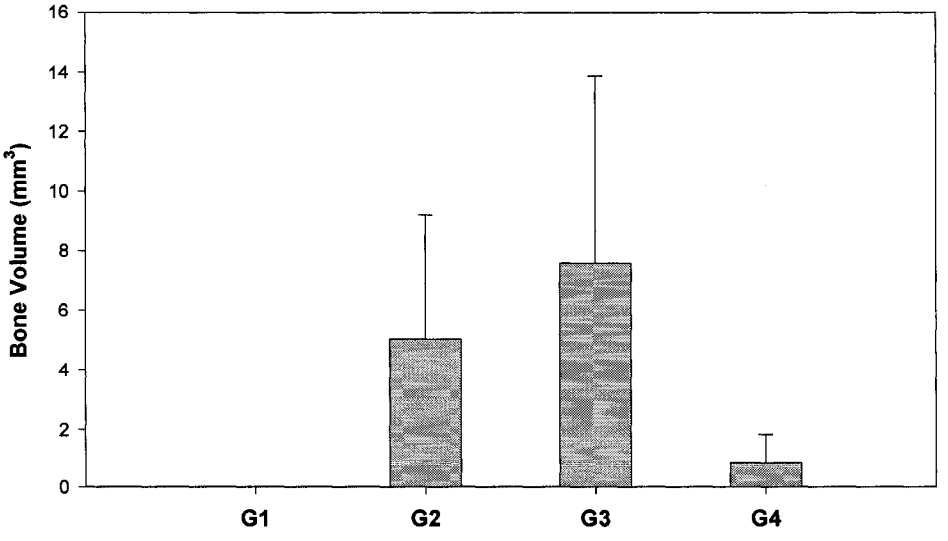

Figure 7-10. Micro-CT images (**A**) and bone volume analysis (**B**) of the osteoinductive effect of NPs at day 16 post-implantation.

References

[1] P. C. Bessa, M. Casal, and R. L. Reis, Bone morphogenetic proteins in tissue engineering: the road from laboratory to clinic, part II (BMP delivery), *J. Tissue Eng. Regen. Med.*, 2 (2008) 81-96.

[2] E. P. Barboza, M. E. L. Duarte, L. Geolas, R. G. Sorensen, G. E. Riedel, and U. M. E. Wikesjo, Ridge augmentation following implantation of recombinant human bone morphogenetic protein-2 in the dog, *J. Periodontol.*, 71 (2000) 488-496.

[3] P. J. Boyne, Application of bone morphogenetic proteins in the treatment of clinical oral and maxillofacial osseous defects, *J. Bone Joint. Surg. Am.*, 83 (2001) S146-S150.

[4] B. Chen, H. Lin, J. Wang, Y. Zhao, B. Wang, W. Zhao, W. Sun, and J. Dai, Homogeneous osteogenesis and bone regeneration by demineralized bone matrix loading with collagen-targeting bone morphogenetic protein-2, *Biomaterials*, 28 (2007) 1027-1035.

[5] J. Levine, J. Bradley, A. E. Turk, J. L. Ricci, J. J. Benedict, G. Steiner, M. T. Longaker, and J. G. McCarthy, Bone morphogenetic protein promotes vascularization and osteoinduction in preformed hydroxyapatite in the rabbit, *Ann. Plast. Surg.*, 39 (1997) 158-168.

[6] U. Ripamonti, L. N. Ramoshebi, T. Matsaba, J. Tasker, J. Crooks, and J. Teare, Bone induction by BMPs/OPs and related family members in primates : the critical role of delivery systems, *J. Bone Joint. Surg. Am.*, 83 (2001) S116-S127.

[7] H. S. M. Sandhu and S. N. M. Khan, Animal models for preclinical assessment of bone morphogenetic proteins in the spine, *Spine,* 27 (2002) S32-S38.

[8] J. M. P. Wozney and V. P. Rosen, Bone morphogenetic protein and bone morphogenetic protein gene family in bone formation and repair, *Clin. Orthop. Relat. Res.*, 346 (1998) 26-37.

[9] S. D. Boden, T. A. Zdeblick, H. S. Sandhu, and S. E. Heim, The use of rhBMP-2 in interbody fusion cages, *Spine*, 25 (2000) 376-381.

[10] S. D. Boden, G. J. J. Martin, M. A. Morone, J. L. Ugbo, and P. A. Moskovitz, Posterolateral lumbar intertransverse process spine arthrodesis with recombinant human bone morphogenetic protein-2/hydroxyapatite-tricalcium phosphate after laminectomy in the nonhuman primate, *Spine*, 24 (1999) 1179.

[11] S. D. M. Boden, Overview of the biology of lumbar spine fusion and principles for selecting a bone graft substitute, *Spine*, 27 (2002) S26-S31.

[12] D. S. Baskin, P. Ryan, V. Sonntag, R. Westmark, and M. Widmayer, A prospective, randomized, controlled cervical fusion study using recombinant human bone morphogenetic protein-2 with the CORNERSTONE-SR^{TM} allograft ring and the ATLANTIS^{TM} anterior cervical plate, *Spine*, 28 (2003) 1219-1224.

[13] E. A. Wang, Bone morphogenetic proteins (BMPs): therapeutic potential in healing bony defects, *Trends Biotechnol.*, 11 (1993) 379-383.

[14] N. Sykaras and L. A. Opperman, Bone morphogenetic proteins (BMPs): how do they function and what can they offer the clinician?, *J. Oral Sci.*, 45 (2003) 57-73.

[15] H. Uludağ, D. D'Augusta, R. Palmer, G. Timony, and J. Wozney, Characterization of rhBMP-2 pharmacokinetics implanted with biomaterial carriers in the rat ectopic model, *J. Biomed. Mater. Res.*, 46 (1999) 193-202.

[16] H. Uludağ, D. 'Augusta, J. Golden, J. Li, G. Timony, R. Riedel, and J. M. Wozney, Implantation of recombinant human bone morphogenetic proteins with biomaterial carriers: A correlation between protein pharmacokinetics and osteoinduction in the rat ectopic model, *J. Biomed. Mater. Res.*, 50 (2000) 227-238.

[17] H. Uludağ, T. Gao, T. J. Porter, W. Friess, and J. M. Wozney, Delivery systems for BMPs: factors contributing to protein retention at an application site, *J. Bone Joint. Surg. Am.*, 83 (2001) S128-S135.

[18] J. M. Lane, BMPs: Why are they not in everyday use?, *J. Bone Joint. Surg. Am.*, 83 (2001) S161-S162.

[19] V. Luginbuehl, L. Meinel, H. P. Merkle, and B. Gander, Localized delivery of growth factors for bone repair, *Eur. J. Pharm. Biopharm.*, 58 (2004) 197-208.

[20] D. Thassu, M. Deleers, and Y. Pathak, *Nanoparticulate Drug Delivery System*, Informa Healthcare USA, Inc., New York 2007.

[21] S. Zhang, G. Wang, X. Lin, M. Chatzinikolaidou, H. Jennissen, M. Laub, and H. Uludağ, Polyethylenimine-coated albumin nanoparticles for BMP-2 delivery, *Biotechnol. Prog.*, 24 (2008) 945-956.

[22] G. T. Hermanson, Modification with synthetic polymers, *Bioconjugate Techniques*, Academic Press, San Diego, 1996, pp. 605-629.

[23] R. I. Mahato, *Biomaterials for Delivery and Targeting of Proteins and Nucleic Acids*, CRC Press, Boca Raton, 2005.

[24] S. Zhang, J. E. I. Wright, N. Özber, and H. Uludağ, The Interaction of cationic polymers and their bisphosphonate derivatives with hydroxyapatite, *Macromol. Biosci.*, 7 (2007) 656-670.

[25] M. Chatzinikolaidou, T. Zumbrink, and H. P. Jennissen, Stability of surface-enhanced ultrahydrophilic metals as a basis for bioactive rhBMP-2 surfaces, *Materialwiss. Werkstofftech.*, 34 (2003) 1106-1112.

[26] H. Lv, S. Zhang, B. Wang, S. Cui, and J. Yan, Toxicity of cationic lipids and cationic polymers in gene delivery, *J. Control Release*, 114 (2006) 100-109.

[27] P. C. Hiemenz and R. Rajagopalan, *Principles of Colloid and Surface Chemistry*, New York, Marcel Dekker, 1997.

[28] J. B. Lian and G. S. Stein, Concepts of osteoblast growth and differentiation: basis for modulation of bone cell development and tissue formation, *Crit. Rev. Oral. Biol. Med.*, 3 (1992) 269-305.

[29] S. R. P. Winn, H. P. Uludağ, and J. O. D. Hollinger, Carrier systems for bone morphogenetic proteins, *Clin. Orthop. Relat. Res.*, 367 Supplement (1999) S95-S106.

[30] R. Z. P. LeGeros, Properties of osteoconductive biomaterials: calcium phosphates, *Clin. Orthop. Relat. Res.*, 395 (2002) 81-98.

[31] S. P. Baldwin and W. Mark Saltzman, Materials for protein delivery in tissue engineering, *Adv. Drug Deliv. Rev.*, 33 (1998) 71-86.

[32] H. Petersen, P. M. Fechner, A. L. Martin, K. Kunath, S. Stolnik, C. J. Roberts, D. Fischer, M. C. Davies, and T. Kissel, Polyethylenimine-graft-poly(ethylene glycol) copolymers: influence of copolymer block structure on DNA complexation and biological Activities as gene delivery system, *Bioconjug. Chem.*, 13 (2002) 845-854.

[33] G. P. Tang, J. M. Zeng, S. J. Gao, Y. X. Ma, L. Shi, Y. Li, H.-P. Too, and S. Wang, Polyethylene glycol modified polyethylenimine for improved CNS gene transfer: effects of PEGylation extent, *Biomaterials*, 24 (2003) 2351-2362.

[34] K. Kunath, A. von Harpe, H. Petersen, D. Fischer, K. Voigt, T. Kissel, and U. Bickel, The structure of PEG-modified poly(ethyleneimines) influences

biodistribution and pharmacokinetics of their complexes with NF-kB decoy in mice, *Pharm. Res.*, 19 (2002) 810-817.

[35] K. Remaut, B. Lucas, K. Raemdonck, K. Braeckmans, J. Demeester, and S. C. DeSmedt, Protection of oligonucleotides against enzymatic degradation by pegylated and nonpegylated branched polyethyleneimine, *Biomacromolecules*, 8 (2007) 1333-1340.

[36] T. Niidome, M. Yamagata, Y. Okamoto, Y. Akiyama, H. Takahashi, T. Kawano, Y. Katayama, and Y. Niidome, PEG-modified gold nanorods with a stealth character for *in vivo* applications, *J. Control Release*, 114 (2006) 343-347.

[37] D. Bazile, C. Prud'homme, M.-T. Bassoullet, M. Marlard, G. Spenlehauer, and M. Veillard, Stealth Me.PEG-PLA nanoparticles avoid uptake by the mononuclear phagocytes system, *J. Pharm. Sci.*, 84 (1995) 493-498.

[38] T. Waku, M. Matsusaki, T. Kaneko, and M. Akashi, PEG brush peptide nanospheres with stealth properties and chemical functionality, *Macromolecules*, 40 (2007) 6385-6392.

[39] Y. Hu, J. Xie, Y. W. Tong, and C. H. Wang, Effect of PEG conformation and particle size on the cellular uptake efficiency of nanoparticles with the HepG2 cells, *J. Control Release*, 118 (2007) 7-17.

[40] S. Mishra, P. Webster, and M. E. Davis, PEGylation significantly affects cellular uptake and intracellular trafficking of non-viral gene delivery particles, *Eur. J. Cell Biol.*, 83 (2004) 97-111.

[41] D. Goula, J. S. Remy, P. Erbacher, M. Wasowicz, G. Levi, B. Abdallah, and B. A. Demeneix, Size, diffusibility and transfection performance of linear PEI/DNA complexes in the mouse central nervous system, *Gene Ther.*, 5 (1998) 712.

[42] M. Ogris, S. Brunner, S. Schuller, R. Kircheis, and E. Wagner, PEGylated DNA/transferrin–PEI complexes: reduced interaction with blood components, extended circulation in blood and potential for systemic gene delivery, *Gene Ther.*, 6 (1999) 595.

[43] G. A. Helm, J. M. Sheehan, J. P. Sheehan, J. A. Jane, C. G. Dipierro, N. E. Simmons, G. T. Gillies, D. F. Kallmes, and T. M. Sweeney, Utilization of type I collagen gel, demineralized bone matrix, and bone morphogenetic protein-2 to enhance autologous bone lumbar spinal fusion, *J. Neurosurg.*, 86 (1997) 93-100.

[44] Y. Takahashi, M. Yamamoto, and Y. Tabata, Enhanced osteoinduction by controlled release of bone morphogenetic protein-2 from biodegradable sponge composed of gelatin and β-tricalcium phosphate, *Biomaterials*, 26 (2005) 4856-4865.

[45] G. Wei, Q. Jin, W. V. Giannobile, and P. X. Ma, The enhancement of osteogenesis by nano-fibrous scaffolds incorporating rhBMP-7 nanospheres, *Biomaterials*, 28 (2007) 2087-2096.

[46] V. Mishra, S. Mahor, A. Rawat, P. N. Gupta, P. Dubey, K. Khatri, and S. P. Vyas, Targeted brain delivery of AZT via transferrin anchored pegylated albumin nanoparticles, *J. Drug Target.*, 14 (2006) 45-53.

[47] H. Maeda, A. Sano, and K. Fujioka, Controlled release of rhBMP-2 from collagen minipellet and the relationship between release profile and ectopic bone formation, *Int. J. Pharm.*, 275 (2004) 109-122.

[48] S. R. Winn, H. Uludağ, and J. O. Hollinger, Sustained release emphasizing recombinant human bone morphogenetic protein-2, *Adv. Drug Deliv. Rev.*, 31 (1998) 303-318.

[49] Y. I. Chung, K. M. Ahn, S. H. Jeon, S. Y. Lee, J. H. Lee, and G. Tae, Enhanced bone regeneration with BMP-2 loaded functional nanoparticle-hydrogel complex, *J. Control Release*, 121 (2007) 91-99.

[50] F. m. Chen, Y. M. Zhao, R. Zhang, T. Jin, H. h. Sun, Z. f. Wu, and Y. Jin, Periodontal regeneration using novel glycidyl methacrylated dextran (Dex-GMA)/gelatin scaffolds containing microspheres loaded with bone morphogenetic proteins, *J. Control Release*, 121 (2007) 81-90.

[51] H. Fan, Y. Hu, L. Qin, X. Li, H. Wu, and R. Lv, Porous gelatin-chondroitin-hyaluronate tri-copolymer scaffold containing microspheres loaded with TGF-beta1 induces differentiation of mesenchymal stem cells *in vivo* for enhancing cartilage repair, *J. Biomed. Mater. Res.*, 77A (2006) 785-794.

[52] S. S. Rengachary, Bone morphogenetic proteins: basic concepts, *Neurosurg. Focus*, 13 (2002) 1-6.

[53] B. Zhao, T. Katagiri, H. Toyoda, T. Takada, T. Yanai, T. Fukuda, U. Chung, T. Koike, K. Takaoka, and R. Kamijo, Heparin potentiates the *in vivo* ectopic bone formation induced by bone morphogenetic protein-2, *J. Biol. Chem.*, 281 (2006) 23246-23253.

[54] R. J. Westerhuis, R. L. van Bezooijen, and P. Klloen, Use of bone morphogenetic proteins in traumatology, *Injury*, 36 (2005) 1405-1412.

CHAPTER VIII

Conclusions and Future Recommendations

The ideal approach for drug delivery to bone is to formulate a specific drug of interest, which may exhibit no particular bone affinity, with a bone-seeking carrier, so that the complex will be deposited at bones after systemic administration. The work presented in this dissertation has contributed to development of engineering proteins with bisphosphonates (BPs) for bone affinity in order to improve their therapeutic potential. It provided the foundation of a colloidal drug delivery system to bone based on albumin nanoparticles (NPs) surface modified with cationic polymers. Moreover, the dissertation contains scientific information for numerous additional studies to expand our knowledge in drug delivery and bone tissue engineering.

BPs have remarkable affinity for bone mineral and rapidly localize in bone after entering the systemic circulation [1], which provides a basis for bone-specific drug delivery systems. It was postulated that conjugating BPs to therapeutic proteins can impart mineral affinity to proteins, improve the targeting of proteins to skeletal tissue, and decrease the extra-skeletal distribution of the administered proteins. Furthermore, a reduction in administered protein dose may be achieved due to the increased targeting efficiency of a bone-targeted protein. The side effects of protein therapy should be minimized in this way. Owing to the structural specialty, BPs preserve a long retention time in the bone with a half life of several months [1]. This is expected to improve the protein retention in bones, which in turn should improve the protein efficacy due to the prolonged localization in bone. Overall, protein-BP conjugation is expected to provide the advantage of controlled (localization and retention) delivery of protein to bone.

Initially, protein-BP conjugation was explored with the linker of SMCC [2-4], MMCCH [5] and EDC/NHS [6]. These linkages are regarded as stable, or slow-cleaving

linkages *in vivo*. They were initially chosen to minimize BP removal from conjugates after a protein-BP conjugate is administered into an animal model. Protein conjugates with cleavable linkage might be desirable since proteins can be liberated from the conjugate *in situ* to interact freely with their cellular targets. Therefore, the cleavable protein-BP conjugate was constructed with disulfide linkage through the linker SPDP (**CHAPTER III**). The conjugates were readily cleaved upon the presence of physiological thiols. This disulfide cleavage of the protein-BP conjugate was further evaluated *in vivo* with a subcutaneous implant model in rats, and compared with the stable thioether linkages [7]. However, the results showed the cleavage of disulfide-linked conjugate was not apparent, with no obvious differences from thioether linkages in the implant binding. This suggested that the disulfide cleavage *in vivo* might be slower than desired, and much slower than *in vitro* conditions. The accessibility of hydroxyapatite (HA)-bound conjugate to physiological thiols could be one reason for the slow cleavage *in vivo*. To elucidate this possibility, systemic administration of the disulfide-linked conjugate and investigation of the conjugate's stability will be required; in addition, determination of the increase in the short half-life of the systemically delivered protein can be obtained by this approach. A faster cleavage may be achieved with thioester linkages, as compared with disulfide linkages, since one study showed a very limited stability (< 24 h in serum) of a thioester-linked BP conjugate [8]. Developing a conjugation scheme with thioester linkages might be desirable in this respect. Such thioester conjugates may enable us to better understand (1) the rates of linkage cleavage *in vivo* and (2) factors controlling protein desorption from minerals.

In conventional protein-BP conjugation, a small targeting moiety (BP with <1 kDa) is linked with a large protein (10-200 kDa). Accordingly, multiple copies of BPs are needed for conjugation for a significant mineral affinity. Yet, retaining bioactivity after conjugation is the central issue with this approach since multiple attachments on protein increase the likelihood of reducing protein bioactivity. The alternative to conventional BPs is molecules that bear multiple copies of BPs [6,9]; with a single attachment site, multiple copies of BPs can be attached to a protein, minimizing the extent of protein modification. The utility of cationic polymers (PLL or PEI) with multiple copies of BPs, was explored in **CHAPTER IV**. A number of BPs were successfully linked to PLL and PEI, respectively, however, the polymer-BP conjugates did not demonstrate increased mineral affinity compared with the unmodified polymers, as examined *in vitro* and *in vivo*. This was due to inherently strong interaction of cationic polymers with HA, which were as effective as BPs in HA binding. To harmonize the mineral affinity from BPs and polymer backbone, future studies need to focus on using negatively charged or neutral polymers, as shown with N-(2-hydroxypropyl)methacrylamide (HPMA [10]). Our laboratory reported the dendritic BPs such as diBPs [6], tetraBPs [9] with a dense phosphonate density and superior mineral affinity compared with conventional BPs (one bisphosphonic group). OctaBPs or decaBPs may be considered in future studies. Furthermore, incorporating BPs into the monomer before polymerization [11] can be attempted in future to create polymeric molecules with bisphosphonic side-groups. Nevertheless, inherent mineral affinity of cationic polymers discovered in this work provided merit of direct utilization of PEI or PLL for targeting therapeutics agents to bone. The *in vivo* studies showed that PEI retained its strong mineral binding character

under physiological conditions [12]. However, whether these cationic polymers will also be effective in seeking bone after systemic administration remains to be determined, since cationic polymers may display non-specific binding to other tissues *in vivo*. Given the simplicity of this approach, the potential of native cationic polymers for bone targeting should be considered.

The determination of affinity constants of BPs, and that of the protein-BP or polymer-BP conjugate would be an alternative way to characterize the bone-binding molecules. The affinity constant for BPs can be calculated from the kinetic studies on HA crystal growth, as shown by Nancollas et al. [13], using a constant composition potentiostatic method. The adsorption of BP molecules on crystal surface was interpreted by a Langmuir equilibrium isotherm, and the kinetic affinity constant was then calculated from the slope of the isotherm. A competitive adsorption method can be alternatively used to determine the affinity constant of BPs and BP conjugate (tetraazacyclododecanetetraacetic acid (DOTA)-BP conjugate) adsorption on HA surface [14]. The adsorption isotherms of the BP or conjugates on HA was described by the Langmuir-Freundlich model since the heterogeneous nature of HA surface ($X / X_m = (Kc)^n / [1 + (Kc)^n]$, where K is the affinity constant, mol/L; X_m is the maximum adsorption capacity, mol/m^2; X is the specific adsorbed amount, mol/m^2; c is the equilibrium concentration in the solution, mol/L; and n is a coefficient with $0 < n < 1$). Their results suggested the size of the conjugates to be the main factor affecting the maximum adsorption capacities of the molecules, with the larger conjugate exhibiting lower maximum adsorption capacity; the conjugate containing shorter spacer between BP and DOTA possessed higher affinity constant. The determination of affinity constants of

BP, protein-BP and polymer-BP conjugates will provide more information on the binding capacities of these molecules, and allow comparison with other bone-binding ligands in the literature.

Despite successful delivery of molecules to bones, the non-metabolizable nature of BPs is a concern especially if a medicinal agent needs to be administered on a regular basis. It might be possible to utilize mineral-binding protein motifs as a guide to develop more physiological molecules for bone targeting. Poly(aspartic acid) and poly(glutamic acids) are prototypical molecules for this reason, where the mineral affinity is afforded by endogenous moieties. *In vivo* targeting for small molecules, fluorescein isothiocyanate (FITC) [15] and 17β-estradiol [16], and recently a polymeric ligand [10], was successfully demonstrated by using poly(amino acids). γ-Carboxyglutamic acid in an α-helix conformation, phosphorylated serines/tyrosines, and lysine/arginine are other moieties found in protein motifs that may be assembled into bone-seeking agents [17-20]. Their ability to be physiologically metabolized makes them worthwhile to explore. Another issue associated with protein-BP conjugate is the chemical modification of protein upon BP attachment. The integrity of protein is at risk by this approach and the bioactivity needs to be assessed on a protein-by-protein basis after BP conjugation. Furthermore, administration of exogenous protein in BP-conjugate might elicit immunological response *in vivo*. It is believed that the more divergent an exogenous protein is from its endogenous form, the more likely it will elicit an immunogenic response [21]. The possible immunogenicity might not only affect the pharmacokinetics (increased reticuloendothelial system uptake) but also the pharmacodynamic properties (osteogenic activity) of protein-BP conjugate.

The development of bone-specific carrier that complexes a therapeutic agent without the need for direct modification of the agent is more likely to maintain the bioactivity of therapeutics. In consideration of this, we developed a nanoparticulate drug delivery system from albumin NPs, with the osteogenic growth factor BMP-2 encapsulated (**CHAPTER V**). BSA NPs are considered suitable for drug delivery since they are naturally biodegradable, non-toxic and non-antigenic. The NPs were surface-modified with PEI by electrostatic interaction, in order to stabilize the NPs and also serve as a mineral binding ligand. This polymeric nanocarrier ensures the isolation of the payload from the bone-seeking agent, and independently engineering each component for an optimal performance is possible. The PEI-coated BMP-2/BSA NPs demonstrated ALP induction activity, and sustained release of BMP-2 as a function of PEI coating. This is advantageous since the release kinetics will influence the osteogenic activity [22]. Unfortunately, NPs failed to induce bone formation in a rat ectopic study due to the increased toxicity after PEI concentration. In order to overcome the toxicity issue, we implemented PEGylation of PEI, which displayed several superior properties: decreased toxicity, reduced NP size and lower zeta potential of NPs. When implanted *in vivo*, the PEI-PEG coated BMP-2/BSA NPs successfully induced new bone formation in the rat ectopic model. With the intention to investigate the correlation between the osteoinduction activity and BMP-2 retention in NPs, the pharmacokinetics of BMP-2 from PEI-PEG coated NPs needs to be determined *in vivo* in future studies. Different PEI-PEG coating concentrations should be considered, since the coating concentration would affect BMP-2 release and, consequently the osteoinduction activity. Owing to the nanosize of this colloidal NPs drug delivery system, systemic administration via

intravenous injection should also be attempted in future studies to assess the bone-targeting efficiency of this delivery system.

As mineral binding is of great importance for bone-targeting drug delivery, the HA affinity of the proposed NPs should be assessed in future studies. Due to the colloidal nature of NPs, the established HA binding assay [4] may need to be amended to suit the NP system. Currently, an extraction method by using HCl for NPs bound HA is being explored in our laboratory to assess the mineral affinity of NPs. The hydrated PEG molecule should antagonize the HA affinity of PEI [12] after substitution to PEI. Fortunately, BPs conjugation to PEI-PEG may recover this affinity and restore the mineral affinity of PEI, as was the case for PLL conjugates [12]. By using BP-conjugated PEI-PEG for NP coating, this polymer may provide a dual advantage of increased biocompatibility (PEG) and osteotropicity (BPs). Future studies need to examine coating the NPs with PEI-PEG-BP conjugates (with different PEG and BP densities) in order to determine the significance of these two fractions on bone-targeting. Moreover, since these modifications on PEI could adversely affect the coating efficiency of NPs, future studies should be focused on NP coating efficiency by the modified PEIs. It is imperative that modification with PEG and/or BP do not compromise the NP coating efficiency of the designed polymers.

The molecular weight (MW) of PEG is thought to influence the HA binding, since the chain length between NP surface and BP will increase as the PEG MW is increased. One study from our group showed that shorter tether between a protein and a BP is more effective in mineral binding [23]. As Molecular Dynamics (MD) is a useful tool in predicting the binding capacity of molecules, MD simulation can be employed in future

studies to identify the relationship between the HA binding of PEI-PEG-BP with different MW of PEG and the maximal probability/radial density of their pendent ligands; The latter parameter is inversely proportional to tether length. In addition to this, MW of PEG chains may impact the resistance to non-specific protein fouling [24]. Lower MW of PEG (MW: 600) with higher grafting densities seemed to be more effective in preventing non-specific protein fouling on surfaces, and it is likely that this may be the case for NP surfaces. This property will be beneficial for systemic administration of NPs. Nevertheless, the effect of PEG MW should be examined in future studies to elucidate its influence on HA binding and protein fouling prevention.

Uptake of the designed NPs with cells derived from bone marrow cavity or osteoblastic cell lines (e.g., mouse calvarial MC3T3-E1 cells) should be conducted in future studies. This will help to understand the mechanism of action for BMP-2 delivered with the NPs. It will also help to determine the biocompatibility of the polymer-coated NPs. The developed polymer-coated BSA NPs system is likely to be a 'generic' drug delivery system, in that it will serve as a carrier for a range of therapeutic agents, rather than molecule-specific which is often the case with protein-BP conjugates. With the final goal of efficiently delivering proteins to bone, the reduction in protein dose and decrease in extra-skeletal distribution are the two critical issues to be satisfied. Future studies should examine the non-skeletal effects of protein interventions since this will ultimately validate the benefit of bone-specific delivery. Given the promise of the bone-targeting approach, significant efforts in this area are expected to overcome the current challenges and generate novel pharmaceuticals for treatment of bone diseases.

References

[1] H. Hirabayashi and J. Fujisaki, Bone-specific drug delivery systems: approaches via chemical modification of bone-seeking agents, *Clin. Pharmacokinet.*, 42 (2003) 1319-1330.

[2] H. Uludağ, T. Gao, G. R. Wohl, D. Kantoci, and R. F. Zernicke, Bone affinity of a bisphosphonate-conjugated protein *in vivo*, *Biotechnol. Prog.*, 16 (2000) 1115-1118.

[3] H. Uludağ and J. Yang, Targeting systemically sdministered proteins to bone by bisphosphonate conjugation, *Biotechnol. Prog.*, 18 (2002) 604-611.

[4] H. Uludağ, N. Kousinioris, T. Gao, and D. Kantoci, Bisphosphonate conjugation to proteins as a means to impart bone affinity, *Biotechnol. Prog.*, 16 (2000) 258-267.

[5] S. A. Gittens, J. R. Matyas, R. F. Zernicke, and H. Uludağ, Imparting bone affinity to glycoproteins through the conjugation of bisphosphonates, *Pharm. Res.*, 20 (2003) 978-987.

[6] G. Bansal, S. A. Gittens, and H. Uludağ, A di(bisphosphonic acid) for protein coupling and targeting to bone, *J. Pharm. Sci.*, 93 (2004) 2788-2799.

[7] J. E. I. Wright, S. A. Gittens, G. Bansal, P. I. Kitov, D. Sindrey, C. Kucharski, and H. Uludağ, A comparison of mineral affinity of bisphosphonate-protein conjugates constructed with disulfide and thioether linkages, *Biomaterials*, 27 (2006) 769-784.

[8] L. Gil, Y. Han, E. E. Opas, G. A. Rodan, R. Ruel, J. G. Seedor, P. C. Tyler, and R. N. Young, Prostaglandin E2-bisphosphonate conjugates: potential agents for treatment of osteoporosis, *Bioorg. Med. Chem.*, 7 (1999) 901-919.

[9] G. Bansal, J. E. I. Wright, C. Kucharski, and H. Uludağ, A dendritic tetra(bisphosphonic acid) for improved targeting of proteins to bone, *Angew. Chem. Int. Ed.*, 44 (2005) 3710-3714.

[10] D. Wang, S. Miller, M. Sima, P. Kopeckova, and J. Kopecek, Synthesis and evaluation of water-soluble polymeric bone-targeted drug delivery systems, *Bioconjug. Chem.*, 14 (2003) 853-859.

[11] L. Wang, M. Zhang, Z. Yang, and B. Xu, The first pamidronate containing polymer and copolymer, *Chem. Commun.*, (2006) 2795-2797.

[12] S. Zhang, J. E. I. Wright, N. Özber, and H. Uludağ, The interaction of cationic polymers and their bisphosphonate derivatives with hydroxyapatite, *Macromol. Biosci.*, 7 (2007) 656-670.

[13] G. H. Nancollas, R. Tang, R. J. Phipps, Z. Henneman, S. Gulde, W. Wu, A. Mangood, R. G. G. Russell and F. H. Ebetino, Novel insights into actions of

bisphosphonates on bone: differences in interactions with hydroxyapatite, *Bone*, 38 (2006) 617-627.

[14] T. Vitha, V. Kubíček, P. Hermann, Z. I. Kolar, H. Th. Wolterbeek, J. A. Peters and I. Lukeš, Complexes of DOTA-bisphosphonate conjugates: probes for determination of adsorption capacity and affinity constants of hydroxyapatite, *Langmuir*, 24 (2008) 1952-1958.

[15] S. Kasugai, R. Fujisawa, Y. Waki, K. Miyamoto, and K. Ohya, Selective drug delivery system to bone: small peptide (Asp)6 conjugation, *J. Bone Miner. Res.*, 15 (2000) 936-943.

[16] K. Yokogawa, K. Miya, T. Sekido, Y. Higashi, M. Nomura, R. Fujisawa, K. Morito, Y. Masamune, Y. Waki, S. Kasugai, and K. I. Miyamoto, Selective delivery of estradiol to bone by aspartic acid oligopeptide and its effects on ovariectomized mice, *Endocrinology*, 142 (2001) 1228-1233.

[17] T. Aizawa, N. Koganesawa, A. Kamakura, K. Masaki, A. Matsuura, H. Nagadome, Y. Terada, K. Kawano, and K. Nitta, Adsorption of human lysozyme onto hydroxyapatite: Identification of its adsorbing site using site-directed mutagenesis, *FEBS Lett.*, 422 (1998) 175-178.

[18] P. V. Hauschka and S. A. Carr, Calcium-dependent α-helical structure in osteocalcin, *Biochemistry*, 21 (1982) 2538-2547.

[19] M. Missbach, M. Jeschke, J. Feyen, K. Mnller, M. Glatt, J. Green, and M. Susa, A novel inhibitor of the tyrosine kinase Src suppresses phosphorylation of its major cellular substrates and reduces bone resorption *in vitro* and in rodent models *in vivo*, *Bone*, 24 (1999) 437-449.

[20] W. Shakespeare, M. Yang, R. Bohacek, F. Cerasoli, K. Stebbins, R. Sundaramoorthi, M. Azimioara, C. Vu, S. Pradeepan, C. Metcalf, C. Haraldson, T. Merry, D. Dalgarno, S. Narula, M. Hatada, X. Lu, M. R. van Schravendijk, S. Adams, S. Violette, J. Smith, W. Guan, C. Bartlett, J. Herson, J. Iuliucci, M. Weigele, and T. Sawyer, Structure-based design of an osteoclast-selective, nonpeptide Src homology 2 inhibitor with *in vivo* antiresorptive activity, *Proc. Natl. Acad. Sci. U.S.A.*, 97 (2000) 9373-9378.

[21] A. Heiss, A. DuChesne, B. Denecke, J. Grotzinger, K. Yamamoto, T. Renne, and W. Jahnen-Dechent, Structural basis of calcification inhibition by α_2-HS glycoprotein/fetuin-A. Formation of colloidal calciprotein particles, *J. Biol. Chem.*, 278 (2003) 13333-13341.

[22] H. Uludağ, D. D'Augusta, J. Golden, J. Li, G. Timony, R. Riedel, and J. M. Wozney, Implantation of recombinant human bone morphogenetic proteins with biomaterial carriers: a correlation between protein pharmacokinetics and osteoinduction in the rat ectopic model, *J. Biomed. Mater. Res.*, 50 (2000) 227-238.

[23] S. Gittens, P. Kitov, J. Matyas, R. Lobenberg, and H. Uludağ, Impact of tether length on bone mineral affinity of protein-bisphosphonate conjugates, *Pharm. Res.*, 21 (2004) 608-616.

[24] L. D. Unsworth, H. Sheardown, and J. L. Brash, Protein-resistant poly(ethylene oxide)-grafted surfaces: chain density-dependent multiple mechanisms of action, *Langmuir*, 24 (2008) 1924-1929.

APPENDIX

Biodistribution of BSA NPs After Subcutaneous Injection

9.1 *In vivo* Biodistribution of NPs

In order to investigate the *in vivo* biodistribution of NPs, BMP-2 was labeled with ^{125}I, and then encapsulated into BSA NPs. The pre-formed BSA NPs was coated with 0.1 mg/mL PEI or 0.1 mg/mL PEI-PEG. The PEI-PEG-3mM was used to coat NPs for this biodistribution study (the same polymer as in the ectopic bone formation study in **CHPATER VII**). The coated NPs and uncoated NPs were dialyzed against sterilized PBS (pH=7.4) overnight before injection. 6~8-week-old female Sprague-Dawley rats were purchased from Biosciences (Edmonton, Alberta). The rats were acclimated for 1 week under standard laboratory conditions (23°C, 12 hours of light/dark cycle) prior to the beginning of the study. While maintained in pairs in sterilized cages, rats were provided standard commercial rat chow, and tap water *ad libitum* for the duration of the study. All procedures involving the rats were approved by the Animal Welfare Committee at the University of Alberta (Edmonton, Alberta).

In this study, 300 μL of radioactive-labeled samples were injected subcutaneously (SC) into each rat. In order to assess the total dose administered, the counts in the 300 μL aliquots of NP solutions were assessed in duplicate prior to injection. The samples tested were the uncoated BMP-2/BSA NPs, 0.1 mg/mL PEI-PEG coated NPs and 0.1 mg/mL PEI coated NPs. The animals were sacrificed at 3 h after the injection via CO_2 asphyxiation and a sample of blood was obtained via cardiac puncture and weighed. The bilateral femora, bilateral tibiae, bilateral kidneys, spleen and a section of liver, which was weighed, were harvested. The counts associated with each harvested tissue were determined, and all values were normalized with the injected dose and expressed as mean

± SD of % injected dose (n = 3 for spleen and liver; and n = 6 for femora, tibiae, and kidneys). The liver sample was normalized by dividing the counts by the weight of excised liver. As a consequence, the reported values for liver are in % injected dose/g of tissue. The volume of the blood counted was calculated by dividing the weight of the sample by the density of rat blood[1] (1.05 g/mL), and the blood counts were divided by the volume of blood harvested, to obtain % dose/mL.

9.2 Results and Discussion

As a preliminary study, three groups, including the uncoated BSA NPs, 0.1 mg/mL PEI-PEG coated BSA NPs and 0.1 mg/mL PEI coated NPs, were investigated for their biodistribution by SC injection **(Figure 9-1)**. The protein biodistribution was assessed 3 h after SC injection. The results indicated that PEI-PEG coating increased the BMP-2 levels in the blood, compared with PEI coating, but this was not higher than the uncoated NPs. The level of PEI-coated NPs was higher in the femur than the PEI-PEG coated NPs; however, this was not evident with tibia. The uncoated NPs showed the highest levels in all the organs, indicating an increased systemic bioavailability. The PEI-PEG coating did not reduce the distribution of NPs in other organs, e.g. spleen, liver and kidney, compared with PEI coating. Since PEGylation might decrease the hydroxyapatite (HA) affinity of PEI, this PEI-PEG coated NPs did not demonstrate specific bone affinity. In future studies, "bone-seeking" moieties, such as bisphosphonates (BPs), should be conjugated to the PEI-PEG conjugate for NPs targeting to bone.

[1] The value of density of blood was obtained from: S. A. Anderson, S. K. Song, J. J. Ackerman, and S. S. Hotchkiss, Sepsis increases intracellular free calcium in brain, *J. Neurochem.*, 72 (1999) 2617-2620.

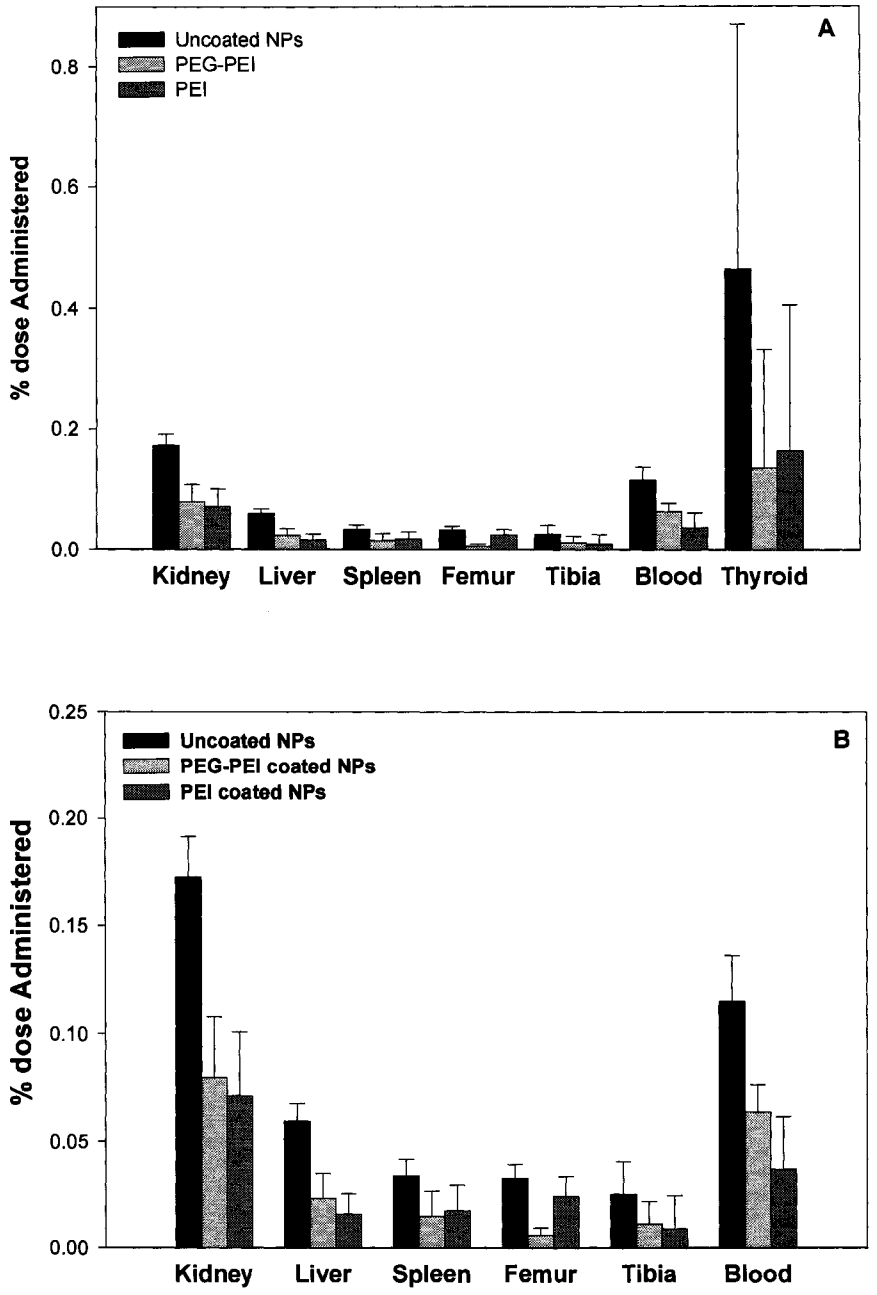

Figure 9-1. Organ distributions of NPs after 3 h of subcutaneous injection. The NPs distribution in thyroid was removed for a better comparison in other organs (**B**).